Luís António Ferreira Rocha

Development of vascularizable hydrogels to promote spinal cord injury repair: from RGD to mimetic ligands

UMinho | 2021

Universidade do Minho
Escola de Medicina

Luís António Ferreira Rocha

Development of vascularizable hydrogels to promote spinal cord injury repair: from RGD to mimetic ligands

março de 2021

Universidade do Minho

Escola de Medicina

Luís António Ferreira Rocha

Development of vascularizable hydrogels to promote spinal cord injury repair: from RGD to mimetic ligands

Tese de Doutoramento em Ciências da Saúde

Trabalho efetuado sob a orientação do
Doutor António Salgado
e do
Doutor David Learmonth

Março de 2021

Agradecimentos

"Following our will and wind we may just go where no one's been" (Maynard James Keenan in Tool - Lateralus)

Em primeiro lugar queria agradecer a orientação científica, bem como o encorajamento e liberdade para perseguir novas experiências, dada pelo "Tó" e pelo David. Um agradecimento ao Rui Sousa por ter aceitado este desafio. A minha profunda gratidão pela forma como o Carles me recebeu em Barcelona, e pela confiança demonstrada no meu trabalho. O meu obrigado pelas discussões, não só sobre ciência, e pela boa relação que desenvolvemos em tão pouco tempo.

À Tó Team, mais especialmente à parte relativa a SCI. Um grupo fantástico de pessoas, do qual felizmente levo alguns amigos. O meu agradecimento pela entre ajuda, companheirismo, discussões científicas, e amizade. Tenho de referir especificamente o Eduardo e o Rui. Obrigado! Não posso também deixar de fora a Susana, que contribuiu notavelmente para a descoberta do meu "eu" científico. Agradecer também ao Jonas pelas conversas profundas e por toda a sua ajuda e companheirismo. Um exemplo para todos. Um agradecimento especial também ao Marco e a uma amizade que cresceu para lá das fronteiras do laboratório.

Finalmente, aos meus pais e da Diana por todo o apoio. Aos meus pais por me terem incutido os princípios de justiça e educação com o seu exemplo de conduta. À Diana, minha partner in crime para a vida, por TUDO! Sem ela nada disto seria possível, desde a candidatura ao fim do doutoramento. Obrigado por me obrigares a ser melhor todos os dias da minha vida *.

The work presented in this thesis was performed in the Life and Health Sciences Research Institute (ICVS), Minho University, Stemmatters – Biotecnologia & Medicina Regenerativa SA and Universitat Politècnica de Catalunya (UPC) . Financial support was provided by National funds, through the Foundation for Science and Technology (FCT) - project UIDB/50026/2020 and UIDP/50026/2020; and by the projects NORTE-01-0145-FEDER-000013 and NORTE-01-0145-FEDER-000023, supported by Norte Portugal Regional Operational Programme (NORTE 2020), under the PORTUGAL 2020 Partnership Agreement, through the European Regional Development Fund (ERDF). Prémios Santa Casa Neurociências - Prize Melo e Castro for Spinal Cord Injury Research (MC-04/17). FEDER, through the Competitiveness Internationalization Operational Program (POCI), and by National funds, through the FCT, under the scope of the projects POCI-01-0145-FEDER-007038; TUBITAK/0007/2014; PTDC/DTP-FTO/5109/2014; POCI-01-0145-FEDER-029206; POCI-01-0145-FEDER-031392; PTDC/MED-NEU/31417/2017. LR is acknowledges FCT by the finantial support (PD/BDE/127835/2016).

STATEMENT OF INTEGRITY

I hereby declare having conducted this academic work with integrity. I confirm that I have not used plagiarism or any form of undue use of information or falsification of results along the process leading to its elaboration.

I further declare that I have fully acknowledged the Code of Ethical Conduct of the University of Minho.

Abstract - Development of vascularizable hydrogels to promote spinal cord injury repair: from RGD to mimetic ligands

A major contributor for the severe deficits spinal cord injury (SCI) patients face lies on the disruption of the blood-spinal cord barrier (BSCB), and consequent deficient angiogenic response. Therefore, during this PhD thesis we proposed to develop vascularizable cell transplantation vehicles based on modified gellan gum (GG) hydrogels aiming to promote SCI repair. We started by understanding whether human umbilical vein endothelial cells (HUVECs) were able to assemble into vascular-like constructs when cultured on in-house GRGDS-modified GG (GG-GRGDS). HUVECs only developed stable vascular-like constructs in the presence of adipose-derived stem cells (ASCs). Moreover, the co-culture secretome had an enrichment on defined neurotrophic factors in comparison to the individual culture of both types of cells. We also observed a significant promotion on axonal growth in comparison to the hydrogels without cells. The next part of the work involved the modification of GG with two integrin-specific ligands (against αvβ3 and α5β1) to improve the bioactivity of the polymer. Cell adhesion studies showed that the αvβ3 mimetic promoted significant adhesion of ASCs to the matrix in comparison to RGD and the other mimetic ligand. This was even more evident for the formulation modified using a GG:ligand ratio of 10:1 (GGp10αv). Despite integrin specificity, it were only observed vascular-like structures only when HUVECs were co-cultured with ASCs. The axonal growth experiments did not reveal a statistical increase when comparing the co-culture with the hydrogel alone. Finally, the *in vivo* evaluation of both in-house GG-GRGDS and GGp10αv on a T8 transection model of SCI showed statistically significant motor improvements for GGp10αv encapsulating ASCs+HUVECs in comparison to lesioned animals. Furthermore, both GG-GRGDS and GGp10αv (with and without cells) lead to significant gains of sensation 8 weeks after SCI. It was also observed that during the acute phase of SCI GGp10αv+cells promoted a marked decrease on pro-inflammatory cytokines such as IL-1 α, IL-1 β, TNF-α and MCP-1 that are associated with the exacerbation of damage following SCI. On the other hand, IL-10 and IL-4, which are more connected to a pro-regenerative inflammation, were augmented relative to injured animals. Even though the histological and proteomic characterization of the tissue is still lacking, these indications point out towards a neuroprotective effect of GGp10αv+cells on injured tissue.
Keywords: integrin-specific biomaterials; mesenchymal stem cells; neurovascular; spinal cord injury; vascular engineering.

Resumo - Desenvolvimento de hidrogéis vascularizáveis para pormover a recuperação de lesões medulares: desde o RGD até ligandos miméticos

Um dos principais contribuintes para os défices observados em pacientes com lesões medulares é a disrupção da componente medular da barreira hematoencefálica, e consequente resposta angiogénica defetiva. Assim, nesta tese propusemos o desenvolvimento de veículos de transplantação celular vascularizáveis baseados em hidrogéis de goma gelano modificado, com o pressuposto de promover a recuperação depois de lesão medular. Começámos por entender se células endoteliais do cordão umbilical (HUVECs) se organizavam em estruturas vasculares quando encapsuladas em GG modificado com GRGDS. Observámos que as HUVECs apenas apresentaram este fenótipo quando encapsuladas em co-cultura com células estaminais derivadas de tecido adipose (ASCs). A análise do secretoma da co-cultura mostrou um enriquecimento em factores neurotróficos definidos em comparação com a cultura isolada de ambas as células. Também se observou uma promoção significativa no crescimento axonal em comparação com os hidrogéis sem células. A próxima parte do trabalho envolveu a modificação de GG com dois ligandos específicos para integrinas ($\alpha v\beta 3$ e $\alpha 5\beta 1$) de modo a melhor a bioatividade do polímero. Estudos de adesão cellular mostraram que o mimético para $\alpha v\beta 3$ promoveu adesão significativa de ASCs em comparação com o RGD e o outro ligando mimético. Isto foi ainda mais evidente para a formulação que usou um rácio GG:ligando de 1:10 (GGp10αv). Apesar da elevada especificidade, só se observaram estruturas vasculares quando as ASCs estavam em co-cultura com as HUVECs. As experiências de crescimento axonal não revelaram aumentos estatísticos quando comparando a co-cultura com hidrogel sem células. Finalmente, a avaliação *in vivo* da co-cultura em GGp10αv, num modelo de transecção em T8, levou a melhorias motoras significativas em comparação ao grupo lesionado. Além disso, tanto o GG-GRGDS como o GGp10αv promoveram ganhos sensoriais significativos às 8 semanas. Durante a fase aguda da condição o GGp10αv+células promoveu uma diminuição de citocinas pro-inflamatórias como IL-1 α, IL-1 β, TNF-α e MCP-1.

Por outro lado, citocinas ligadas a uma resposta inflamatória mais regenerativa como IL-10 e IL-4 estavam aumentadas em comparação com animais lesionados. Apesar de a caracterização histológica e proteómica do tecido estar em falta, estas indicações apontam para um efeito neuroprotetor promovido pela condição experimental GGp10αv+células no tecido medular lesionado.
Palavras-chave: biomateriais com especificidade para integrinas; células estaminais mesenquimatosas; engenharia vascular; lesões medulares; neurovascular.

Table of contents

Abbreviations list

A

AAV – Adeno-associated virus

AI – Artificial intelligence

Ang – Angiopoietin

ASCs – Adipose-derived stem cells

ATR-FTIR – Attenuate Total Reflectanceode

B

BBB – Basso, Beattie and Bresnahan

BDNF – Brain-derived neurotrophic factor

bFGF – basic fibroblast growth factor

BM-MSCs – Bone marrow stem cells

Bp – Base pair

BSCB – Blood-spinal cord barrier

C

Ca^{2+} – Calcium

CAM – Chick chorioallantoic membrane

CCL – Chemokine C-C motif ligand

CD – Cluster of differentiation

CF – Carboxyfluorescein

CNS – Central nervous system

CPG – Central pattern generator

CSF – Cerebrospinal fluid

CSPGs – Chondroitin sulfate proteoglycans

Cyr – Cysteine-rich

D

DAMP – Danger-associated molecular pattern

DCC – Deleted Colorectal Carcinoma receptor

DMT-MM – 4-(4,6-Dimethoxy-1,3,5-triazin-2-yl)-4-methylmorpholinium chloride

DRG – Dorsal root ganglia

DSCAM – Down's syndrome cell adhesion molecule

E

E – Embryonic day

ECM – Extracellular matrix

ECs – endothelial cells

EGM – Endothelial growth media

EGS – Endothelial growth supplement

EPCs – Endothelial progenitor cells

ET – Endothelin

EMA – European Medicines Agency

F

FBS – Fetal bovine serum

FCS – Fetal calf serum

FDA – Food and Drug Administration

FGF – fibroblast growth factor

fGGp – fluorescent ligand conjugate

FTIR – Fourier-transform infrared spectroscopy

FTM – First-trimester

G

GABA – Gamma-aminobutyric acid

GDNF – Glial cell line-derived neurotrophic factor

GG – Gellan gum

GGp – Purified gellan gum

GGpα5 – α5β1 mimetic-modified GGp

GGpαv – αvβ3 mimetic-modified GGp

GGpRGD – RGD-modified GGp

Glut-1 – Glucose transporter-1

H

HAMECs – human adipose microvascular endothelial cells

HGF – hepatocyte growth factor

HIF 1-α – hypoxia-inducible factor 1-α

HLA-DR – human leukocyte antigen DR isotype

HMGB1 – high-mobility group protein B1

HUCPVCs – human umbilical cord perivascular cells

HUVECs – human umbilical vein endothelial cells

I

ICC – Immunocytochemistry

IGF – Insulin growth factor

IKVAV – Ile-Lys-Val-Ala-Val

IL – Interleukin

iNOS – Inducible nitric oxide synthase

iPSCs – induced pluripotent stem cells

K

K^+ – Potassium

L

LIF – Leukemia inhibitory factor

LDV – Leu-Asp-Val

M

Mal-GRGDS – Maleimide-modified GRGDS MAG – Myelin-associated glycoprotein

MCP-1 – Monocyte chemoattractant protein 1

MES - 2-(N-morpholino)ethanesulfonic acid

MFSD2A – major facilitator superfamily domain-containing protein 2a

MHC – Major histocompatibility complex

miR – MicroRNA

MNs – Motor neurons

MRI – Magnetic resonance imaging

MSCs – Mesenchymal stem cells

Mw – Molecular weight

N

Na^+ – Sodium

NGF – Nerve growth factor

Ngr1 – Nogo receptor 1

NPCs – Neural progenitor cells

NT-3 –Neurotrophin-3

NVU – Neurovascular unit

O

OECs – Olfactory ensheathing cells

OMgp – Oligodendrocyte-myelin glycoprotein

P

P – Postnatal day

PCL – Poly(ε-caprolactone)

PDGF – platelet-derived growth factor

PEG – Polyethylene glycol

Pen/strep – Penicillin-streptomycin

PFA – Paraformaldehyde

PLGA – Poly(lactic-co-glycolide)

PLGF – Placental growth factor

PLLA – Poly(L-lactic acid)

PNS – Peripheral nervous system

PNVP – Perineural vascular plexus

R

RGD –Arg-Gly-Asp

RGDS – Arg-Gly-Asp-Ser

ROS – Reactive oxygen species

RT – Room temperature

S

SAPs – Self-assembling peptides

SCI – Spinal cord injury

sFlt-1 – Soluble fms-related tyrosine kinase 1

T

TBI – Traumatic brain injury

TGF-β – Transforming growth factor beta

TNF-α – Tumor necrosis factor alpha

Tubb3 – β-Tubulin III

U

Unc5 – Uncoordinated 5 subfamily

UTX – Ubiquitously Transcribed tetratricopeptide repeat

V

VEGF – Vascular endothelial growth factor

VEGFR – Vascular endothelial growth factor receptor 2

Y

YIGSR – Tyr-Ile-Gly-Ser-Arg

Z

ZO-1 – zona occludens 1

Figures list

Chapter 1

the release of cytotoxic products that lead to cell death. B, During the subacute phase (2-4 days after injury) further ischemia (continuation) and persistent inflammatory cell infiltration occurs which increased cell death as well as the formation of microcavities and the disruption of the architecture of the spinal cord. Astrocytes begin to proliferate and deposit fibrotic ECM components. C, during the intermediate to chronic phases (2 weeks to 6 months) it exists an ongoing axonal degeneration and the glial scar matures, being a formidable barrier to axonal regeneration. Cystic cavities merge and further hamper axonal regrowth and cellular migration. ECM: Extracellular matrix. Adapted from 144.

Chapter 2

(BDNF, β-NGF, IGF-1 and S-100 B) showing a positive effect of the interaction of both cells on the secretion of these molecules. B, The secretome of HUVECs presented decreased amounts of the quantified angiogenic molecules, with exception to EGF, whereas ASCs+HUVECs upregulated Angiogenin and CXCL-5 and ASCs promoted increased expression of CXCL-1/2/3. The relative expression values are shown in a logarithmic scale.

Figure 2.6 – Vessel recruitment capacity of ASCs encapsulated in GG-GRGDS following 3 days of implantation on CAM. A, Representative *in ovo* and *ex ovo* images of each condition. B, Quantification of the number of vessels converging to the hydrogels demonstrated that these ASCs significantly impacted this parameter in comparison to the hydrogel without cells, which shows how these cells may affect the SCI vascular milieu following implantation. Scale bar: 1 mm. Results are shown as mean±SEM (n=12/14); ***p<0.001.

Supplementary figure 2.1 – Total panel of molecules detected on A, Neurodiscovery and B, Angiogenesis Array and their relative expression.

Chapter 3

Figure 3.1 – Chemical structure and binding affinities of A, the α5β1 mimetic, B, the αvβ3 mimetic and C, common linear GGGGRGDS. Binding affinities were obtained from 8,20.

Figure 3.2 – Representative confocal micrographs of GGp hydogels conjugated with fluorescent ligands. I. unmodified GGp. II. A, 10:1 GGp:ligand ; B, fGGp20 . There are no major differences among the same stoichiometry group, however fluorescence clearly decreased on the 20:1 hydrogels, a reflection of the grafting of a lesser quantity of fluorescent molecules.

Figure 3.3 – FTIR spectra for modified GGpRGD. A, GGp10RGD; B, GGp20RGD. The amide bond peaks are highlighted in circles to each modification, accompanied by the corresponding wavelength.

Figure 3.4 – FTIR spectra for modified GGpα5. A, GGpα510; B, GGpα520. The amide bond peaks are highlighted in circles to each modification, accompanied by the corresponding wavelength.

Figure 3.5 – FTIR spectra for modified GGpαv. A, GGpαv10; B, GGpαv20. The amide bond peaks are highlighted in circles to each modification, accompanied by the corresponding wavelength.

Figure 3.6 – Representative images of the ASCs cultured on native and modified GGp at day 3 of culture. The adhesion of ASCs is clearly enhanced on GGp10αv. Scale bar: 100 μm.

Figure 3.7 – Representative images of each of the studied GGp formulations at day 7 of culture. GGp10αv clearly promoted the adhesion and extensive spreading and interconnection of ASCs to the three-dimensional matrix. Scale bar: 100 μm.

of each experimental paradigm on the swimming test did not show differences among injured animals and treated animals. Data is shown as mean±SEM (n=4/10). *p<0.05; **p<0.01 between GGp10αv and injured animals; #p<0.05 between GG-GRGDS and injured animals.

Figure 4.2 – Sensory evaluation of the studied animals using the Von Frey filament test. Animals on the treated groups increased sensory recovery when comparing to SCI animals. With exception to rats that received GGp10αv+cells, the other experimental groups showed signs of hypersensitivity as their 50 % threshold was consistently lower than the value obtained for the Sham animals. Data is presented as mean±SEM (n=4/10). *p<0.05; **p<0.01; p<0.001.

Figure 4.3 – Molecular analysis of the recollected sera 48 h following SCI using Rat Cytokine Array C2 from Raybiotech. A, Representative heat map of the panel for the different groups was generated using the BROAD Institute's R implementation of Morpheus with Euclidean distance hierarchical clustering. B, Relative expression of selected anti-inflammatory and pro-inflammatory cytokines with a known role on SCI. Data are shown as mean Log2 (fold change) relative to the normalization of each cytokine to the internal controls of each membrane.

Figure 4.4 – Analysis of the recollected sera 3 weeks following SCI. A, Representative heat map of the panel for the different groups was generated using the BROAD Institute's R implementation of Morpheus with Euclidean distance hierarchical clustering. B, Relative expression of selected anti-inflammatory and pro-inflammatory cytokines with a known role on SCI. Data are shown as mean Log2 (fold change) relative to the normalization of each cytokine to the internal controls of each membrane.

Figure 4.5 – Analysis of the recollected sera from the animals studied during the in vivo 8 weeks after SCI. The molecular analysis was performed using the Rat Cytokine Array C2 from Raybiotech. A, Representative heat map of the panel for the different groups was generated using the BROAD Institute's R implementation of Morpheus with Euclidean distance hierarchical clustering. B, Relative expression of selected anti-inflammatory and pro-inflammatory cytokines with a known role on SCI. Data are shown as mean Log2 (fold change) relative to the normalization of each cytokine to the internal controls of each membrane.

Tables list

Chapter 1

Chapter 2

Chapter 3

Thesis aims and layout

The main aims of this thesis were to develop vascularizable gellan gum (GG) hydrogels, by combining adipose-derived stem cells (ASCs) and human umbilical vein endothelial cells (HUVECs) with the final aim to promote the recovery from spinal cord injury (SCI).

This involved the initial study regarding the interaction of both types of cells in in-house GRGDS-modified GG (GG-GRGDS), as well as the *in vivo* capacity of ASCs to reshape the vascular milieu. Given the fundamental role of integrin activation during angiogenesis and vascularization, the next objective was to study the bioactivity of purified gellan gum (GGp) when αvβ3 and α5β1 integrin peptidomimetics were grafted in comparison to linear RGD. Finally, it was done the *in vivo* evaluation of the transplantation of both GG-GRGDS and GGp modified with the αvβ3 peptidomimetic using a polymer:ligand ratio of 10:1 (GGp10av) encompassing ASCs and HUVECs in a rat T8 transection model.

The thesis is divided in 5 chapters as follows:

CHAPTER 1 comprises a general introduction that covers the parallelism between central nervous system (CNS) and vascular system. A characterization of SCI and associated vascular damages, as well as therapies that impacted the local vasculature and lead to functional gains, is also included. Moreover, general aspects regarding the development of biomaterials with αvβ3 α5β1 specific peptidomimetics are also covered. This chapter includes portions from previously published papers by the author (Rocha *et al*, Biotechnol Adv, 36(1):208-227 and Rocha *et al*, Front Pharmacol, 9:164).

CHAPTER 2 reports the effects of encapsulating ASCs with HUVECs on the vascular organization of the endothelial cells (ECs) after encapsulation in GG-GRGDS. Additionally, the co-culture impact on axonal growth of dorsal root ganglia (DRG) explants, as well as the neuroregulatory and angiotrophic nature of their secretome, and the capacity of ASCs to reshape the vascular milieu were tested. We observed that HUVECs only assembled into vascular-like structures in the presence of ASCs, with the co-culture promoting a significant increase in DRG neurite outgrowth in comparison to the hydrogel alone. Moreover, the secretome of the co-culture presented increased amounts of different neurotrophic factors including brain-derived neurotrophic factor (BDNF) or neural growth factor (NGF). Finally, we demonstrated in an *in* vivo scenario [using the chick chorioallantoic membrane assay (CAM)], that apart from their action on the formation of mature vascular networks, ASCs can also reshape the vascular milieu by blood vessel recruitment. This work is already published (Rocha *et al*, Front Cell Dev Biol, 8:489).

CHAPTER 3 presents the results obtained for the modification of GGp with both integrin peptidomimetics (for αvβ3 and α5β1 integrins) and their comparison in terms of bioactivity with linear RGD. In this chapter

each ligand was grafted onto GGp using two different polymer:ligand ratios: 10:1 and 20:1. After the necessary chemical characterization, cell adhesion assays using ASCs demonstrated that GGp modified with GGp10αv promoted a substantial increase on the adhesion of the cells to the matrix in comparison to the other conditions. Opposingly, no biological activity was observed on GGpα5. Similarly to Chapter 2, HUVECs only developed into mature vascular-like constructs when co-cultured with ASCs. This highlights the complexity of the vascularization process, and the need to include several cues to its successful instruction. Neurite outgrowth experiments showed that ASCs encapsulated on GGp10αv lead to a significant increase of the parameter, with no differences observed between the co-culture and the hydrogel alone.

CHAPTER 4 reports the motor and sensory data, as well as the effect on the systemic inflammation on different timepoints of SCI, of the transplantation of GG-GRGDS and GGp10αv encapsulating ASCs and HUVECs in a T8 transection model of the condition. We demonstrated that GGp10αv promoted an overall significant motor recovery in comparison to lesioned animals, whereas the recovery achieved by GG-GRGDS+ ells only achieved statistical significance 8 weeks post-SCI. Regarding sensory recovery, both GG-GRGDS and GGp10αv (either encapsulating ASCs+HUVECs or not) promoted a significant gain at the end of the *in vivo* (8 weeks timepoint). Finally, it is also demonstrated that GGp10αv+cells promoted a marked decreased on pro-inflammatory mediators such as IL-1 α and β, TNF-α and MCP-1 during the acute phase of the condition (48 h after SCI). This was accompanied by an increase on the expression of anti-inflammatory mediators IL-4 and IL-10. Even though the decreased expression of pro-inflammatory mediators was not noticed for GG-GRGDS+cells, animals of the group had the highest expression of IL-4, IL-10 and IL-13 during the acute phase of SCI.

CHAPTER 5 comprises the general discussion of the results reported during this thesis, as well as future experiments that could be done to reinforce the findings reported on this document.

CHAPTER 1

Introduction

1. Development of central nervous system vascularization and importance to its homeostasis

1.1. Parallelism between central nervous system and vascular development and organization

Almost 500 years ago, in 1543, the Belgian anatomist Andreas Vesalius reported that blood vessels and nerves organized in a similar stereotypical patterning and arborization, laying the foundation for the next generations to explore the mechanisms and reasons behind this curious observation (Figure 1.1) [1]. However, the similarities are not restricted to their parallel organization as both systems are composed of afferent and efferent branches, are used to adequately transport information to the entire body (the nervous system uses electrical signaling whereas the vascular system relies on soluble molecules and leukocyte trafficking), share the same growing and inhibitory cues and use analogous structures at the phenotypical and molecular level to support growth (the axonal growth cone and the endothelial cell tip) (Figure 1.2) [2,3].

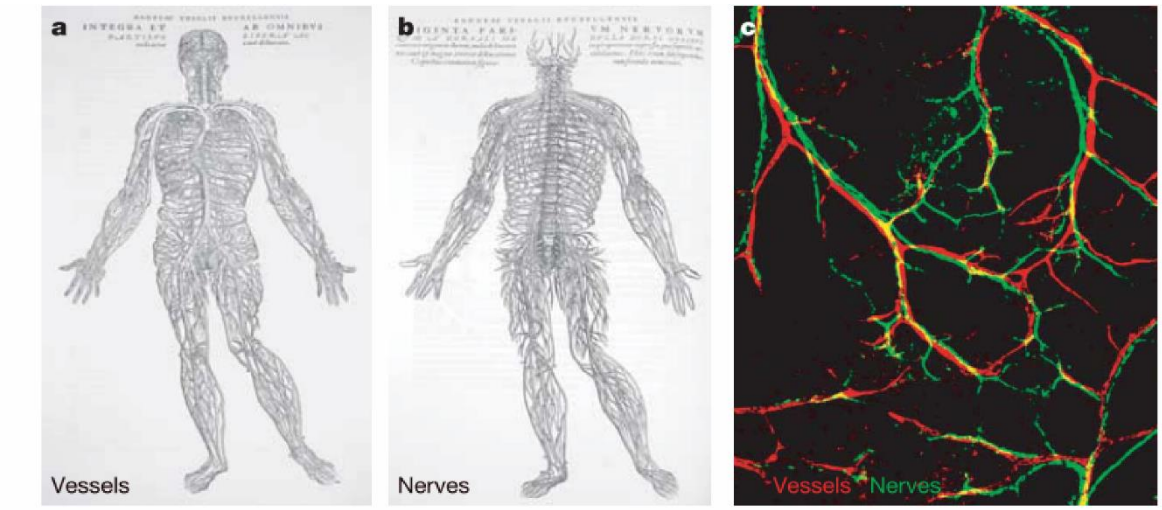

Figure 1.1 – Parallel organization between vessel and nerves. **A, B** the first drawings of Andreas Vesalius showing the similar arborization patterns between vascular and nervous networks. **C**, Fluorescence micrograph detailing the same. Adapted from 1.

In evolutionary terms, the nervous system arose as organisms became more complex and needed to coordinate and integrate complex tasks [4]. It consisted of a very primitive network of diffuse nerves that allowed the predecessors of current ctenophores (sea gooseberry, sea walnut or Venus' girdle) and cnidarians (hydra, jellyfish or corals) to control body physiology, motor activity and gastric movements [5,6]. The distribution of oxygen on these organisms was achieved by simple diffusion and so there was no need for the presence of a vascular system to distribute it, meaning that the necessity for the development of a nervous system appeared first in evolution. Indeed, the increase in animal size and complexity

decurrent from the evolutionary course meant the diffusive distribution of oxygen was no longer effective, since it is a slow process that is only effective over small distances (less than 1 mm) [7]. To overcome this evolutionary constraint, triploblast ancestors developed a primitive vascular system around 600-700 million years ago, whereas an endothelium that allowed better flow dynamics and the appearance of barriers between circulating fluid and tissue only evolved in an ancestral vertebrate around 540-510 million years ago [7].

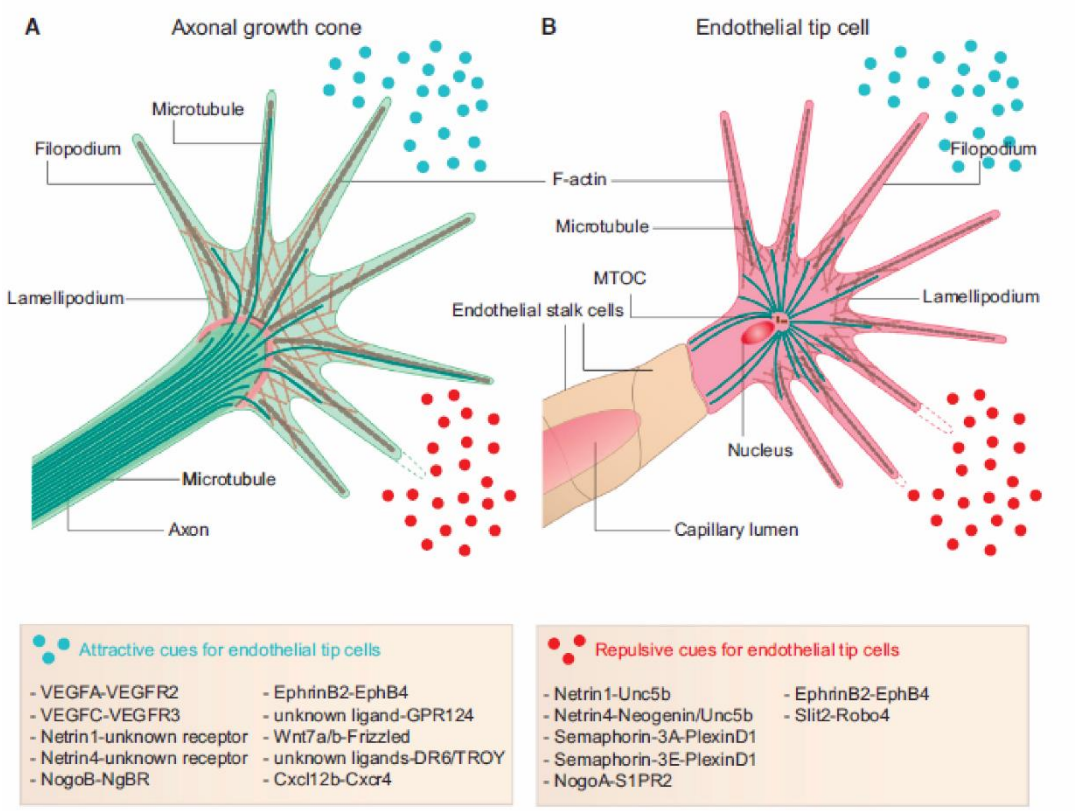

Figure 1.2 – The structure similarities between the neuronal growth cone and the vascular endothelial tip cell. Both use lamellipodia and filopodia to sense the environmental cues to determine their migration pattern. The major difference lies on the fact that the tip cell is an independent cellular entity, whereas the growth cone is a subcellular structure. **A**, Representation of the growth cone of an axon and **B**, the representation of an endothelial cell tip. The structures are attracted (blue) and repulsed (red) by the same molecular cues in another parallelism between the nervous and vascular systems. Adapted from 8.

The apparent overlapping between both systems is not restricted to humans, being also evident in invertebrates like earthworms or in vertebrate animals such as fish [9]. In earthworms, nerve cords develop parallel to blood vessels while in fish their motoneuron axons are aligned with the dorsal aorta and the neural tube is accompanied throughout its extension by the dorsal vasculature [10–12]. Therefore, it seems

that organisms presenting a homology between nervous and vascular systems were favored during evolution, being this selection criteria conserved across radically distinct species both on their complexity and organization. A probable reason for this lies on the high metabolic need the nervous system has, which lead to the selection of organisms capable of rapidly supply it to ensure proper homeostasis.

One of the two branches of the nervous system, the central nervous system (CNS) encompasses three distinct parts: brain, spinal cord and retina. Its development in mice starts at embryonic day 7.5 (E7.5) and initially consists of neuroectodermal cells enclosed in an embryonic germ layer termed the neural plate which is located atop the notochord and the paraxial mesoderm (Figure 1.3) [13]. Subsequently, the neural plate starts to elongate along the anteroposterior axis, folds and finally forms the neural tube around E8.5 and E10. This structure presents the first signs of regionalization as it is divided into the rostral primary brain vesicles (forebrain, midbrain and hindbrain) and the caudal spinal cord [9,14]. Around the same time, neural tube progenitors start to proliferate and differentiate, exhibiting dorsoventral pattering, and the migration of neurons and glia begins to be observed [15,16].

The development of the CNS vasculature occurs coincidently, reinforcing the interdependence of both phenomena, and starts with the recruitment of angioblasts by the neural tube which then differentiate into endothelial cells (ECs), coalesce and form a perineural vascular plexus (PNVP) [17]. CNS parenchymal vascularization is accomplished by angiogenesis (formation of new blood vessels from pre-existing ones) when vessel sprouts from the PNVP start to invade the embryonic tissue until reaching the ventricular side [18]. Then, vessels on this side ramify to encircle the ventricle and start migrating towards the pial side, finally branching at different levels of the tissue and start to anastomose to achieve a highly interconnected capillary plexus that allows an efficient nutrient distribution [14]. This vascularization process is observed both in embryonic hindbrain and spinal cord but differs from how the embryonic forebrain (telencephalon) becomes vascularized. Within this part of the embryonic brain, vascularization occurs by the colonization of blood vessels, not only from the PNVP, but also from an independent periventricular vascular plexus originated from a protuberant basal vessel located in what will be the basal ganglia [14,17].

1.2. Central nervous system vascularization signaling cues

1.2.1. VEGF-A

The establishment of the initial CNS vascular architecture heavily relies on the crosstalk between developing neurons and vasculature. Therefore, initial recruitment of angioblasts to the perineural region is mediated by the secretion of vascular endothelial growth factor A (VEGF-A) by the neural tube cells. Even though commonly known for its angiotrophic properties, increasing evidence has pointed out that

VEGF-A rose initially as a neurotrophic factor [3]. In fact, species devoid of a vascular system possess VEGF-A orthologs that shape neuronal development, supporting the idea that the vascular system adapted neuronal molecules as signaling cues for its development [19,20]. VEGF-A interacts with vascular endothelial growth factor receptor 2 (VEGFR2) expressed by angioblasts and stimulates their migration towards the perineural space and consequent establishment of the stereotypical PNVP [21]. Likewise, this is one of the pathways utilized for the angiogenic colonization of embryonic neuronal parenchyma by enabling to discern which ECs suffer tip (responsible to lead the migration and sense the angiogenic cues) or stalk cell (elongate and proliferate behind the sprout to form the lumen and allow perfusion) identity [9]. This specification is a dynamic process where different ECs compete for the tip cell position, upon stimulation with VEGF-A, and the upregulation of VEGFR2 and downregulating VEGFR1 is favored [22]. Upon the establishment of the tip cell identity, these instruct adjacent ECs these to assume a stalk cell identity [23,24]. Therefore, this tip/stalk cell balance is essential for proper vascularization of neuronal tissue and disturbing it leads to abnormal vascular phenotypes within tissue [25]. The main source of VEGF-A during CNS vascular development are neurons, however following remodeling of the vascular milieu [around postnatal day 24 (P24)] glial cells assume this role [8].

Both mice and human VEGF-A possess several alternative splicing isoforms that allow the exertion of its angiogenic guiding effect at short and long ranges [26–28]. Three of these are considered the major VEGF-A isoforms, being composed of 121 (VEGF121), 165 (VEGF165) and 189 (VEGF189) amino acids in humans which correspond to mouse isoforms VEGF120, VEGF164 and VEGF188 (each lacking one amino acid) [28]. These variants are capable to induce endothelial cell differentiation and proliferation, hence their individual expression allows to revert vascular defects and lethality associated to total Vegfa knockout in mice [26,29]. Nevertheless, each isoform has a specific role in angiogenic development as their affinities to the extracellular matrix (ECM) differ which allow the creation of a VEGF gradient that is pivotal for CNS vascularization [28].

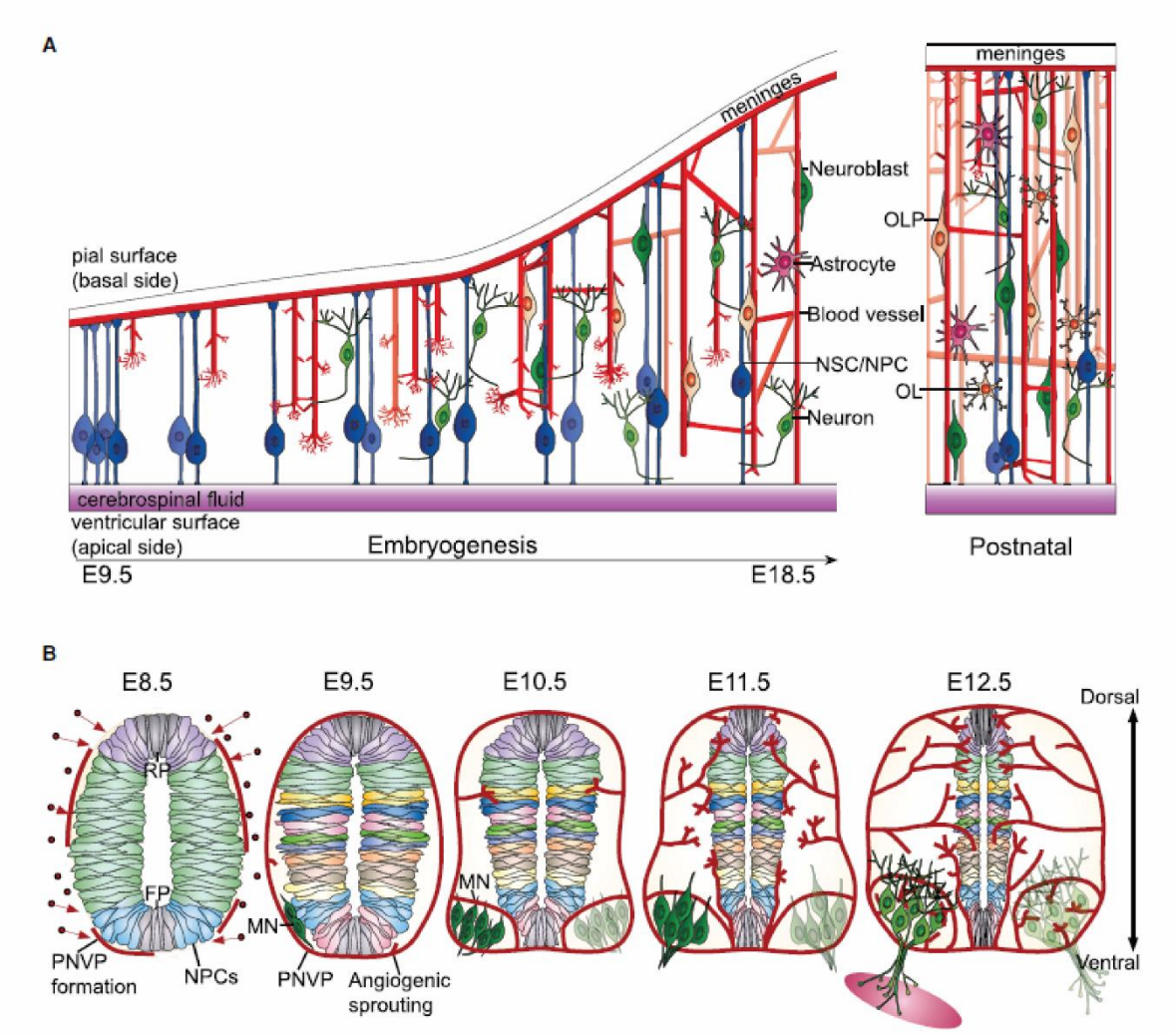

Figure 1.3 – Vascular development of the CNS. **A**, Neurogenesis and the formation of the PNVP begin around E9 and E10 in the germinal zone of the mouse cortex. Then, the sprouting vessels extend radial branches from the PNVP to the ventricle. The vascular component starts to be stereotypically patterned, anastomosing into a highly branched network. **B**, Around the same time, in mice, mesodermal angioblasts are recruited by NPCs to the periphery of the neural tube/spinal cord to form the PNVP. MNs start to differentiate at E9.5, around the same that vessel sprouts start to penetrate radially the spinal cord. Initially, MN regions (MN columns) and the FP remain avascular (until E12.5). The extension of the vascular network to the entire spinal cord happens at E12.5, where capillaries grow and branch into MN columns. **PNVP:** Perineural vascular plexus; **E:** Embryonic day; **NPC:** Neuronal progenitor cell; **MN:** Motor neuron. Adapted from 14.

To reach a proper vascular stereotypical patterning during CNS development, neuronal cells express the VEGF-A soluble fms-related tyrosine kinase 1 (sFlt-1) decoy receptor that titrates its availability and controls VEGF signaling [17]. Specifically in the developing spinal cord, motor neurons (MNs) express sFlt-1 in agreement to the developmental interval where MN columns remain avascular. The overexpression of VEGF or in alternative the knockout of sFlt-1 precipitates the ingression of ECs into MN columns, thus showing how the decoy receptor modulates proper CNS vascularization [30].

1.2.2. Wnt/β-catenin pathway

The Wnt/β-catenin represents another key signaling pathway involved in CNS developmental vascularization [31–33]. Concretely, between E10.5 and E11.5 neural progenitor cells (NPCs) located in the forebrain and spinal cord express Wnt7a and Wnt7b that by interacting with Frizzled (Fzd) receptors present on CNS induce the stabilization of β-catenin, finally leading to the expression of genes involved in cell proliferation, adhesion and morphogenesis that allow the stereotypical development of CNS intraparenchymal vasculature [31,33]. Several manipulations of this pathway induced serious malformations to CNS vasculature and lead to a higher risk of CNS hemorrhage, proving the importance of the signaling pathway on proper CNS vascular homeostasis [31,33]. These malformations traduced in a nearly complete abolishment of sprouting angiogenesis in the forebrain and ventral spinal cord (but not in the cortex and hindbrain), leading to a thicker and multilayered PNVP on which ECs mostly did not show a defined lumen [31,33]. .

Apart from the VEGF and Wnt signaling pathways, which also directly impact neuronal development [28,34], CNS vascular development shares the signaling effects of the four classes of neuronal guiding molecules (Semaphorins, Netrins, Slits and Ephrins) to establish its final organization [1,4].

1.2.3. Semaphorins

Semaphorins are mostly inhibitory molecules for both axonal guidance and angiogenesis and regulate the latter through Plexin receptors (a proper connection between semaphorin signaling through Nrp-1 on CNS angiogenesis has yet to be totally proved) [8]. Thus, the expression of Semaphorin3A is observed in ECs from the PNVP that will invade embryonic CNS at mouse E12.5, thus indicating an active role of this molecule in shaping the CNS vascular environment [35]. Semaphorin3A is also a regulator of mouse CNS vascular branching as it was observed a deficient branching of cranial blood vessels at E9.5 in mice lacking the expression of this molecule [35]. Moreover, the overexpression of Semaphorin3A/F, Nrp-1 or Plexin-A1 significantly disturbed the remodeling of chick PNVP into a mature vascular organization [35].

Nevertheless, the role of Semaphorin3A on developmental angiogenesis remains controversial since different studies showed that the knockout of Semaphorin3A had no effect on vasculature, namely on EC adhesion and migration by this molecule [36,37]. Thus, more studies are needed to really understand in depth the role of Semaphorin3A on angiogenic development.

Contrarily to Semaphorin3A, the negative effects of Semaphorin3E on angiogenesis are well established and characterized [38–40]. Plexin-D1, the receptor for Semaphorin3E, is abundantly expressed in the retinal endothelial migration front (both in tip and stalk cells), but not mature vessels, during retina vascularization [39,40]. In contrast, during the same developmental period (P2-P6) the expression of Semaphorin3E is not exclusive of retinal angiogenic sites, suggesting that it is Plexin-D1 and not the ligand who defines the angiogenic patterning on this structure [39,41]. Additionally, this ligand/receptor pair is also responsible to regulate the endothelial tip/stalk cell balance by interfering with VEGF-A/VEGFR2 signaling pathway [39]. However, the importance of Semaphorin3E for the establishment of the PNVP and the vascular colonization of embryonic neuronal parenchyma remains to be elucidated [8].

1.2.4. Netrins

Another class of axonal guidance molecules, netrins interact with a plethora of receptor families to influence neuronal and vascular patterning. These include the Deleted Colorectal Carcinoma receptor (DCC) subfamily, the Uncoordinated 5 (Unc5) subfamily, integrins, the adenosine receptor AR2b and Down's syndrome cell adhesion molecule (DSCAM) [3]. For example, Netrin1 binds to intraneural vascular plexus ECs through Unc5b, being the receptor expressed between E10.5 and E12.5 of mouse development, indicating a time-dependent effect of this axonal/vascular guidance molecule during CNS vascularization[42]. This phenotype is also observed in chick and quail embryos and interestingly upon EC quiescence this receptor is downregulated, which backs the notion regarding the contribution of Unc5b to constrain CNS angiogenesis [43]. However, another subset of works has found that Netrin-1 acts as a pro-angiogenic and not anti-angiogenic molecule, opening the debate regarding its absolute function, or whether it indeed has a complex dual role, during vascular development [44–46].

These antagonistic effects might be related to their interaction with distinct types of receptors, be a result from various netrin concentrations in embryonic neuronal tissue or be a consequence of triggering cell type-dependent signaling [47]. Indeed, recently Tu *et al.* [46], demonstrated that Netrin-1 interacts with ECs through CD146 and that this receptor might be responsible for its role as a stimulator of angiogenesis.

Similarly to Netrin-1, Netrin-4 has been described as having the same dichotomic role on angiogenesis [44,48–50]. The expression of this netrin family member is prevalent along zebrafish CNS ECs, where its

morpholino-mediated knockout produced serious vascular deficits [50]. The authors reported that the pattern of Netrin-4 expression was not followed by its putative receptors, opening the possibility of these angiogenic effects being mediated by alternative signaling mechanisms [49]. Thus, the *in vitro* stimulation of ECs with Netrin-4 increased the phosphorylation of JNK1/2, Akt, FAK, Akt, ERK1/2 while enhancing their angiogenic and tube formation capacity, survival and proliferation [50]. Since these are common VEGF pathway downstream targets, it suggests a possible crosstalk between Netrin-4 and VEGF signaling [8].

The anti-angiogenic effects of Netrin-4 occur when the signaling molecule binds to Neogenin, which is followed by the recruitment of Unc5B and inhibition of angiogenesis through VEGF signaling disruption [48]. Netrin-4 reduced tube formation capacity, as well as migration and branching of ECs stimulated with VEGF *in vitro*. *In vivo*, Netrin-4 suppressed choroidal neovascularization following laser injury and its overexpression inhibited VEGF and fibroblast growth factor-2 (FGF-2)-induced angiogenesis [48]. The latter observation has led to theorize Netrin-4 as an important negative feedback regulator of pathological angiogenesis, with future clinical value [48]. Whether the same happens during CNS vascular development or pathology is still to be fully elucidated. Nevertheless, the embryonic development is a complex phenomenon orchestrated by well-defined events, that depend on developmental time, signaling cues or the type of involved cells. Therefore, given the dual role of Netrin-1 and Netrin-4 on angiogenesis the characterization of the precise circumstances that dictate whether the molecule behaves as pro or anti-angiogenic still needs to be clarified to fully understand their role during CNS vascular development.

1.2.5. Slits

Slit ligands are expressed at the ventral midline where they bind to Roundabout receptors (Robo) on axonal growth cones and act as a chemorepulsive cue to control which axons cross to the other side of the body and establish bilateral neuronal communication [51]. As with the other axonal guidance family of molecules and receptors, the vascular system has adopted Slit/Robo signaling mechanisms during development and homeostasis [52–55]. In the retina, Slit2 is expressed by bipolar neurons that extend underneath the vasculature and its knockout in mice originated an exuberant reduction in retinal vessel branching and growth [55].

Robo4 is exclusively expressed by ECs and initial works postulated that the interaction between Slit2 and this receptor could reduce pathological angiogenesis and vascular leak in the retina while inhibiting VEGF-induced EC migration, tube formation and permeability *in vitro* [53,56]. However, molecular biology evidence has showed that Robo4 lacked essential amino acid residues to bind Slit2, and indeed further experiments in knockout mice failed to establish a direct connection between Robo4 and Slit2 [52,55,57]. Since ECs co-express Robo1/2 and Robo4 an alternative hypothesis arose where Slit2 interacts with receptor

heterodimers, which in fact was observed by Sheldon and coworkers in a study that showed that Slit2 interacted with Robo1/Robo4 heterodimers to induce EC migration [58]. Similarly to netrins, more research is necessary to fully understand the effects of Slit and Robo signaling on CNS vascularization. This encompasses the context on which they either act as pro or anti-angiogenic and even the complete set of ligands and receptors involved on the mediation of their effects.

1.2.6. Ephrins

The Ephrin family of neuronal/vascular guidance molecules and respective Eph receptors act on a unique way since their signaling effects are felt both on the cell expressing the ligand (reverse signaling) an on the cell expressing the receptor (forward signaling) [59]. During development Ephrin/Eph are instrumental to maintain vascular patterning by ensuring the separation between developing arteries and veins [60,61]. This is accomplished by the repulsion between EphrinB2-expressing arterial-fated ECs and EphB4-expressing venous-fated ECs [60,61]. Adding to this fundamental role on vascular stereotyping, EphrinB2 reverse signaling regulates tip cell guidance by being involved on the internalization of VEGFR2 and VEGFR3, a fundamental mechanism for VEGF-induced angiogenesis [62,63].

1.2.7. Nogo-A

Nogo-A is a protein mostly known for being an inhibitory cue of axonal growth, something important to guarantee proper CNS connectivity during homeostasis, but simultaneously contributing decisively for the failure of neuronal regeneration following injury [64]. Recent works have also identified this membrane protein to be a negative regulator of CNS angiogenesis [65,66]. Genetic deletion of this protein or the administration of a Nogo-A neutralizing antibody increased the vascular density in the hippocampus, cortex, corpus callosum and superior colliculus at P8. These results are not due to an increment in vessel caliber or length, but instead result from the insertion of new capillary networks by vessel sprouting and branching showing that the promotion of angiogenesis by Nogo-A function ablation results in vessels with a normal phenotype [66]. The inhibitory effects of Nogo-A in angiogenesis are mediated by its Delta 20 inhibitory segment since its administration to brain microvascular ECs induced the retraction of cytoskeleton migratory projections, impacting cell spreading and adhesion on a dose-dependent way. The other inhibitory segment to neuronal growth, Nogo-66, did not impact these parameters which shows that the action of Nogo-A in ECs and angiogenesis is specific to these processes [65]. These results extend the range of action of anti-Nogo therapies beyond the classical axonal growth stimulation in injured CNS, where Nogo-A inactivation can be used to not only induce neuronal growth but also promote CNS angiogenesis and vascularization. The latter is also impaired in several CNS conditions and contributes

decisively to their pathophysiology. On this regard, knocking out either Nogo-A or its receptor S1PR2 as well as inactivating the protein via antibody administration stimulated the revascularization of the penumbra surrounding the ischemic core in a mouse stroke model [67]. This revascularization was accompanied by enhanced neuronal survival and functional recovery. Indeed, elucidating whether the results obtained from Nogo-A inactivation are just due to its effect on axonal growth or CNS vascularization or result from a more holistic action on injured tissue will be extremely valuable to fully understand the entire potential of such therapies.

1.3. Central nervous system vasculature regulates the behavior of neural stem cells

CNS blood vessels are a key component of neurogenic niches during development and homeostasis, where NSCs reside in close association with vasculature [14]. There are two main neurogenic regions in the adult mammalian brain: the subgranular zone located in the dentate gyrus of the hippocampus, and the subventricular zone adjacent to the lateral ventricles [68]. In another example of the parallelism between vascular and neuronal development, the timing of angiogenesis closely follows the degree of neurogenesis (the generation of new neurons from NSCs) in different CNS structures including the forebrain [69], hindbrain [69,70] and spinal cord [21,30]. Even though the expanding neuronal tissue requires proper oxygen and nutrient supply to meet its high metabolic demands, blood vessels act as more than simple transporters serving also as modulators of NSC behavior [71]. This is observed during the embryonic development of the mouse hindbrain, where the knockout of Nrp-1 in ECs (and not on NPCs) originated deficient vascularization of the germinal zone accompanied by the precocious differentiation of NSCs at the expense of their self-renewal [72]. Thus, this mutation originated a depleted pool of NSCs with aberrant mitotic patterns that were independent of hindbrain oxygenation [72].

The angiogenic process in the developing mouse forebrain, however, stimulates the differentiation of NSCs by alleviating tissue hypoxia [73]. Indeed, the ingression of blood vessels in this part of the embryonic brain matches in a temporo-spatial manner its rate of neurogenesis. Inhibition of forebrain angiogenesis by GPR124 genetic deletion impaired proper tissue oxygenation and increased the proliferation of NSCs sacrificing their differentiation, in a process controlled by the expression of hypoxia-inducible factor 1-α (HIF 1-α). The authors reverted the phenotype by increasing oxygen levels and showed that at least in this region of the developing brain tissue oxygenation provided by blood vessels is fundamental to govern the state of NSCs [73]. This contrasts to what was previously detailed for the developing hindbrain [72] and can be due to differences in NSC populations or even due to different extents of vascular defects generated by each genetic model. Nevertheless, both studies highlight the importance of blood vessels for NSC

functioning. In the future it should be interesting to use the same gene deletion model and study if these differences are maintained to understand whether it really exists a regional-specific effect of hypoxia/oxygenation in NSC proliferation/differentiation during development.

In the developing mouse telencephalon, ventral progenitors need to engage with blood vessels to divide and generate neocortical interneurons [74]. The interaction seems to be partially mediated, at least, by Integrin β1 since its deletion in NSCs reduced their proliferation and neurogenesis, leading to defective synaptic activity [74]. Dorsal progenitors, on the other hand, do not need to interact with embryonic telencephalon vasculature to divide and give rise to differentiated neurons [74]. Interestingly, dorsal, and ventral, progenitors of the telencephalon originate excitatory and inhibitory neurons, respectively, thus showing that different classes of neurons may require specific stimuli to develop properly.

The action of ECs is partially explained by their capacity to secrete soluble factors that influence the phenotype of NSCs [75,76]. Accordingly, the seminal work of Shen an colleagues [75] demonstrated that NSCs cultured in the presence of ECs presented increased proliferation and self-renewal capacity through a paracrine mechanism. Upon the removal of the ECs, NSCs remained proliferative for about 4 days, after which they started to differentiate giving rise to increased quantities of neurons in comparison to NSCs cultured alone [75]. Since the publication of this work, others have followed and continued to prove that the paracrine signaling of ECs is vital to maintain NSCs in a proliferative undifferentiated state [77–79].

NSCs in the adult CNS directly contact the vasculature at sites with increased vessel permeability which gives them privileged access to nutrients and soluble cues [80,81]. This interaction is fundamental to maintain quiescent NSCs in this state in the adult CNS, being mediated by endothelial-expressed EphrinB2 and Jagged1 [82]. The former suppresses MAPK signaling to enforce quiescence, whereas the latter controls NSC identity. Intriguingly, ECs are also able to regulate NSC quiescence in the adult brain by secreting neurotrophin-3 (NT-3), a growth factor commonly associated to neuronal growth, by inducing NSCs to produce nitric oxide that acts as a cytostatic factor [83].

1.4. Central nervous system vessels act as physical guidance tracks for neuronal migration

In addition to the trophic support and nutrient provision to newborn neurons, CNS vasculature also serves as scaffolds for neuronal migration from germinal zones to their final destination [84–86]. In the developed mammalian CNS, the olfactory bulb represents one of the few exceptions that still renovates its neuronal population. To achieve it, neuronal progenitors originated from NSCs in the subventricular zone must migrate along the blood vessels of the rostral migratory stream towards the olfactory bulb where they finally differentiate [87]. These blood vessels are disposed parallelly and orientated in a caudal-to-rostral

direction, an organization that is required for their physical support of neuronal migration [88]. This architecture is fundamental for their role as physical tracks for neuronal migration, as its disruption precludes neuronal precursors to migrate from the subventricular zone [89,90]. Inside the olfactory bulb neuroblasts stop their parallel migration and start to migrate radially [91]. Still, vessel organization within this structure reflects this shift and remains parallel to the radial routes of neuroblast migration [84]. To attract neuroblasts, ECs cells secrete brain-derived neurotrophic factor (BDNF) that interacts with neuroblasts via its low-affinity p75NTR receptor, inducing their migration [85]. Neuroblasts control the rate of migration by an indirect mechanism. These neuronal precursors release GABA, leading to the insertion of the high-affinity BDNF TrkB receptor on the plasma membrane of astrocytes contacting blood vessels. This allows to trap free BDNF and refrain neuroblast migration[85]. Interestingly, the interaction of BDNF with TrkB causes the internalization of the receptor meaning that this is a highly dynamic process mediated by the constant trafficking of TrkB on astrocytes [91]. VEGF-A signaling through VEGFR2 has also been implicated to stimulate neuroblast migration across the blood vessels of the rostral migratory path. Accordingly, its intracerebroventricular infusion increased the migratory flux of the precursors [92]. Knockout mice for VEGFR1 have also showed increased neuroblast migration and so it seems that the receptor regulates the process in homeostatic conditions [92]

Besides the migratory path towards the olfactory bulb, neuroblasts of the subventricular zone also travel along blood vessels towards lower cortical layers in the first four postnatal weeks [93]. The migration occurs through the corpus callosum and astrocytes associated to blood vessels are key in coordinating the proper organization of the vascular route [93,94]. Accordingly, downregulating VEGF specifically in this astrocytic population disturbs the development of the vascular scaffold and alters the neuroblast migration patterns [94].

Gamma-aminobutyric acid (GABA) interneurons from the ventral telencephalon migrate to the developing neocortex following two main courses. that are coincident with the two developing vascular networks of the dorsal telencephalon (pial-derived vessels and periventricular vessels) [9]. These networks arise in a ventral-to-dorsal way and both the migration of their blood vessels and GABA neurons are controlled by the same homeobox transcription factors, which seems to indicate an association between both phenomena [86]. By deleting the GABA receptor β in the endothelium or abolishing the release of GABA from ECs, Li *et al.* [95], demonstrated this association as these animals developed showed defective periventricular angiogenesis. Furthermore, this phenotype lead to the inhibition of GABAergic migration along the vascular route and further shows the importance of blood vessels in the guidance of neurons [95].

The tangential migration of young neurons across blood vessels also occurs in the human brain during infancy. Throughout this period, these precursors use the blood vessels of not only the rostral migratory stream, but also the medial migratory stream to reach the olfactory bulb and the medial prefrontal cortex, respectively [96]. Further investigation is needed to fully understand how vascular perturbations during human development and infancy impact neuronal migration and development and whether additional blood vessel-based routes exist in the CNS.

1.5. The neurovascular unit

During CNS development and homeostasis ECs astrocytes, pericytes and neurons form an anatomical and functional whole, which was termed the neurovascular unit (NVU), that regulates cerebral blood flow according to its necessities and helps to establish the barriers between the CNS and its periphery (Figure 1.4) [87,97]. The term was coined in 2001 during the first Stroke Progress Review Group meeting of the National Institute of Neurological Disorders and Stroke of the NIH to highlight the intimate relationship between brain cells and their vasculature [98]. The close association between all the NVU constituents is mediated by tight junctions and adhesion molecules, such as cadherins and integrins [99].

The NVU is a highly dynamic structure where each of its components can influence the others to maintain homeostasis [99]. For instance, neurons are capable to detect very slight fluctuations in their nutrient and oxygen supply and communicate it to interneurons or astrocytes on their periphery by chemical and electrical signals [99]. Both cell types act as mediators between neurons and blood vessels to ensure the appropriate response regarding vascular tone and blood supply to the area. Accordingly, areas where neuronal activity is more exuberant higher have a higher energy demand to operate and induce an increase in blood flow on that particular region. This diverges from low activity zones, where blood flow is maintained at basal level, meaning that the hemodynamic response can be an accurate way to measure brain activity [100].

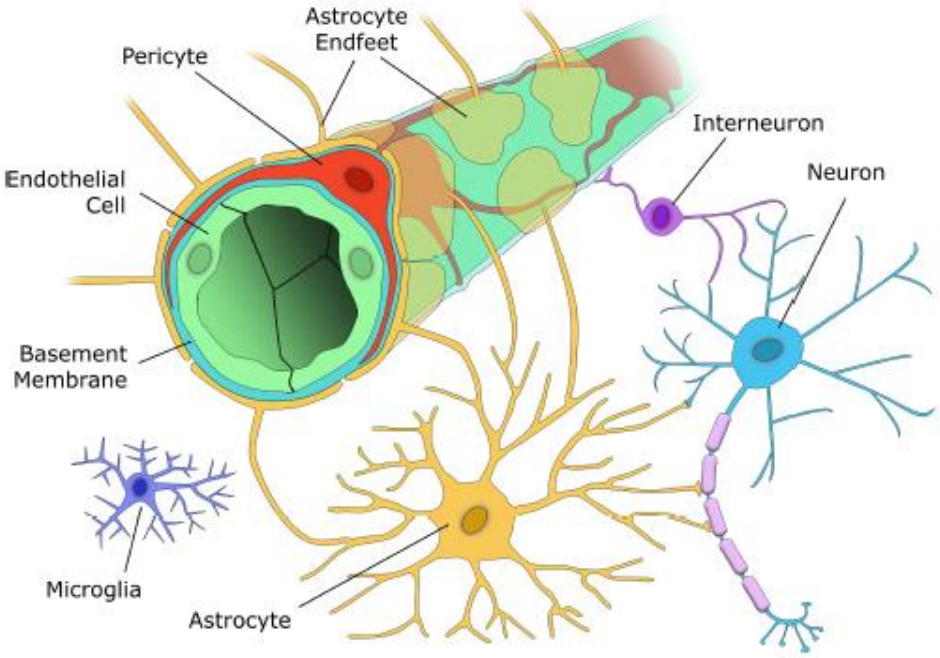

Figure 1.4 – The neurovascular unit. This regulatory structure is composed by ECs, pericytes, astrocytic endfeet and neurons being responsible to regulate CNS blood flow. Adapted from 101.

1.6. Central nervous system barriers

The NVU is also fundamental to establish both the blood-brain barrier and the blood-spinal cord barrier (BSCB). Both control the transport of biomolecules and other substances across the endothelium and are pivotal to seal the CNS and exclude pathogens, neurotoxic components and even immune and blood-borne cells that otherwise would be nefarious to the CNS [9]. To achieve it, CNS ECs exhibit several unique characteristics such as: (1) tight junctions that avoid the paracellular passage of hydrophilic molecules[102]; (2) the expression of specific transporters that regulate the influx and efflux of molecules; (3) having low rates of transcytosis, limiting transcellular transport through the endothelium; and (4) expressing low quantities of leukocyte adhesion molecules to constrain the passage of immune cells.

These properties are not inherent to CNS ECs, as different studies showed that it is actually the neuronal milieu that motivates their phenotypical appearance [103,104]. This was elegantly showed by Stewart and Willey [104] by transplanting avascular chick/quail brain fragments into the coelomic cavity. These fragments were colonized by vessels that acquired blood brain barrier features, whereas the vascular colonization of embryonic mesoderm avascular fragments that were grafted into the CNS did not show such phenotype [104].

The genesis of barriers in mice initiates between E10 and E15, when the first characteristics of the blood brain barrier appear and start sealing the leaky vasculature originated by the colonization of the neural

tube by the PNVP [105]. During this stage of the embryonic development ECs are already sealed, specialized transport systems are established and finally pericytes start to associate with capillaries to reinforce the barrier [106–108].

Following this period, the blood brain barrier continues to maturate and only then astrocytes join and provide further support through the formation of perivascular endfeet around capillaries [105]. These glial cells secrete laminin and this is important to stabilize pericytes by preventing their differentiation into a contractile phenotype that disrupts the blood brain barrier [109].. Additional molecular candidates for the effects of astrocytes on maintaining the blood brain barrier intact include interleukin-6 (IL-6) [110], glial cell line-derived neurotrophic factor (GDNF) [111], basic fibroblast growth factor (bFGF) [112].

Capillary blood vessels are ensheathed by pericyte projections along the entire organism, being on the CNS where the highest pericyte-to-EC ratio are found [113]. CNS ECs recruit pericytes during the first phases of CNS vascularization through the secretion of platelet-derived growth factor B (PDGF-B) and these cells contribute to establish the blood brain barrier by decreasing vascular permeability [108,114]. Impairments in PDGF-B signaling contribute to a deficient pericyte coverage, leading to a dysfunctional barrier function in mice, underlying the importance of pericytes to appropriate blood brain barrier development and stabilization [115]. These disturbances continue throughout adulthood, where pericyte-deficient mice show age-dependent microvascular deficiency and loss of cerebral capillaries [106,115]. Accordingly, pericytes provide support to ECs and participate on their differentiation and maturation, by enhancing tight junction formation, and decreasing both leukocyte adhesion molecule expression and transcytosis [116,117]. Indeed, pericyte loss was associated with the infiltration of different blood-derived neurotoxic molecules, which may enhance microvascular degeneration and lead to the obstruction of capillary blood flow, eventually causing hypoxia and vascular-associated neurodegeneration [115,118].

The molecular trades between CNS and blood (or vice versa) generally occur through specialized transporters, being gases and lipophilic molecules smaller than 400 Da the only exceptions since both can freely diffuse through the endothelium of CNS blood vessels [119]. The transportation of molecules across the blood brain barrier can be categorized into four distinct types: 1) passive diffusion of lipophilic molecules; 2) passage using soluble carrier transporters; 3) selective transport by ATP-binding cassette transporters; 4) vesicle trafficking by transcytosis [102]. These are fundamental for barriergenesis and their mutation or faulting genetic expression give rise to vascular and blood brain barrier disfunctions that lead to cognitive disabilities [120–122].

Soluble carrier transporters guarantee the proper uptake of fatty acids, hormones, amino acids, carbohydrates, or ions [105]. This class includes the glucose transporter-1 (Glut-1), which is ubiquitously

expressed on CNS ECs and whose deficiency provokes development impairments, seizures, ataxia and microencephaly [123]. ATP-binding cassette transporters intervene in the clearance of CNS metabolic waste products and are thought to be fundamental in CNS protection against nefarious substances [102]. As previously mentioned, CNS ECs present extremely low molecular transportation through vesicular trafficking, a process that is generally inhibited in homeostatic conditions by major facilitator superfamily domain-containing protein 2a (MFSD2A) [124,125]. Nevertheless, biomolecules without specific transporters rely on transcytosis to enter CNS. Among these are albumin, insulin or iron-bound transferrin [102]. Particularly the transferrin receptor has been used as a means to enable the delivery of drugs into the brain, circumventing the blood brain barrier [126].

Analogously to the brain, the spinal cord is sealed of its surrounding environment by a barrier having the same elements and functions as the blood brain barrier called the BSCB. Still, the BSCB has its own physiological characteristics and so it is considered as an independent structural entity [127]. Accordingly, in the spinal cord the microvasculature displays glycogen deposits that may act as an energy reservoir that might be readily used according to tissue demands [128]. Further differences are found in permeability as the spinal cord shows increased permeability to polysaccharides and cytokines in comparison to the brain [129,130]. The BSCB expresses decreased amounts of the tight junction proteins zona occludens 1 (ZO-1) and occludin, being accompanied by a smaller number and coverage of pericytes (specially in the anterior horn). These two features probably account for the differential permeability observed between spinal cord and brain ECs[131,132]. Pericyte deficiencies in the spinal cord originate the disruption of the BSCB leading to the accumulation of serum proteins and neurotoxic blood components in motor neurons, and finally to the death of these cells [132]. This experimental result highlights that even though the BSCB is more permeable than the blood brain barrier its barrier function is fundamental to guarantee the proper isolation of the spinal cord against nefarious components, securing its homeostatic balance.

The central role of the blood brain barrier and the BSCB in guarding the CNS from noxious effects implicates that their compromise and disfunction takes part in the pathophysiology of several neurological conditions. Some of these associations are direct such as in CNS vascular disorders or trauma, whereas their interplay in neurodegeneration as either cause or consequence remains to be fully elucidated [105].

The most common hallmarks of blood brain barrier or BSCB disruption are decreased expression of tight junction proteins or the loss of barrier transporters [105]. These originate the infiltration and accumulation of toxic blood components, chemicals and cells as well as inefficient nutrient supply and debris clearance (protein aggregates or myelin fragments) of the diseased CNS [117]. As a multidimensional player in the progression and control of CNS conditions, CNS barriers have been the target of therapies that intend to

reinstate their function and understand whether their modulation ameliorates the poor prognosis associated with such diseases. Some of these therapies have showed interesting results in preclinical models of traumatic brain injury (TBI), amyotrophic lateral sclerosis (ALS) and stroke[133].

As detailed on this section, CNS barriers exert key influence during the development and homeostasis of the CNS, keeping it safe from neurotoxic components while maintaining the appropriate nutrient supply and clearing waste products that otherwise would be nefarious. These are complex structures that implicate the coordination and communication between distinct types of cells to function properly. The importance of CNS barriers is highlighted by the presence of barrier dysfunction in most CNS pathologies and so their modulation is an attractive therapeutic target. More research is still needed to comprehend their role on the pathophysiology of these conditions. This will allow to establish the precise window of intervention therapies aiming to restore barrier function have and to establish whether it can effectively contribute to contain CNS diseases.

1.6.1. The vascular organization of the spinal cord

Neurons in the spinal cord also experience a high energy demand, which is perhaps reflected on the intricate degree of vascularization this CNS component presents, especially within the gray matter where neuron cell bodies are located [134]. The vasculature of the spinal is collateralized, which confers it a certain degree of resistance to hypoxia [135]. Blood circulation on the spinal cord occurs through arteries and veins encompassing the tissue, generally termed spinal microcirculation, whereas the intraparenchymal blood flow occurs through capillaries and venules and is referred as spinal microcirculation (Figure 1.5) [136].

Arterial blood arrives to the spinal cord mostly by the longitudinally-orientated anterior spinal artery and the two posterior spinal arteries, and both are branches of the vertebral artery and the median sacral artery rostrally and caudally, respectively [137]. Along the segments of the spinal cord several arteries entry the vertebrae foramen, branching into the anterior and posterior longitudinal spinal canal arteries and the radicular artery [134]. The latter travels alongside the nerve root, dividing into an anterior and posterior radicular artery that penetrates the dura mater and anastomoses with the anterior and posterior spinal arteries, thus providing further blood supply to the tissue [138].The lateral portion of the spinal cord receives its blood supply through the arterial vasocorona (or pial plexus), which results from extensive anastomosis between anterior and posterior arteries, connects both [138]. To supply the anterior portion of the spinal vascular network, the anterior artery branches into the sulcocommissural artery that together with the arterial vasocorona vascularizes the corticospinal and spinothalamic tracts, the anterior horns, the intermediolateral cell column and the central portion of the gray matter [135]. In contrast dorsal horns and

columns are supplied by ramifications originated in the posterior spinal arteries [138]. Interestingly, regions of the spinal where the highest density of neurons is found like the cervical and lumbar enlargements also show the highest degree of vascularization and arterial caliber, which contrast with the thoracic region where there are less and smaller vessels [139]. This perhaps reflects the metabolic demand of those particular areas and the need to provide them with increased nutrient and oxygen supplies to assure their proper function.

Venous drainage from the spinal cord into the extrinsic venous system is done by sulcal (central) and radial (peripheral) veins [138]. This intrinsic system is directed towards the outer surface of the spinal cord where it assembles into a venous ring and connect with the superficial spinal cord venous system [140]. Then, venous blood coming from the spinal cord goes into the anterior and posterior median spinal veins, coursing along both anterior and posterior nerve roots through the radiculomedullary veins [138]. These lead to the paravertebral and intervertebral venous plexus and eventually to segmental veins that drain into the ascending lumbar and azygos venous systems and finally to the superior vena cava [138].

The convenient vascular function is essential to guarantee the normal functioning of the spinal cord, guaranteeing the nurturing of cells with adequate nutrients and preventing the accumulation of neurotoxic molecules. Therefore, whenever a perturbation of this system occurs, either by infarction or trauma, severe motor, autonomic and sensory impairments are observed. The next section will be focused on the contribution of the disruption of the vascular architecture of the spinal cord vascular architecture and consequent BSCB compromise to the pathophysiology of SCI.

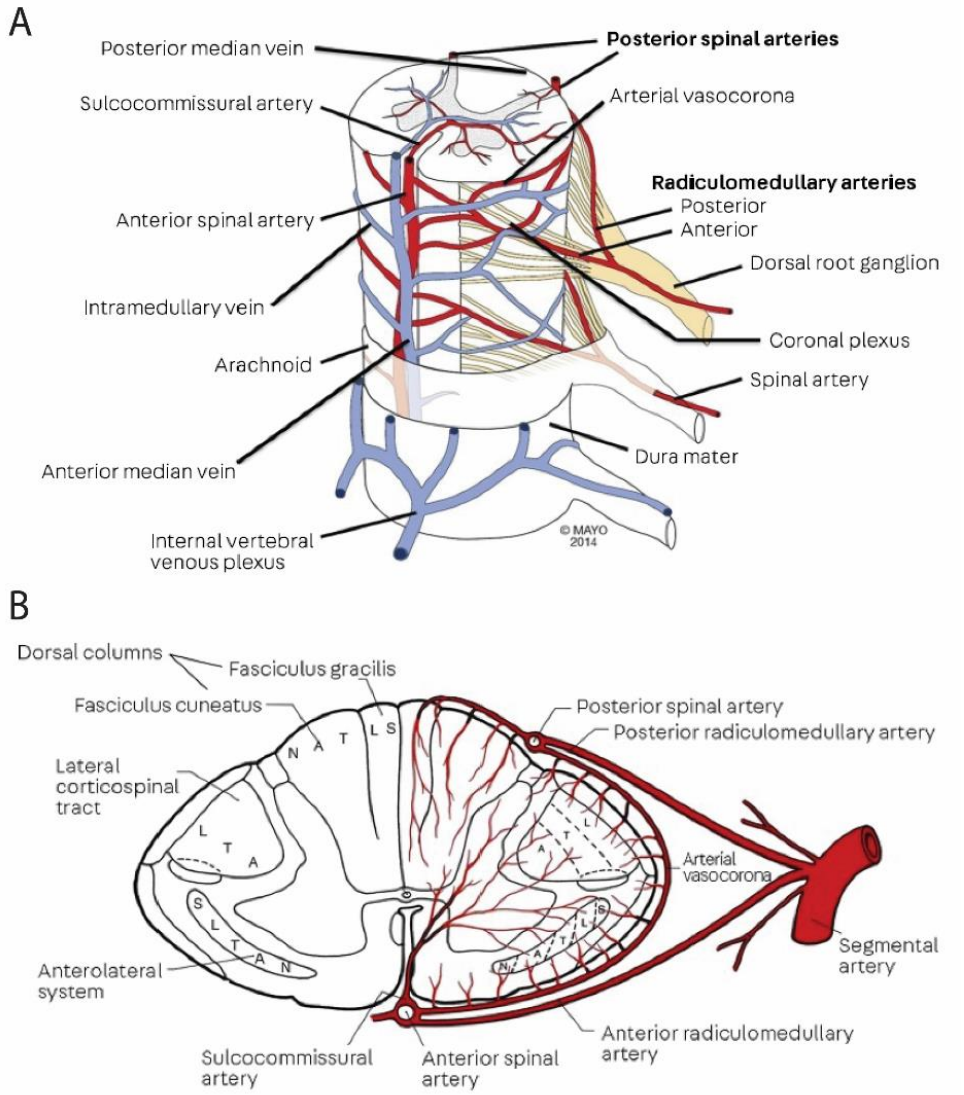

Figure 1.5 – Vascular organization of the spinal cord. **A**, the three-dimensional arterial and venous vascular anatomy of the spinal cord. **B,** cross-sectional depiction of the vascular perfusion within the spinal cord. The somatotopic arrangement of fibers within tracts is denoted by letters. **A:** arm; **L:** lumbar area; **Neck:** neck; **S:** sacral area; **T:** thoracic area. Adapted from 135.

1.7. Characterization of spinal cord injury and associated vascular damage

1.7.1. Incidence, management, and pathophysiology of spinal cord injury

According to the latest estimates, approximately 27 million individuals worldwide live with deficits provoked by SCI, accounting to an incidence of approximately 0.93 million cases per year (Figure 1.6) [141]. Generally, SCI results from traumatic events derived from falls and traffic incidents, with the particular exception of conflict zones where lesions are a consequence of physical violence or acts of terrorism [141]. Damage to the spinal cord can also be inflicted by non-traumatic events including cord infarction, spinal abscess, spinal canal stenosis or transverse myelitis [142]. Even though their management and care has

dramatically improved, patients with SCI continue to have superior mortality rates in comparison to uninjured individuals belonging to the same age group [143]. Additional factors associated to their lowered life expectancy are: 1) patient age; 2) the severity of the lesion (whether it is complete or partial); 3) higher injury levels (cervical injuries originate severe autonomic dysfunctions like breathing difficulties, cardiac dysrhythmias or hypotension whereas lumbar SCIs associate with the loss of bladder and bowel control and erectile dysfunction); 4) the existence of multiorgan damage associated to the lesion [144]. The devastating impairments experienced by SCI patients (where motor loss is perhaps the most visible one) have a profound impact on their day-to-day well-being. This inspires the extensive search for effective treatment options that restore some degree of functionally on the affected traits and enable this population to regain quality of life.

The last decades saw a clear deepening in comprehending the pathophysiology of SCI, unfortunately without the company of major breakthroughs regarding patient treatment, meaning that their clinical interventions remains mostly palliative. Following SCI the first interventions intend to immobilize the patient, preventing further damage to occur, being normally followed by the surgical stabilization and decompression of the spinal cord [145]. The rationale behind decompressing the injured spinal cord is to alleviate the mechanical compression of the tissue and restore its blood flow, thus stopping additional acute ischemic damage [146]. Another important aspect to control during this period is the arterial pressure of the patient, as hypotension is a commonly observed in SCI individuals and it can contribute to inadequate spinal cord perfusion and exacerbate the damage to the tissue [147].

To date there are no consensual therapeutic approaches to contain the progression of SCI and protect neuronal tissue from additional degradation. Nevertheless, promising preclinical data supported the study of the acute use of methylprednisolone sodium succinate in SCI patients in different clinical trials [148–151]. Methylprednisolone is a synthetic corticosteroid and a potent anti-inflammatory molecule that also inhibits lipid peroxidation, contributing to maintain the integrity of the BSCB and to prevent ischemia by enhancing spinal cord blood flow, thus acting as a neuroprotective agent [145]. The clinical data obtained encouraged a substantial number of clinicians to administer the drug within the first 8 hours following SCI [152]. This was supported by the fact that enrolled patients that started to receive a 24-hour infusion of high doses of methylprednisolone during the first 8 hours post-injury showed some degree of motor recovery [151,153]. The use of methylprednisolone remains controversial and a matter of extensive debate in the SCI community being mainly driven by the increased risk of adverse effects following its administration (gastrointestinal hemorrhages, sepsis, wound infections and pulmonary embolisms) which counterbalance its modest clinical gains [154]. The void that still exists regarding neuroprotective agents

motivates the ongoing search for such therapeutics. Therefore, different approaches that showed preclinical potential await total clinical validation, including the administration of riluzole or minocycline, hypothermia and stem cell therapy [154]. Following the acute phase of SCI the focus of caregivers is to handle patient spasticity, dysautonomia and neuropathic pain while executing bowel and bladder training programs and educating SCI patients to deal with these disabilities [145]. This is accompanied by physical therapy protocols that intend to induce plasticity in broken neuronal circuits by stimulating the affected limbs with repetitive movements and with it lead to some degree of motor recovery [155]. The pathophysiology of SCI can be divided into 4 distinct periods: acute (less than 48 hours following injury); subacute (48 hours to 14 days); intermediate (14 days to 6 months) and chronic (more than 6 months) (Figure 1.7) [144]. The traumatic event triggering spinal cord damage is commonly called primary injury and involves the compression of the tissue by dislocation of the vertebral column, causing either the compression or total transection of the spinal cord [145]. This is immediately followed by neuronal disruption, the breakdown of the BSCB and the appearance of micro-hemorrhages in the tissue within minutes, spinal cord swelling and ischemic damage [156]. The disruption of descending sympathetic tracts may lead to autonomic dysregulation and its manifestations include patient hypotension, bradycardia and temperature imbalances in what is commonly called neurogenic shock (occurs in lesions above T6 but mostly on cervical lesions) [157].

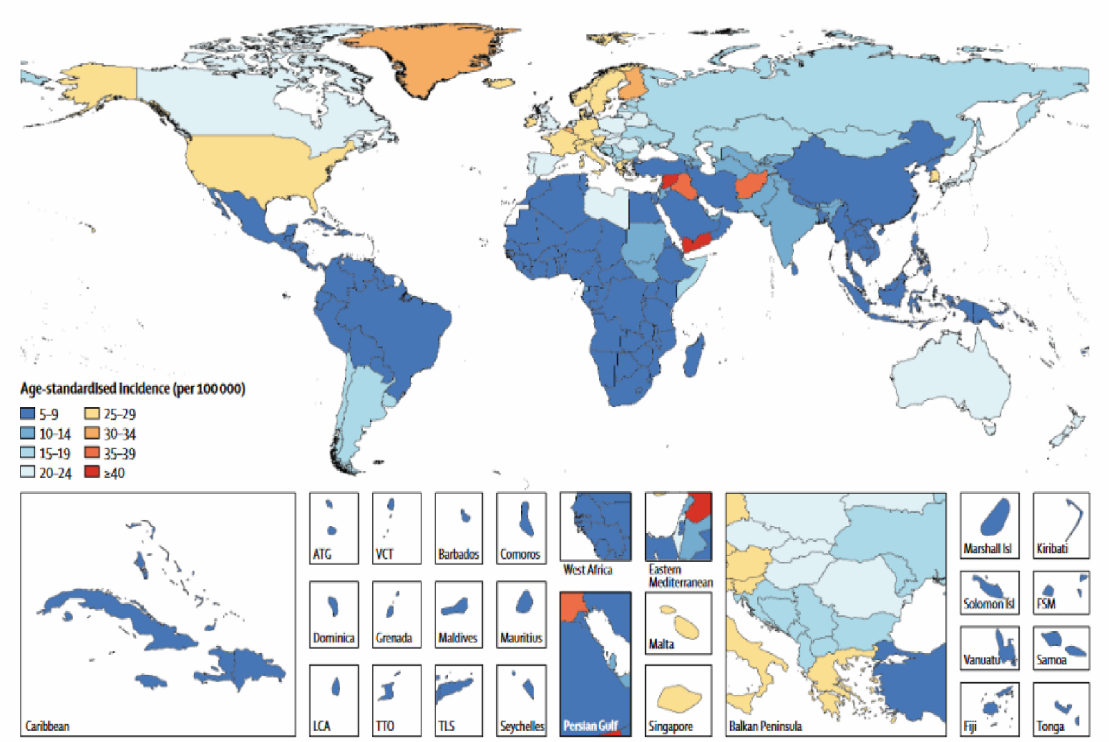

Figure 1.6 – The incidence of SCI per 100,000 people in 2006 by location and standardized to age. Adapted from 141.

These occurrences cause the initiation of a complex cascade of secondary events that last weeks until eventually the wound is closed and a glial scar is formed [127]. During this phase, spinal cord damage extends from the lesion epicenter originating the death of neuronal cells that may survived the initial traumatic event and the complication of the prognosis of SCI patients [158]. One of the most studied events associated with this phase of the condition is glutamatergic excitotoxicity, which occurs due to the release and accumulation of elevated quantities of the neurotransmitter from dying neurons and astrocytes [159]. These excessive amounts of glutamate lead to an uncontrolled influx of sodium (Na^+), potassium (K^+) and calcium (Ca^{2+}) into neuronal cells which provokes further cell death by ionic balance disruption and Ca^{2+}-mediated secondary messenger cascades [159–161]. Glutamate excitotoxicity is also involved in mitochondrial dysfunction during SCI [162]. This organelle acts as a Ca^{2+} scavenger and the accumulation of high concentrations in mitochondria during SCI opens the mitochondrial permeability transition pore which eventually leads to the cessation of ATP synthesis and consequently to cell death [163,164]. Loss of ATP synthesis inactivates ATP-dependent ionic pumps, thus additionally contributing to the ionic imbalance in cells following SCI [162]. Furthermore, mitochondrial dysfunction contributes to the increase of reactive oxygen species (ROS) in the injury milieu that will disrupt the cell membrane of neuronal cells by lipid peroxidation, cause DNA oxidative damage and protein oxidation, aggravating the damage triggered by the lesion [165–167].

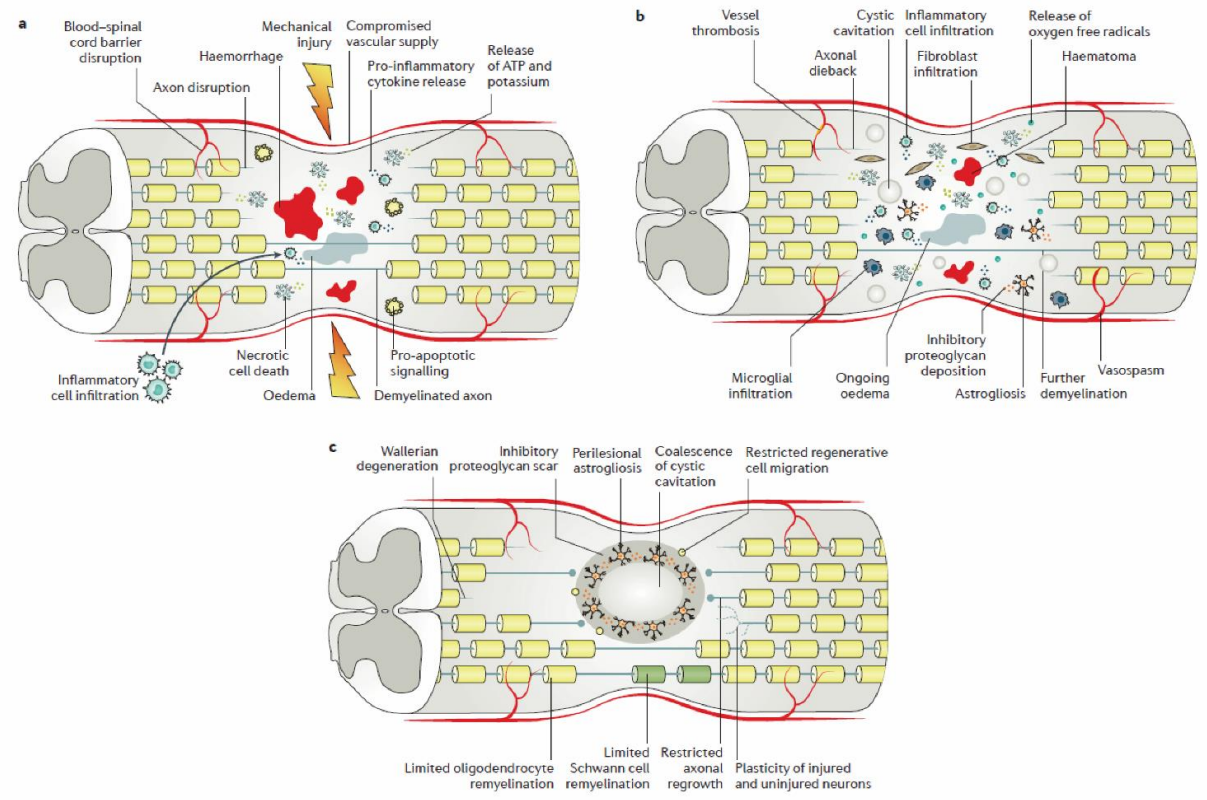

Figure 1.7 – Pathophysiology of traumatic SCI. **A,** the mechanical trauma initiates a secondary injury cascade during the acute phase (0-48 hours) that includes ischemia, inflammatory cell infiltration and the release of cytotoxic products that lead to cell death. **B,** During the subacute phase (2-4 days after injury) further ischemia (continuation) and persistent inflammatory cell infiltration occurs which increased cell death as well as the formation of microcavities and the disruption of the architecture of the spinal cord. Astrocytes begin to proliferate and deposit fibrotic ECM components. **C,** during the intermediate to chronic phases (2 weeks to 6 months) it exists an ongoing axonal degeneration and the glial scar matures, being a formidable barrier to axonal regeneration. Cystic cavities merge and further hamper axonal regrowth and cellular migration. **ECM:** Extracellular matrix. Adapted from 144.

The inflammatory response also plays a major role in the secondary injury, decisively contributing to the deleterious local environment. Inflammation is triggered when immune cells respond to danger-associated molecular patterns (DAMPs) and become reactive [168]. Alarmins are a type of DAMPs involved in SCI inflammation which are released from apoptotic and necrotic cells and include ATP, IL-1α, IL-33, tumor necrosis factor (TNF-α), histones or high-mobility group protein B1 (HMGB1) [169]. Microglia are the resident CNS immune cells and the first to respond to SCI and migrate towards the lesion site, becoming activated due to the interaction with alarmins [170]. The polarization of microglia towards the pro-inflammatory M1-like state contributes to increase the neuronal loss and astrogliosis as well as the inflammatory response by producing chemokines (e.g chemokine ligand 3 - CCL3), inducing the release of CCL2 from reactive

astrocytes or liberating ROS [171–173]. Activated microglia have also an important function in clearing neuronal cell debris but at the same time these cells can also phagocytose dendrites, playing a role in enhancing synaptic damage [174,175].

BSCB disruption exposes the spinal cord to the infiltration of circulating immune cells. Neutrophils are the first to arrive and infiltrate the injured spinal cord approximately 3-6 h following SCI in response to chemoattractant gradients, being mostly present in necrotic areas of the tissue [176]. They contribute to exponentiate the inflammatory response by releasing pro-inflammatory molecules and ROS that activate other immune and glial cells, increasing damage to the tissue [127,177,178]. Peripheric monocytes penetrate the tissue and differentiate mostly into the pro-inflammatory M1 phenotype 1 week following SCI, repeating the process approximately 60 days after the injury [179]. Apart from producing cytotoxic factors that enhance apoptosis, M1 macrophages promote axonal retraction and dieback by contacting with the dystrophic tips of axons in a process that seems to be mediated MMP-9 [180–182]. Macrophages migrate to the center and borders of the lesion, where similarly to microglia, phagocytose cell and tissue debris, being however more susceptible to cell death following after this process [174].

Adding to the extremely harsh environment that impairs neuronal survival and expands the initial damage to the spinal cord, several additional SCI and CNS traumatic hallmarks limit the regenerative capacity of surviving neurons and consequently the intrinsic capacity of recovery. The disruption of myelin sheaths following trauma originates proteic debris that are potent inhibitory cues for axonal growth, including Nogo-A, oligodendrocyte-myelin glycoprotein (OMgp) and myelin-associated glycoprotein (MAG) [183–185]. Upon binding to Nogo receptor 1 (Ngr1) and co-receptors, these inhibitory molecules induce the activation of the Rho/Rock signaling pathway which destabilizes the axonal cytoskeleton, leading to the collapse of the growth cone and translating into the impairment of axonal growth [186]. The upregulation of classical axonal repulsive molecules such as Slit2, SEMA4D and EphrinB3 after SCI complicates even more axonal regeneration in this context [187–189]. Regarding the modulation of myelin-associated debris, there is hope that an antibody targeting Nogo-A will achieve clinical translation and be integrated in SCI clinical practice [190]. The therapy has showed robust preclinical potential and is currently being evaluated in a multicentric Phase II clinical trial (NISCI, NCT03935321), following proving to be safe to administer to SCI patients and capable of reverting complete into incomplete lesions in some of the individuals [191–194].

Various types of cells in the injured milieu like activated microglia, astrocytes, oligodendrocyte precursors or macrophages deposit chondroitin sulfate proteoglycans (CSPGs) in the penumbra and core of the lesion [170]. CSPGs consist on a core protein with glycosaminoglycan side chains and are fundamental to suppress plasticity and stabilize neuronal circuits in normal conditions but prove detrimental to axonal

regeneration following SCI [195]. These components of the native CNS ECM inhibit axonal regeneration by activating the Rho/Rock pathway, inhibiting the Akt pathway and Erk1/2 phosphorylation [196,197]. The deposition of CSPGs is accompanied by the formation of a physical barrier surrounding the severely damaged area named glial scar. It is composed of reactive astrocytes, activated microglia and NG2^{+} oligodendrocyte precursors and serves as a barrier to axonal regeneration [198]. The glial scar formation begins to be formed in the subacute phase of SCI and maturates during the intermediate and chronic stages of the condition [199]. Within the glial scar there is a mixture of fibroblast, pericytes and macrophages that is characterized by the presence of a dense fibrotic ECM that also does not favor axonal growth, in what is usually referred as the fibrotic component of the glial scar [200–203]. In humans the glial scar encompasses an extracellular fluid-filled cystic cavity posing both a barrier to axonal growth and cellular migration that can develop into syringomyelia (a very large cyst spanning several segments of the spinal cord) [144].

There is an ongoing debate in the community whether the glial scar acts as a physical barrier to axonal regeneration or if it is a necessary process to contain the spreading of spinal cord damage. The former is supported by the already discussed inhibitory components of the glial scar and the fact that lower vertebrates, which maintain a formidable CNS regenerative capacity, do it without the necessity of forming such a structure [204]. Additionally, it is well established that contrarily to CNS, peripheral nervous system (PNS) nerves can regenerate and establish functional synapses [205]. This distinct behavior is thought to be in part mediated by decisive differences in their injury environment and is backed by the fact that PNS segments grafted to the CNS do not regenerate whereas CNS injured neurons use PNS tissue as bridges to elongate their axons [198,206,207]. Nevertheless, distinct different works have demonstrated over the years that the genetic ablation of reactive astrocytes or more recently STAT3 signaling astrocytes (a vital pathway for glial scar formation) does not benefit axonal regeneration or the SCI injury mileu [208–211]. Indeed, loss of these astrocytic populations and by inheritance of glial scar formation increases neuronal death, demyelination and the injury size, highlighting the role of the glial scar in containing the propagation of neurotoxins and inflammatory cells, thus protecting the healthy tissue [209–211]. Anderson *et al.* [208] demonstrated that the sustainable delivery of neurotrophic molecules induces higher axonal regrowth over scar-forming astrocytes than the same condition in animals lacking the expression of these cells. Thus, the authors theorized that it is not the glial scar by itself, but the lack of molecules that induce axonal growth, that block regeneration during the pathophysiology of SCI [208]. The same is possibly not true for the cellular components of the fibrotic scar. Recently Dias and colleagues have showed that inhibiting the proliferation of pericytes reduces the deposition of fibrotic tissue into the lesion core, originates the

growth of corticospinal tract axons that integrate into functional circuits, decreases inflammation and improves mice sensorimotor recovery [201].

A considerable body of research has been devoted to circumvent the repulsive action of CSPGs. These may involve: (1) their enzymatic degradation using Chondroitinase ABC [212,213]; (2) preventing their formation and deposition by genetic or molecular mechanisms [214,215]; (3) inhibiting their effect by targeting their signaling pathways or receptors [216,217]. Despite the promising preclinical results there is currently no such therapy being evaluated in human clinical trials, despite the promising results observed recently in a clinical trial enrolling SCI dogs receiving Chondroitinase ABC which may support its evaluation in humans [218].

Severed axons, once separated from their soma, begin to deteriorate immediately following SCI in a process denominated Wallerian Degeneration. This event is present during the entire pathophysiology of SCI and can destroy considerable parts of white matter tracts. Even the axons of surviving demyelinated neurons are susceptible to Wallerian Degeneration due to poor remyelination following SCI as consequence of failed oligodendrocyte maturation due to the nefarious local environment [219–221].

The incident triggering SCI is usually quite simple, a laceration or compression of the spinal cord following a traffic accident or fall, but the myriad of actions that follows it is rather complex, producing an overwhelming nefarious stimulus to the injured tissue. These events are sometimes redundant or provide just the right stimulus for others to escalate their damage potential, as this section intended to demonstrate. Even though the adult CNS reacts with some degree of plasticity following injury, the degree of recovery is unpredictable and depends on: 1) type and extent of lesion; 2) how fast the patient gets to the hospital; 3) general health condition of the patient prior to SCI; 4) genetic predisposal to recovery. Given these variables, nowadays the best therapeutic approaches are probably still to intervene in the acute phase of SCI to stop several injury cascades to escalade and produce profound harm to the spinal cord, hence protecting the tissue. Instantaneously after the primary injury the BSCB breaks and allows the beginning of the secondary injury. Given the importance of vessel disruption to initiate the pathophysiology of SCI, the next section will:

- characterize BSCB and spinal cord vessel disruption following SCI;
- detail its contribution to the progression of SCI;
- elaborate on the host endogenous attempts to regain vascular perfusion;
- advance the therapeutic opportunities that the modulation of the spinal cord vasculature offers to stop the progression of SCI.

1.7.2. Characterization of vascular damage associated to spinal cord injury

The protective and trophic function of the vascular network supplying the spinal cord, in which the BSCB is included, is compromised following the trauma that causes SCI. ECs immediately lose their tight junctions and glycocalyx (hence their structural integrity) which dictates an increase in vascular permeability and BSCB breakdown [127]. This originates tissue edema due to the unregulated influx of water and ions (also contributes do ionic imbalance) as well as severe intraparenchymal hemorrhage that starts on the grey matter and rapidly spreads to adjacent white matter [134]. The intramedullary bleeding can continue for days and evidence has showed that its extension across spinal cord tissue correlates with the area occupied by the cystic cavity [222–224]. Lack of blood flow to the injured spinal cord, vasospasms triggered by the release of platelet-derived factors, vasoconstriction by endothelin (ET) and vasogenic edema cause tissue ischemia which originates oxidative stress and contributes to necrotic cell death [225]. Recent data shows that hypoxia continues to be present during the chronic phase of SCI in the caudal part of the lesion, demonstrating that the injured tissue is not capable of regaining adequate perfusion [226]. The overstimulation of the sympathetic and its reflex parasympathetic system during the first minutes after SCI hemodynamically converts into acute hypertension and bradycardia or reflexive tachycardia [227]. Once this period ends the sympathetic activity dramatically decreases and patients suffering mostly high-level injuries enter in neurogenic shock due to unopposed parasympathetic stimulus through the vagus nerve (remains intact following SCI since it mostly follows a nonspinal route) [228,229]. Patients having injuries above T6 commonly experience orthostatic hypotension, reflex bradycardia, low resting blood pressure or loss of diurnal blood pressure fluctuation [227]. The severity of these events depends whether the descending sympathetic fibers are partially spared or not and so patients with complete injuries experience greater cardiovascular disturbances [230,231]. Additionally, the loss of autonomic control coupled with decrease blood flow to the inferior limbs and lack of muscle activity due to paralysis can also originate deep vein thrombosis, especially during the first 10 days following SCI [232,233]. This incident is capable to cause pulmonary embolism if the thrombi dislocates into the lungs, where it might cause pulmonary embolism and eventually lead to death [227].

Without a functional BSCB, peripheric pro-inflammatory mediators (TNF-α, IL-1 β, nitric oxide, MMP-9 or fibrinogen) are free to infiltrate the injury site where they contribute to enhance the secondary injury [234,235]. For instance, fibrinogen is essential to appropriate blood coagulation, and thus to contain the hemorrhagic damage associated to SCI [234]. However, fibrinogen also activates resident microglia and promotes astrogliosis, deleteriously contributing to the injury environment [236,237]. The disruption of the BSCB also alters the expression of different transport systems in which the TNF-α and leukemia inhibitory factor

(LIF) are included. The accumulation of TNF-α during the acute phase of SCI contributes to exacerbate inflammation, apoptotic neuronal death, astrocyte toxicity and myelin degradation [238]. Following SCI, LIF activates microglia acting as another agent that supports the inflammatory environment in the lesion site [239]. On the hand, this cytokine may have a beneficial action on oligodendrocytes since its administration to a SCI mice model prevented oligodendrocyte apoptosis, subsequently protecting surviving neurons from demyelination [240,241]. Fundamental to maintain the constant glucose supply to neurons, the presence of Glut-1 is also abolished in the injured spinal cord during the first two weeks and may contribute to metabolic imbalances in neuronal cells at least during this period [242]. The expression of the glucose transporter starts to be observed after two weeks and associates with blood vessels that are in close proximity to astrocytes [242]. However, it is still unknown whether the restoration of Glut-1 is sufficient to supply metabolic needs of surviving neurons in the perilesional area and whether possible glucose impairments are only observed in the lesion core or its proximity.

The absence of proper barrier function allows peripheric inflammatory cells to infiltrate the injured spinal cord without control, which, as already referred is a key event for the pathophysiology of SCI. To efficiently migrate to the injured spinal cord, inflammatory cells rely on a multitude of MMPs to degrade the basal lamina (in which tight junction proteins are included) of the remaining blood vessels [243]. Neutrophils are the first immune cells to arrive to the spinal cord and use MMP-3, MMP-8 and MMP-9 during the migratory process [244–247]. These MMPs are upregulated on neutrophils immediately following SCI and contribute to BSCB destruction, inflammatory cell migration and increased vascular permeability. Likewise, blood-born macrophages use MMP-12 to disrupt the basement membrane of spinal cord ECs further contributing to increase BSCB compromise [248]. Nevertheless, it must be mentioned that not all classes of MMPs prove to be deleterious during SCI. For instance, MMP-2 participates in the wound healing phase of the condition where it can degrade specific CSPGs [249]. The loss of MMP-2 expression leads to a more extensive glial scar, reduces white matter sparing and aggravates motor function [249]. Furthermore, this MMP is also implicated in vascular remodeling following SCI since its depletion decreases EC proliferation during the first two weeks following SCI and originates a significant vascular decline 21 days post-injury [250]. Mechanistically, MMP-2 may act by activating integrin αvβ3 (an integrin deeply involved in angiogenesis) to induce EC proliferation and not by facilitating cellular migration and matrix remodeling [250]. The knockout of MMP-2 is compensated by the upregulation of MMP-9 that transiently supports angiogenesis in the initial stages of SCI, but leads to vascular regression if its expression remains elevated in the injured spinal cord [250].

The Angiopoietin (Ang) family of growth factors, especially Ang-1 and Ang-2, is also differentially expressed in the vasculature of the spinal cord during SCI [251–253]. Both proteins have equal affinity towards the Tie2 receptor, where they exert antagonistic effects. The expression of Ang-1 is markedly decreased during SCI, meaning that its function of suppressing vascular leakage and inducing vessel maturation is compromised, contributing to the severe vascular dysfunction observed [251,252]. On the other hand, it was showed that Ang-2 is persistently upregulated during SCI, where its role in maintaining vascular permeability or as a stimulus to the compensatory angiogenic response is still to be totally clarified [253,254]. Neutrophil elastase is a proteolytic enzyme secreted by neutrophils in response to pro-inflammatory stimulus and a molecular player that affects the expression of Ang-1, contributing to the disruption of the BSCB and its persistent permeability increase in SCI [255].

Increased vascular permeability is further induced by alterations in vasoactive molecules like ETs. ETs are a type of peptides whose synthesis is enhanced following CNS injury. McKenzie and coworkers [256] implicated ET-1 as a participant in enhancing vascular permeability following SCI by showing that the expression of the peptide was increased in spinal cord regions where there were signs of clear barrier disruption [256]. ET-1 produces long periods of vasospasms following CNS vascular damage which results in neuronal ischemic damage and disruption of the blood brain barrier, being speculated that this is the mechanism by which the peptide contributes to the pathophysiology of SCI [134,257]. This hypothesis was further supported by the generation of ROS and consequent associated damage following the intrathecal administration of ET-1 in a model of brain injury [258]. Additional molecular players that are thought to contribute to BSCB permeability during SCI are arachidonic acid, nitric oxide, kinins, leukotrienes, histamine, opioids or serotonin [128].

Whether the vascular permeability following SCI reduces to the point where it allows to conveniently reestablish the BSCB is still an open question. Studies addressing this issue generally report a decrease on permeability along time but its progression varies depending on the method the authors use to assess it [259]. Noble and Wrathall used horseradish peroxidase to characterize BSCB permeability following mild, moderate and severe contusive SCI [224]. The authors concluded that the leakage was maximum 3h to 24h after injury and the permeability was gradually restored until 14 days following the event [224]. Furthermore, the study also demonstrated that protein extravasation is proportional to the severity of SCI in a clear indication that the degree of vascular disruption is coupled to the initial trauma, with a marked contribution to spinal cord damage [224]. The same temporal dynamics regarding BSCB permeability was observed by Figley *et al.* using Evans Blue [260]. Another work using [^{14}C]-α-aminoisobutyric acid to assess this parameter showed that increases in vascular permeability are not only restricted to the lesion epicenter but also

observed in rostral and caudal areas (approximately 3 cms in each direction) [261]. Regarding the progression of BSCB permeability after injury, Popovich and coworkers demonstrated that its maximum is observed during the first days for gray matter, a secondary wave of largely enhanced permeability is observed in matter tracts between two to four weeks subsequent to SCI [261]. However, a study employing magnetic resonance imaging (MRI) determined that the permeability of the BSCB remains elevated even 8 weeks after injury, opening the possibility that the window of time where peripheric elements can contribute to the aggravation of SCI is larger than initially thought [262]. The answer to this question remains to be totally addressed as there is a lack exhaustive studies demonstrating how different neurotoxic molecules or even inflammatory cells are affected by the endogenous attempts to restore permeability. The temporal dynamics regarding the reestablishment (or not) of different BSCB transporters or tight junctions would also be a decisive contribution to the field. Nevertheless, only after a careful modulation of the BSCB permeability in injuries at different levels of the spinal and at different stages of the condition would enlighten the full potential of such therapies to protect the tissue and enable functional ameliorations.

Similarly to the endogenous response that attempts to recover the permeability of the BSCB, the vascular milieu of the spinal cord also tries to respond to the loss of vasculature due to SCI. Vascular remodeling starts three to four days following injury through angiogenesis, continuing up to one week, where the maximum blood vessel density in the lesioned area is observed [260,263–265]. However, the rate of vascular recovery differs between studies. Dray and coworkers [265] reported a 540% vessel density increase in SCI animals in comparison to healthy controls during this period, whereas Whetstone *et al.,* reported a return to basal levels in the same timepoint [242]. Following this phase of vigorous angiogenesis, the vast majority of the newly formed blood vessels is pruned and only a few stable remain directed towards the lesion [265]. However, most of these blood vessels do not contact with neurons, astrocytes or pericytes in a clear indication of neurovascular disruption following lesion [200,263]. Additionally, pericytes enwrapped around spinal cord capillaries are overactivated and constrict blood vessels following SCI, making the caudal area of the lesion in a constant state of hypoxia during the chronic phase of the condition [226]. This happens because pericytes ectopically express L-amino acid decarboxylase which lead to the synthesis of trace amines that abnormally activate pericytic monoamine receptors, hence contracting these cells and consequently associated capillaries [226]. Furthermore, following SCI pericytes seem to swell and increase the area of endothelial coverage in what might be a compensatory mechanism to counteract increased BSCB permeability, according to a recent report by Xu and colleagues [266]. These authors also found increased quantities of caveolae and vacuoles inside ECs of lesioned animals, which probably contribute

to increased BSCB permeability and/or function as an adaptation that grants the transportation of biomolecules in the absence of proper barrier carriers [266].

SCI originates epigenetic alterations in local ECs that alter their functioning and compromise the observed vascular response [267]. One of the consequences of these changes involves the upregulation of molecules that are deleterious to their EC survival, including thrombospondin 1 and proapoptotic signals like caspase-3, caspase-6 and RhoB [268]. The aberrant function of ECs in the SCI milieu is also manifested by their capacity to act as amateur myelin phagocytes [269]. Even though myelin debris are axonal growth repellents, as briefly discussed, their engulfment by ECs triggers an endothelial-to-mesenchymal transition that makes these cells promote inflammation by signaling the recruitment of macrophages and depositing fibrotic components of the glial scar [269]. It seems now clear that SCI instigates different phenotypic changes in ECs belonging to the injury environment that contribute to the harsh local environment. The impact of such changes in the pathophysiology of SCI needs to continue to be characterized to fully comprehend its extension and how the modulation of endothelial function can contribute to the development of more holistic treatments against the condition.

As detailed in the first section, the CNS and the vascular system share signaling cues which help to pattern them in an intimacy that surely is not driven by chance and where ECs aid the guidance of axons to their final destinations. Therefore, a therapy aiming to protect and enhance the vasculature of the spinal cord following injury may indeed contribute to promote axonal growth and guidance, reshaping neuronal circuits and reinstating their functionality. Dray and colleagues [270] reported that attempts of axonal growth following SCI privilege axons which are in close proximity to blood vessels, clearly demonstrating the inseparable interaction of both systems even following CNS trauma. Interestingly, the study also showed that the rate of axonal sprouts following blood vessels correlated with the endogenous angiogenic response to vascular disruption following SCI (grew from 3 up until day 7/8 and then decreased until day 15) [270]. However, the axonal guidance properties of blood vessels on these conditions were less clear as the authors observed that some of the axonal sprouts were actually guided across the lesion site, whereas others grew away from the injury epicenter [270]. It is worth noting that this is an observational study where no clinical intervention was attempted, and one may ask: (1) how the guidance of growing axons is affected by an angiogenic response that allows to recover convenient perfusion? (2) how the conservation of endothelial phenotype affects the growth and guidance of axons and ultimately sensory, autonomic, and motor function? (3) do such interventions contribute to restore appropriate neurovascular coupling? (4) if so, what kind of metabolic shifts neurons experience and how these contribute to stimulate regeneration? (5) how does the inflammatory response following SCI gets affected

by vascular modulation? These are some of the questions that will be partially answered in the next section where approaches that regulate spinal cord vasculature following injury, as well as their contribution to functional recovery, will be detailed. The detailed list of works modulating SCI vasculature is found on Table 1.1.

The present section aimed to describe what is known about the impact vascular disruption has on the onset of SCI, as well as its contribution to the severity of the condition and the inhibitory environment for regeneration found on the tissue. Being present since the infliction of the initial trauma, and actually taking part in some of the key hallmarks of the condition including tissue hemorrhage and edema, hypoxia, free radical formation, metabolic imbalances, infiltration of inflammatory cells and blood-derived neurotoxic molecules, attests the importance of the event to the pathophysiology of SCI. Moreover, the implications of vascular loss are not restricted to the acute phase of the condition since the angiogenic response and the recovery of BSCB is inefficient and affects neuronal homeostasis across the different phases of SCI, as described.

1.8. Modulation of the spinal cord vasculature to achieve functional recovery after spinal cord injury

1.8.1. Administration of angiotrophic factors and other therapeutic agents

The central role of vascular damage and BSCB loss in triggering the secondary cascade of damage following SCI raises the hypothesis that protecting the spinal cord vasculature and/or even stimulating angiogenesis after injury might be an attractive option to avoid further damage to the tissue. Moreover, as already mentioned, the benefits of such approaches might even enhance axonal regeneration through the trophic support and the scaffolding effect blood vessels exert on neurons and their axons. Indeed different SCI therapeutic approaches have linked functional ameliorations with increased angiogenesis and preserved vascular and BSCB integrity [271–277]. Kaneko *et al.* [271], gave a clear indication on the potential of using shared neuronal and vascular signaling cues to simultaneously stimulate neuronal regeneration and angiogenesis for SCI treatment. The authors inhibited the axonal and vascular growth repellent SEMA3A in transected rats, detailing that its neutralization increased angiogenesis, neuronal regeneration and myelination leading to enhanced motor recovery [271]. In line with this, one can speculate whether the promising results obtained with the anti-Nogo A immunotherapy in SCI patients also result from its boosting effect on the vasculature of the spinal cord, similarly to what was depicted in the brain [65,66]. This is an open question that needs to be answered to give a more comprehensive view on the mode of action of this therapy. Eventually it may originate further refinements on the application of the anti-Nogo A

antibody and conduce to better clinical outcomes concerning individuals with SCI, while further elucidating the role of revascularization on post-SCI outcome.

The previous section also elucidated that not only the lesion environment is deleterious to the vascular response following SCI, but also the angiotrophic molecules are unregulated and unable to create a permissive environment for proper angiogenesis and vascular stabilization. Therefore, an active line of research studies the possible administration of angiotrophic factors to stimulate angiogenesis after SCI and its impact on recovery [278–285].

Given the hopes around the application of VEGF in vascular therapies it is natural that this growth factor remains the most applied in SCI under the same context. The results have been ambiguous given that some studies reported a protective effect of the local administration of VEGF on the vasculature of the spinal cord following injury that originated some degree of motor recovery [278,286] whereas Benton *et al.*, demonstrated a negative on the pathophysiology of SCI [287]. It has to be highlighted that one of the potential drawbacks of using VEGF as a therapeutic agent for SCI lies on its action on vascular permeability (something corroborated by different experimental approaches) [287,288]. According to the current evidence, the use of VEGF for SCI treatment must be carefully considered due to its action on vascular permeability, which by itself may exacerbate associated secondary damage. Furthermore, dose, method of administration, which isoform to use and duration of the treatment has to investigated and optimized [289]. An appropriate manner to circumvent the exacerbated BSCB permeability associated to VEGF is to co-deliver it with growth factors that promote vascular stability [252,290]. In line with this, the sustained delivery of Ang-1 to VEGF through adeno-associated virus (AAV) was explored and granted vascular stabilization which was accompanied by the reduction on lesion volume and functionally translated into some improvement in the locomotor behavior [252]. Apart from its function in reducing vascular permeability, Ang-1 contributes to the stabilization and maturation of blood vessels during the final phases of angiogenesis, and so it acts as a vasoprotective molecule in the context of SCI [280,291]. When combined with a laminin-based mimetic possessing increased affinity to $\alpha v\beta 3$ or $\alpha 5\beta 1$ integrins (mainly present in ECs), the therapy originated a robust locomotor recovery in a SCI mice model [280]. Interestingly, the authors showed that the vascularization near the injury site directly correlated with the amount of epicenter white matter and the functional gains obtained, especially during the first week after injury infliction. This study also elegantly showed how the modulation of vascular permeability can influence the infiltration of inflammatory cells by clearly showing reduced numbers of leukocytes in spinal cord tissue as early as 24h after lesion, which continued until the end of the experiment (42 days) [280].

The modulation of endogenous MMPs that actively participate in the disruption of the BSCB also provides a relevant therapeutic target to avoid part of the vascular damage associated to SCI. Thus, the knockout of MMP-3, MMP-9 and MMP-12 in SCI animal models decreased BSCB permeability and the penetration of inflammatory cells into the injured tissue, helping to contain the secondary injury cascade of events [244–246,248]. The same was observed by directly inhibiting MMP-8 immediately after SCI, or indirectly by preventing neutrophil migration with a neutrophil elastase inhibitor [247]. This work additionally demonstrated that the inhibition of MMP-8 decreased inflammatory markers like TNF-α and inducible nitric oxide synthase (iNOS) and increased the expression of TJs in the affected spinal cord vasculature. A different experimental work revealed that inhibiting neutrophil elastase resulted in the upregulation of Ang-1 following SCI which protected TJs from degradation and decreased different inflammation markers (IL-1β, iNOS, TNF-α) [255]. The modulation of the injury environment reduced microglial and macrophage activation, impeding the spinal cord tissue from degradation, and contributing to significant motor improvements.

Ni *et al.*, found that following SCI there is a marked upregulation of the Ubiquitously Transcribed tetratricopeptide repeat on chromosome X (UTX) in local ECs, which originates epigenetic changes that inhibit angiogenesis through the expression of microRNA 24 (miR-24) [267]. By abolishing the expression of UTX in ECs the authors reduced the expression of miR-24 and were able to enhance angiogenesis and promote long term vascular gains in the epicenter of the lesion. Moreover, the sole prevention of this epigenetic alteration in ECs lead to significant gains of motor function (confirmed by a recovery on motor evoked potentials) as well as to better sensory outcomes. The study found changes of other epigenetic regulators, but these were transient and not consistent across the analyzed different timepoints [267]. Nevertheless, the study of the impact that these alterations have on the faulting vascularization following SCI, and how their modulation may circumvent it and allow better functional outcomes is a relevant question that remains to be answered. MiR-126 is highly present in ECs where it governs the response of these cells to VEGF by repressing its negative regulators [292]. Stimulating the expression of miR-126, which is naturally decreased following SCI, resulted in increased angiogenesis, reduced the influx of inflammatory cells by probably increasing BSCB permeability, lead to white matter sparing and promoted robust motor recovery [279]. The study also found that the treatment lead to the increased activation of ERK and AKT, two pathways that are activated by VEGF to promote angiogenesis, that might be the key effectors of miR-126 on this biological phenomenon. Whether miR-126 acts solely on ECs or its promising effects come from the modulation of other cell types and SCI events is still to be investigated.

1.8.2. Cell transplantation to promote spinal cord injury vascularization

The transplantation of cells or tissue grafts to overcome the limited ability of the CNS to regenerate is a concept that dates from the first part of the XX century when Jorge Francisco Tello (a pupil of Ramon y Cajal) observed the growth of retinal axons into peripheral nerve tissue transplanted onto severed optical nerves [293]. This observation made scientists speculate that the inability of the CNS to properly regenerate comes from the inhibitory environment formed following damage and not from its intrinsic lack of capacity to do so. The use of similar approaches, where peripheral nerves were grafted onto different zones of the spinal cord and the medulla oblongata, originated the robust growth of spinal axons into the PNS grafts and help to establish the use of tissue or cell transplantation as a possible therapy against CNS damage [207,294].

Neural stem cells and their capacity to differentiate into the three neuronal lineages gave researchers further tools to develop effective therapies by replacing lost neuronal cells and tissue [295,296]. Therefore, it enabled the use of embryonic CNS tissue or cells, which although remains controversial, represents a better alternative to the not only highly invasive isolation but also limited repairing capacity of their adult counterparts [297]. Pioneering studies have showed the feasibility and safety of such methodologies to replace lost or damaged neuronal tissue, paving the way for this field of research [298,299]. Regarding SCI, the first studies in animal models demonstrated that fetal spinal grafts supported the growth of host axons across the newborn tissue and promoted the communication between the graft and the native tissue, as well as its integration [300]. Similarly to the first approaches on adult brain pathologies, the grafting of fetal spinal cord tissue has proven to be both feasible and safe in humans with SCI [301]. The regulatory reluctance regarding these therapeutic approaches, which makes it difficult to access and study human fetal or embryonic tissue due to ethical concerns, has probably delayed understanding their full translational capability. However, the finding of the Yamanaka Factors (Sox2, c-Myc, Klf4, Oct3/4) in 2006, a cocktail of transcriptional factors that enable the reversion of virtually every cell to the state of pluripotency [coined as induced pluripotent stem cell (iPSC)] overcame the aforementioned reservations and provided a fundamental boost for stem cell therapy [302]. This means that one can easily collect a skin sample from a patient and through the transient induction of the expression of the Yamanaka Factors revert those cells to the state of pluripotency. Preclinical evidence in SCI animal models revealed the iPSCs are safe to use, not causing the formation of teratomas [303]. Furthermore, the transplants gave interesting indications regarding their capacity of differentiating into the three distinct neuronal populations, host integration and synapse formation and axonal regrowth [303–305]. These results opened the opportunity to evaluate the transplantation human-derived iPSCs in a Phase I clinical trial in SCI patients [306]. The candidates for cell-

based SCI therapies do not run out on fetal and embryonic grafts nor on iPSCs and include NPCs [307,308], OPCs [309,310], endothelial progenitor cells (EPCs) [311,312] MSCs [274,313]. The majority of the referred cell types have been or will be evaluated in clinical trials for SCI treatment, but to date none of these has the approval from major regulatory agencies like the Food and Drug Administration (FDA) or the European Medicines Agency (EMA) for clinical use [314].

The use of cell therapy to promote SCI vascularization has been centered on the use of EPCs, and MSCs. The obtained results will be detailed on the next subsections and are summarized in Table 1.1.

Table 1.1 – Spinal cord injury interventions that traduced into vascular gains and enable gains of function.

	SPECIE	MODEL	THER. FACTORS	DELIVERY METHOD	MAJOR RESULTS	REF
DELIVERY OF SOLUBLE FACTORS	Rat	T8 contusion	Antagomir-223	Intrathecal administration	Increased expression of CD31 and microvascular density; decreased expression of apoptotic proteins; enhanced hindlimb motor function.	507
	Rat	T9/T10 contusion	Agomir-126	Intrathecal administration	Upregulated VCAM1 expression and angiogenesis; inhibited leukocyte extravasation; decreased inflammation; tissue sparing.	279
	Mouse	T9 contusion	Ang-1 and KAFDITYVRLKF (C16 peptide)	Intravenous injection	Preserved epicenter vessels and white matter; prevented the exacerbation of inflammation; significant motor improvements.	280
	Rat	T9 contusion	VEGF	Injected into the lesioned area	Promoted higher blood vessel density; Decreased apoptosis; Improved motor function.	278
	Rat	T10 compression	MMP-8I	Intravenous injection	Increased tight junction expression; decreased inflammatory markers; reduced vascular permeability.	247
	Rat	C7-T1 compression	hIgG	Intravenous administration	Increased tight junction expression and vascular integrity; protected spinal cord vasculature; enhanced functional blood flow; promoted tissue preservation; Increased motor recovery.	276
	Mouse	T10 contusion	Pericyte exosomes	Intravenous injection	Improved blood flow regulation and tissue oxygenation; protected BSCB and upregulated tight junction proteins; decreased tissue edema; Enhanced motor behavior	508
	Rat	T7 compression	Chondroitinase ABC + PDGF-AA + bFGF + EGF	Intrathecal delivery	Promoted the proliferation of endothelial cells; Inhibited the proliferation of macrophages/microglia; guided the differentiation of endogenous spinal NPCs into oligodendrocytes	509
	Rat	T10 compression	Sivelestat sodium	Intraperitoneal administration	Prevented tight junction degradation and enhanced Ang-1 expression; Promoted blood vessel formation; Reduced glial scar; Lead to hindlimb motor recovery.	255
CELL TRANSPLANTATION	Rat	T9 contusion	BM-MSCs	Intravenous injection	Decreased BSCB leakage; Improved locomotion; Enhanced EC marker expression	363
	Rat	C7-T1 contusion	Brain stromal cells	Intraspinal delivery	Less lesion volume, BSCB permeability and hemorrhage. Induced IL-10 upregulation. Improved functional recovery	274
	Mouse	T10 compression	Bone Marrow-derived EPCs	Intravenous delivery	Enhanced neovascularization and astrogliosis.	311
	Rat	C7-T1 compression	First-trimester HUPVCs/ term-birth HUPVCs or BM-MSCs	Intravenous infusion	First-trimester HUPVCs increased grip strength; Cell infusions reduced glial scar; Increased myelin, axonal and vascular densities.	277

(Continues)

NANOPARTICLE DELIVERY AND SOLE BIOMATERIAL IMPLANTATION	Rat	T9-10 hemisection	PLG bridges delivering VEGF and FGF-2	Spinal cord implantation	Enhanced EC infiltration and blood vessel formation; Bridges were substrates for axonal infiltration.	[282]
	Rat	T9 transection	PLGA Nanospheres modified with 3β-[N-(N',N'- Dimethylaminoethane) Carbamoyl] Cholesterol encompassing the VEGF gene	Local implantation	Better motor outcomes than SCI animals; Induced axonal regeneration and increased local angiogenesis.	[510]
	Rat	T9-10 hemisection	Alginate hydrogels supplemented with fibrinogen and encapsulating VEGF	Intraspinal injection	Induced neuronal fiber growth and angiogenesis; Permeated EC infiltration.	[284]
	Rat	T9 contusion	PLGA microspheres containing Ang-1, bFGF and VEGF	Lesion epicenter	Enhanced spinal vascular repopulation and axonal growth; Prevented oligodendrocyte death; Significant motor recovery.	[285]
	Rat	C6 hemisection	Graphene oxide porous scaffold	Implanted in the spinal cord	Supported vascular infiltration, coincidently with regenerating axons; Increased angiogenesis; Induced a pro-regenerative macrophage phenotype.	[511]
	Rat	C6 hemisection	Graphene oxide scaffold	Local implantation	Elicited vascular colonization; Promoted axonal elongation and increased myelination in excitatory neurons; Reduced perilesional damage.	[460]
BIOMATERIAL CELL-BASED THERAPIES	Rat	T10-11 transection	Gelatin sponge within a thin PLGA film encapsulating BM-MSCs	Spinal cord implantation	Promoted neovascularization of the injury environment; Reduced lesion cavity; Weakened inflammation.	[447]
	Rat	T9-10 hemisection	PLGA encapsulating adipose tissue ECs and NPCs	Local implantation	Fourfold increased on functional vessels; Enhanced expression of BSCG makes; Increased axonal regeneration	[323]
	Rat	T9-10 hemisection	PLGA encapsulating BM-MSCs	Lesion epicenter	Improved both motor and sensory phenotypes; Transplanted MSCs promoted angiogenesis, modulated inflammation, and had a neurotrophic action; Reestablished lumbar motor circuitry.	[275]
	Rat	T9 hemisection	Prevascularized nerve conduit based on MSC cell sheets	Spinal cord implantation	Attenuated glial scar formation and increased the intensity of axonal fibers; Better motor outcomes.	[512]
	Rat	C5 contusion	RADA-16 SAP containing cerebral microvascular ECs	Local implantation	Reduced inflammation and glial scar formation; Enhanced neuronal density across the lesioned site.	[456]
	Rat	T10 transection	PLGA/PLLA scaffold with dental pulp MSCs and HAMECs	Spinal cord implantation	Promoted SCI revascularization, especially in sensory areas; Increased axon regeneration and myelination; Lead to sensory recovery.	[457]
	Mouse	T9 hemisection	Silk fibroin scaffolds conjugated with ADAMTS13-expressing HUVECs	Local implantation	Fomented vascular infiltration and the formation of microvascular assemblies; Increased presence of neurons; Better motor outcomes.	[513]

1.8.3. Endothelial progenitor cells

EPCs were firstly identified in 1997 by Asahara and colleagues as a population of putative endothelial progenitors with the capacity to differentiate into ECs and promote angiogenesis and vasculogenesis [315]. Their clinical relevance became apparent in 2003 when a study in the New England Journal of Medicine suggested that their circulating numbers could be used as a biological marker for cardiovascular disease, something still being studied and debated [316–318]. Despite the ongoing debates concerning their identity and functions during vascular repair, the capacity of EPCs to differentiate, integrate and produce new vascular structures have caught the eye of researchers from the regenerative medicine field [319]. Therefore, their therapeutic application in cardiovascular and ischemic conditions has being the object of study during the last few years [320].

Following SCI there is an increase in circulating EPCs, peaking three days after the event, which migrate into the lesioned tissue and have an active role in the vascular response to the injury [311,321]. Regarding their therapeutical application in SCI, the current results are restricted to animal models of the condition [311,322,323]. The intravenous injection of EPCs into SCI mouse animal models allowed to observe the recruitment of the transplanted cells to the lesion site where they contributed to neovascularization, astrogliosis and functional recovery [311]. The study also demonstrated that the effect of EPCs on astrogliosis is mediated by the Jagged1-Notch signaling pathway, since the deletion of the Jagged1 gene in EPCs abolished the effect of the cells on astrogliosis [322]. This signaling pathway has been previously implicated on defining the fate of endogenous spinal cord NSCs towards the astrocytic and not the neuronal lineage following lesion [324]. Furthermore, deletion of Jagged1 dramatically decreased the integration of transplanted EPCs into the vascular niche of the lesion site and contributed to the formation of abnormal vessels that resemble the phenotype of leaky vessels appearing in CNS pathologies [322]. The latter is probably a reflection of the reduced astrogliosis in knockout mice, since as already mentioned, these are required to maintain CNS vessels in a healthy and stable phenotype. The reports detailing the use of EPCs to promote SCI vascularization are still scarce, but the reported results instigate to continue to investigate their therapeutic potential. Studies detailing their impact on the infiltration of inflammatory cells as well as understanding whether EPCs show the hallmarks of CNS endothelium are interesting questions to pursue.

1.8.4. Mesenchymal stem cells

The discovery of MSCs is credited to Friedenstein and his collaborators when in 1966 they observed that a minor subset of cells from the bone marrow demonstrated osteogenic capacity following ectopic transplantation [325]. MSCs were distinguishable from other bone marrow cells by their capacity to quickly

adhere to plastic, presenting a fibroblast-like shape and generating single-cell derived colonies [326]. The term "mesenchymal stem cell" was firstly applied by Caplan in 1991 to reflect their multipotent nature, something that was confirmed later on [327,328]. However, the lack of consensus regarding whether they fulfil all the requirements to be classified as a stem cell (concretely their self-renewal and *in vivo* differentiation capacity) originated the alteration of their domination to "mesenchymal stromal cells" [329]. Despite this continuous discussion, the characteristics that a cell must present to be classified has a MSC are rigorously defined. According to the International Society for Cellular Therapy MSCs have to mandatorily: 1) adhere to plastic; 2) express the surface markers cluster of differentiation (CD) 105, CD73 and CD90; 3) lack the expression of CD45, CD34, CD14 or CD11b, CD79-α or CD19 and human leukocyte antigen DR isotype (HLA-DR); 4) be able to differentiate *in vitro* into osteoblasts, adipocytes and chondroblasts [330]. Numerous tissues have cells that satisfy the requirements to be classified as MSCs, including adipose tissue, umbilical cord, dental pulp, amniotic fluid and endometrium [331]. The therapeutic application of MSCs possesses several advantages in comparison to other cell types since these can be isolated in a minimally invasive manner (sometimes from surgical leftovers like adipose tissue or umbilical cord), are easy to culture *in vitro*, have high proliferative rates, show minimal signs of senescence along accumulated passages and do not elicit a host immune response as MSCs lack the expression of major histocompatibility complex II (MHC II) markers [329,332,333].

Due to their capacity to differentiate into distinct types of cells *in vitro* the initial rationale of using MSCs was to replace injured tissue [334]. However, as the understanding of their biology evolved it became evident that their therapeutic spectrum was broader, and in fact nowadays it is well established that MSCs can promote tissue regeneration by modulating the local environment instead of differentiating into a specific type of cell [335,336]. The mechanisms by which MSCs contribute to ameliorate the local environment involve its immunomodulation into a pro-regenerative phenotype, the secretion of molecules and vesicles (the secretome) that promote tissue repair and the recruitment of endogenous MSCs to the injury site [327].

These properties have put MSCs in the forefront for regenerative medicine applications. and according to clinicaltrials.gov this has translated into 1125 ongoing or terminated clinical trials for conditions ranging from Crohn's Disease to Covid-19. The same source documents the existence of 34 clinical trials on SCI patients. The first therapeutic approval for the use of MSCs for SCI treatment was accomplished in Japan at the end 2018, but scientists have raised concerns as the clinical trial supporting the approval lacked a control group, a small number of patients (13) and the data remains unpublished [337]. Nevertheless, the evaluation of distinct MSC therapies in humans was only possible due to the large body of evidence collected from their administration to SCI animal models [338]. In these studies the cells proved to be safe

to administer, while exerting immunomodulatory and neurotrophic effects that protect spinal cord tissue from further degradation and enhance axonal regeneration, eventually leading to some degree of functional recovery [313,339–344]. Despite this, more clinical evidence is needed to robustly show the safety and therapeutic impact of MSCs in the sensory, motor, and autonomic functionalities of SCI patients before thinking on the widespread approval of such therapies. Some of the concerns are related with their possible tumorigenicity by either differentiating or secreting growth factors that may promote the growth of tumor cells [334]. Additional translation bottlenecks involve: 1) creating standardized procedures to isolate, culture and conveniently store different populations of MSCs before clinical use; 2) understand the genetical, epigenetic and phenotypic differences of distinct populations of MSCs and according to it choose the appropriate source to treat a given condition [336].

A fundamental part of the proposed therapeutic effect MSCs offer lies on the secretome of these cells. It is an extremely rich source of cytokines, growth factors and extracellular vesicles that engage the paracrine activation of important immunomodulatory, anti-apoptotic, anti-fibrotic, neuroprotective and neurotrophic, and angiogenic pathways [345,346]. Therefore, MSCs are strong promoters of angiogenesis by secreting molecules that include VEGF-A, FGF-2, Angiogenin, Ang-1 and Ang-2, IL-6, monocyte chemoattractant protein 1 (MCP-1), placental growth factor (PLGF) or cysteine-rich 61 (Cyr61) [327]. Furthermore, the secretome of MSCs is also composed of miRs that positively affect vascularization such as miR-210, miR-221/222, miR-296, miR-126, miR17-5, miR-132, miR-92a or miR-18a [347]. However, the impact MSCs exert on vascularization is not restricted to their secretome as numerous studies showed that their direct contact with ECs is essential for the development of fully matured vascular structures [348–350]. On such experimental scenarios, MSCs contribute to degrade the ECM and facilitate the migration of ECs, acting as stabilizers of the vascular structures by enwrapping around vascular tubes and providing trophic support to ECs [351,352]. Different MSC populations have showed an impact on angiogenesis in which amniotic MSCs [353,354], adipose-derived stem cells (ASCs) [355,356], bone marrow stem cells (BM-MSCs) [357,358], Wharton Jelly-derived MSCs [359,360] or dental pulp MSCs [361,362] are included.

The impact of faulting vascularization on the secondary injury-associated damage following SCI, as well as the clear angiotrophic and angioregulatory action of MSCs has made some research groups to study whether the beneficial effects of these cells on SCI showed any links with vascular improvements [274,275,363–365]. Several of the referred studies have indeed found significantly increased amounts of blood vessels in the lesion site and its periphery in the groups treated with MSCs, showing that the modulation of the vascular response following SCI is probably one of the hallmarks of the application of these cells to treat the condition [363,365]. The effect of MSCs in spinal cord vasculature is not confined to increase angiogenesis,

affecting also BSCB permeability. Matsushita *et al.*,[363] demonstrated intravenously injected BM-MSCs into a contusive SCI rat model and observed an extensive reduction on vascular permeability at the lesion site in two analyzed timepoints (2 and 6 weeks post-SCI). The authors linked these observations with the increase expression of endothelial barrier antigen (a marker of the integrity of CNS barriers) and von Willebrand Factor (whose decreased expression has been connected to faulty CNS vascular permeability), although without altering the endothelial-pericyte coupling [363]. A distinct work showed that the infusion of MSCs (in this case isolated from the umbilical cord and brain) markedly reduced BSCB permeability and intraparenchymal hemorrhage as early as 24h post-SCI, leading to lesions with smaller volumes [274]. Furthermore, both types of MSCs protected the functionality of the blood vessels of the injury epicenter during the acute phase of SCI, and these effects on local vasculature aided to promote some degree of functional recovery on the animals receiving the brain-derived MSCs. The authors speculated that the observed impact on spinal cord vasculature could be, at least partially, mediated by IL-10 as the cytokine was systemically upregulated 24h following SCI [274]. This IL has been showed to prevent the adhesion of monocytes to vasculature, while reducing the expression of MMPs and the degradation of the its basement membrane [366].

To elucidate the contribution tissue source age, Vawda and coworkers [367] compared the therapeutic performance term-birth human umbilical cord perivascular cells (HUCPVCs) and first-trimester HUCPVCs (FTM HUCPVCs) in a cervical compression rat model. Previous characterization of both cell sources showed that FTM HUCPVCs possess a higher proliferative and *in* vitro differentiation capacity than HUCPVCs collected after birth, potentially indicating that cells from younger sources are more attractive for regenerative medicine uses [368]. Both reduced vascular and intraparenchymal hemorrhage permeability 24h after SCI, as well as lesion volume in comparison to lesioned animals, however FTM HUCPVCs had a higher impact on the latter two vascular parameters. Moreover, FTM HUCPVCs and HUCPVCs increased the vascular and clearly inhibited astrogliosis and CSPG deposition. Despite these promising histological findings there were no differences regarding the recovery of hindlimb function between treated and non-treated animals, with animals in the FTM HUCPVCs group showing significant increased grip strength test relative to lesioned animals [367].

Concerning the studies where the vascular response post-SCI was assessed using the transplantation of MSCs, the word of Vawda *et al.*,[367] is the only one evaluating (even if preliminarily) possible differences on the capacity of modulate vascularization depending on tissue source age. This feature should be further dissected, and extended to other sources of MSCs, to understand whether the age-dependent differences

on the proliferative and differentiation capacity these authors observed are unanimously present across MSCs.

Additional studies should also understand whether such differences are translated into the secretome of MSCs, what sources are the most affected and how it affects the capacity of well-defined batches of MSCs (both age, donor and source) to shape the vascular milieu following SCI. On this regard, our group recently demonstrated by proteomic analysis that it exist evident differences between the secretome of BM-MSCs, HUPVCs and ASCs a fact that may direct the application of each source to specific CNS conditions [369]. This work demonstrated that the secretome of BM-MSCs is richer in molecules targeting oxidative stress while the secretome of ASCs and HUPVCs has a more interesting profile to target excitotoxicity.

Even though the impact of MSCs in SCI vascularization seem to be robust, future works should perform exhaustive characterizations regarding the expression of TJ proteins, metabolic transporters, relief of tissue hypoxia and infiltration of inflammatory cells. These are fundamental features for a fully functional BSCB and mitigate the severity of secondary injury events.

The detailed studies consisted on the intravenous and two of these successfully followed the fate of the grafted cells to find that the vast majority did not home to the lesion but instead to peripheral organs like the liver, lungs, spleen [274,363]. Therefore, it means that the observed effects on SCI vascularization are mediated systemically and by the secretome of these cells. As referred on this subsection, the most robust results on vascularization appear when MSCs are on the same environment as ECs as the former are important to stabilize and help mature vascular networks. To guarantee the presence of MSCs on the injury milieu, other delivery forms should be optimized in which the local implantation of biomaterials is included. The advantages concerning such delivery platforms and how they may provide interesting tools to promote SCI revascularization will be discussed in the next subsection.

1.9. Biomaterials as tools to modulate angiogenesis and vascularization

Biomaterials can aid the modulation of the vascular response following SCI via two distinct mechanisms, namely acting as vehicles for the delivery of pro-angiogenic molecules [285] or as ECM-mimetic platforms that support cell growth and proliferation [370]. The capacity that biomaterials must protect cells and therapeutic agents from the harsh conditions found in SCI lesion sites puts them in a privileged position for the development of targeted regenerative therapies. Furthermore, this is complemented by the possibility of tailoring their mechanical properties to match native ECM and to their biocompatible and biodegradable characteristics [371]. Biocompatibility reduces the risk of triggering toxic or immunological responses within the CNS, a feature that if not fulfilled could induce chronic inflammation at the

biomaterial interface resulting in the restrain of the scaffold by an avascular glial scar [372–374]. The natural degradation processes of biomaterials under physiological conditions, without originating toxic metabolites, represents another advantage in SCI as it eliminates the need of follow-up surgical procedures for their subsequent removal. Tuning the degradation of these materials allows control of the rate of release of angiogenic factors thereby enabling the optimization of bioavailability and therapeutic concentration [373].

1.9.1. Extracellular matrix-like platforms to support angiogenesis and vascularization

In their native environment, cells are embedded in a three-dimensional ECM responsible for providing adequate mechanical and physical cues that provide instructions to engage in specific behaviors [375]. Additionally, the ECM confers to cells mechanical support and protection from the external environment [374]. This structure interacts with angiogenic gs, to coordinate their bioavailability, concentration and signaling [376]. For instance, VEGF disseminates across the interstitial space and binds both to the ECM and receptors on the surface of cells creating a concentration gradient that attracts endothelial sprouts in the direction of hypoxic regions [377]. Cell-derived proteases regulate the availability of functional growth factors linked to the matrix through their capacity to degrade ECM constituents or by cleaving these molecules into isoforms with reduced bioactivity that are incapable of binding to the ECM. [378].

Given the importance of the ECM during angiogenesis, developing precise analogs of this structure to therapies that aim to restore vascular perfusion seems particularly promising. On this front, biomaterials seem a perfect fit due to their ability to mimic the mechanical properties of the ECM and to provide specific molecular cues. [379]. Commonly, these biomaterials can be of natural origin (ECM-derived or otherwise) or synthetic. Hydrogels from ECM-derived proteins like fibrin, collagen or gelatin are normally used and can be modified regarding their mechanical properties, degradability, cell adhesion and GF-bearing capacity to a limited extent [380]. Natural non-proteic biomaterials, including alginate [381], pectin [382], dextran [383] and gellan gum (GG) [384], are bioinert and require functionalization with appropriate adhesion motifs to acquire biological activity. Additionally, mechanical properties and degradation profiles are adjustable by varying the degree and nature of crosslinking or by including cell degradable peptides, respectively [385]. On the other hand, synthetic biomaterials such as polyethylene glycol (PEG), poly(ε-caprolactone) (PCL) and poly(lactic-co-glycolide) (PLGA) are excellent alternatives to natural polymers due to the possibility to modulate their properties to a greater extent. Moreover, they can be obtained in a reproducible manner, which enables control over molecular weight, mechanical strength, degradation, crosslinking degree and cell adhesive behavior [386]. Therefore, incorporating cell adhesion motifs together

with protease-sensitive sites represents a common strategy to induce angiogenesis and vascularization of natural and synthetic materials and the biomaterial-tissue interface [387–390]. Interestingly, by controlling the spatial distribution and density of these molecular cues it is possible to modulate not only the maturation and formation of newborn blood vessels but also the rate at which they degrade the engineered ECM and infiltrate into host tissue or *vice versa* [390,391]. Thus, these types of materials can be considered blank canvasses to create tunable platforms that can modulate the angiogenic response in a specific way unlike ECM-derived materials.

The development of biomaterial-based strategies to promote vascularization can be done by simple cell seeding on the constructs, spheroids and bioprinting.

1.9.2. Cell seeding

Cell seeding is the most often used *in vitro* pre-vascularization approach. Here, cells that will form the future vessels are seeded onto scaffolds either engineered separately or consisting of natural decellularized ECM. The use of decellularized tissue has the advantage of promptly having available the intricate 3D architecture of the vascular system [392,393]. Therefore, cells can be directly delivered into the channels that were, and will become again, the vascular network of the tissue before decellularization.

Several studies of scaffold pre-vascularization have depended on the ability of ECs to spontaneously organize and form vascular networks [394–396]. ECs start by forming a primitive network on the initially avascular scaffold in a similar process to vasculogenesis. Then, ECs further organize in a similar way to angiogenesis. Even though these cells are able of assembling into complex networks, often without addition of growth factors or specific cues, culture conditions and the type of cells used during co-culture with ECs are of extreme importance. Thus, these factors can influence the morphology of the newly formed vascular network. Therefore, depending on these, the obtained network will vary from immature and possessing limited amounts of lumen to more mature networks with well-developed lumen [396,397]. Levenberg *et al.*, showed that culturing mural precursor cells like embryonic fibroblasts and MSCs with ECs helps maturating the network and its stabilization [395]. This is also reflected by an increased vessel lumen, which will augment the quantity of blood that can be delivered to the tissue. In addition, these cells help regulating vascular permeability which results in less fluid being leaked into the tissue and lower interstitial fluid pressure [398]. Pericytes are other type of cells with beneficial action towards stabilization of newly-formed endothelial tubes [399]. Stratman *et al.* proved that the crosstalk between ECs and pericytes induces ECs to deposit ECM proteins like collagen type IV, laminin and fibronectin contributing in turn to stabilize the vascular network [400]. Koike and coworkers also proved that mural cells are fundamental for

obtaining stable vascular networks [401]. In this seminal study, co-cultures of human umbilical vein endothelial cells (HUVECs) and mural precursor cells developed into stable vascular networks that lasted for periods up to one year *in vivo*. In contrast, constructs engineered with HUVECs alone showed minimal perfusion and disappeared after 60 days. Even though, as mentioned, after seeding HUVECs form vascular networks and can be perfused upon implantation, these cells are difficult to harvest in large amounts under clinical conditions and have limited proliferation during the culture phase. Furthermore, this type of ECs are heterogeneous and present several different features depending on the organ from which they were harvested (molecular permeability, homeostasis, immune tolerance, angiogenic potential and vascular tone) [402,403]. Despite these disadvantages, HUVECs are frequently used in *in vitro* studies. Contrarily to most ECs, HUVECs are available for extraction from unwanted umbilical cords, are easy to obtain and present an interesting expansion profile which make them an attractive source of ECs. Unfortunately, HUVECs often render unstable vessels and their transplantation is capable of inducing an immune response from the host [404]. Several studies demonstrated that EPCs represent a promising cell population to be used on prevascularized scaffolds [405–409]. These cells represent a small population of circulating $CD34^+$ cells with the capacity of accomplishing phenotypical features of ECs *in vitro* [315,410]. Importantly, EPCs have higher proliferative potential than ECs and are easily obtained [411]. Accordingly, these cells circulate in peripheral blood and can be obtained from it by non-invasive procedures. Moreover, EPCs are also present in blood from the umbilical cord, another source of high concentrations of these progenitor cells [412,413]. Considering the time they take to appear after being cultivated *in vitro*, EPCs can be divided into two distinct groups. Thus, early EPCs appear less than 1 week after culture whereas late EPCs take 2 to 4 weeks to appear and present a cobblestone-like morphology [315]. Late EPCs are the most interesting for the development of pre-vascularized constructs since they are able of differentiating into ECs and form capillary-like structures. On the other hand, early EPCs have an indirect action towards vessel formation. Thus, by secreting angiogenic growth factors, this type of EPCs has a paracrine action on angiogenesis [414]. Additional cell types with capacity to achieve complex vascular networks in scaffolds include MSCs [415–418], iPSC-derived ECs [419] and amniotic fluid-derived stem cells [420,421].

1.9.3. Spheroids

Spheroids represent another way of producing pre-vascularized constructs [422–424]. These cell aggregates are form by self-assembly and can be obtained *in vitro* when cells are unable of attaching to a surface and consequently have to interact with each other [425]. Since spheroids represent 3D cellular structures, their organization resembles what is found physiologically. Moreover, these aggregates present high

concentrations of cell-to-cell contacts, cell-matrix interactions and produce high amounts of growth factors. In addition, cells within spheroids are more resistant to hypoxia and apoptosis and have enhanced differentiation potential when compared to 2D cell culture [426,427]. Therefore, these features make them particularly interesting to be studied as potential promoters of scaffold vascularization. Recently, Mishra *et al.* utilized a poly(propylene fumarate)/fibrin hydrogel to coculture HUVEC/ MSC and develop a pre-vascularized scaffold for bone regeneration [424]. These authors proved that allowing the spheroid cells to organize into vascular networks before *in vivo* implantation improves the connection within the vasculature of the host. In a different study, Laschke and coworkers proved that ASCs spheroids seeded into polyurethane scaffolds are capable of initiating blood vessel formation. Upon implantation in an animal model, this type of MSCs induced a strong angiogenic host tissue response which resulted in improved scaffold vascularization and high functional microvessel density [428].

1.9.4. Bioprinting

3D bioprinting has enormous potential in the development of prevascularized structures. The application of this technique allows precise control over the location of cells in spatially defined locations within 3D environments [429]. Therefore, the complex architecture of a vascular network can be both addressed and controlled by directly designing it onto a scaffold. Additionally, scientists can exactly control the cellular densities of the newly patterned vessels and organize different cell types to mimic their natural assembly in blood vessels. Bioprinting is able of forming 3D vascular networks and structures by additively depositing cell suspensions containing vascular cells inside, or not, an appropriate matrix (bioink) [430]. These networks can be engineered by discretely depositing cells as droplets or spheroids adjacently to each other in the intended form. Creating a vascular network using this type of bioprinting relies on the capacity of spheroids to spontaneously join and self-assembly into blood vessels. The other way of engineering a pre-vasculature using bioprinting is by direct-writing, where cells are continuously administered as vascular cell suspensions inside an appropriate matrix. Thus, using this type of bioprinting, a vasculature more similar to the one to be replaced/needed can be obtained [431]. The potential of bioprinting was demonstrated in a study by Norotte *et al* [432]*.* These authors utilized several types of vascular cells aggregated into separated units (either multicellular spheroids or cylinders) to print layer-by-layer vessel-like structures with agarose rods as molding template. During post-printing these cellular structures started to aggregate and developed into fully biological vascular tubular structures. Using a different approach Cui and coworkers developed a 3D polylactic acid bioprinted vascularized bone construct having a fully interconnected microvascular network that mimicked native bone [433]. This

innovative scaffold was then subjected to several surface modifications to optimize its capacity towards cell adhesion and smart release of growth factors. Afterwards the authors repopulated the vasculature of the scaffold with hMSCs and HUVECs under different culture conditions. Interestingly, these authors were able of modulating angiogenesis and osteogenesis through the delivery of specific growth factors entrapped on the surface of the construct with spatiotemporal coordination.

1.9.5. Enhancers of the delivery of angiogenic growth factors

Delivery of angiogenic growth factors has been acknowledged as a promising tool to stimulate angiogenesis and restore vascular perfusion. Nevertheless, clinical translation has proven difficult as these molecules have short *in vivo* half-lives, dosages are sub-optimal and poor retention kinetics [380].

Biomaterials provide a route to circumvent some of these problems as they can protect growth factors' from degradation and can be tuned to release them in a controllable way [434]. Consequently, these platforms can be designed to create a chemical gradient during the release of growth factors, mimicking *in vivo* angiogenesis, and affecting the rate of EC invasion, its direction, structure and network formation [435,436]. Biomaterials can be functionalized with more than one type of growth factors and further replicate native angiogenesis, a process that depends on distinct concentration gradients and bioavailability of these molecules [437–440]. Indeed, both synthetic and natural biomaterials have been used either by physically entrapping the growth factors or by establishing chemical bonds with the matrix [284,441–443]. Perhaps the best approach to enhance the angiogenic response would be to combine the delivery of growth factors with molecules capable of inducing their expression, such as sonic hedgehog. Sonic hedgehog induces the expression of VEGF, Ang-1 and Ang-2, increasing their concentration and leading to the formation of more functional and stable vessels *in vivo* [444,445]. This methodology enables cells to regulate the secretion of growth factors, whilst helping the formation of microgradients and granting the possibility of expressing different growth factors simultaneously [404].

1.10. Integration of biomaterials in spinal cord injury vascularization therapies

As depicted in the previous sections, biomaterials can provide interesting platforms to enhance these particular therapies and in fact have shown the capacity to modulate angiogenesis and vascularization following SCI [370,446–451]. Accordingly, Duan *et al.* utilized NT-3 loaded chitosan tubes to fill the void left by the transection of rat spinal cords and found that this material promoted nerve growth, neurogenesis and functional recovery of the animals. Thus, this study found an upregulation on genes related to vascular development, angiogenesis and hypoxia response in the NT-3 treatment group, when compared to

uninjured and untreated animals [273]. Despite the rationale of the study was not to directly impact the vascular response following SCI it clearly demonstrates that enhancing vascularization is an important part of SCI therapies.

Differently, Rauch *et al.*, [323] created a co-culture system consisting of ECs and NPCs in a biodegradable PLGA scaffold and tested its ability to form functional vessels in an SCI hemisection model. After implantation, this system created a suitable environment for vessel inosculation and angiogenesis in the experimental group, contributing to a 3.5 (PLGA implantation without cells group) and 5-fold (lesioned animals group) increase in number of functional vessels at injury epicenter eight weeks after SCI. The crosstalk between ECs and NPCs was fundamental due to the secretion of nitric oxide by NPCs, which induces the production of VEGF and brain-derived neurotrophic factor on ECs and creates a positive feedback on NO production, promoting vessel formation and stabilization. Notably, the co-culture platform seemed to promote some degree of re-establishment in the BSCB since half of the vessels in the experimental group were positive to endothelial barrier antigen. In contrast, all the other cohorts (untreated, PLGA implantation, PLGA and ECs implantation and PLGA harboring NPCs group) had no expression of this marker [370]. Even though the authors did not assess BSCB functionality and observed limited regeneration, this work underlines the potential of integrating biomaterial-based ECs transplantation into SCI experimental treatments due to their capacity of reestablishing perfusion and BSCB, helping to modulate a regenerative phenotype.

Self-assembling peptides (SAPs) represent a class of scaffolds with robust impact on vascularization and angiogenesis [452–455]. To understand whether combining a SAP (RADA-16I) with microvessels displaying BSCB phenotype provided a beneficial effect on the inflammatory response and scar formation, Tran *et al.* [456] implanted the prevascularized platform on a cervical contusion SCI rat model. The authors used two different microvessel densities and demonstrated that the transplanted vascular structures had a similar alignment to host axons, potentially an indicative of some degree of neurovascular coupling. Additionally, both treatment paradigms significantly decreased microglial activation and scar formation and promoted the ingrowth of host axons [456]. Although promising, the work did not present behavior data to assess whether these histological findings were linked to functional recovery. Furthermore, there were no indications of anastomosis between the transplanted microvessels and host vasculature, as well as measures of *in vivo* BSCB and indications of NVU coupling with astrocytes and pericytes. Guo and coworkers [457]also implanted a prevascularized scaffold composed of poly(L-lactic acid) (PLLA)/PLGA in a rat thoracic model. The scaffold harbored a co-culture between human dental pulp MSCs and human adipose microvascular endothelial cells (HAMECs) that assembled into vascular structures prior to

implantation. Following 8 weeks of implantation, the prevascularized biomaterial originated the robust vascularization of the injured area, particularly on ascending sensory tracts. This feature may explain the distinct behavioral results of the study since the motor recovery of the treated animals was quite modest, whereas the biomaterial platform led to increased recovery of sensory function. Similarly, to the previously mentioned study, no data regarding extensive NVU coupling and integration of the microvascular structures was presented.

The regenerative capacity of graphene oxide scaffolds was evaluated by López-Dolado *et al.*, [448] in a hemisection rat model due to its capacity of inducing neuronal and astrocytic growth and neurogenesis. Upon implantation, these scaffolds promoted angiogenesis inside their structure, showing abundant and functional new vessels in their proximity in comparison to lesioned animals without scaffold implantation. Additionally, the scaffolds also seemed to have immunomodulatory capacity due to an increased presence of pro-regenerative macrophages on its interface. On the other hand, infiltration of neurons into the scaffolds was very low and no measurements on functional outcomes were assessed [448]. Nevertheless, this study presents some encouraging results and it is worth underlining the outstanding conductible properties of graphene, a feature that can play a pivotal role in therapies that apply electric stimulation to induce neural growth [458,459]. Further refinements into the previously referred approach involved the development of soft graphene foams that enabled the infiltration of functional blood vessels and myelinated excitatory axons, while reducing the perilesional damage [460].

Ropper and coworkers implanted a PLGA scaffold encapsulating MSCs in a thoracic hemisection rat model to study the potential of this system in SCI recovery. This treatment induced significant moto-sensory improvements regarding untreated animals or the groups where either scaffold insertion or MSCs transplantation occurred. Additionally, treatment with MSCs encapsulated in PLGA lead to significant decreases in lesion volume and improvements in neuropathic pain in comparison to controls. Furthermore, histological analysis of spinal cord sections showed an increased angiogenesis around the epicenter (observable by a significant increase in laminin concentration on the treatment group) which together with neurotrophic, anti-inflammatory and neurogenic mechanisms helps explaining the obtained moto-sensory improvements of this experimental approach. Nevertheless, therapeutic differences between the direct application of MSCs and their prior encapsulation in PLGA may reside in the protective action of the polymer towards the inhospitable environment found on SCI, which was transduced in augmented MSCs survival upon implantation for that group [275]. The positive impact of MSCs on the angiogenesis and vascularization of SCI was probably driven by the secretome of these cells which is extremely rich in pro-angiogenic growth factors [461]. Accordingly, several researchers have taken advantage

of the aforementioned features of biomaterials to explore delivery of angiogenic growth factors in SCI animal models and assess their impact on recovery following injury [282,284,285,462,463]. Combinatorial approaches utilizing different angiogenic growth factors perhaps represent the best way of attaining better functional outcomes following SCI. Consequently, Yu et al. delivered PLGA microspheres containing VEGF, Ang-1 and bFGF into the injury site of a contusion rat model and observed increased axonal growth on the treated animals in comparison to animals that received the empty microspheres. The authors associated these results with increased density of functional vessels and neural precursors recruitment to the injury site. Moreover, these cells closely associated with blood vessels opening the possibility of the microvascular network having a role on axonal guidance and growth across the lesion cavity. This study also found increased expression levels of miR-210 in treated animals, an inducer of VEGF expression, and suppression of ephrin-A3, a finding that demonstrates that increased neurogenesis found on the treated group was probably directly due to the growth factors administration, broadening their spectrum of action [285].

The utilization of biomaterials to promote SCI revascularization, mainly through the delivery of cells, has started to demonstrate the privileged nature of these platforms to address this phenomenon and promote functional recovery following SCI. The reasons were already addressed and include providing a physical matrix that grants the appropriate cues for cells to exert their biological functions, the delivery of neuronal tissue-compliant substitutes that promote the infiltration of host cells as well as their interaction with transplanted cells, enhancing the survival of delivered cells by protecting them from the harsh environment found on SCI. Despite the promising results, several challenges remain and include: exhaustively characterize the vascular phenotype of transplanted ECs, to understand whether these develop the hallmarks of BSCB; assess if these cells integrate functional vascular networks; characterize the effects of biomaterial-based approaches on vascular permeability and how it affects the infiltration of inflammatory cells; study whether either the stimulation of endogenous ECs or even the vascular structures formed by transplanted ECs provide trophic support and physical tracks for growing axons.

1.11. The use of peptidomimetic ligands to promote angiogenesis in an integrin-specific manner

The angiogenic response is highly influenced by integrin-mediated adhesion of ECs to the basal membrane, in which $\alpha v\beta 3$ and $\alpha 5\beta 1$ are included and have been extensively studied [464]. For instance, different experimental approaches have showed that $\alpha v\beta 3$ is pivotal for EC survival and migration during angiogenesis [465,466]. This glycoprotein is expressed by ECs in response to angiogenic growth factors and its inhibition leads to the disruption of vascular networks in quail embryos by preventing lumen formation

and vascular patterning [465,467]. Integrin $\alpha5\beta1$ interacts with fibronectin, being downregulated on quiescent endothelium and extensively upregulated on ECs during pathological and non-pathological angiogenic processes [468,469]. Similarly to $\alpha v\beta3$, the expression of this integrin increased following the exposure of ECs to growth factors including bFGF or IL-8, but not VEGF [469,470].

Most adhesive ligands used for biofunctionalization of biomaterials involve the use of ECM-derived peptides that do not possess integrin specificity and lose biological activity due to conformation changes upon grafting to the materials or even due to the crosslinking reactions during the formation of hydrogels [471]. Therefore, the development of biomaterials with increased specificity towards specific integrins would enable to target specific biological phenomena like angiogenesis. The following subsection will provide the developments regarding this type of materials, starting from the rationale behind using Arg-Gly-Asp (RGD) as a promoter of biological activity and ending with the application of ligands with elevated integrin specificity.

1.11.1. RGD-integrin interaction features and peptidomimetic design

1.11.1.1 *Elucidation of the RGD-integrin interaction and peptidomimetic ligand advantages*

Initially, the shortest molecular motif in fibronectin able of binding cells to ECM was defined by Pierschbacher and Ruoslathi as being Arg-Gly-Asp-Ser (RGDS) [472]. Their pioneering work consisted of designing synthetic peptides endowed with this sequence and studying their effect on the adhesion of fibroblasts to surfaces displaying fibronectin. Soluble RGDS prevented fibroblast adhesion to the latter surfaces while promoting the adhesion of these cells when coated to sepharose beads. Moreover, it was proved that contrarily to the other three fragments, serine, was not essential to the bioactivity of the peptide and could be replaced by other amino acids [473]. Pierschbacher and Ruoslathi also verified that the RGD sequence was also present in other proteins such as collagen type I, thrombin and fibrinogen and that these motifs had the same cell binding effect [472,473]. These results encouraged efforts to understand if a homology between different ECM proteins and the presence of RGD as the cell adhesion sequence existed. Indeed, the RGD sequence was discovered in laminin, von Willebrand factor, vitronectin and osteopontin and these observations put the tripeptide as a putative candidate for universal cell adhesion motif [474–477]. Curiously, RGD also appears in snake venom disintegrins, a type of strong integrin inhibitors that can inhibit platelet aggregation and angiogenesis, with variable selectivity and potency towards integrins recognizing RGD [478,479].

Notwithstanding, and despite possessing cell adhesion properties, RGD alone is unable of presenting cell-specificity and its effects are highly dependent on the conformation and spatial organization of the peptide

[480,481]. Complementing these features, peptides in the native state present poor pharmacokinetics, such as low metabolic stability, poor absorption after oral ingestion, rapid excretion, low diffusion in some organs and may have undesired effects due to off-target interaction with several other receptors [482]. RGD, of course, is no exception and scientists have tried to improve both the biological activity and specificity of the peptide or peptide-like molecules through specific structural and functional modifications, whilst maintaining their bioactivity. This approach looks to biomolecules, in this case peptides, as a starting point to find new molecules with secondary structures, and additional fundamental structural characteristics analogous to the native peptide, being classified as peptidomimetic molecules [481]. The final goal is to obtain a biomolecule with enhanced binding affinity towards a given receptor or target molecule. Additional advantages of peptidomimetic molecules are their extended biological activity, due to a smaller susceptibility to premature enzymatic degradation, and improved oral bioavailability [483]. Therefore, these ligands have proved to be excellent cell adhesion inhibitors in their soluble form both *in vitro* and *in vivo*, even when ECM proteins are present [484,485]. Furthermore, due to their strong affinity towards integrins (in the nanomolar range) involved in cancer angiogenesis they are regarded as not only trackers of tumor vasculature but also inhibitors of tumor progression [486,487]

A fundamental advance towards a deeper understanding of the interaction between RGD and integrins was achieved by resolving the crystallographic structure of $\alpha v\beta 3$ integrin [488]. Xiong and coworkers reported the crystal structure of the extracellular segment of this integrin complexed with cilengitide (a cyclic peptide presenting RGD). The findings of this study helped establishing a general model of interaction between integrins and RGD, facilitating both the design of RGD peptidomimetics with enhanced affinity towards integrins and docking studies of these compounds.

1.11.1.2 *Peptidomimetic rational design*

Design of peptidomimetic ligands is focused in finding ways of mimicking the pharmacophoric elements of the original peptide. Therefore, for their proper development it is extremely important to have a profound understanding of both the peptide and its receptor and their electronic and three-dimensional conformational characteristics. Additional considerations include the substitution of amide bonds if the biological activity remains untouched. These interactions can also be replaced when they are outside the zone of the active site. In the long term, the objective of these changes will be the substitution of the initial peptidic backbone with a non-peptidic one. Flexibility is also a very important feature to consider during the development of peptidomimetic molecules. However, this characteristic remains untouched during the development of first generation peptidomimetics as long as the molecule maintains its biological

activity. Further refinements will include introducing elements that infer rigidity to side-chains of the new molecule in order to improve its initial bioactivity [481]. Nevertheless, during the initial steps of peptidomimetic design it is preferable to preserve the side chains having biological relevance and possible adjustments to enhance activity are only included in second generation peptidomimetics. Normally, introduction of constraints into the biomolecule, chain length modifications and isosteric replacements are considered [489]. Moreover, the nature of the amino acid sequences flanking the bioactive sequence also impacts ligand specificity [490]. Another crucial factor to consider during the development of peptidomimetic ligands that intend to be coupled to materials lies on the utilized spacer unit. Thus, Pallarola et al. studied the effect of three different spacers (polyproline, aminohexanoic acid and PEG) and concluded that a simple variation on the spacer motif could determine higher or lower integrin binding affinity [491]. A final concern during the development of peptidomimetics is to use the acquired knowledge of the three-dimensional bioactive conformation to rapidly develop the ideal peptidomimetic compound, without wasting time creating numerous molecules without relevant bioactivity [481].

The conversion of the initial peptide into a peptidomimetic compound is approached hierarchically, by introducing incremental chemical modifications that will additionally help elucidating the structure-activity relationship [489]. First, the biologically active peptide suffers alanine scanning and his biological activity is measured. As the name suggests this step is based on the substitution of different amino acids of the original peptidic sequence by alanine. Observing the bioactivity of the resulting molecule will help understanding if a given amino acid is biologically relevant or not [481]. Next in hierarchy is the reduction in size of the initial peptide [489]. With this methodology it is possible to assess the minimum sequence that interacts with the target. Concretely, this process identifies the sequence bearing the pharmacophore. To achieve it a sequential removal of amino acids either from *N*- or *C*-termini and the subsequent biological activity measurement is done. [481]. Afterwards, replacing amino acids of the parent peptide with D-amino acids and measuring the activity of the obtained molecule enlightens the structural organization of the biologically active conformation due to a change in the configuration and conformation of the side chains [481,489]. The clarification of the role each amino acid in the bioactive peptide has can also be done by creating *N*-methylated peptides [481]. Lastly, the bioactive conformation can be defined with the help of the insertion of local and/or global constraints because the initial peptide is in a loose conformation that presents low activity [489].

Regarding to what specific characteristic a peptidomimetic molecule emulates, this can be fitted into three different categories: type-I, type-II and type-III mimetics [481]. Type-I mimetics were the first peptidomimetic molecules to be described and mimic local topographic features of the native compound while still

carrying all the features responsible for the interaction with the target molecule. It is frequent that these biomolecules match the peptidic backbone atom for atom by introducing isosteres into it [492]. Functional mimetics, or type-II mimetics, replicate the basis of the interaction between the native peptide and the target without concern for mimicking the structural arrangements of the initial molecule. When the first appeared, these peptidomimetics were thought to be equivalent to the original peptides in terms of structure, but characterization of both biomolecules found that they bind to different sub-sites in a large number of receptors [493,494]. Despite this, both types of peptidomimetics described are valuable resources to replace peptides with molecules possessing higher binding affinity or greater selectivity towards a given target. However, type-III mimetics are considered the ideal approach in designing peptidomimetic ligands. Such biomolecules present a scaffold with a different structure regarding the initial peptide and although they appear quite unrelated, they possess all the necessary groups in a well-defined spatial orientation to facilitate favorable molecular interactions. Thus, they are generally termed functional-structural mimetics [481,492].

1.11.1.3 *The potential of peptidomimetic ligands with integrin selectivity for proper development of vascular networks in regenerative medicine methodologies*

To counteract the already mentioned drawbacks of using RGD or other peptidic adhesive ligands, some groups have used different RGD-containing molecules like small cyclic RGD peptides and protein fragments. Notwithstanding, this type of ligands fail to target specific integrins, which represents a disadvantage if the intention is to guide cells towards a response directed by a defined integrin. Other approaches employ biomaterials functionalized with combinations of different peptidic ligands that exhibit integrin specificity. Normally, these mixtures do not fulfil their potential due to difficulties in controlling their spatial arrangement [471]. Developing peptidomimetic ligands with selectivity for specific integrins thus seems an interesting approach to enhance the angiogenic properties of biomaterials for regenerative medicine purposes. Additionally, peptidomimetic molecules may be designed having the appropriate conformation to engage integrins and elicit their biological responses whilst having better pharmacokinetic parameters than proteins or peptides [481]. Nevertheless, the majority of integrins display similar RGD binding regions making the synthesis of highly selective ligands, whilst displaying high affinity, to distinct integrin subtypes challenging. Therefore, some ligands presenting subtype selectivity have a residual, but still significant, affinity towards other integrins [495]. Although their use for regenerative medicine purposes remains undermined, some labs have considered them as promising tools in biomaterial functionalization [496–501]. Consequently, in a pioneering study Marchand-Brynaert *et al.* developed an RGD peptidomimetic

molecule based on an L-tyrosine scaffold that was afterwards immobilized in a poly(ethylene terephthalate) film [502]. Interestingly, this ligand presented cell adhesion properties comparable to RGD, but inferior to the same material functionalized with fibronectin. Even though these results are not totally satisfying, it helped to demonstrate that peptidomimetic ligands could provide good alternatives for the biofunctionalization of intrinsically inert materials. Development of this peptidomimetic ligand has continued and in a subsequent study it showed higher adhesion capacity than RGD [503]. More recently, Rechenmacher and coworkers modified a peptidomimetic compound previously developed by their group with nanomolar affinity towards either α5β1 or αvβ3 [504]. This modification intended to facilitate the immobilization of the molecule on materials with different surface chemistries. Initially, these authors optimized the length of the spacer motif (lysine-based) and number of anchor units (phosphonic acid). Thus, the modified peptidomimetic showed a nine-fold increase in α5β1 binding (in comparison to controls) for higher spacer lengths and seemed independent of the number of phosphonic acids (2, 3 or 4). By culturing either α5β1-expressing or αvβ3-expressing fibroblasts with TiO_2 nanoarrays that had the optimized compound immobilized, this study showed that this chemical modification did not alter affinity, nor the selectivity of the ligand. Therefore, the former cells adhered and extended their processes in culture conditions, whereas the latter cells maintained a round, typically non-adherent morphology. As a proof that this method also allowed the immobilization of a αvβ3-sellective ligand, the authors immobilized a peptidomimetic ligand with nanomolar affinity to this integrin utilizing the same strategy. After improving the solubility of this peptidomimetic molecule, αvβ3-containing fibroblasts were cultured with TiO_2-peptidomimetic nanoarrays. Contrarily to the other ligand, these fibroblasts rapidly adhered to the titanium oxide nanoparticles. On the other hand, α5β1-containing fibroblasts did not interact with the functionalized nanoparticles. This result is in line with a previous study of the same authors where they used these compounds but immobilized them into gold, via thiol [505]. These reports established that peptidomimetic ligands are able of being immobilized onto the surface of materials without losing their affinity and selectivity. Consequently, it opened excellent perspectives for the development of materials capable of equally attracting specific types of cells or guiding cellular responses of interest. Given that peptidomimetics can discriminate between integrins, immobilizing these ligands onto biomaterials may help elucidating the role that different integrins have on mechanotransduction. Likewise, Rahmouni *et al.* developed PEG hydrogels nanopatterned with gold nanoparticles on the surface and possessing variable bending stiffness [499]. Then, these hydrogels were functionalized with α5β1- or αvβ3-integrin specific ligands and by culturing fibroblasts within them the authors assessed the traction forces exerted by the adhesion mediated by each of these integrins. In this work, it is showed that cells adhering to α5β1

integrins employed higher maximum forces in the material than cells binding to αvβ3. Despite their preliminary nature, these results demonstrate that one must not only develop integrin-specific materials but also physically tailor them to correspond to the mechanical needs of cells if the intention is to guide them towards a given response. In another effort to understanding the behavior of α5β1 and αvβ3 during cell adhesion, Guasch *et al.* orthogonally functionalized alternated stripes of gold and metal oxide with peptidomimetic ligands specific to αvβ3 and α5β1, respectively [501]. Thus, to accomplish an orthogonal functionalization these researchers used an αvβ3 ligand with a thiol group and an α5β1 molecule with phosphonic acid. This work intended to correlate the focal adhesion points during cellular adhesion with the location of these integrins and assess the role cells have in positioning these receptors. Therefore, U20S osteosarcoma cells seeded in the functionalized material exhibited an expression of both integrins in the zone of the α5β1-specific ligand, i.e. independently of integrin affinity, whereas cells in the αvβ3-selective zones only presented clusters of this integrin. According to Guasch and coworkers [501], this colocalization can be motivated by a crosstalk between the activated α5β1 and αvβ3 integrins that overcomes the affinity of the latter towards its ligand. Although the activation of αvβ3 integrins in this area is unlikely, due to the high selectivity of the peptidomimetic ligand, α5β1 might recruit αvβ3 integrins by inside-out signaling ensuring their colocalization prior to cell migration. Interestingly, the initial width of the gold stripes (7-8 μm) proved to be insufficient to motivate the expression of αvβ3 on this area. Consequently, U20S cells only started to express αvβ3 on the gold stripes after increasing the width of this surface. Hindering of the peptidomimetic ligand by its lateral confinement was discarded due to the expression of αvβ3 on metal oxide stripes with 7-8 μm. Instead, the explanation to this experimental observation might lie on the different roles α5β1 and αvβ3 integrins have during cell adhesion. Therefore, cells seemed not to sense the appropriate mechanical stimulus to express αvβ3 integrins, which again shows the importance of mechanotransduction in cell behavior, concretely in integrin expression. These results need to be explored to gather more knowledge about the different roles each integrin possesses during cell adhesion, if objective is developing smart-instructive materials. Consequently, peptidomimetic ligands seem the best option to ensure it as they can be tailored to have nanomolar specificity to an intended integrin. To explore the importance of mechanotransduction in bone regeneration, Mauro *et al.* developed RGD-like poly(amido-amine) hydrogels with tunable stiffness reinforced by montmorillonite [498]. This reinforcement originated swollen hydrogels with a shear storage modulus (G') 20 times higher than conventional hydrogels. Thus, these hydrogels presented excellent mechanical properties to be used in bone regeneration. This was corroborated when these authors culture pre-osteoblastic MC3T3-E1 mouse cells and observed that their hydrogels fomented cell adhesion and proliferation while inducing a clear

differentiation towards the osteoblastic phenotype. Fraioli *et al.*, however, were the first to report that peptidomimetic ligands with specificity to αvβ3 and α5β1 could enhance adhesion, proliferation and differentiation of cells towards an osteogenic phenotype [506]. Accordingly, two peptidomimetics presenting specificity to either αvβ3 or α5β1 were immobilized onto titanium surfaces. To guarantee that the effects seen on the cells were only due to the bioactivity of both ligands, these authors reduced the roughness of titanium surfaces as rough surfaces are known to positively influence of osteoblastic-like cells. Remarkably, the action of these highly specific ligands conducted SaOS-2 cells to differentiate into osteoblast-like cells while improving the cellular adhesion and proliferation in an equal extension to native ECM proteins.

The use of peptidomimetics for surface coating and regenerative medicine applications is still in its infancy but has presented promising results to date in the guidance of specific cellular responses. Although none of the reported studies is conducted with the purpose of enhancing the formation of a vascular network in a regenerative medicine therapy these works use peptidomimetic molecules specific to integrins involved in angiogenesis (αvβ3 and α5β1). The described results show that the effect of these molecules on cellular adhesion can be equivalent to the action of ECM proteins and conduct cellular differentiation to an intended cell type. Therefore, this opens excellent opportunities for the use of peptidomimetic ligands as vascularization enhancers in regenerative medicine constructs. It is important to underline, though, that the development of these ligands is rather intricate, involving *in silico* studies to understand the spatial orientation of the chemical mimetics and deep knowledge in organic chemistry. Nevertheless, the possibility of enhancing the vascular response of cells and guiding their behavior towards the creation of complex vascular networks may help dictating the success of a therapy in this field. Another important fact to retain is that peptidomimetics do not represent the holy grail in directed vascular responses. Therefore, as it is shown in this section, there are many factors involved in the creation of vascular networks. These include: a correct spatiotemporal administration of growth factors, the use of cell types that mimic the organization of vascular structures *in vivo* and having environments that resemble the mechanical properties cells find in their habitat. Consequently, a multidisciplinary approach that addresses all these challenges will bring us closer to developing complex, functional, vascular networks that grant the success of regenerative medicine constructs upon implantation.

1.12. Concluding remarks

The intimate relationship between the CNS and the vascular system ranges from the beginning of embryonic development, where both systems develop concomitantly while sharing the same cues, to

be finally shaped with similar stereotypical organization. Vascular networks are important to grant the appropriate nutrient/blood flow supply to the CNS, to serve as barriers to the entry of exogenous neurotoxic molecules and as substrates of neuronal migration. SCI is a highly severe CNS traumatic event with a very limited clinical prognosis. Vascular disruption occurs in the moment of lesion infliction and is responsible for the initiation of the secondary cascade of lesion that expands tissue damage and leads to the severe motor, autonomic and sensory disfunctions SCI patients face. The limited vascular response observed following SCI means that the vascular supply to the injured spinal cord is inefficient to deliver nutrients and oxygen. Affected ECs do not display associations in NUVs, presenting a dysfunctional BSCB phenotype that allows the entry of neurotoxic molecules and cells from the periphery that prove deleterious for the pathophysiology of the condition. Therefore, the central role of vascular disruption to the progression of SCI makes the modulation of this parameter a promising therapeutic opportunity. An interesting way to address this issue is to use biomaterials (more concretely hydrogels) as vehicles for the transplantation of ECs with the purpose to enhance their maturation into vascular networks, development of BSCB properties, and anastomose with the host tissue. Hydrogels provide the appropriate physical environment and chemical cues to induce cell growth and proliferation while protecting transplanted cells from the nefarious environment found on SCI. Moreover, numerous *in vitro* data has shown that MSCs are able to act as stabilizers of newly formed vascular structures by granting trophic support to ECs. These properties make MSCs the ideal candidates to be included on the aforementioned SCI vascular therapies by co-culturing them with ECs. Further refinements to this cell transplantation strategy may include the functionalization of biomaterials with integrin specific ligands. These molecules possess an extremely high affinity towards integrins of interest and allow to specifically induce biological processes of interest such as angiogenesis. GG is an ideal candidate to be included in such a therapy since it is FDA approved (facilitating clinical translation) and possesses an ideal backbone to graft such ligands. Therefore, the combination of GG (to which integrin specific ligands are coupled) with the co-culture of MSCs and ECs seems an interesting therapeutic rationale to be applied in SCI.

References

1. Carmeliet, P. & Tessier-Lavigne, M. Common mechanisms of nerve and blood vessel wiring. *Nature* **436**, 193–200 (2005).
2. Nourshargh, S., Hordijk, P. L. & Sixt, M. Breaching multiple barriers: leukocyte motility through venular walls and the interstitium. *Nat. Rev. Mol. Cell Biol.* **11**, 366–378 (2010).
3. Segura, I., De Smet, F., Hohensinner, P. J., Almodovar, C. R. de & Carmeliet, P. The neurovascular link in health and disease: an update. *Trends Mol. Med.* **15**, 439–451 (2009).
4. Quaegebeur, A., Lange, C. & Carmeliet, P. The neurovascular link in health and disease: Molecular mechanisms and therapeutic implications. *Neuron* **71**, 406–424 (2011).
5. Miller, G. On the Origin of the nervous system. *Science* (2009) doi:10.1126/science.325_24.
6. Arendt, D., Tosches, M. A. & Marlow, H. From nerve net to nerve ring, nerve cord and brain — evolution of the nervous system. *Nat. Rev. Neurosci.* **17**, 61–72 (2016).
7. Monahan-Earley, R., Dvorak, A. M. & Aird, W. C. Evolutionary origins of the blood vascular system and endothelium. *J. Thromb. Haemost.* **11**, 46–66 (2013).
8. Wälchli, T. *et al.* Wiring the Vascular Network with Neural Cues: A CNS Perspective. *Neuron* **87**, 271–96 (2015).
9. Segarra, M., Aburto, M. R., Hefendehl, J. & Acker-Palmer, A. Neurovascular Interactions in the Nervous System. *Annu. Rev. Cell Dev. Biol.* **35**, 615–635 (2019).
10. Hama, K. The Fine Structure of Some Blood Vessels of the Earthworm, Eisenia foetida. *J. Biophys. Biochem. Cytol.* **7**, 717–724 (1960).
11. Kwon, H.-B. *et al.* The parallel growth of motoneuron axons with the dorsal aorta depends on Vegfc/Vegfr3 signaling in zebrafish. *Development* **140**, 4081–4090 (2013).
12. Wild, R. *et al.* Neuronal sFlt1 and Vegfaa determine venous sprouting and spinal cord vascularization. *Nat. Commun.* **8**, (2017).
13. Nikolopoulou, E., Galea, G. L., Rolo, A., Greene, N. D. E. & Copp, A. J. Neural tube closure: cellular, molecular and biomechanical mechanisms. *Development* **144**, 552–566 (2017).
14. Paredes, I., Himmels, P. & Ruiz de Almodóvar, C. Neurovascular Communication during CNS Development. *Dev. Cell* **45**, 10–32 (2018).
15. Wilson, L. & Maden, M. The mechanisms of dorsoventral patterning in the vertebrate neural tube. *Dev. Biol.* **282**, 1–13 (2005).
16. Dessaud, E., McMahon, A. P. & Briscoe, J. Pattern formation in the vertebrate neural tube: a sonic hedgehog morphogen-regulated transcriptional network. *Development* **135**, 2489–2503 (2008).
17. Tata, M. & Ruhrberg, C. Cross-talk between blood vessels and neural progenitors in the developing brain. *Neuronal Signal.* **2**, 1–13 (2018).

18. Tata, M., Ruhrberg, C. & Fantin, A. Vascularisation of the central nervous system. *Mech. Dev.* **138 Pt 1**, 26–36 (2015).
19. Ruiz de Almodovar, C., Lambrechts, D., Mazzone, M. & Carmeliet, P. Role and Therapeutic Potential of VEGF in the Nervous System. *Physiol. Rev.* **89**, 607–648 (2009).
20. Tarsitano, M., De Falco, S., Colonna, V., McGhee, J. D. & Persico, M. G. The C. elegans pvf-1 gene encodes a PDGF/VEGF-like factor able to bind mammalian VEGF receptors and to induce angiogenesis. *FASEB J.* **20**, 227–233 (2006).
21. Hogan, K. A. The neural tube patterns vessels developmentally using the VEGF signaling pathway. *Development* **131**, 1503–1513 (2004).
22. Jakobsson, L. *et al.* Endothelial cells dynamically compete for the tip cell position during angiogenic sprouting. *Nat. Cell Biol.* **12**, 943–953 (2010).
23. Lobov, I. B. *et al.* Delta-like ligand 4 (Dll4) is induced by VEGF as a negative regulator of angiogenic sprouting. *Proc. Natl. Acad. Sci. U. S. A.* **104**, 3219–24 (2007).
24. Leslie, J. D. *et al.* Endothelial signalling by the Notch ligand Delta-like 4 restricts angiogenesis. *Development* (2007) doi:10.1242/dev.003244.
25. Potente, M., Gerhardt, H. & Carmeliet, P. Basic and therapeutic aspects of angiogenesis. *Cell* (2011) doi:10.1016/j.cell.2011.08.039.
26. Carmeliet, P. *et al.* Impaired myocardial angiogenesis and ischemic cardiomyopathy in mice lacking the vascular endothelial growth factor isoforms VEGF164 and VEGF188. *Nat. Med.* (1999) doi:10.1038/8379.
27. Stalmans, I. *et al.* Arteriolar and venular patterning in retinas of mice selectively expressing VEGF isoforms. *J. Clin. Invest.* **109**, 327–336 (2002).
28. Mackenzie, F. & Ruhrberg, C. Diverse roles for VEGF-A in the nervous system. *Development* **139**, 1371–1380 (2012).
29. Ruhrberg, C. Spatially restricted patterning cues provided by heparin-binding VEGF-A control blood vessel branching morphogenesis. *Genes Dev.* **16**, 2684–2698 (2002).
30. Himmels, P. *et al.* Motor neurons control blood vessel patterning in the developing spinal cord. *Nat. Commun.* **8**, (2017).
31. Daneman, R. *et al.* Wnt/β-catenin signaling is required for CNS, but not non-CNS, angiogenesis. *Proc. Natl. Acad. Sci. U. S. A.* (2009) doi:10.1073/pnas.0805165106.
32. Corada, M. *et al.* The Wnt/β-Catenin Pathway Modulates Vascular Remodeling and Specification by Upregulating Dll4/Notch Signaling. *Dev. Cell* **18**, 938–949 (2010).
33. Stenman, J. M. *et al.* Canonical Wnt Signaling Regulates Organ-Specific Assembly and Differentiation of CNS Vasculature. *Science (80-.).* **322**, 1247–1250 (2008).

34. Mulligan, K. A. & Cheyette, B. N. R. Wnt Signaling in Vertebrate Neural Development and Function. *J. Neuroimmune Pharmacol.* **7**, 774–787 (2012).

35. Serini, G. *et al.* Class 3 semaphorins control vascular morphogenesis by inhibiting integrin function. *Nature* (2003) doi:10.1038/nature01784.

36. Vieira, J. M., Schwarz, Q. & Ruhrberg, C. Selective requirements for NRP1 ligands during neurovascular patterning. *Development* (2007) doi:10.1242/dev.002402.

37. Pan, Q. *et al.* Blocking Neuropilin-1 Function Has an Additive Effect with Anti-VEGF to Inhibit Tumor Growth. *Cancer Cell* **11**, 53–67 (2007).

38. Lamont, R. E., Lamont, E. J. & Childs, S. J. Antagonistic interactions among Plexins regulate the timing of intersegmental vessel formation. *Dev. Biol.* (2009) doi:10.1016/j.ydbio.2009.04.037.

39. Fukushima, Y. *et al.* Sema3E-PlexinD1 signaling selectively suppresses disoriented angiogenesis in ischemic retinopathy in mice. *J. Clin. Invest.* (2011) doi:10.1172/JCI44900.

40. Kim, J., Oh, W.-J., Gaiano, N., Yoshida, Y. & Gu, C. Semaphorin 3E-Plexin-D1 signaling regulates VEGF function in developmental angiogenesis via a feedback mechanism. *Genes Dev.* **25**, 1399–1411 (2011).

41. Kim, K., Ohashi, K., Utoh, R., Kano, K. & Okano, T. Preserved liver-specific functions of hepatocytes in 3D co-culture with endothelial cell sheets. *Biomaterials* **33**, 1406–1413 (2012).

42. Lu, X. *et al.* The netrin receptor UNC5B mediates guidance events controlling morphogenesis of the vascular system. *Nature* **432**, 179–186 (2004).

43. Larrivée, B. *et al.* Activation of the UNC5B receptor by Netrin-1 inhibits sprouting angiogenesis. *Genes Dev.* (2007) doi:10.1101/gad.437807.

44. Wilson, B. D. Netrins Promote Developmental and Therapeutic Angiogenesis. *Science (80-.).* **313**, 640–644 (2006).

45. Kye, W. P. *et al.* The axonal attractant Netrin-1 is an angiogenic factor. *Proc. Natl. Acad. Sci. U. S. A.* (2004) doi:10.1073/pnas.0405984101.

46. Tu, T. *et al.* CD146 acts as a novel receptor for netrin-1 in promoting angiogenesis and vascular development. *Cell Res.* **25**, 275–287 (2015).

47. Castets, M. & Mehlen, P. Netrin-1 role in angiogenesis: To be or not to be a pro-angiogenic factor? *Cell Cycle* (2010) doi:10.4161/cc.9.8.11197.

48. Lejmi, E. *et al.* Netrin-4 inhibits angiogenesis via binding to neogenin and recruitment of Unc5B. *Proc. Natl. Acad. Sci. U. S. A.* **105**, 12491–12496 (2008).

49. Hoang, S. *et al.* Netrin-4 enhances angiogenesis and neurologic outcome after cerebral ischemia. *J. Cereb. Blood Flow Metab.* **29**, 385–397 (2009).

50. Lambert, E., Coissieux, M. M., Laudet, V. & Mehlen, P. Netrin-4 acts as a pro-angiogenic factor during

zebrafish development. *J. Biol. Chem.* **287**, 3987–3999 (2012).

51. Kidd, T., Bland, K. S. & Goodman, C. S. Slit is the midline repellent for the Robo receptor in Drosophila. *Cell* (1999) doi:10.1016/S0092-8674(00)80589-9.
52. Blockus, H. & Chédotal, A. Slit-robo signaling. *Dev.* (2016) doi:10.1242/dev.132829.
53. Jones, C. A. *et al.* Robo4 stabilizes the vascular network by inhibiting pathologic angiogenesis and endothelial hyperpermeability. *Nat. Med.* **14**, 448–453 (2008).
54. Dubrac, A. *et al.* Targeting NCK-Mediated Endothelial Cell Front-Rear Polarity Inhibits Neovascularization. *Circulation* (2016) doi:10.1161/CIRCULATIONAHA.115.017537.
55. Rama, N. *et al.* Slit2 signaling through Robo1 and Robo2 is required for retinal neovascularization. *Nat. Med.* **21**, 483–491 (2015).
56. Jones, C. A. *et al.* Slit2-Robo4 signalling promotes vascular stability by blocking Arf6 activity. *Nat. Cell Biol.* (2009) doi:10.1038/ncb1976.
57. Koch, A. W. *et al.* Robo4 Maintains Vessel Integrity and Inhibits Angiogenesis by Interacting with UNC5B. *Dev. Cell* **20**, 33–46 (2011).
58. Sheldon, H. *et al.* Active involvement of Robo1 and Robo4 in filopodia formation and endothelial cell motility mediated via WASP and other actin nucleation-promoting factors . *FASEB J.* (2009) doi:10.1096/fj.07-098269.
59. Pitulescu, M. E. & Adams, R. H. Eph/ephrin molecules–a hub for signaling and endocytosis. *Genes Dev.* **24**, 2480–2492 (2010).
60. Adams, R. H. *et al.* Roles of ephrinB ligands and EphB receptors in cardiovascular development: demarcation of arterial/venous domains, vascular morphogenesis, and sprouting angiogenesis. *Genes Dev.* **13**, 295–306 (1999).
61. Wang, H. U., Chen, Z. F. & Anderson, D. J. Molecular distinction and angiogenic interaction between embryonic arteries and veins revealed by ephrin-B2 and its receptor Eph-B4. *Cell* (1998) doi:10.1016/S0092-8674(00)81436-1.
62. Sawamiphak, S. *et al.* Ephrin-B2 regulates VEGFR2 function in developmental and tumour angiogenesis. *Nature* **465**, 487–491 (2010).
63. Wang, Y. *et al.* Ephrin-B2 controls VEGF-induced angiogenesis and lymphangiogenesis. *Nature* (2010) doi:10.1038/nature09002.
64. Schwab, M. E. Functions of Nogo proteins and their receptors in the nervous system. *Nat. Rev. Neurosci.* **11**, 799–811 (2010).
65. Wälchli, T. *et al.* Nogo-A is a negative regulator of CNS angiogenesis. *Proc. Natl. Acad. Sci. U. S. A.* (2013) doi:10.1073/pnas.1216203110.
66. Wälchli, T. *et al.* Nogo-A regulates vascular network architecture in the postnatal brain. *J. Cereb. Blood*

Flow Metab. (2017) doi:10.1177/0271678X16675182.

67. Rust, R. *et al.* Nogo-A targeted therapy promotes vascular repair and functional recovery following stroke. *Proc. Natl. Acad. Sci. U. S. A.* **116**, 14270–14279 (2019).
68. Bond, A. M., Ming, G. & Song, H. Adult Mammalian Neural Stem Cells and Neurogenesis: Five Decades Later. *Cell Stem Cell* **17**, 385–395 (2015).
69. Vasudevan, A., Long, J. E., Crandall, J. E., Rubenstein, J. L. R. & Bhide, P. G. Compartment-specific transcription factors orchestrate angiogenesis gradients in the embryonic brain. *Nat. Neurosci.* **11**, 429–439 (2008).
70. Ulrich, F., Ma, L. H., Baker, R. G. & Torres-Vázquez, J. Neurovascular development in the embryonic zebrafish hindbrain. *Dev. Biol.* **357**, 134–151 (2011).
71. Bjornsson, C. S., Apostolopoulou, M., Tian, Y. & Temple, S. It takes a village: constructing the neurogenic niche. *Dev. Cell* **32**, 435–46 (2015).
72. Tata, M. *et al.* Regulation of embryonic neurogenesis by germinal zone vasculature. *Proc. Natl. Acad. Sci. U. S. A.* **113**, 13414–13419 (2016).
73. Lange, C. *et al.* Relief of hypoxia by angiogenesis promotes neural stem cell differentiation by targeting glycolysis. *EMBO J.* **35**, 924–941 (2016).
74. Tan, X. *et al.* Vascular Influence on Ventral Telencephalic Progenitors and Neocortical Interneuron Production. *Dev. Cell* (2016) doi:10.1016/j.devcel.2016.02.023.
75. Shen, Q. Endothelial Cells Stimulate Self-Renewal and Expand Neurogenesis of Neural Stem Cells. *Science (80-.).* **304**, 1338–1340 (2004).
76. Kokovay, E. *et al.* Adult SVZ Lineage Cells Home to and Leave the Vascular Niche via Differential Responses to SDF1/CXCR4 Signaling. *Cell Stem Cell* **7**, 163–173 (2010).
77. Sosa, M. A. G. *et al.* Interactions of primary neuroepithelial progenitor and brain endothelial cells: Distinct effect on neural progenitor maintenance and differentiation by soluble factors and direct contact. *Cell Res.* **17**, 619–626 (2007).
78. Vissapragada, R. *et al.* Bidirectional crosstalk between periventricular endothelial cells and neural progenitor cells promotes the formation of a neurovascular unit. *Brain Res.* **1565**, 8–17 (2014).
79. Li, Q., Ford, M. C., Lavik, E. B. & Madri, J. A. Modeling the neurovascular niche: VEGF- and BDNF-mediated cross-talk between neural stem cells and endothelial cells: An in vitro study. *J. Neurosci. Res.* **84**, 1656–1668 (2006).
80. Chaker, Z., Codega, P. & Doetsch, F. A mosaic world: puzzles revealed by adult neural stem cell heterogeneity. *Wiley Interdiscip. Rev. Dev. Biol.* **5**, 640–658 (2016).
81. Tavazoie, M. *et al.* A Specialized Vascular Niche for Adult Neural Stem Cells. *Cell Stem Cell* (2008) doi:10.1016/j.stem.2008.07.025.

82. Ottone, C. *et al.* Direct cell-cell contact with the vascular niche maintains quiescent neural stem cells. *Nat. Cell Biol.* **16**, 1045–1056 (2014).

83. Delgado, A. C. *et al.* Endothelial NT-3 Delivered by Vasculature and CSF Promotes Quiescence of Subependymal Neural Stem Cells through Nitric Oxide Induction. *Neuron* **83**, 572–585 (2014).

84. Bovetti, S. *et al.* Blood vessels form a scaffold for neuroblast migration in the adult olfactory bulb. *J. Neurosci.* **27**, 5976–5980 (2007).

85. Snapyan, M. *et al.* Vasculature guides migrating neuronal precursors in the adult mammalian forebrain via brain-derived neurotrophic factor signaling. *J. Neurosci.* **29**, 4172–4188 (2009).

86. Won, C. *et al.* Autonomous vascular networks synchronize GABA neuron migration in the embryonic forebrain. *Nat. Commun.* **4**, (2013).

87. Eichmann, A. & Thomas, J.-L. Molecular Parallels between Neural and Vascular Development. *Cold Spring Harb. Perspect. Med.* **3**, a006551–a006551 (2013).

88. Licht, T. & Keshet, E. The vascular niche in adult neurogenesis. *Mech. Dev.* **138**, 56–62 (2015).

89. Licht, T. *et al.* VEGF is required for dendritogenesis of newly born olfactory bulb interneurons. *Development* **137**, 261–271 (2010).

90. Licht, T., Dor-Wollman, T., Ben-Zvi, A., Rothe, G. & Keshet, E. Vessel maturation schedule determines vulnerability to neuronal injuries of prematurity. *J. Clin. Invest.* (2015) doi:10.1172/JCI79401.

91. Saghatelyan, A. Role of blood vessels in the neuronal migration. *Semin. Cell Dev. Biol.* **20**, 744–750 (2009).

92. Wittko, I. M. *et al.* VEGFR-1 regulates adult olfactory bulb neurogenesis and migration of neural progenitors in the rostral migratory stream in vivo. *J. Neurosci.* **29**, 8704–8714 (2009).

93. Le Magueresse, C. *et al.* Subventricular zone-derived neuroblasts use vasculature as a scaffold to migrate radially to the cortex in neonatal mice. *Cereb. Cortex* (2012) doi:10.1093/cercor/bhr302.

94. Bozoyan, L., Khlghatyan, J. & Saghatelyan, A. Astrocytes control the development of the migration-promoting vasculature scaffold in the postnatal brain via VEGF signaling. *J. Neurosci.* **32**, 1687–1704 (2012).

95. Li, S. *et al.* Endothelial cell-derived GABA signaling modulates neuronal migration and postnatal behavior. *Cell Res.* **28**, 221–248 (2018).

96. Paredes, M. F. *et al.* Extensive migration of young neurons into the infant human frontal lobe. *Science (80-.).* **354**, (2016).

97. Harder, D. R., Zhang, C. & Gebremedhin, D. Astrocytes Function in Matching Blood Flow to Metabolic Activity. *Physiology* **17**, 27–31 (2002).

98. Iadecola, C. The Neurovascular Unit Coming of Age: A Journey through Neurovascular Coupling in Health and Disease. *Neuron* vol. 96 17–42 (2017).

99. Muoio, V., Persson, P. B. & Sendeski, M. M. The neurovascular unit - concept review. *Acta Physiol.* **210**, 790–798 (2014).

100. Raichle, M. E. & Mintun, M. A. BRAIN WORK AND BRAIN IMAGING. *Annu. Rev. Neurosci.* **29**, 449–476 (2006).

101. Brown, L. S. *et al.* Pericytes and neurovascular function in the healthy and diseased brain. *Frontiers in Cellular Neuroscience* (2019) doi:10.3389/fncel.2019.00282.

102. Langen, U. H., Ayloo, S. & Gu, C. Development and Cell Biology of the Blood-Brain Barrier. *Annu. Rev. Cell Dev. Biol.* **35**, 591–613 (2019).

103. Janzer, R. C. & Raff, M. C. Astrocytes induce blood–brain barrier properties in endothelial cells. *Nature* **325**, 253–257 (1987).

104. Stewart, P. A. & Wiley, M. J. Developing nervous tissue induces formation of blood-brain barrier characteristics in invading endothelial cells: A study using quail-chick transplantation chimeras. *Dev. Biol.* **84**, 183–192 (1981).

105. Sweeney, M. D., Zhao, Z., Montagne, A., Nelson, A. R. & Zlokovic, B. V. Blood-brain barrier: From physiology to disease and back. *Physiol. Rev.* **99**, 21–78 (2019).

106. Armulik, A. *et al.* Pericytes regulate the blood–brain barrier. *Nature* **468**, 557–561 (2010).

107. Ben-Zvi, A. *et al.* Mfsd2a is critical for the formation and function of the blood-brain barrier. *Nature* (2014) doi:10.1038/nature13324.

108. Daneman, R., Zhou, L., Kebede, A. A. & Barres, B. A. Pericytes are required for blood–brain barrier integrity during embryogenesis. *Nature* **468**, 562–566 (2010).

109. Yao, Y., Chen, Z. L., Norris, E. H. & Strickland, S. Astrocytic laminin regulates pericyte differentiation and maintains blood brain barrier integrity. *Nat. Commun.* (2014) doi:10.1038/ncomms4413.

110. Sun, D., Lytle, C. & O'Donnell, M. E. IL-6 secreted by astroglial cells regulates Na-K-Cl cotransport in brain microvessel endothelial cells. *Am. J. Physiol. - Cell Physiol.* **272**, (1997).

111. Igarashi, Y. *et al.* Glial cell line-derived neurotrophic factor induces barrier function of endothelial cells forming the blood-brain barrier. *Biochem. Biophys. Res. Commun.* **261**, 108–112 (1999).

112. Sobue, K. *et al.* Induction of blood-brain barrier properties in immortalized bovine brain endothelial cells by astrocytic factors. *Neurosci. Res.* **35**, 155–164 (1999).

113. Frank, R. N., Dutta, S. & Mancini, M. A. Pericyte coverage is greater in the retinal than in the cerebral capillaries of the rat. *Investig. Ophthalmol. Vis. Sci.* (1987).

114. Hellström, M., Kalén, M., Lindahl, P., Abramsson, A. & Betsholtz, C. Role of PDGF-B and PDGFR-beta in recruitment of vascular smooth muscle cells and pericytes during embryonic blood vessel formation in the mouse. *Development* **126**, 3047–55 (1999).

115. Bell, R. D. *et al.* Pericytes Control Key Neurovascular Functions and Neuronal Phenotype in the Adult

Brain and during Brain Aging. *Neuron* **68**, 409–427 (2010).

116. Sá-Pereira, I., Brites, D. & Brito, M. A. Neurovascular Unit: a Focus on Pericytes. *Mol. Neurobiol.* **45**, 327–347 (2012).

117. Obermeier, B., Daneman, R. & Ransohoff, R. M. Development, maintenance and disruption of the blood-brain barrier. *Nat. Med.* **19**, 1584–1596 (2013).

118. Winkler, E. A., Bell, R. D. & Zlokovic, B. V. Central nervous system pericytes in health and disease. *Nature Neuroscience* vol. 14 1398–1405 (2011).

119. Pardridge, W. M. Drug transport across the blood-brain barrier. *Journal of Cerebral Blood Flow and Metabolism* (2012) doi:10.1038/jcbfm.2012.126.

120. Guemez-Gamboa, A. *et al.* Inactivating mutations in MFSD2A, required for omega-3 fatty acid transport in brain, cause a lethal microcephaly syndrome. *Nat. Genet.* (2015) doi:10.1038/ng.3311.

121. Winkler, E. A. *et al.* GLUT1 reductions exacerbate Alzheimer's disease vasculo-neuronal dysfunction and degeneration. *Nat. Neurosci.* (2015) doi:10.1038/nn.3966.

122. Vatine, G. D. *et al.* Modeling Psychomotor Retardation using iPSCs from MCT8-Deficient Patients Indicates a Prominent Role for the Blood-Brain Barrier. *Cell Stem Cell* (2017) doi:10.1016/j.stem.2017.04.002.

123. de Vivo, D. C. *et al.* Defective glucose transport across the blood-brain barrier as a cause of persistent hypoglycorrhachia, seizures, and developmental delay. *N. Engl. J. Med.* (1991) doi:10.1056/NEJM199109053251006.

124. Andreone, B. J. *et al.* Blood-Brain Barrier Permeability Is Regulated by Lipid Transport-Dependent Suppression of Caveolae-Mediated Transcytosis. *Neuron* (2017) doi:10.1016/j.neuron.2017.03.043.

125. Chow, B. W. & Gu, C. Gradual Suppression of Transcytosis Governs Functional Blood-Retinal Barrier Formation. *Neuron* (2017) doi:10.1016/j.neuron.2017.02.043.

126. Qian, Z. M., Li, H., Sun, H. & Ho, K. Targeted drug delivery via the transferrin receptor-mediated endocytosis pathway. *Pharmacological Reviews* vol. 54 561–587 (2002).

127. Tran, A. P., Warren, P. M. & Silver, J. The biology of regeneration failure and success after spinal cord injury. *Physiol. Rev.* **98**, 881–917 (2018).

128. Sharma, H. Pathophysiology of Blood-Spinal Cord Barrier in Traumatic Injury and Repair. *Curr. Pharm. Des.* **11**, 1353–1389 (2005).

129. Pan, W., Banks, W. A. & Kastin, A. J. Permeability of the blood-brain and blood-spinal cord barriers to interferons. *J. Neuroimmunol.* **76**, 105–111 (1997).

130. Prockop, L. D., Naidu, K. A., Binard, J. E. & Ransohoff, J. Selective permeability of [3H]-D-mannitol and [14C]-carboxyl-inulin across the blood-brain barrier and blood-spinal cord barrier in the rabbit. *J. Spinal Cord Med.* **18**, 221–226 (1995).

131. Ge, S. & Pachter, J. S. Isolation and culture of microvascular endothelial cells from murine spinal cord. *J. Neuroimmunol.* **177**, 209–214 (2006).

132. Winkler, E. A., Sengillo, J. D., Bell, R. D., Wang, J. & Zlokovic, B. V. Blood-spinal cord barrier pericyte reductions contribute to increased capillary permeability. *J. Cereb. Blood Flow Metab.* **32**, 1841–1852 (2012).

133. Griffin, J. H., Zlokovic, B. V. & Mosnier, L. O. Activated protein C: Biased for translation. *Blood* vol. 125 2898–2907 (2015).

134. Mautes, A. E., Weinzierl, M. R., Donovan, F. & Noble, L. J. Vascular events after spinal cord injury: contribution to secondary pathogenesis. *Phys. Ther.* **80**, 673–87 (2000).

135. Kramer, C. L. Vascular Disorders of the Spinal Cord. *Continuum (Minneap. Minn).* **24**, 407–426 (2018).

136. Sharma, H. S. Early microvascular reactions and blood–spinal cord barrier disruption are instrumental in pathophysiology of spinal cord injury and repair: novel therapeutic strategies including nanowired drug delivery to enhance neuroprotection. *J. Neural Transm.* **118**, 155–176 (2011).

137. Rubin, M. N. & Rabinstein, A. A. Vascular Diseases of the Spinal Cord. *Neurologic Clinics* vol. 31 153–181 (2013).

138. Santillan, A. *et al.* Vascular anatomy of the spinal cord. *J. Neurointerv. Surg.* **4**, 67–74 (2012).

139. Suh, T. H. Vascular system of the human spinal cord. *Arch. Neurol. Psychiatry* **41**, 659 (1939).

140. Felten, D. L., O'Banion, M. K. & Maida, M. S. Vasculature. in *Netter's Atlas of Neuroscience* vol. 58 93–124 (Elsevier, 2016).

141. James, S. L. *et al.* Global, regional, and national burden of traumatic brain injury and spinal cord injury, 1990–2016: a systematic analysis for the Global Burden of Disease Study 2016. *Lancet Neurol.* **18**, 56–87 (2019).

142. New, P. W. & Marshall, R. International Spinal Cord Injury Data Sets for non-traumatic spinal cord injury. *Spinal Cord* **52**, 123–132 (2014).

143. Spinal cord injury facts and figures at a glance. *J. Spinal Cord Med.* **35**, 197–198 (2012).

144. Ahuja, C. S. *et al.* Traumatic spinal cord injury. *Nat. Rev. Dis. Prim.* **3**, 17018 (2017).

145. Silva, N. A., Sousa, N., Reis, R. L. & Salgado, A. J. From basics to clinical: A comprehensive review on spinal cord injury. *Prog. Neurobiol.* **114**, 25–57 (2014).

146. Carlson, G. D. *et al.* Early time-dependent decompression for spinal cord injury: Vascular mechanisms of recovery. *J. Neurotrauma* **14**, 951–962 (1997).

147. Ryken, T. C. *et al.* The acute cardiopulmonary management of patients with cervical spinal cord injuries. *Neurosurgery* **72**, 84–92 (2013).

148. Braughler, J. M. & Hall, E. D. Effects of multi-dose methylprednisolone sodium succinate

administration on injured cat spinal cord neurofilament degradation and energy metabolism. *J. Neurosurg.* **61**, 290–295 (1984).

149. Hall, E. D. & Braughler, J. M. Effects of intravenous methylprednisolone on spinal cord lipid peroxidation and (Na+ + K+)-ATPase activity. *J. Neurosurg.* **57**, 247–253 (1982).

150. Bracken, M. B. *et al.* Administration of methylprednisolone for 24 or 48 hours or tirilazad mesylate for 48 hours in the treatment of acute spinal cord injury: Results of the Third National Acute Spinal Cord Injury randomized controlled trial. *J. Am. Med. Assoc.* (1997) doi:10.1097/00132586-199808000-00011.

151. Bracken, M. B. *et al.* A Randomized, Controlled Trial of Methylprednisolone or Naloxone in the Treatment of Acute Spinal-Cord Injury. *N. Engl. J. Med.* **322**, 1405–1411 (1990).

152. Eck, J. C., Nachtigall, D., Humphreys, S. C. & Hodges, S. D. Questionnaire Survey of Spine Surgeons on the Use of Methylprednisolone for Acute Spinal Cord Injury. *Spine (Phila. Pa. 1976).* **31**, E250–E253 (2006).

153. Bracken, M. B. Steroids for acute spinal cord injury. *Cochrane database Syst. Rev.* **1**, CD001046 (2012).

154. Sámano, C. & Nistri, A. Mechanism of Neuroprotection Against Experimental Spinal Cord Injury by Riluzole or Methylprednisolone. *Neurochem. Res.* **44**, 200–213 (2019).

155. Sandrow-Feinberg, H. R. & Houlé, J. D. Exercise after spinal cord injury as an agent for neuroprotection, regeneration and rehabilitation. *Brain Research* vol. 1619 12–21 (2015).

156. McDonald, J. W. & Sadowsky, C. Spinal-cord injury. in *Lancet* vol. 359 417–425 (Elsevier Limited, 2002).

157. Meister, R., Pasquier, M., Clerc, D. & Carron, P. N. Neurogenic shock. *Rev. Med. Suisse* **10**, 403–479 (2014).

158. Fitch, M. T., Doller, C., Combs, C. K., Landreth, G. E. & Silver, J. Cellular and molecular mechanisms of glial scarring and progressive cavitation: In vivo and in vitro analysis of inflammation-induced secondary injury after CNS trauma. *J. Neurosci.* **19**, 8182–8198 (1999).

159. Park, E., Velumian, A. A. & Fehlings, M. G. The role of excitotoxicity in secondary mechanisms of spinal cord injury: A review with an emphasis on the implications for white matter degeneration. *Journal of Neurotrauma* vol. 21 754–774 (2004).

160. Farooque, M., Hillered, L., Holtz, A. & Olsson, Y. Changes of extracellular levels of amino acids after graded compression trauma to the spinal cord: An experimental study in the rat using microdialysis. *J. Neurotrauma* (1996) doi:10.1089/neu.1996.13.537.

161. Liu, D., Xu, G. Y., Pan, E. & McAdoo, D. J. Neurotoxicity of glutamate at the concentration released upon spinal cord injury. *Neuroscience* (1999) doi:10.1016/S0306-4522(99)00278-X.

162. Scholpa, N. E. & Schnellmann, R. G. Mitochondrial-based therapeutics for the treatment of spinal cord injury: Mitochondrial biogenesis as a potential pharmacological target. *Journal of Pharmacology and Experimental Therapeutics* vol. 363 303–313 (2017).

163. Epstein, F. H., Lipton, S. A. & Rosenberg, P. A. Excitatory amino acids as a final common pathway for neurologic disorders. *New England Journal of Medicine* (1994) doi:10.1056/NEJM199403033300907.

164. Lu, J., Ashwell, K. W. S. & Waite, P. Advances in secondary spinal cord injury: Role of apoptosis. *Spine* (2000) doi:10.1097/00007632-200007150-00022.

165. Jia, Z. *et al.* Oxidative stress in spinal cord injury and antioxidant-based intervention. *Spinal Cord* **50**, 264–274 (2012).

166. Sullivan, P. G., Krishnamurthy, S., Patel, S. P., Pandya, J. D. & Rabchevsky, A. G. Temporal characterization of mitochondrial bioenergetics after spinal cord injury. *J. Neurotrauma* **24**, 991–999 (2007).

167. Bains, M. & Hall, E. D. Antioxidant therapies in traumatic brain and spinal cord injury. *Biochimica et Biophysica Acta - Molecular Basis of Disease* vol. 1822 675–684 (2012).

168. Rice, T., Larsen, J., Rivest, S. & Yong, V. W. Characterization of the early neuroinflammation after spinal cord injury in mice. *J. Neuropathol. Exp. Neurol.* **66**, 184–195 (2007).

169. Gadani, S. P., Walsh, J. T., Lukens, J. R. & Kipnis, J. Dealing with Danger in the CNS: The Response of the Immune System to Injury. *Neuron* (2015) doi:10.1016/j.neuron.2015.05.019.

170. Bradbury, E. J. & Burnside, E. R. Moving beyond the glial scar for spinal cord repair. *Nat. Commun.* **10**, 1–15 (2019).

171. Davalos, D. *et al.* ATP mediates rapid microglial response to local brain injury in vivo. *Nat. Neurosci.* **8**, 752–8 (2005).

172. Kataoka, A., Tozaki-Saitoh, H., Koga, Y., Tsuda, M. & Inoue, K. Activation of P2X 7 receptors induces CCL3 production in microglial cells through transcription factor NFAT. *J. Neurochem.* **108**, 115–125 (2009).

173. Panenka, W. *et al.* P2X7-like receptor activation in astrocytes increases chemokine monocyte chemoattractant protein-1 expression via mitogen-activated protein kinase. *J. Neurosci.* (2001) doi:10.1523/jneurosci.21-18-07135.2001.

174. Greenhalgh, A. D. & David, S. Differences in the phagocytic response of microglia and peripheral macrophages after spinal cord Injury and its effects on cell death. *J. Neurosci.* (2014) doi:10.1523/JNEUROSCI.4912-13.2014.

175. David, S. & Kroner, A. Repertoire of microglial and macrophage responses after spinal cord injury. *Nat. Rev. Neurosci.* **12**, 388–399 (2011).

176. Carlson, S. L., Parrish, M. E., Springer, J. E., Doty, K. & Dossett, L. Acute Inflammatory Response in Spinal Cord Following Impact Injury. *Exp. Neurol.* **151**, 77–88 (1998).

177. Gris, D. Transient Blockade of the CD11d/CD18 Integrin Reduces Secondary Damage after Spinal Cord Injury, Improving Sensory, Autonomic, and Motor Function. *J. Neurosci.* **24**, 4043–4051 (2004).

178. Summers, C. *et al.* Neutrophil kinetics in health and disease. *Trends Immunol.* **31**, 318–324 (2010).

179. Popovich, P. G., Wei, P. & Stokes, B. T. Cellular inflammatory response after spinal cord injury in sprague-dawley and lewis rats. *J. Comp. Neurol.* **377**, 443–464 (1997).

180. Busch, S. A., Horn, K. P., Silver, D. J. & Silver, J. Overcoming Macrophage-Mediated Axonal Dieback Following CNS Injury. *J. Neurosci.* **29**, 9967–9976 (2009).

181. Evans, T. A. *et al.* High-resolution intravital imaging reveals that blood-derived macrophages but not resident microglia facilitate secondary axonal dieback in traumatic spinal cord injury. *Exp. Neurol.* **254**, 109–120 (2014).

182. Horn, K. P., Busch, S. A., Hawthorne, A. L., Van Rooijen, N. & Silver, J. Another barrier to regeneration in the CNS: Activated macrophages induce extensive retraction of dystrophic axons through direct physical interactions. *J. Neurosci.* (2008) doi:10.1523/JNEUROSCI.2488-08.2008.

183. Chen, M. S. *et al.* Nogo-A is a myelin-associated neurite outgrowth inhibitor and an antigen for monoclonal antibody IN-1. *Nature* (2000) doi:10.1038/35000219.

184. McKerracher, L. *et al.* Identification of myelin-associated glycoprotein as a major myelin-derived inhibitor of neurite growth. *Neuron* **13**, 805–811 (1994).

185. Wang, K. C. *et al.* Oligodendrocyte-myelin glycoprotein is a Nogo receptor ligand that inhibits neurite outgrowth. *Nature* (2002) doi:10.1038/nature00867.

186. Filbin, M. T. Myelin-associated inhibitors of axonal regeneration in the adult mammalian CNS. *Nat. Rev. Neurosci.* **4**, 703–713 (2003).

187. Moreau-Fauvarque, C. *et al.* The transmembrane semaphorin Sema4D/CD100, an inhibitor of axonal growth, is expressed on oligodendrocytes and upregulated after CNS lesion. *J. Neurosci.* **23**, 9229–9239 (2003).

188. Benson, M. D. *et al.* Ephrin-B3 is a myelin-based inhibitor of neurite outgrowth. *Proc. Natl. Acad. Sci. U. S. A.* **102**, 10694–10699 (2005).

189. Duffy, P. *et al.* Myelin-derived ephrinB3 restricts axonal regeneration and recovery after adult CNS injury. *Proc. Natl. Acad. Sci. U. S. A.* **109**, 5063–5068 (2012).

190. Sartori, A. M., Hofer, A. S. & Schwab, M. E. Recovery after spinal cord injury is enhanced by anti-Nogo-A antibody therapy — from animal models to clinical trials. *Current Opinion in Physiology* vol. 14 1–6 (2020).

191. Kucher, K. *et al.* First-in-Man Intrathecal Application of Neurite Growth-Promoting Anti-Nogo-A

Antibodies in Acute Spinal Cord Injury. *Neurorehabil. Neural Repair* **32**, 578–589 (2018).

192. Schneider, M. P. *et al.* Anti-Nogo-A antibodies as a potential causal therapy for lower urinary tract dysfunction after spinal cord injury. *J. Neurosci.* **39**, 4066–4076 (2019).
193. Maier, I. C. *et al.* Differential effects of anti-Nogo-A antibody treatment and treadmill training in rats with incomplete spinal cord injury. *Brain* **132**, 1426–1440 (2009).
194. Chen, K. *et al.* Sequential therapy of anti-Nogo-A antibody treatment and treadmill training leads to cumulative improvements after spinal cord injury in rats. *Exp. Neurol.* **292**, 135–144 (2017).
195. Führmann, T., Anandakumaran, P. N. & Shoichet, M. S. Combinatorial Therapies After Spinal Cord Injury: How Can Biomaterials Help? *Adv. Healthc. Mater.* **6**, 1–21 (2017).
196. Koprivica, V. *et al.* Neuroscience: EGFR activation mediates inhibition of axon regeneration by myelin and chondroitin sulfate proteoglycans. *Science (80-.).* **310**, 106–110 (2005).
197. Dyck, S. M. *et al.* Chondroitin Sulfate Proteoglycans Negatively Modulate Spinal Cord Neural Precursor Cells by Signaling Through LAR and RPTPσ and Modulation of the Rho/ROCK Pathway. *Stem Cells* **33**, 2550–2563 (2015).
198. Adams, K. L. & Gallo, V. The diversity and disparity of the glial scar. *Nat. Neurosci.* **21**, 9–15 (2018).
199. Alizadeh, A., Dyck, S. M. & Karimi-Abdolrezaee, S. Traumatic Spinal Cord Injury: An Overview of Pathophysiology, Models and Acute Injury Mechanisms. *Front. Neurol.* **10**, (2019).
200. Goritz, C. *et al.* A Pericyte Origin of Spinal Cord Scar Tissue. *Science (80-.).* **333**, 238–242 (2011).
201. Dias, D. O. *et al.* Reducing Pericyte-Derived Scarring Promotes Recovery after Spinal Cord Injury. *Cell* (2018) doi:10.1016/j.cell.2018.02.004.
202. Soderblom, C. *et al.* Perivascular fibroblasts form the fibrotic scar after contusive spinal cord injury. *J. Neurosci.* **33**, 13882–13887 (2013).
203. Norenberg, M. D., Smith, J. & Marcillo, A. The pathology of human spinal cord injury: defining the problems. *J. Neurotrauma* **21**, 429–40 (2004).
204. Cregg, J. M. *et al.* Functional regeneration beyond the glial scar. *Experimental Neurology* (2014) doi:10.1016/j.expneurol.2013.12.024.
205. Huebner, E. A. & Strittmatter, S. M. Axon regeneration in the peripheral and central nervous systems. *Results Probl. Cell Differ.* **48**, 339–351 (2009).
206. Schwab, M. E. & Bartholdi, D. Degeneration and regeneration of axons in the lesioned spinal cord. *Physiol. Rev.* **76**, 319–370 (1996).
207. David, S. & Aguayo, A. Axonal elongation into peripheral nervous system 'bridges' after central nervous system injury in adult rats. *Science (80-.).* **214**, 931–933 (1981).
208. Anderson, M. A. *et al.* Astrocyte scar formation aids central nervous system axon regeneration. *Nature* **532**, 195–200 (2016).

209. Faulkner, J. R. Reactive Astrocytes Protect Tissue and Preserve Function after Spinal Cord Injury. *J. Neurosci.* **24**, 2143–2155 (2004).

210. Wanner, I. B. *et al.* Glial Scar Borders Are Formed by Newly Proliferated, Elongated Astrocytes That Interact to Corral Inflammatory and Fibrotic Cells via STAT3-Dependent Mechanisms after Spinal Cord Injury. *J. Neurosci.* **33**, 12870–12886 (2013).

211. Bush, T. G. *et al.* Leukocyte infiltration, neuronal degeneration, and neurite outgrowth after ablation of scar-forming, reactive astrocytes in adult transgenic mice. *Neuron* **23**, 297–308 (1999).

212. Bradbury, E. J. *et al.* Chondroitinase ABC promotes functional recovery after spinal cord injury. *Nature* (2002) doi:10.1038/416636a.

213. Barritt, A. W. *et al.* Chondroitinase ABC promotes sprouting of intact and injured spinal systems after spinal cord injury. *J. Neurosci.* (2006) doi:10.1523/JNEUROSCI.2980-06.2006.

214. Grimpe, B. A Novel DNA Enzyme Reduces Glycosaminoglycan Chains in the Glial Scar and Allows Microtransplanted Dorsal Root Ganglia Axons to Regenerate beyond Lesions in the Spinal Cord. *J. Neurosci.* **24**, 1393–1397 (2004).

215. Takeuchi, K. *et al.* Chondroitin sulphate N-acetylgalactosaminyl-transferase-1 inhibits recovery from neural injury. *Nat. Commun.* (2013) doi:10.1038/ncomms3740.

216. Lang, B. T. *et al.* Modulation of the proteoglycan receptor PTPσ promotes recovery after spinal cord injury. *Nature* (2015) doi:10.1038/nature13974.

217. Fisher, D. *et al.* Leukocyte common antigen-related phosphatase is a functional receptor for chondroitin sulfate proteoglycan axon growth inhibitors. *J. Neurosci.* (2011) doi:10.1523/JNEUROSCI.1737-11.2011.

218. Hu, H. Z., Granger, N., Balakrishna Pai, S., Bellamkonda, R. V. & Jeffery, N. D. Therapeutic efficacy of microtube-embedded chondroitinase ABC in a canine clinical model of spinal cord injury. *Brain* (2018) doi:10.1093/brain/awy007.

219. Fehlings, M. G. & Tator, C. H. The relationships among the severity of spinal cord injury, residual neurological function, axon counts, and counts of retrogradely labeled neurons after experimental spinal cord injury. *Exp. Neurol.* (1995) doi:10.1016/0014-4886(95)90027-6.

220. Kotter, M. R., Li, W. W., Zhao, C. & Franklin, R. J. M. Myelin impairs CNS remyelination by inhibiting oligodendrocyte precursor cell differentiation. *J. Neurosci.* (2006) doi:10.1523/JNEUROSCI.2615-05.2006.

221. Syed, Y. A. *et al.* Antibody-mediated neutralization of myelin-associated EphrinB3 accelerates CNS remyelination. *Acta Neuropathol.* (2016) doi:10.1007/s00401-015-1521-1.

222. Balentine, J. D. Pathology of experimental spinal cord trauma. I. The necrotic lesion as a function of vascular injury. *Lab. Investig.* (1978).

223. Mihai, G. *et al.* Longitudinal comparison of two severities of unilateral cervical spinal cord injury using magnetic resonance imaging in rats. *J. Neurotrauma* **25**, 1–18 (2008).

224. Noble, L. J. & Wrathall, J. R. Distribution and time course of protein extravasation in the rat spinal cord after contusive injury. *Brain Res.* **482**, 57–66 (1989).

225. Sinescu, C. *et al.* Molecular basis of vascular events following spinal cord injury. *J. Med. Life* **3**, 254–261 (2010).

226. Li, Y. *et al.* Pericytes impair capillary blood flow and motor function after chronic spinal cord injury. *Nat. Med.* **23**, 733–741 (2017).

227. Popa, C. *et al.* Vascular dysfunctions following spinal cord injury. *J. Med. Life* **3**, 275–85 (2010).

228. Krassioukov, A. V. *et al.* Assessment of autonomic dysfunction following spinal cord injury: Rationale for additions to international standards for neurological assessment. in *Journal of Rehabilitation Research and Development* vol. 44 103–112 (J Rehabil Res Dev, 2007).

229. Krassioukov, A. & Claydon, V. E. The clinical problems in cardiovascular control following spinal cord injury: An overview. in *Progress in Brain Research* vol. 152 223–229 (Elsevier, 2006).

230. Furlan, J. C., Fehlings, M. G., Shannon, P., Norenberg, M. D. & Krassioukov, A. V. Descending Vasomotor Pathways in Humans: Correlation between Axonal Preservation and Cardiovascular Dysfunction after Spinal Cord Injury. *J. Neurotrauma* (2003) doi:10.1089/089771503322686148.

231. Ellaway, P. H. *et al.* Towards improved clinical and physiological assessments of recovery in spinal cord injury: a clinical initiative. *Spinal Cord* **42**, 325–337 (2004).

232. Mackiewicz-Milewska, M. *et al.* Deep venous thrombosis in patients with chronic spinal cord injury. *J. Spinal Cord Med.* **39**, 400–404 (2016).

233. Green, D., Rossi, E. C., Yao, J. S. T., Flinn, W. R. & Spies, S. M. Deep vein thrombosis in spinal cord injury: Effect of prophylaxis with calf compression, aspirin, and dipyridamole. *Paraplegia* **20**, 227–234 (1982).

234. Rebhun, J., Madorsky, J. G. B. & Glovsky, M. M. Proteins of the complement system and acute phase reactants in sera of patients with spinal cord injury. *Ann. Allergy* **66**, 335–338 (1991).

235. Garcia, E., Aguilar-Cevallos, J., Silva-Garcia, R. & Ibarra, A. Cytokine and Growth Factor Activation In Vivo and In Vitro after Spinal Cord Injury. (2016) doi:10.1155/2016/9476020.

236. Adams, R. A. *et al.* The fibrin-derived γ377-395 peptide inhibits microglia activation and suppresses relapsing paralysis in central nervous system autoimmune disease. *J. Exp. Med.* (2007) doi:10.1084/jem.20061931.

237. Schachtrup, C. *et al.* Fibrinogen Triggers Astrocyte Scar Formation by Promoting the Availability of Active TGF- after Vascular Damage. *J. Neurosci.* **30**, 5843–5854 (2010).

238. Pan, W. & Kastin, A. Cytokine Transport Across the Injured Blood-Spinal Cord Barrier. *Curr. Pharm.*

Des. **14**, 1620–1624 (2008).

239. Kerr, B. J. & Patterson, P. H. Potent pro-inflammatory actions of leukemia inhibitory factor in the spinal cord of the adult mouse. *Exp. Neurol.* (2004) doi:10.1016/j.expneurol.2004.04.012.

240. Azari, M. F. *et al.* Leukemia inhibitory factor arrests oligodendrocyte death and demyelination in spinal cord injury. *J. Neuropathol. Exp. Neurol.* (2006) doi:10.1097/01.jnen.0000235855.77716.25.

241. Kerr, B. J. & Patterson, P. H. Leukemia inhibitory factor promotes oligodendrocyte survival after spinal cord injury. *Glia* **51**, 73–79 (2005).

242. Whetstone, W. D., Hsu, J. Y. C., Eisenberg, M., Werb, Z. & Noble-Haeusslein, L. J. Blood-spinal cord barrier after spinal cord injury: Relation to revascularization and wound healing. *J. Neurosci. Res.* **74**, 227–239 (2003).

243. Kumar, H., Ropper, A. E., Lee, S. H. & Han, I. Propitious Therapeutic Modulators to Prevent Blood-Spinal Cord Barrier Disruption in Spinal Cord Injury. *Mol. Neurobiol.* **54**, 3578–3590 (2017).

244. Lee, J. Y., Choi, H. Y., Ahn, H. J., Ju, B. G. & Yune, T. Y. Matrix metalloproteinase-3 promotes early blood-spinal cord barrier disruption and hemorrhage and impairs long-term neurological recovery after spinal cord injury. *Am. J. Pathol.* **184**, 2985–3000 (2014).

245. De Castro, R., Burns, C. L., McAdoo, D. J. & Romanic, A. M. Metalloproteinase increases in the injured rat spinal cord. *Neuroreport* **11**, 3551–3554 (2000).

246. Noble, L. J., Donovan, F., Igarashi, T., Goussev, S. & Werb, Z. Matrix metalloproteinases limit functional recovery after spinal cord injury by modulation of early vascular events. *J. Neurosci.* **22**, 7526–35 (2002).

247. Kumar, H. *et al.* Matrix Metalloproteinase-8 Inhibition Prevents Disruption of Blood–Spinal Cord Barrier and Attenuates Inflammation in Rat Model of Spinal Cord Injury. *Mol. Neurobiol.* **55**, 2577–2590 (2018).

248. Wells, J. E. A. *et al.* An Adverse Role for Matrix Metalloproteinase 12 after Spinal Cord Injury in Mice. *J. Neurosci.* **23**, 10107–10115 (2003).

249. Hsu, J.-Y. C. *et al.* Matrix Metalloproteinase-2 Facilitates Wound Healing Events That Promote Functional Recovery after Spinal Cord Injury. *J. Neurosci.* **26**, 9841–9850 (2006).

250. Trivedi, A. *et al.* Deficiency in matrix metalloproteinase-2 results in long-term vascular instability and regression in the injured mouse spinal cord. *Exp. Neurol.* **284**, 50–62 (2016).

251. Ritz, M.-F., Graumann, U., Gutierrez, B. & Hausmann, O. Traumatic spinal cord injury alters angiogenic factors and TGF-beta1 that may affect vascular recovery. *Curr. Neurovasc. Res.* **7**, 301–10 (2010).

252. Herrera, J. J., Sundberg, L. M., Zentilin, L., Giacca, M. & Narayana, P. A. Sustained expression of vascular endothelial growth factor and angiopoietin-1 improves blood-spinal cord barrier integrity and functional recovery after spinal cord injury. *J. Neurotrauma* **27**, 2067–76 (2010).

253. Durham-Lee, J. C., Wu, Y., Mokkapati, V. U. L., Paulucci-Holthauzen, A. A. & Nesic, O. Induction of angiopoietin-2 after spinal cord injury. *Neuroscience* **202**, 454–464 (2012).

254. Ng, M. T. L., Stammers, A. T. & Kwon, B. K. Vascular Disruption and the Role of Angiogenic Proteins After Spinal Cord Injury. *Transl. Stroke Res.* **2**, 474–491 (2011).

255. Kumar, H. *et al.* Neutrophil elastase inhibition effectively rescued angiopoietin-1 decrease and inhibits glial scar after spinal cord injury. *Acta Neuropathol. Commun.* **6**, 1–18 (2018).

256. Mckenzie, A. L., Hall, J. J., Aihara, N., Fukuda, K. & Noble, L. J. Immunolocalization of Endothelin in the Traumatized Spinal Cord: Relationship to Blood–Spinal Cord Barrier Breakdown. *J. Neurotrauma* **12**, 257–268 (1995).

257. Macrae, I. M., Robinson, M. J., Graham, D. I., Reid, J. L. & McCulloch, J. Endothelin-1-Induced Reductions in Cerebral Blood Flow: Dose Dependency, Time Course, and Neuropathological Consequences. *J. Cereb. Blood Flow Metab.* **13**, 276–284 (1993).

258. Armstead, W. M. Role of endothelin in pial artery vasoconstriction and altered responses to vasopressin after brain injury. *J. Neurosurg.* **85**, 901–907 (1996).

259. Bartanusz, V., Jezova, D., Alajajian, B. & Digicaylioglu, M. The blood-spinal cord barrier: morphology and clinical implications. *Ann. Neurol.* **70**, 194–206 (2011).

260. Figley, S. A., Khosravi, R., Legasto, J. M., Tseng, Y.-F. & Fehlings, M. G. Characterization of Vascular Disruption and Blood–Spinal Cord Barrier Permeability following Traumatic Spinal Cord Injury. *J. Neurotrauma* **31**, 541–552 (2014).

261. Popovich, P. G., Horner, P. J., Mullin, B. B. & Stokes, B. T. A Quantitative Spatial Analysis of the Blood–Spinal Cord Barrier. *Exp. Neurol.* **142**, 258–275 (1996).

262. Tatar, I., Chou, P. C., Desouki, M. M., El Sayed, H. & Bilgen, M. Evaluating regional blood spinal cord barrier dysfunction following spinal cord injury using longitudinal dynamic contrast-enhanced MRI. *BMC Med. Imaging* **9**, 10 (2009).

263. Casella, G. T. B., Marcillo, A., Bunge, M. B. & Wood, P. M. New vascular tissue rapidly replaces neural parenchyma and vessels destroyed by a contusion injury to the rat spinal cord. *Exp. Neurol.* **173**, 63–76 (2002).

264. Loy, D. N. *et al.* Temporal progression of angiogenesis and basal lamina deposition after contusive spinal cord injury in the adult rat. *J. Comp. Neurol.* **445**, 308–324 (2002).

265. Dray, C., Rougon, G. & Debarbieux, F. Quantitative analysis by in vivo imaging of the dynamics of vascular and axonal networks in injured mouse spinal cord. *Proc. Natl. Acad. Sci. U. S. A.* **106**, 9459–64 (2009).

266. Xu, J. *et al.* Ultrastructural features of neurovascular units in a rat model of chronic compressive spinal cord injury. *Front. Neuroanat.* **11**, 1–14 (2018).

267. Ni, S. *et al.* UTX/KDM6A Deletion Promotes Recovery of Spinal Cord Injury by Epigenetically Regulating Vascular Regeneration. *Mol. Ther.* **27**, 2134–2146 (2019).

268. Benton, R. L. *et al.* Transcriptomic Screening of Microvascular Endothelial Cells Implicates Novel Molecular Regulators of Vascular Dysfunction after Spinal Cord Injury. *J. Cereb. Blood Flow Metab.* **28**, 1771–1785 (2008).

269. Zhou, T. *et al.* Microvascular endothelial cells engulf myelin debris and promote macrophage recruitment and fibrosis after neural injury. *Nat. Neurosci.* **22**, 421–435 (2019).

270. Dray, C., Rougon, G. & Debarbieux, F. Quantitative analysis by in vivo imaging of the dynamics of vascular and axonal networks in injured mouse spinal cord. *Proc. Natl. Acad. Sci.* **106**, 9459–9464 (2009).

271. Kaneko, S. *et al.* A selective Sema3A inhibitor enhances regenerative responses and functional recovery of the injured spinal cord. *Nat. Med.* **12**, 1380–1389 (2007).

272. Glaser, J., Gonzalez, R., Sadr, E. & Keirstead, H. S. Neutralization of the chemokine CXCL10 reduces apoptosis and increases axon sprouting after spinal cord injury. *J. Neurosci. Res.* **84**, 724–34 (2006).

273. Duan, H. *et al.* Transcriptome analyses reveal molecular mechanisms underlying functional recovery after spinal cord injury. *Proc. Natl. Acad. Sci.* **112**, 201510176 (2015).

274. Badner, A. *et al.* Early Intravenous Delivery of Human Brain Stromal Cells Modulates Systemic Inflammation and Leads to Vasoprotection in Traumatic Spinal Cord Injury. *Stem Cells Transl. Med.* **5**, 991–1003 (2016).

275. Ropper, A. E. *et al.* Defining recovery neurobiology of injured spinal cord by synthetic matrix-assisted hMSC implantation. *Proc. Natl. Acad. Sci.* 201616340 (2017) doi:10.1073/pnas.1616340114.

276. Chio, J. C. T. *et al.* The effects of human immunoglobulin G on enhancing tissue protection and neurobehavioral recovery after traumatic cervical spinal cord injury are mediated through the neurovascular unit. *J. Neuroinflammation* **16**, 1–18 (2019).

277. Vawda, R. *et al.* Early Intravenous Infusion of Mesenchymal Stromal Cells Exerts a Tissue Source Age-Dependent Beneficial Effect on Neurovascular Integrity and Neurobehavioral Recovery After Traumatic Cervical Spinal Cord Injury. *Stem Cells Transl. Med.* **8**, 639–649 (2019).

278. Widenfalk, J. *et al.* Vascular endothelial growth factor improves functional outcome and decreases secondary degeneration in experimental spinal cord contusion injury. *Neuroscience* **120**, 951–960 (2003).

279. Hu, J., Zeng, L., Huang, J., Wang, G. & Lu, H. MiR-126 promotes angiogenesis and attenuates inflammation after contusion spinal cord injury in rats. *Brain Res.* **1608**, 191–202 (2015).

280. Han, S. *et al.* Rescuing vasculature with intravenous angiopoietin-1 and αvβ3 integrin peptide is protective after spinal cord injury. *Brain* **133**, 1026–1042 (2010).

281. Kim, H. M., Hwang, D. H., Lee, J. E., Kim, S. U. & Kim, B. G. Ex vivo VEGF delivery by neural stem cells enhances proliferation of glial progenitors, angiogenesis, and tissue sparing after spinal cord injury. *PLoS One* **4**, e4987 (2009).

282. De Laporte, L. *et al.* Vascular endothelial growth factor and fibroblast growth factor 2 delivery from spinal cord bridges to enhance angiogenesis following injury. *J. Biomed. Mater. Res. - Part A* **98 A**, 372–382 (2011).

283. Kang, C. E., Baumann, M. D., Tator, C. H. & Shoichet, M. S. Localized and Sustained Delivery of Fibroblast Growth Factor-2 from a Nanoparticle-Hydrogel Composite for Treatment of Spinal Cord Injury. *Cells Tissues Organs* **197**, 55–63 (2013).

284. Des Rieux, A. *et al.* Vascular endothelial growth factor-loaded injectable hydrogel enhances plasticity in the injured spinal cord. *J. Biomed. Mater. Res. - Part A* **102**, 2345–2355 (2014).

285. Yu, S. *et al.* Angiogenic microspheres promote neural regeneration and motor function recovery after spinal cord injury in rats. *Sci. Rep.* **6**, 33428 (2016).

286. Liu, Y. *et al.* An engineered transcription factor which activates VEGF-A enhances recovery after spinal cord injury. *Neurobiol. Dis.* **37**, 384–393 (2010).

287. Benton, R. L. & Whittemore, S. R. VEGF165 therapy exacerbates secondary damage following spinal cord injury. *Neurochem. Res.* **28**, 1693–703 (2003).

288. Patel, C. B. *et al.* Effect of VEGF treatment on the blood-spinal cord barrier permeability in experimental spinal cord injury: Dynamic contrast-enhanced magnetic resonance imaging. *J. Neurotrauma* (2009) doi:10.1089/neu.2008.0860.

289. Bartholdi, D., Rubin, B. P. & Schwab, M. E. VEGF mRNA Induction Correlates With Changes in the Vascular Architecture Upon Spinal Cord Damage in the Rat. *Eur. J. Neurosci.* **9**, 2549–2560 (1997).

290. Lutton, C. *et al.* Combined VEGF and PDGF Treatment Reduces Secondary Degeneration after Spinal Cord Injury. *J. Neurotrauma* **29**, 957–970 (2012).

291. Wong, A. L. *et al.* Tie2 expression and phosphorylation in angiogenic and quiescent adult tissues. *Circ. Res.* **81**, 567–74 (1997).

292. Fish, J. E. *et al.* miR-126 Regulates Angiogenic Signaling and Vascular Integrity. *Dev. Cell* (2008) doi:10.1016/j.devcel.2008.07.008.

293. Assinck, P., Duncan, G. J., Hilton, B. J., Plemel, J. R. & Tetzlaff, W. Cell transplantation therapy for spinal cord injury. *Nat. Neurosci.* **20**, 637–647 (2017).

294. Richardson, P. M., Issa, V. M. K. & Aguayo, A. J. Regeneration of long spinal axons in the rat. *J. Neurocytol.* **13**, 165–82 (1984).

295. Temple, S. Division and differentiation of isolated CNS blast cells in microculture. *Nature* (1989) doi:10.1038/340471a0.

296. Gage, F. H. Mammalian neural stem cells. *Science* (2000) doi:10.1126/science.287.5457.1433.

297. Björklund, A. & Lindvall, O. Cell replacement therapies for central nervous system disorders. *Nat. Neurosci.* **3**, 537–44 (2000).

298. Freed, C. R. *et al.* Transplantation of human fetal dopamine cells for Parkinson's disease. Results at 1 year. *Arch. Neurol.* **47**, 505–12 (1990).

299. Freeman, T. B. *et al.* Transplanted fetal striatum in Huntington's disease: phenotypic development and lack of pathology. *Proc. Natl. Acad. Sci. U. S. A.* **97**, 13877–82 (2000).

300. Bregman, B. S. *et al.* Recovery of Function after Spinal Cord Injury: Mechanisms Underlying Transplant-Mediated Recovery of Function Differ after Spinal Cord Injury in Newborn and Adult Rats. *Exp. Neurol.* **123**, 3–16 (1993).

301. Wirth, E. D. *et al.* Feasibility and safety of neural tissue transplantation in patients with syringomyelia. *J. Neurotrauma* (2001) doi:10.1089/089771501750451839.

302. Takahashi, K. & Yamanaka, S. Induction of pluripotent stem cells from mouse embryonic and adult fibroblast cultures by defined factors. *Cell* **126**, 663–76 (2006).

303. Tsuji, O. *et al.* Therapeutic potential of appropriately evaluated safe-induced pluripotent stem cells for spinal cord injury. *Proc. Natl. Acad. Sci.* **107**, 12704–12709 (2010).

304. Lu, P. *et al.* Long-Distance Axonal Growth from Human Induced Pluripotent Stem Cells after Spinal Cord Injury. *Neuron* (2014) doi:10.1016/j.neuron.2014.07.014.

305. Nori, S. *et al.* Grafted human-induced pluripotent stem-cell-derived neurospheres promote motor functional recovery after spinal cord injury in mice. *Proc. Natl. Acad. Sci.* **108**, 16825–16830 (2011).

306. Tsuji, O. *et al.* Concise Review: Laying the Groundwork for a First-In-Human Study of an Induced Pluripotent Stem Cell-Based Intervention for Spinal Cord Injury. *Stem Cells* (2019) doi:10.1002/stem.2926.

307. Lu, P. *et al.* Long-Distance Growth and Connectivity of Neural Stem Cells after Severe Spinal Cord Injury. *Cell* **150**, 1264–1273 (2012).

308. Cummings, B. J. *et al. Human neural stem cells differentiate and promote locomotor recovery in spinal cord-injured mice*. *PNAS* vol. 102 www.pnas.orgcgidoi10.1073pnas.0507063102 (2005).

309. Keirstead, H. S. *et al.* Human embryonic stem cell-derived oligodendrocyte progenitor cell transplants remyelinate and restore locomotion after spinal cord injury. *J. Neurosci.* **25**, 4694–4705 (2005).

310. Sharp, J., Frame, J., Siegenthaler, M., Nistor, G. & Keirstead, H. S. Human embryonic Stem Cell-Derived Oligodendrocyte Progenitor Cell Transplants Improve Recovery after Cervical Spinal Cord Injury. *Stem Cells* **28**, N/A-N/A (2009).

311. Kamei, N. *et al.* Contribution of bone marrow-derived endothelial progenitor cells to neovascularization and astrogliosis following spinal cord injury. *J. Neurosci. Res.* **90**, 2281–2292 (2012).

312. Kamei, N. *et al.* Ex-vivo expanded human blood-derived CD133+ cells promote repair of injured spinal cord. *J. Neurol. Sci.* **328**, 41–50 (2013).

313. Nakajima, H. *et al.* Transplantation of mesenchymal stem cells promotes an alternative pathway of macrophage activation and functional recovery after spinal cord injury. *J. Neurotrauma* **29**, 1614–1625 (2012).

314. Silvestro, S., Bramanti, P., Trubiani, O. & Mazzon, E. Stem cells therapy for spinal cord injury: An overview of clinical trials. *International Journal of Molecular Sciences* vol. 21 (2020).

315. Asahara, T. *et al.* Isolation of putative progenitor endothelial cells for angiogenesis. *Science* **275**, 964–7 (1997).

316. Hill, J. M. *et al.* Circulating endothelial progenitor cells, vascular function, and cardiovascular risk. *N. Engl. J. Med.* **348**, 593–600 (2003).

317. Fadini, G. P., Losordo, D. & Dimmeler, S. Critical reevaluation of endothelial progenitor cell phenotypes for therapeutic and diagnostic use. *Circ. Res.* **110**, 624–37 (2012).

318. Farinacci, M. *et al.* Circulating endothelial cells as biomarker for cardiovascular diseases. *Res. Pract. Thromb. Haemost.* **3**, 49–58 (2019).

319. Seow, M., Chong, K., Ng, W. K., Kok, J. & Chan, Y. Tissue Engineering and Regenerative Medicine Concise Review: Endothelial Progenitor Cells in Regenerative Medicine: Applications and Challenges. doi:10.5966/sctm.2015-0227.

320. Keighron, C., Lyons, C. J., Creane, M., O'Brien, T. & Liew, A. Recent advances in endothelial progenitor cells toward their use in clinical translation. *Front. Med.* **5**, 354 (2018).

321. Yuan, X. *et al.* Systemic microcirculation dysfunction after low thoracic spinal cord injury in mice. *Life Sci.* **221**, 47–55 (2019).

322. Kamei, N. *et al.* Endothelial progenitor cells promote astrogliosis following spinal cord injury through Jagged1-dependent notch signaling. *J. Neurotrauma* **29**, 1758–1769 (2012).

323. Rauch, M. F. *et al.* Engineering angiogenesis following spinal cord injury: A coculture of neural progenitor and endothelial cells in a degradable polymer implant leads to an increase in vessel density and formation of the blood-spinal cord barrier. *European Journal of Neuroscience* vol. 29 132–145 (2009).

324. Yamamoto, S. *et al.* Transcription Factor Expression and Notch-Dependent Regulation of Neural Progenitors in the Adult Rat Spinal Cord. *J. Neurosci.* **21**, 9814–9823 (2001).

325. Friedenstein, A. J., Piatetzky-Shapiro, I. & Petrakova, & K. V. *Osteogenesis in transplants of bone marrow cells. Embryol. exp. Morph* vol. 16 (1966).

326. Friedenstein, A. J., Chailakhjan, R. K. & Lalykina, K. S. The development of fibroblast colonies in monolayer cultures of guinea-pig bone marrow and spleen cells. *Cell Tissue Kinet.* **3**, 393–403 (1970).

327. Bronckaers, A. *et al.* Mesenchymal stem/stromal cells as a pharmacological and therapeutic approach to accelerate angiogenesis. *Pharmacol. Ther.* **143**, 181–196 (2014).

328. Pittenger, M. F. *et al.* Multilineage potential of adult human mesenchymal stem cells. *Science* **284**, 143–7 (1999).

329. Meyerrose, T. *et al.* Mesenchymal stem cells for the sustained in vivo delivery of bioactive factors. *Adv. Drug Deliv. Rev.* **62**, 1167–1174 (2010).

330. Dominici, M. *et al.* Minimal criteria for defining multipotent mesenchymal stromal cells. The International Society for Cellular Therapy position statement. *Cytotherapy* **8**, 315–7 (2006).

331. Macrin, D., Joseph, J. P., Pillai, A. A. & Devi, A. Eminent Sources of Adult Mesenchymal Stem Cells and Their Therapeutic Imminence. *Stem cell Rev. reports* **13**, 741–756 (2017).

332. De Ugarte, D. A. *et al.* Comparison of multi-lineage cells from human adipose tissue and bone marrow. *Cells Tissues Organs* (2003) doi:10.1159/000071150.

333. Zuk, P. A. *et al.* Multilineage cells from human adipose tissue: Implications for cell-based therapies. in *Tissue Engineering* (2001). doi:10.1089/107632701300062859.

334. Han, Y. *et al.* Mesenchymal Stem Cells for Regenerative Medicine. *Cells* **8**, (2019).

335. Uccelli, A., Moretta, L. & Pistoia, V. Mesenchymal stem cells in health and disease. *Nature Reviews Immunology* vol. 8 726–736 (2008).

336. Andrzejewska, A., Lukomska, B. & Janowski, M. Concise Review: Mesenchymal Stem Cells: From Roots to Boost. *Stem Cells* **37**, 855–864 (2019).

337. Japan should put the brakes on stem-cell sales. *Nature* vol. 565 535–536 (2019).

338. Cofano, F. *et al.* Mesenchymal stem cells for spinal cord injury: Current options limitations, and future of cell therapy. *International Journal of Molecular Sciences* vol. 20 (2019).

339. Rosocha, an, Vanick, I., JergováJergov, S. & Cížek, M. Transplants of Human Mesenchymal Stem Cells Improve Functional Recovery After Spinal Cord Injury in the Rat. *Cell. Mol. Neurobiol.* **26**,.

340. Osaka, M. *et al.* Intravenous administration of mesenchymal stem cells derived from bone marrow after contusive spinal cord injury improves functional outcome. *Brain Res.* **1343**, 226–235 (2010).

341. Yang, C. *et al.* Repeated injections of human umbilical cord blood-derived mesenchymal stem cells significantly promotes functional recovery in rabbits with spinal cord injury of two noncontinuous segments. *Stem Cell Res. Ther.* **9**, (2018).

342. Hakim, R. *et al.* Mesenchymal stem cells transplanted into spinal cord injury adopt immune cell-like characteristics. *Stem Cell Res. Ther.* **10**, (2019).

343. Morita, T. *et al.* Intravenous infusion of mesenchymal stem cells promotes functional recovery in a model of chronic spinal cord injury. *Neuroscience* **335**, 221–231 (2016).

344. Oshigiri, T. *et al.* Intravenous infusion of mesenchymal stem cells alters motor cortex gene expression

in a rat model of acute spinal cord injury. *J. Neurotrauma* **36**, 411–420 (2019).

345. Salgado, A. J. *et al.* Mesenchymal stem cells secretome as a modulator of the neurogenic niche: basic insights and therapeutic opportunities. *Front. Cell. Neurosci.* **9**, (2015).

346. Eleuteri, S. & Fierabracci, A. Insights into the secretome of mesenchymal stem cells and its potential applications. *International Journal of Molecular Sciences* vol. 20 (2019).

347. Watt, S. M. *et al.* The angiogenic properties of mesenchymal stem/stromal cells and their therapeutic potential. *Br. Med. Bull.* **108**, 25–53 (2013).

348. Merfeld-Clauss, S., Gollahalli, N., March, K. L. & Traktuev, D. O. Adipose tissue progenitor cells directly interact with endothelial cells to induce vascular network formation. *Tissue Eng. - Part A* (2010) doi:10.1089/ten.tea.2009.0635.

349. Verseijden, F. *et al.* Adult Human Bone Marrow– and Adipose Tissue–Derived Stromal Cells Support the Formation of Prevascular-like Structures from Endothelial Cells In Vitro. *Tissue Eng. Part A* **16**, 101–114 (2010).

350. Rohringer, S. *et al.* Mechanisms of vasculogenesis in 3D fibrin matrices mediated by the interaction of adipose-derived stem cells and endothelial cells. *Angiogenesis* (2014) doi:10.1007/s10456-014-9439-0.

351. Tao, H., Han, Z., Han, Z. C. & Li, Z. Proangiogenic Features of Mesenchymal Stem Cells and Their Therapeutic Applications. *Stem Cells International* (2016) doi:10.1155/2016/1314709.

352. Stapor, P. C., Sweat, R. S., Dashti, D. C., Betancourt, A. M. & Murfee, W. L. Pericyte Dynamics during Angiogenesis: New Insights from New Identities. *J. Vasc. Res.* **51**, 163–174 (2014).

353. Kim, S.-W., Zhang, H.-Z., Guo, L., Kim, J.-M. & Kim, M. H. Amniotic mesenchymal stem cells enhance wound healing in diabetic NOD/SCID mice through high angiogenic and engraftment capabilities. *PLoS One* **7**, e41105 (2012).

354. Kim, S.-W. *et al.* Amniotic mesenchymal stem cells have robust angiogenic properties and are effective in treating hindlimb ischaemia. *Cardiovasc. Res.* **93**, 525–34 (2012).

355. Matsuda, K. *et al.* Adipose-Derived Stem Cells Promote Angiogenesis and Tissue Formation for In Vivo Tissue Engineering. *Tissue Eng. Part A* **19**, 1327–1335 (2013).

356. Rubina, K. *et al.* Adipose stromal cells stimulate angiogenesis via promoting progenitor cell differentiation, secretion of angiogenic factors, and enhancing vessel maturation. *Tissue Eng. - Part A* (2009) doi:10.1089/ten.tea.2008.0359.

357. Zhang, N., Li, J., Luo, R., Jiang, J. & Wang, J. A. Bone marrow mesenchymal stem cells induce angiogenesis and attenuate the remodeling of diabetic cardiomyopathy. *Exp. Clin. Endocrinol. Diabetes* (2008) doi:10.1055/s-2007-985154.

358. Kachgal, S. & Putnam, A. J. Mesenchymal stem cells from adipose and bone marrow promote

angiogenesis via distinct cytokine and protease expression mechanisms. *Angiogenesis* (2011) doi:10.1007/s10456-010-9194-9.

359. Edwards, S. S. *et al.* Functional analysis reveals angiogenic potential of human mesenchymal stem cells from Wharton's jelly in dermal regeneration. *Angiogenesis* **17**, 851–866 (2014).
360. Choi, M. *et al.* Proangiogenic features of Wharton's jelly-derived mesenchymal stromal/stem cells and their ability to form functional vessels. *Int. J. Biochem. Cell Biol.* (2013) doi:10.1016/j.biocel.2012.12.001.
361. Gandia, C. *et al.* Human Dental Pulp Stem Cells Improve Left Ventricular Function, Induce Angiogenesis, and Reduce Infarct Size in Rats with Acute Myocardial Infarction. *Stem Cells* **26**, 638–645 (2008).
362. Bronckaers, A. *et al.* Angiogenic Properties of Human Dental Pulp Stem Cells. *PLoS One* **8**, e71104 (2013).
363. Matsushita, T. *et al.* Diffuse and persistent blood–spinal cord barrier disruption after contusive spinal cord injury rapidly recovers following intravenous infusion of bone marrow mesenchymal stem cells. *Exp. Neurol.* **267**, 152–164 (2015).
364. Zeng, X. *et al.* Bone marrow mesenchymal stem cells in a three-dimensional gelatin sponge scaffold attenuate inflammation, promote angiogenesis, and reduce cavity formation in experimental spinal cord injury. *Cell Transplant.* **20**, 1881–99 (2011).
365. Quertainmont, R. *et al.* Mesenchymal stem cell graft improves recovery after spinal cord injury in adult rats through neurotrophic and pro-angiogenic actions. *PLoS One* **7**, 39500 (2012).
366. Mostafa Mtairag, E. *et al.* Effects of interleukin-10 on monocyte/endothelial cell adhesion and MMP-9/TIMP-1 secretion. *Cardiovasc. Res.* (2001) doi:10.1016/S0008-6363(00)00287-X.
367. Vawda, R. *et al.* Early Intravenous Infusion of Mesenchymal Stromal Cells Exerts a Tissue Source Age-Dependent Beneficial Effect on Neurovascular Integrity and Neurobehavioral Recovery After Traumatic Cervical Spinal Cord Injury. *Stem Cells Transl. Med.* sctm.18-0192 (2019) doi:10.1002/sctm.18-0192.
368. Hong, S. H. *et al.* Ontogeny of human umbilical cord perivascular cells: Molecular and fate potential changes during gestation. *Stem Cells Dev.* (2013) doi:10.1089/scd.2012.0552.
369. Pires, A. O. *et al.* Unveiling the Differences of Secretome of Human Bone Marrow Mesenchymal Stem Cells, Adipose Tissue-Derived Stem Cells, and Human Umbilical Cord Perivascular Cells: A Proteomic Analysis. *Stem Cells Dev.* **25**, 1073–1083 (2016).
370. Rauch, M. F. *et al.* Engineering angiogenesis following spinal cord injury: a coculture of neural progenitor and endothelial cells in a degradable polymer implant leads to an increase in vessel density and formation of the blood-spinal cord barrier. *Eur. J. Neurosci.* **29**, 132–45 (2009).

371. Haggerty, A. E., Marlow, M. M. & Oudega, M. Extracellular matrix components as therapeutics for spinal cord injury. *Neurosci. Lett.* **652**, 50–55 (2017).

372. Orive, G., Anitua, E., Pedraz, J. L. & Emerich, D. F. Biomaterials for promoting brain protection, repair and regeneration. *Nat. Rev. Neurosci.* **10**, 682–692 (2009).

373. Sensharma, P., Madhumathi, G., Jayant, R. D. & Jaiswal, A. K. Biomaterials and cells for neural tissue engineering: Current choices. *Mater. Sci. Eng. C* **77**, 1302–1315 (2017).

374. Slaughter, B. V, Khurshid, S. S., Fisher, O. Z., Khademhosseini, A. & Peppas, N. A. Hydrogels in regenerative medicine. *Adv. Mater.* **21**, 3307–29 (2009).

375. Guvendiren, M. & Burdick, J. A. Engineering synthetic hydrogel microenvironments to instruct stem cells. *Curr. Opin. Biotechnol.* **24**, 841–6 (2013).

376. Martino, M. M. *et al.* Extracellular matrix and growth factor engineering for controlled angiogenesis in regenerative medicine. *Front. Bioeng. Biotechnol.* **3**, 45 (2015).

377. Vempati, P., Popel, A. S. & Mac Gabhann, F. Formation of VEGF isoform-specific spatial distributions governing angiogenesis: computational analysis. *BMC Syst. Biol.* **5**, 59 (2011).

378. Briquez, P. S., Clegg, L. E., Martino, M. M., Gabhann, F. Mac & Hubbell, J. A. Design principles for therapeutic angiogenic materials. *Nat. Rev. Mater.* **1**, 15006 (2016).

379. Devolder, R. & Kong, H. J. Hydrogels for in vivo-like three-dimensional cellular studies. *Wiley Interdiscip. Rev. Syst. Biol. Med.* **4**, 351–365 (2012).

380. Browne, S. & Pandit, A. Engineered systems for therapeutic angiogenesis. *Curr. Opin. Pharmacol.* **36**, 34–43 (2017).

381. Dalheim, M. Ø. *et al.* Efficient functionalization of alginate biomaterials. *Biomaterials* **80**, 146–156 (2016).

382. Neves, S. C. *et al.* Biofunctionalized pectin hydrogels as 3D cellular microenvironments. *J. Mater. Chem. B* **3**, 2096–2108 (2015).

383. Riahi, N., Liberelle, B., Henry, O. & De Crescenzo, G. Impact of RGD amount in dextran-based hydrogels for cell delivery. *Carbohydr. Polym.* **161**, 219–227 (2017).

384. Gomes, E. D. *et al.* Combination of a peptide-modified gellan gum hydrogel with cell therapy in a lumbar spinal cord injury animal model. *Biomaterials* **105**, 38–51 (2016).

385. Lau, T. T. & Wang, D.-A. Bioresponsive hydrogel scaffolding systems for 3D constructions in tissue engineering and regenerative medicine. *Nanomedicine (Lond).* **8**, 655–68 (2013).

386. Zhu, J. & Marchant, R. E. Design properties of hydrogel tissue-engineering scaffolds. *Expert Rev. Med. Devices* **8**, 607–26 (2011).

387. Chwalek, K., Tsurkan, M. V, Freudenberg, U. & Werner, C. Glycosaminoglycan-based hydrogels to modulate heterocellular communication in in vitro angiogenesis models. *Sci. Rep.* **4**, 4414 (2015).

388. Tsurkan, M. V. *et al.* Defined Polymer-Peptide Conjugates to Form Cell-Instructive starPEG-Heparin Matrices In Situ. *Adv. Mater.* **25**, 2606–2610 (2013).

389. Jha, A. K. *et al.* Matrix metalloproteinase-13 mediated degradation of hyaluronic acid-based matrices orchestrates stem cell engraftment through vascular integration. (2016) doi:10.1016/j.biomaterials.2016.02.023.

390. Hanjaya-Putra, D. *et al.* Spatial control of cell-mediated degradation to regulate vasculogenesis and angiogenesis in hyaluronan hydrogels. *Biomaterials* **33**, 6123–6131 (2012).

391. Hanjaya-Putra, D. *et al.* Controlled activation of morphogenesis to generate a functional human microvasculature in a synthetic matrix. *Blood* **118**, 804–15 (2011).

392. Ott, H. C. *et al.* Perfusion-decellularized matrix: using nature's platform to engineer a bioartificial heart. *Nat. Med.* **14**, 213–221 (2008).

393. Song, J. J. & Ott, H. C. Organ engineering based on decellularized matrix scaffolds. *Trends Mol. Med.* **17**, 424–32 (2011).

394. Chen, X. *et al.* Prevascularization of a fibrin-based tissue construct accelerates the formation of functional anastomosis with host vasculature. *Tissue Eng. Part A* **15**, 1363–1371 (2009).

395. Levenberg, S. *et al.* Engineering vascularized skeletal muscle tissue. *Nat. Biotechnol.* **23**, 879–84 (2005).

396. Chen, Y. C. *et al.* Functional human vascular network generated in photocrosslinkable gelatin methacrylate hydrogels. *Adv. Funct. Mater.* **22**, 2027–2039 (2012).

397. Kunz-Schughart, L. A. *et al.* Potential of fibroblasts to regulate the formation of three-dimensional vessel-like structures from endothelial cells in vitro. *Am. J. Physiol. Cell Physiol.* **290**, C1385-98 (2006).

398. Goel, S. *et al.* Normalization of the vasculature for treatment of cancer and other diseases. *Physiol. Rev.* **91**, 1071–121 (2011).

399. Saunders, W. B. *et al.* Coregulation of vascular tube stabilization by endothelial cell TIMP-2 and pericyte TIMP-3. *J. Cell Biol.* **175**, 179–191 (2006).

400. Stratman, A. N. & Davis, G. E. Endothelial cell-pericyte interactions stimulate basement membrane matrix assembly: influence on vascular tube remodeling, maturation, and stabilization. *Microsc. Microanal.* **18**, 68–80 (2012).

401. Koike, N. *et al.* Tissue engineering: creation of long-lasting blood vessels. *Nature* **428**, 138–139 (2004).

402. Aird, W. C. Phenotypic heterogeneity of the endothelium: I. Structure, function, and mechanisms. *Circ. Res.* **100**, 158–73 (2007).

403. Baldwin, J. *et al.* In vitro pre-vascularisation of tissue-engineered constructs A co-culture perspective.

Vasc. Cell **6**, 1–16 (2014).

404. Baiguera, S. & Ribatti, D. Endothelialization approaches for viable engineered tissues. *Angiogenesis* **16**, 1–14 (2013).
405. Aronson, J. P. *et al.* A novel tissue engineering approach using an endothelial progenitor cell-seeded biopolymer to treat intracranial saccular aneurysms. *J. Neurosurg.* **117**, 546–54 (2012).
406. Serrano, M. C. *et al.* Progenitor-derived endothelial cell response, platelet reactivity and haemocompatibility parameters indicate the potential of NaOH-treated polycaprolactone for vascular tissue engineering. *J. Tissue Eng. Regen. Med.* **5**, 238–247 (2011).
407. Sobhan, P. K. *et al.* Immortalized functional endothelial progenitor cell lines from umbilical cord blood for vascular tissue engineering. *Tissue Eng. Part C. Methods* **18**, 890–902 (2012).
408. Duttenhoefer, F. *et al.* 3D scaffolds co-seeded with human endothelial progenitor and mesenchymal stem cells: evidence of prevascularisation within 7 days. *Eur. Cell. Mater.* **26**, 49–64; discussion 64-5 (2013).
409. Guerrero, J. *et al.* Cell interactions between human progenitor-derived endothelial cells and human mesenchymal stem cells in a three-dimensional macroporous polysaccharide-based scaffold promote osteogenesis. *Acta Biomater.* **9**, 8200–8213 (2013).
410. Finkenzeller, G., Torio-Padron, N., Momeni, A., Mehlhorn, A. T. & Stark, G. B. In Vitro Angiogenesis Properties of Endothelial Progenitor Cells: A Promising Tool for Vascularization of Ex Vivo Engineered Tissues. *Tissue Eng.* **13**, 1413–1420 (2007).
411. Sales, V. L. *et al.* Transforming growth factor-beta1 modulates extracellular matrix production, proliferation, and apoptosis of endothelial progenitor cells in tissue-engineering scaffolds. *Circulation* **114**, I193-9 (2006).
412. Murohara, T. *et al.* Transplanted cord blood-derived endothelial precursor cells augment postnatal neovascularization. *J. Clin. Invest.* **105**, 1527–1536 (2000).
413. Hristov, M., Erl, W. & Weber, P. C. Endothelial progenitor cells: isolation and characterization. *Trends Cardiovasc. Med.* **13**, 201–6 (2003).
414. Hur, J. *et al.* Characterization of two types of endothelial progenitor cells and their different contributions to neovasculogenesis. *Arterioscler. Thromb. Vasc. Biol.* **24**, 288–93 (2004).
415. Almalki, S. G., Llamas Valle, Y. & Agrawal, D. K. MMP-2 and MMP-14 Silencing Inhibits VEGFR2 Cleavage and Induces the Differentiation of Porcine Adipose-Derived Mesenchymal Stem Cells to Endothelial Cells. *Stem Cells Transl. Med.* **6**, 1385–1398 (2017).
416. Hsieh, S.-C. *et al.* Prominent Vascularization Capacity of Mesenchymal Stem Cells in Collagen–Gold Nanocomposites. *ACS Appl. Mater. Interfaces* **8**, 28982–29000 (2016).
417. Miranville, A. *et al.* Improvement of postnatal neovascularization by human adipose tissue-derived

stem cells. *Circulation* **110**, 349–355 (2004).

418. Pill, K., Hofmann, S., Redl, H. & Holnthoner, W. Vascularization mediated by mesenchymal stem cells from bone marrow and adipose tissue: a comparison. *Cell Regen. (London, England)* **4**, 8 (2015).
419. Belair, D. G. *et al.* Human vascular tissue models formed from human induced pluripotent stem cell derived endothelial cells. *Stem Cell Rev.* **11**, 511–25 (2015).
420. Benavides, O. M. *et al.* In situ vascularization of injectable fibrin/poly(ethylene glycol) hydrogels by human amniotic fluid-derived stem cells. *J. Biomed. Mater. Res. - Part A* **103**, 2645–2653 (2015).
421. Verseijden, F. *et al.* Adult human bone marrow- and adipose tissue-derived stromal cells support the formation of prevascular-like structures from endothelial cells in vitro. *Tissue Eng. Part A* **16**, 101–14 (2010).
422. Verseijden, F. *et al.* Prevascular structures promote vascularization in engineered human adipose tissue constructs upon implantation. *Cell Transplant.* **19**, 1007–20 (2010).
423. Rouwkema, J., Westerweel, P. E., de Boer, J., Verhaar, M. C. & van Blitterswijk, C. a. The use of endothelial progenitor cells for prevascularized bone tissue engineering. *Tissue Eng. Part A* **15**, 2015–27 (2009).
424. Mishra, R. *et al.* Effect of prevascularization on in vivo vascularization of poly(propylene fumarate)/fibrin scaffolds. *Biomaterials* **77**, 255–266 (2016).
425. Laschke, M. W. & Menger, M. D. Life is 3D: Boosting Spheroid Function for Tissue Engineering. *Trends Biotechnol.* **35**, 133–144 (2017).
426. Yoon, H. H., Bhang, S. H., Shin, J.-Y., Shin, J. & Kim, B.-S. Enhanced Cartilage Formation via Three-Dimensional Cell Engineering of Human Adipose-Derived Stem Cells. *Tissue Eng. Part A* **18**, 1949–1956 (2012).
427. Bhang, S. H., Lee, S., Shin, J.-Y., Lee, T.-J. & Kim, B.-S. Transplantation of cord blood mesenchymal stem cells as spheroids enhances vascularization. *Tissue Eng. Part A* **18**, 2138–47 (2012).
428. Laschke, M. W. *et al.* Three-dimensional spheroids of adipose-derived mesenchymal stem cells are potent initiators of blood vessel formation in porous polyurethane scaffolds. *Acta Biomater.* **9**, 6876–6884 (2013).
429. Mandrycky, C., Wang, Z., Kim, K. & Kim, D.-H. 3D bioprinting for engineering complex tissues. *Biotechnol. Adv.* **34**, 422–434 (2015).
430. Jakab, K., Damon, B., Neagu, A., Kachurin, A. & Forgacs, G. Three-dimensional tissue constructs built by bioprinting. *Biorheology* **43**, 509–13 (2006).
431. Hoying, J. B. & Williams, S. K. Biofabrication of vascular networks. in *Essentials of 3D Biofabrication and Translation* 317–335 (2015). doi:10.1016/B978-0-12-800972-7.00019-0.
432. Norotte, C., Marga, F. S., Niklason, L. E. & Forgacs, G. Scaffold-free vascular tissue engineering using

bioprinting. *Biomaterials* **30**, 5910–5917 (2009).

433. Cui, H., Zhu, W., Holmes, B. & Zhang, L. G. Biologically Inspired Smart Release System Based on 3D Bioprinted Perfused Scaffold for Vascularized Tissue Regeneration. *Adv. Sci.* **3**, 1600058 (2016).
434. Abdeen, A. A. & Saha, K. Manufacturing Cell Therapies Using Engineered Biomaterials. *Trends in Biotechnology* (2017) doi:10.1016/j.tibtech.2017.06.008.
435. Akar, B. *et al.* Biomaterials with persistent growth factor gradients in vivo accelerate vascularized tissue formation. *Biomaterials* **72**, 61–73 (2015).
436. Guo, X. *et al.* Creating 3D angiogenic growth factor gradients in fibrous constructs to guide fast angiogenesis. *Biomacromolecules* **13**, 3262–71 (2012).
437. Assal, Y., Mie, M. & Kobatake, E. The promotion of angiogenesis by growth factors integrated with ECM proteins through coiled-coil structures. *Biomaterials* **34**, 3315–23 (2013).
438. Richardson, T. P., Peters, M. C., Ennett, A. B. & Mooney, D. J. Polymeric system for dual growth factor delivery. *Nat. Biotechnol.* **19**, 1029–34 (2001).
439. Rufaihah, A. J. *et al.* Dual delivery of VEGF and ANG-1 in ischemic hearts using an injectable hydrogel. *Acta Biomater.* **48**, 58–67 (2017).
440. Shin, Y. *et al.* In vitro 3D collective sprouting angiogenesis under orchestrated ANG-1 and VEGF gradients. *Lab Chip* **11**, 2175–2181 (2011).
441. Wang, Y. *et al.* Degradable PLGA scaffolds with basic fibroblast growth factor: experimental studies in myocardial revascularization. *Texas Hear. Inst. J.* **36**, 89–97 (2009).
442. Anderson, S. M., Siegman, S. N. & Segura, T. The effect of vascular endothelial growth factor (VEGF) presentation within fibrin matrices on endothelial cell branching. *Biomaterials* **32**, 7432–7443 (2011).
443. Mittermayr, R. *et al.* Controlled release of fibrin matrix-conjugated platelet derived growth factor improves ischemic tissue regeneration by functional angiogenesis. *Acta Biomater.* **29**, 11–20 (2016).
444. Pola, R. *et al.* The morphogen Sonic hedgehog is an indirect angiogenic agent upregulating two families of angiogenic growth factors. *Nat. Med.* **7**, 706–711 (2001).
445. Rivron, N. C. *et al.* Sonic Hedgehog-activated engineered blood vessels enhance bone tissue formation. *Proc. Natl. Acad. Sci. U. S. A.* **109**, 4413–8 (2012).
446. King, V. R., Alovskaya, A., Wei, D. Y. T., Brown, R. A. & Priestley, J. V. The use of injectable forms of fibrin and fibronectin to support axonal ingrowth after spinal cord injury. *Biomaterials* **31**, 4447–4456 (2010).
447. Zeng, X. *et al.* Bone marrow mesenchymal stem cells in a three-dimensional gelatin sponge scaffold attenuate inflammation, promote angiogenesis, and reduce cavity formation in experimental spinal cord injury. *Cell Transplant.* **20**, 1881–1899 (2011).
448. López-Dolado, E., González-Mayorga, A., Gutiérrez, M. C. & Serrano, M. C. Immunomodulatory and

angiogenic responses induced by graphene oxide scaffolds in chronic spinal hemisected rats. *Biomaterials* **99**, 72–81 (2016).

449. Bakshi, A. *et al.* Mechanically engineered hydrogel scaffolds for axonal growth and angiogenesis after transplantation in spinal cord injury. *J. Neurosurg. Spine* **1**, 322–329 (2004).

450. Chedly, J. *et al.* Physical chitosan microhydrogels as scaffolds for spinal cord injury restoration and axon regeneration. *Biomaterials* **138**, 91–107 (2017).

451. Hurtado, A. *et al.* Robust CNS regeneration after complete spinal cord transection using aligned poly-l-lactic acid microfibers. *Biomaterials* **32**, 6068–6079 (2011).

452. Narmoneva, D. A. *et al.* Self-assembling short oligopeptides and the promotion of angiogenesis. *Biomaterials* (2005) doi:10.1016/j.biomaterials.2005.01.005.

453. Liu, X. *et al.* In vivo studies on angiogenic activity of two designer self-assembling peptide scaffold hydrogels in the chicken embryo chorioallantoic membrane. *Nanoscale* **4**, 2720 (2012).

454. Davis, M. E. *et al.* Injectable Self-Assembling Peptide Nanofibers Create Intramyocardial Microenvironments for Endothelial Cells. *Circulation* **111**, 442–450 (2005).

455. Sieminski, A. L., Semino, C. E., Gong, H. & Kamm, R. D. Primary sequence of ionic self-assembling peptide gels affects endothelial cell adhesion and capillary morphogenesis. *J. Biomed. Mater. Res. Part A* **87A**, 494–504 (2008).

456. Tran, K. A. *et al.* Vascularization of self-assembled peptide scaffolds for spinal cord injury repair. *Acta Biomater.* **104**, 76–84 (2020).

457. Guo, S. *et al.* Prevascularized Scaffolds Bearing Human Dental Pulp Stem Cells for Treating Complete Spinal Cord Injury. *Adv. Healthc. Mater.* **2000974**, 2000974 (2020).

458. Akhavan, O., Ghaderi, E., Shirazian, S. A. & Rahighi, R. Rolled graphene oxide foams as three-dimensional scaffolds for growth of neural fibers using electrical stimulation of stem cells. *Carbon N. Y.* **97**, 71–77 (2016).

459. Li, N. *et al.* Three-dimensional graphene foam as a biocompatible and conductive scaffold for neural stem cells. *Sci. Rep.* **3**, 1604 (2013).

460. Domínguez-Bajo, A. *et al.* Myelinated axons and functional blood vessels populate mechanically compliant rGO foams in chronic cervical hemisected rats. *Biomaterials* **192**, 461–474 (2019).

461. Ranganath, S. H., Levy, O., Inamdar, M. S. & Karp, J. M. Harnessing the mesenchymal stem cell secretome for the treatment of cardiovascular disease. *Cell Stem Cell* **10**, 244–58 (2012).

462. Wen, Y. *et al.* Spinal cord injury repair by implantation of structured hyaluronic acid scaffold with PLGA microspheres in the rat. *Cell Tissue Res.* **364**, 17–28 (2016).

463. Kang, C. E., Baumann, M. D., Tator, C. H. & Shoichet, M. S. Localized and sustained delivery of fibroblast growth factor-2 from a nanoparticle-hydrogel composite for treatment of spinal cord injury.

Cells Tissues Organs **197**, 55–63 (2012).

464. Avraamides, C. J., Garmy-Susini, B. & Varner, J. A. Integrins in angiogenesis and lymphangiogenesis. *Nat. Rev. Cancer* **8**, 604–617 (2008).

465. Brooks, P. C., Clark, R. A. & Cheresh, D. a. Requirement of vascular integrin alpha v beta 3 for angiogenesis. *Science* **264**, 569–71 (1994).

466. Brooks, P. C. *et al.* Integrin alpha v beta 3 antagonists promote tumor regression by inducing apoptosis of angiogenic blood vessels. *Cell* **79**, 1157–64 (1994).

467. Drake, C. J., Cheresh, D. A. & Little, C. D. An antagonist of integrin alpha v beta 3 prevents maturation of blood vessels during embryonic neovascularization. *J. Cell Sci.* **108 (Pt 7**, 2655–61 (1995).

468. Muether, P. S. *et al.* The role of integrin α5β1 in the regulation of corneal neovascularization. *Exp. Eye Res.* **85**, 356–365 (2007).

469. Kim, S., Bell, K., Mousa, S. A. & Varner, J. A. Regulation of angiogenesis in vivo by ligation of integrin alpha5beta1 with the central cell-binding domain of fibronectin. *Am. J. Pathol.* **156**, 1345–1362 (2000).

470. Boudreau, N. J. & Varner, J. A. The homeobox transcription factor Hox D3 promotes integrin alpha5beta1 expression and function during angiogenesis. *J. Biol. Chem.* **279**, 4862–8 (2004).

471. Mas-Moruno, C. *et al.* αvβ3- or α5β1-Integrin-Selective Peptidomimetics for Surface Coating. *Angew. Chemie - Int. Ed.* **55**, 7048–7067 (2016).

472. Pierschbacher, M. D. & Ruoslahti, E. Cell attachment activity of fibronectin can be duplicated by small synthetic fragments of the molecule. *Nature* **309**, 30–33 (1984).

473. Pierschbacher, M. D. & Ruoslahti, E. Variants of the cell recognition site of fibronectin that retain attachment-promoting activity. *Proc. Natl. Acad. Sci. U. S. A.* **81**, 5985–5988 (1984).

474. Plow, E. F., Pierschbacher, M. D., Ruoslahti, E., Marguerie, G. A. & Ginsberg, M. H. The effect of Arg-Gly-Asp-containing peptides on fibrinogen and von Willebrand factor binding to platelets. *Proc. Natl. Acad. Sci. U. S. A.* **82**, 8057–61 (1985).

475. Oldberg, A., Franzén, A. & Heinegård, D. Cloning and sequence analysis of rat bone sialoprotein (osteopontin) cDNA reveals an Arg-Gly-Asp cell-binding sequence. *Proc. Natl. Acad. Sci. U. S. A.* **83**, 8819–23 (1986).

476. Grant, D. S. *et al.* Two different laminin domains mediate the differentiation of human endothelial cells into capillary-like structures in vitro. *Cell* **58**, 933–943 (1989).

477. Suzuki, S., Oldberg, A., Hayman, E. G., Pierschbacher, M. D. & Ruoslahti, E. Complete amino acid sequence of human vitronectin deduced from cDNA. Similarity of cell attachment sites in vitronectin and fibronectin. *EMBO J.* **4**, 2519–24 (1985).

478. Gould, R. J. *et al.* Disintegrins: a family of integrin inhibitory proteins from viper venoms. *Proc. Soc.*

Exp. Biol. Med. **195**, 168–71 (1990).

479. Swenson, S., Ramu, S. & Markland, F. S. Anti-angiogenesis and RGD-containing snake venom disintegrins. *Curr. Pharm. Des.* **13**, 2860–71 (2007).

480. Ruoslahti, E. & Pierschbacher, M. D. Arg-Gly-Asp: a versatile cell recognition signal. *Cell* **44**, 517–518 (1986).

481. Trabocchi, A. & Guarna, A. *Peptidomimetics in Organic and Medicinal Chemistry*. *Peptidomimetics in Organic and Medicinal Chemistry: The Art of Transforming Peptides in Drugs* (John Wiley & Sons, Ltd, 2014). doi:10.1002/9781118683033.

482. Giannis, A. & Kolter, T. Peptidomimetics for Receptor Ligands?Discovery, Development, and Medical Perspectives. *Angew. Chemie Int. Ed. English* **32**, 1244–1267 (1993).

483. Olson, G. L. *et al.* Concepts and progress in the development of peptide mimetics. *J. Med. Chem.* **36**, 3039–3049 (1993).

484. Ravindranathan, P. *et al.* Peptidomimetic targeting of critical androgen receptor–coregulator interactions in prostate cancer. *Nat. Commun.* **4**, 1923 (2013).

485. Henderson, N. C. *et al.* Targeting of αv integrin identifies a core molecular pathway that regulates fibrosis in several organs. *Nat. Med.* **19**, 1617–24 (2013).

486. Baum, R. P. *et al.* First-In-Human Study Demonstrating Tumor-Angiogenesis by PET/CT Imaging with (68)Ga-NODAGA-THERANOST, a High-Affinity Peptidomimetic for αvβ3 Integrin Receptor Targeting. *Cancer Biother. Radiopharm.* **30**, 152–9 (2015).

487. Sartori, A. *et al.* Synthesis of Novel c(AmpRGD)-Sunitinib Dual Conjugates as Molecular Tools Targeting the αvβ3 Integrin/VEGFR2 Couple and Impairing Tumor-Associated Angiogenesis. *J. Med. Chem.* **60**, 248–262 (2017).

488. Xiong, J.-P. Crystal Structure of the Extracellular Segment of Integrin alpha Vbeta 3 in Complex with an Arg-Gly-Asp Ligand. *Science (80-.).* **296**, 151–155 (2002).

489. Marshall, G. R. A hierarchical approach to peptidomimetic design. *Tetrahedron* **49**, 3547–3558 (1993).

490. Bochen, A. *et al.* Biselectivity of isoDGR peptides for fibronectin binding integrin subtypes α5β1 and αvβ6: conformational control through flanking amino acids. *J. Med. Chem.* **56**, 1509–19 (2013).

491. Pallarola, D. *et al.* Interface immobilization chemistry of cRGD-based peptides regulates integrin mediated cell adhesion. *Adv. Funct. Mater.* **24**, 943–956 (2014).

492. Ripka, A. S. & Rich, D. H. Peptidomimetic design. *Curr. Opin. Chem. Biol.* **2**, 441–452 (1998).

493. Sautel, M. *et al.* Neuropeptide Y and the nonpeptide antagonist BIBP 3226 share an overlapping binding site at the human Y1 receptor. *Mol. Pharmacol.* **50**, 285–292 (1996).

494. Schwartz, T. W. Locating ligand-binding sites in 7TM receptors by protein engineering. *Curr. Opin. Biotechnol.* **5**, 434–44 (1994).

495. Kapp, T. G. *et al.* A Comprehensive Evaluation of the Activity and Selectivity Profile of Ligands for RGD-binding Integrins. *Sci. Rep.* **7**, 39805 (2017).

496. Klim, J. R. *et al.* Small-Molecule-Modified Surfaces Engage Cells through the αvβ3 Integrin. *ACS Chem. Biol.* **7**, 518–525 (2012).

497. Marelli, U. K., Rechenmacher, F., Sobahi, T. R. A., Mas-Moruno, C. & Kessler, H. Tumor Targeting via Integrin Ligands. *Front. Oncol.* **3**, 222 (2013).

498. Mauro, N. *et al.* RGD-mimic polyamidoamine-montmorillonite composites with tunable stiffness as scaffolds for bone tissue-engineering applications. *J. Tissue Eng. Regen. Med.* **11**, 2164–2175 (2017).

499. Rahmouni, S. *et al.* Hydrogel micropillars with integrin selective peptidomimetic functionalized nanopatterned tops: A new tool for the measurement of cell traction forces transmitted through αvβ3- or α5β1-integrins. *Adv. Mater.* **25**, 5869–5874 (2013).

500. Fraioli, R. *et al.* Surface guidance of stem cell behavior: Chemically tailored co-presentation of integrin-binding peptides stimulates osteogenic differentiation in vitro and bone formation in vivo. *Acta Biomater.* **43**, 269–281 (2016).

501. Guasch, J. *et al.* Segregation versus colocalization: orthogonally functionalized binary micropatterned substrates regulate the molecular distribution in focal adhesions. *Adv. Mater.* **27**, 3737–47 (2015).

502. Marchand-Brynaert, J. *et al.* Biological evaluation of RGD peptidomimetics, designed for the covalent derivatization of cell culture substrata, as potential promotors of cellular adhesion. *Biomaterials* **20**, 1773–1782 (1999).

503. Rerat, V. *et al.* αvβ3 Integrin-Targeting Arg-Gly-Asp (RGD) Peptidomimetics Containing Oligoethylene Glycol (OEG) Spacers. *J. Med. Chem.* **52**, 7029–7043 (2009).

504. Rechenmacher, F. *et al.* A molecular toolkit for the functionalization of titanium-based biomaterials that selectively control integrin-mediated cell adhesion. *Chem. - A Eur. J.* **19**, 9218–9223 (2013).

505. Rechenmacher, F. *et al.* Functionalizing αvβ3- or α5β1-selective integrin antagonists for surface coating: A method to discriminate integrin subtypes in vitro. *Angew. Chemie - Int. Ed.* **52**, 1572–1575 (2013).

506. Fraioli, R. *et al.* Mimicking bone extracellular matrix: Integrin-binding peptidomimetics enhance osteoblast-like cells adhesion, proliferation, and differentiation on titanium. *Colloids Surfaces B Biointerfaces* **128**, 191–200 (2015).

507. Liu, D. *et al.* Administration of Antagomir-223 Inhibits Apoptosis, Promotes Angiogenesis and Functional Recovery in Rats with Spinal Cord Injury. *Cell. Mol. Neurobiol.* **35**, 483–491 (2015).

508. Yuan, X. *et al.* Exosomes Derived From Pericytes Improve Microcirculation and Protect Blood–Spinal Cord Barrier After Spinal Cord Injury in Mice. *Front. Neurosci.* **13**, 1–14 (2019).

509. Karimi-Abdolrezaee, S., Schut, D., Wang, J. & Fehlings, M. G. Chondroitinase and growth factors enhance activation and Oligodendrocyte differentiation of endogenous neural precursor cells after spinal cord injury. *PLoS One* **7**, (2012).

510. Gwak, S. J., Yun, Y., Yoon, D. H., Kim, K. N. & Ha, Y. Therapeutic use of 3β-[N-(N',N'-dimethylaminoethane) carbamoyl] cholesterol-modified PLGA nanospheres as gene delivery vehicles for spinal cord injury. *PLoS One* **11**, 1–14 (2016).

511. López-Dolado, E., González-Mayorga, A., Gutiérrez, M. C. & Serrano, M. C. Immunomodulatory and angiogenic responses induced by graphene oxide scaffolds in chronic spinal hemisected rats. *Biomaterials* **99**, 72–81 (2016).

512. Fan, Z., Liao, X., Tian, Y., Xuzhuzi, X. & Nie, Y. A prevascularized nerve conduit based on a stem cell sheet effectively promotes the repair of transected spinal cord injury. *Acta Biomater.* **101**, 304–313 (2020).

513. Zhong, J. *et al.* A Prevascularization Strategy Using Novel Fibrous Porous Silk Scaffolds for Tissue Regeneration in Mice with Spinal Cord Injury. *Stem Cells Dev.* **29**, 615–624 (2020).

CHAPTER 2

L.A. Rocha, E.D. Gomes, J.L. Afonso, S. Granja, F. Baltazar, N.A. Silva, M.S. Shoichet, R.A. Sousa, D.A. Learmonth, A.J. Salgado

In vitro evaluation of ASCs and HUVECs co-cultures in 3D biodegradable hydrogels on neurite outgrowth and vascular organization

(Frontiers in Cell and Developmental Biology: doi.org/10.3389/fcell.2020.00489)

(2021)

Title

In vitro evaluation of ASCs and HUVECs co-cultures in 3D biodegradable hydrogels on neurite outgrowth and vascular organization.

Authors

L.A. Rocha[1,2,3], E.D. Gomes[1,2], J.L. Afonso[1,2], S. Granja[1,2], F. Baltazar[1,2], N.A. Silva[1,2], M.S. Shoichet[4], R.A. Sousa[3], D.A. Learmonth3, A.J. Salgado[1,2]

Affiliations

[1]Life and Health Sciences Research Institute (ICVS), School of Medicine, University of Minho, Campus Gualtar, 4710-057 Braga, Portugal

[2]ICVS/3B's - PT Government Associate Laboratory, Braga/Guimarães, Portugal

[3]Stemmatters, Biotecnologia e Medicina Regenerativa SA, Barco, Portugal

[4]Institute of Biomaterials and Biomedical Engineering, University of Toronto, Toronto, Ontario M5S 3E1, Canada

Corresponding author

António Salgado (PhD), Life and Health Sciences Research Institute (ICVS), School of Medicine, University of Minho, Campus Gualtar, 4710-057 Braga, Portugal.

Phone number: +351 253 604 947

E-mail: asalgado@med.uminho.pt

Abstract

Vascular disruption following SCI decisively contributes to the poor functional recovery prognosis facing patients with the condition. Using a previously developed gellan gum hydrogel to which the adhesion motif GRGDS was grafted (GG-GRGDS), this work aimed to understand the ability of ASCs to impact vascular organization of HUVECs and how this in turn affects neurite outgrowth of dorsal root ganglia (DRG) explants. Our data shows that culturing these cells together lead to a synergistic effect as showed by increased stimulation of neuritogenesis on DRG. Importantly, HUVECs were only able to assemble into vascular-like structures when cultured in the presence of ASCs, which shows the capacity of these cells in reorganizing the vascular milieu. Analysis of selected neuroregulatory molecules showed that the co-culture upregulated the secretion of several neurotrophic factors. On the other hand, ASCs and ASCs+HUVECs presented a similar profile regarding the presence of angiotrophic molecules herein analyzed. Finally, the implantation of GG-GRGDS hydrogels encapsulating ASCs in the chick chorioallantoic membrane (CAM) lead to increases in vascular recruitment towards the hydrogels in comparison to GG-GRGDS alone. This indicates that the combination of ASCs with GG-GRGDS hydrogels could promote re-vascularization in trauma-related injuries in the CNS and thus control disease progression and induce functional recovery.

Keywords: vascularization; spinal cord injury; neurovascular; biomaterial; cell therapy; secretome; Adipose-derived stem cells.

Introduction

According to latest estimations, approximately 27 million people worldwide live with disabilities caused by SCI [1]. This condition causes severe motor, autonomic and sensory deficits. To date, treatment options are restricted to palliative care [2]. Disruption of the vascular architecture of the spinal cord occurs concomitantly with injury and originates intraparenchymal hemorrhage, tissue edema and swelling that leads to tissue ischemia [3]. Consequently, the BSCB is compromised and blood-borne molecules and inflammatory cells infiltrate the tissue indiscriminately [4]. Vascular damage initiates in gray matter and progressively extends into surrounding white matter leading to disrupted myelin and axonal and periaxonal swelling [5]. Altogether, these events exacerbate the already deleterious injury environment and contribute to the poor recovery scenario facing SCI patients. Endogenous attempts of revascularization (through angiogenesis) are observed from day 3 and peak about 1 week following injury, where some reports showed a return to basal vascular levels or even a 5-fold increase in vascular density at SCI injury site [6–8]. This compensatory mechanism fails to integrate newly formed vessels into functional neurovascular units and most are pruned 2 weeks after injury. Additionally, Glut-1 transporters, which act as constant glucose transporters across the BSCB, are only reestablished at this time point and leave surviving neurons in a persistent metabolic imbalance [8]. Recently it was shown that vascular perfusion below injury during the chronic phase of SCI was half that in comparison to normal spinal cords or above injury, resulting in local chronic hypoxia, and that transiently reestablishing oxygenation levels lead to brief motor recovery [9]. This finding highlights the relevance of vascularization therapies for SCI, showing that even though specific neuronal circuits bellow injury may remain functional, chronic hypoxia and insufficient nutrient supply dictates their inability to undergo normal homeostasis. Thus, different approaches, either directly targeting vascularization [10–13] or not, concretely using neurotrophin-3-loaded chitosan [14], chitosan microhydrogels [15] or a PLGA scaffold to deliver MSCs [16], revealed that modulation of this parameter is intricately involved in enhanced SCI recovery.

In this regard, transplantation of MSCs following SCI has shown protective effects to local vasculature [17–19]. Additionally, MSCs are also capable of promoting neuroprotection and modulation of the immune response towards a more regenerative-prone environment, which broadens the range of their effect and make them a promising candidate to treat SCI [20–22]. These effects have been extensively connected to the panel of molecules that MSCs secrete (secretome), including neurotrophic factors [BDNF, nerve growth factor (NGF) or GDNF], pro-angiogenic molecules (VEGF, bFGF or Ang-1) or immunomodulatory molecules [MCP-1, transforming growth factor beta (TGF-β) or TNF-α] though this profile varies across distinct MSC sources [23,24]. Among MSCs, ASCs are a clinically-relevant population for cell therapy applications as their

isolation takes advantage of otherwise discarded tissue, being minimally invasive and their transplantation does not elicit host immune response [25,26]. Despite the richness of ASCs' secretome in angiogenic factors, different reports demonstrated limited capacity to produce fully branched vascular networks, contrasting to direct contact experiments where ASCs lead to the development of matured vascular structures, highlighting the advantage of including these cells in SCI therapies targeting vascularization [27–29]. Thus, including this type of MSCs in such therapies is appealing as it could possibly enable the modulation of vasculature towards homeostasis and overcome the host deficient response. Furthermore, endothelial cells positively affect neuronal proliferation and neurogenesis, being able to act as physical tracks for axonal growth [30–33]. The development of a cell therapy based on the transplantation of ASCs benefits from their capacity in protecting spared neurons, modulating the environment to a regenerative phenotype, whilst acting on the preservation of the BSCB and enhancing vascular organization following SCI. This can, in turn, contribute to quickly restore the compromised BSCB, controlling the infiltration of inflammatory cells and other inappropriate agents, preventing prolonged tissue hypoxia, providing simultaneously physical cues for neuronal regeneration.

To improve poor survival rates associated with cell transplantation, hydrogels are being used as they enable replication of the physical properties of the native CNS, whilst providing appropriate cues for cell survival, proliferation and integration into host tissue [34,35]. Taking this into consideration, in this work we intended to develop a co-culture system based on the encapsulation of ASCs and HUVECs within an in-house developed GG matrix modified with the adhesion motif GRGDS [36,37]. This gellan gum-based biomaterial has been previously reported as suitable to culture distinct neuronal cells and ASCs, which later translated into improved functional outcomes following its implantation in a SCI animal model.

The main goals of the present work were to study the simultaneous impact of ASCs in the vascular organization of HUVECs and neurite extension of dorsal root ganglia (DRG) explants, as well as to understand how the angiogenic and neuroregulatory nature of their secretome is altered by the presence of HUVECs in 3D conditions. Finally, we assessed the capacity of ASCs encapsulated in GG-GRGDS hydrogels to recruit blood vessels in a simple *in vivo setting* using the CAM assay.

Materials and Methods

Coupling of maleimide-GRGDS to furan-Gellan Gum

The coupling of GRGDS to GG was done using a two-step methodology where first gellan gum is modified with furan by creating an amide bond, through the activation of its -COOH groups, and then coupled to maleimide-modified GRGDS (mal-GRGDS) taking advantage of Diels-Alder cyclization chemistry between the maleimide group of the peptide and the furan group of GG in accordance to previously described protocols [36,37]. A 1 % (w/V) gellan gum (GG, Sigma, USA) solution was dissolved in 100 mM 2-(N-morpholino)ethanesulfonic acid (MES, Sigma, USA) buffer at pH 5.5 and 37 °C. Then, a 750 mM 4-(4,6-Dimethoxy-1,3,5-triazin-2-yl)-4-methylmorpholinium chloride (DMT-MM, Sigma, USA) solution is added in a 1:4 molar ratio (GG:DMT-MM) to activate the-COOH groups of the polymer, which is followed by the addition of furfurylamine (Acros Organics, Belgium) using the same molar ratio. The reaction continues for 24 h and afterwards the obtained products are dialyzed in membranes with a cutoff of 12-14 kDa (Spectrum Labs, USA) to purify the modified polymer from reaction by-products alternatively against distilled water and PBS (0.1 M, pH 7.2) for 5 days. GG-furan was recovered as a white powder by removing its aqueous content by lyophilization. To immobilize the peptide in furan-GG, 1.2 mg/mL of the modified polymer was dissolved in 100 mM MES buffer at pH 5.5 and 37 °C. After complete dissolution, mal-GRGDS peptide (Anaspec, USA) was added in a 1:5 molar ration (furan:maleimide) and the reaction continued under vigorous stirring for 48h. The purification of the peptide-modified GG is done by dialysis (Mw cutoff 12-14 kDa) against distilled water and PBS (0.1 M, pH 7.2) in alternance. Removal of water by lyophilization allowed to obtain GRGDS-modified GG (GG-GRGDS) as a white powder. To quantify the amount of peptide immobilized onto the backbone of GG we performed an amino acid analysis. The protocol consists on the acidic hydrolysis of the peptide with 6 N HCl for 24 h followed by derivatization with phenylisothiocyanate. HPLC was used to quantify the derivatized hydrolizates. A defined amount of mal-GRGDS previously incubated with native gellan gum suffered the same derivatization protocol and amino acid analysis and was used as a control.

Cell isolation and culture

ASCs were isolated by LaCell LLC from the lipoaspirates of consenting donors according to Dubois and coworkers [38] under a protocol previously approved by an institutional review panel at LaCell LLC. Upon isolation, ASCs were cultured in α-MEM (Invitrogen, USA) supplemented with 10 % fetal bovine serum (FBS, Biochrom AG, Germany) and 1 % (V/V) penicillin-streptomycin (pen/strep, Invitrogen, USA) at 37 °C and 5 % CO_2 (V/V) with medium exchanges every 3 days.

HUVECs were obtained from the umbilical cord of healthy consenting patients from the Gynecology and Obstetrics Service of Hospital de Braga using a protocol approved by the review board of the Ethical Commission for Health of Braga Hospital (CESHB). After rinsing and cleaning the umbilical cord with PBS, a cannula was inserted into the umbilical vein. Then, the vein was washed with PBS to remove blood clots and excesses of blood. Afterwards, the other extremity of the umbilical cord was closed with forceps and the vein was filled with α-MEM containing 0.2 % (w/V) (210 U/mL) Type I Collagenase (Gibco, Thermo Fischer Scientific, USA) and 1 % pen/strep. To allow for digestion, the umbilical cord was transferred into a cell culture incubator [T= 37 °C and 5 % (V/V) CO_2] for 15 minutes. Before opening, the cord was massaged to guarantee a homogenous digestion and then its content transferred to a 50 mL Falcon, being subsequently washed with α-MEM having 10 % FBS (w/V) and 1 % pen/strep, PBS and finally with a syringe filled with air. This was followed by the centrifugation of the suspension for 10 minutes at 1200 rpm, removal of the supernatant and resuspension of the pellet in Endothelial Growth Media (EGM, R&D Systems, USA) supplemented with 1x Endothelial Growth Supplement (EGS, R&D Systems, USA) and 1 % (V/V) pen/strep. The cellular suspension was then equally divided into the wells of a 6-well plate (pre-coated with 1 % (w/V) Type B bovine gelatin (Sigma, USA) and cultured in EGM (R&D Systems, USA) supplemented with 1x EGS (R&D Systems, USA) and 1 % (V/V) pen/strep at 37 °C and 5 % (V/V) CO_2 overnight to allow the attachment of HUVECs. The following day media was changed to remove unattached cells and debris and from this point onwards media is exchanged every two days to keep purifying the culture. Upon confluence, part of the cells were stored in liquid nitrogen until further use and the rest were transferred to a T75 flask pre-coated with gelatin and cultured as previously described.

Hydrogel preparation

Lyophilized GG-GRGDS and unmodified GG was exposed to UV lights for 15 minutes [39]. To produce hydrogels for the 3D environment experiments, a 1 % (w/V) solution composed of equal parts of GG-GRGDS and unmodified GG was prepared and dissolved at 40 °C in ultra-pure water. Prior to the experiments the polymeric solution was ionically crosslinked by adding 10 % (V/V) of a 0.3 % (w/V) $CaCl_2$ [to a final concentration of 0.03 % (w/V)]. The volume of hydrogels for the experiments was 50 µL.

3D cell cultures – ASCs, HUVECs and their co-culture

Prior to their encapsulation in GG-GRGDS ASCs and HUVECs were cultured as detailed in **Cell isolation and culture** and the hydrogels prepared according to **Hydrogel preparation**. The pellets with the appropriate number of ASCs and HUVECs were resuspended homogenously in the corresponding volume

of GG-GRGDS at a cell density of 30000 cells/50 µL of hydrogel and cultured under previously described conditions for each cell type. The encapsulation of cells for co-culture experiments was done in a 1:1 ASCs:HUVECs ratio by mixing the appropriate volume of each cell suspension obtained subsequently to individual 2D cultures which was followed by centrifugation at 1200 rpm for 5 minutes to obtain the cell mixture pellet. The appropriate volume of GG-RGDS was then added to the pellet allowing formation of hydrogels with the previously referred density (15000 ASCs + 15000 HUVECs/50 µL of hydrogel) being cultured using α-MEM with 10 % (V/V) FBS and 1 % (V/V) pen/strep.

Dorsal root ganglia isolation and culture

DRG explants were used to understand the capacity that co-culturing ASCs and HUVECs in GG-GRGDS has in inducing neurite outgrowth from the explants in comparison to each cell type cultured alone and GG-GRGDS without cells. Furthermore, using the same experimental setting this organotypic model allowed to assess the modulation of genes related to axonal growth and cytoskeleton dynamics (GAP43 and β-Tubulin III, respectively) along their time in culture. The isolation of DRG explants was effectuated using a previously detailed protocol [37,40]. Thus, DRG from the thoracic regions of the spine of neonatal pups (P5-7) were removed and placed in cold 1x HBSS without Ca^{2+} and Mg^{2+} (Invitrogen, USA) with 1 % (V/V) pen/strep. The remains of peripheral nerve processes were properly cleaned from DRG and then the explants were placed on top of the hydrogels across the 4 groups (no cells, ASCs, HUVECs, ASCs+HUVECs). The cell culture continued for 7 days in Neurobasal medium supplemented with 1x B27 (Invitrogen, USA), 2 mM L-glutamine (Invitrogen, USA), 6 mg/mL D-glucose (Sigma, USA) and 1 % (V/V) pen/strep with medium changes every two days and under a humidified atmosphere [37 °C and 5 % (V/V) CO_2] before fixating the samples using PFA and performing immunocytochemistry (ICC) to understand neurite outgrowth as well as the morphology of ASCs and HUVECs inside the hydrogels.

DRG collection for PCR analysis followed the same extraction and culture methodology and was done at multiple timepoints: 12 h, 24 h, 1 day, 4 days and 7 days following culture in the hydrogels referring to the 4 s. Pools of 2 DRG were collected at each timepoint to eppendorfs containing TripleXtractor (Grisp, Portugal) (a phenol and guanidine isothiocyanate-based solution to extract high quality RNA) and then subjected to RNA isolation or in alternative were rapidly frozen at -80 °C until further use. Cell encapsulation was performed 24 h before DRG culture and followed the methodology detailed in **3D cell cultures – ASCs, HUVECs and their co-culture.**

Immunocytochemistry and Phalloidin/DAPI staining

After 7 days of culture hydrogels and explants were fixed in 4 % PFA (Panreac, Spain) for 45 minutes at room temperature (RT). This step was followed by washing the samples 3 times with PBS and by permeabilizing cell membranes with 0.3 % (V/V) Triton X-100 (Sigma, USA) for 10 minutes. To block non-specific binding sites, samples were incubated in PBS with 10 % (V/V) fetal calf serum (FCS, Biochrom AG, Germany) for 1 h 30 min. Primary antibodies were then properly diluted in PBS 10 % FCS and added to the samples for 48 h at 4 °C. Mouse anti-neurofilament 200 kDa antibody (1:200, Millipore, USA) was used to unveil neurites and rabbit anti-CD 31 (1:20, Abcam, United Kingdom) to identify HUVECs. Following 3 washes using PBS with 0.5 % (V/V) FCS, Alexa Fluor 488 goat anti-rabbit (1:1000, Invitrogen, USA) and Alexa Fluor 647 goat anti-mouse (1:1000, Invitrogen, USA) were diluted in PBS and added to the hydrogels overnight at 4 °C. Following 3 washes with PBS, a PBS solution with 1 µg/mL of DAPI (Invitrogen, USA) and 0.1 µg/mL (Sigma, USA) was added to the hydrogels for 45 minutes at RT. Imaging was performed on a confocal point-scanning microscope Olympus FV1000.

Neurite extension and outgrowth analysis

The area occupied by the neurites of each DRG explant was calculated using the ImageJ (NIH) plugin Neurite-J [41] and using a previously developed protocol [40]. Therefore, after defining the scale, the area referring to the body of the DRG was defined and the threshold contrast properly corrected to emphasize its neurites. The image is automatically translated to 8 bits and using the function "Analyze particles" the area corresponding to the extension the neurites is calculated. The longest neurite was also quantified using Neurite-J after identifying again the DRG body the plugin automatically creates concentric rings with 25 µm intervals and is defining as the length at which the last ring is capable of intersecting neurites.

Analysis of the vascular organization of HUVECs in GG-GRGDS

To analyze the vascular arrangement of HUVECs encapsulated in GG-GRGDS either in the presence or not of ASCs, AngioTool64 Version 0.6a was used [42]. After opening the images referring to the fluorescence channel utilized for CD31 and defining the scale, the background and small particles were removed by defining the appropriate signal threshold in the software. After this correction the software automatically quantifies different parameters related to vascular organization such as total vessel length, vessel area, vessel percentage area and number of junctions.

RNA extraction and qRT-PCR analysis

Total RNA was extracted from pools of 2 DRG using TripleXtractor and following the instructions provided by the manufacturers. After quantifying the RNA using a NanoDrop 1000 spectrophotometer (ThermoFisher Scientific, USA) the samples were diluted to approximately 1 μg/μL and 1 μg of sample transcribed into cDNA using the Xpert cDNA Synthesis Mastermix (Grisp, Portugal) to the manufacturer's protocol. Primers were designed using the Primer-BLAST tool (NCBI, USA) and the name of the genes, GenBank accession numbers and sequences are found on Table 2.1. The qRT-PCR reactions were done in a CFX96 real-time instrument (BioRad, USA) with the XPert Fast SYBR. mastermix and using equal cDNA concentrations for each sample following the manufacturer's instructions. The expression levels of target genes [GAP-43 and β-Tubulin III (Tubb3)] were normalized against housekeeping genes (GAPDH and HPRT-1) and presented as fold-change mRNA levels in comparison to the control group. The fold-change levels were calculated using the $2^{\Delta\Delta_{CT}}$ method.

Table 2.1 – Forward and reverse sequences of the primers used for qRT-PCR analysis and respective GenBank accession number, gene symbol, name and product size.

GENBANK NUMBER	SYMBOL	GENE NAME	PRIMER SEQUENCE (5' →3')	SIZE (BP)
NM_017195.3	GAP43	Growth Associated Protein 43	**Fw:** CAA GCT GAG GAG GAG AAA GAA GC **Rv:** GCA GGA GAG ACA GGG TTC AGG T	158
NM_139254.2	Tubb3	Tubulin beta III	**Fw:** AGA CCC CAG CGG CAA CTA TGT **Rv:** CCA GCA CCA CTC TGA CCG AA	204
NM_017008.4	GAPDH	Glyceraldehyde 3-phosphate dehydrogenase	**Fw:** CAG TGC CAG CCT CGT CTC AT **Rv:** TGG TGA TGG GTT TCC CGT TGA	247
NM_012583.2	HPRT1	Hypoxanthine phosphoribosyltransferase 1	**Fw:** CCT CAG TCC CAG CGT CGT GAT TA **Rv:** TCC AGC AGG TCA GCA AAG AAC T	231

Secretome collection from 3D cultures

The collection of the secretome from 3D cell culture sections was performed after culturing and maintaining cells across the 3 conditions (ASCs, HUVECs and their co-culture) for 6 days as detailed in **3D cell cultures – ASCs, HUVECs and their co-culture.** Subsequently, the hydrogels were washed 3 times with PBS and Neurobasal with 1 % (V/V) pen/strep. This is followed by their incubation with Neurobasal with 1 % (V/V) pen/strep during 24 h after which their secretome is collected, centrifuged at 1200 rpm for 5 min and the supernatant recovered and stored at -80 °C until further use.

Neurotrophic and Angiogenic profile of 3D secretomes

The evaluation of the angiogenic and neurotrophic profile of the previously obtained secretomes was performed using the Human Neuro Discovery Array C1 and Human Angiogenesis Array C1 (RayBiotech, USA) following the manufacturer's guidelines. Briefly, each membrane was blocked for unspecific interactions using blocking buffer for 30 minutes at RT which was followed by its removal and incubation with 1 mL of secretome overnight at 4 °C. Afterwards, the secretome was aspirated and the membranes washed using the washing buffers provided by the kit. Subsequently, 1 mL of biotinylated antibody cocktail was pipetted into each membrane and incubated for 2 h at RT. The antibody cocktail was removed, and the membranes washed using the same washing protocol. Then, 2 mL of 1x HRP-Streptavidin was added to each well and incubated for 2 h at RT. The membranes were once again washed and prior to their revealing, 500 µL of a 1:1 mixture containing Detection buffer C and D was added for 2 minutes at RT. Finally, the chemiluminescence image of each membrane was obtained using a Sapphire Biomolecular Imager (Azure Biosystems, USA). The intensity of each dot was quantified using the AzureSpot software (Azure Biosystems, USA) by designing an 8x8 dot grid adjusted to include each individual point. Absolute values were normalized for the mean of the positive control of each membrane and the background subtracted to allow the comparison between membranes and secretomes.

Chick chorioallantoic membrane (CD)assay

This simple *in vivo* system was used to evaluate the chemotactic capacity of GG-GRGDS hydrogels encapsulating ASCs in recruiting blood vessels towards the hydrogel in comparison to GG-GRGDS alone and collagen. The protocol was initiated by incubating white fertilized chicken eggs at 37 °C and under a 40 % humidified atmosphere for 3 days. After carefully cleaning the eggs with chlorohexidine and putting the egg racks in a laminar-flow hood a small hole in the smallest extremity of the egg was made 2 mL of albumin removed with a 20G needle in a syringe to dissociate the CAM from the egg shell. Embryo viability was assessed after creating a circular window (approximately 3 cm) that allowed to check it and granted access to the CAM. Then, the opening was sealed with parafilm and the remaining eggs allowed to return to the incubated where they stayed for 1 week. At this point, GG-GRGDS hydrogels encapsulating ASCs, GG-GRGDS alone and collagen were transferred to a zone with no major vascularization on top of a CAM, following opening the eggs and checking for their viability. GG-GRGDS hydrogels were produced 24 h before implantation as detailed in **Hydrogel preparation** and ASCs encapsulated according to **3D cell cultures – ASCs, HUVECs and their co-culture.** GG-GRGDS hydrogels with no cells were incubated in α-MEM supplemented with 10 % (w/V) FBS and 1 % pen/strep. Collagen hydrogels were done at the same

time by mixing rat tail Collagen Type I [3.61 mg/mL, 89.6 % (V/V), BD Biosciences, USA] with 10 % (V/V) of 10x DMEM concentrated medium (Invitrogen, USA) and 0.4 % (V/V) of a 7.5 % (w/V) $NaHCO_3$ solution. 50 µL hydrogel drops were then made and incubated for 2 h at 37 °C and 5% CO_2[40] for polymerization to occur. Then, the collagen hydrogels were incubated in α-MEM supplemented with 10 % (w/V) FBS and 1 % pen/strep until CAM implantation. Following 3 days of implantation the hydrogels were photographed *in ovo* using a stereomicroscope (Olympus S2x16) and the embryos sacrificed at -80 °C for 10 min and fixated in 4 % PFA at RT. The CAM portion harboring each hydrogel was dissected and excised using small scissors and transferred to 6-well plates. *Ex ovo* images of each CAM were taken and the total number of vessels directly converging to the hydrogels quantified using ImageJ which allowed to discriminate differences in this parameter between experimental groups.

Statistical analysis

Statistical analysis was performed using GraphPad Prism version 7.04 for Windows (GraphPad Software). Neurite outgrowth as well as CAM experiments were analyzed by performing one-way ANOVA followed by the Bonferroni *post-hoc* test. Welch's *t*-test allowed to assess differences among groups for the vascular arrangement experiments and two-way ANOVA with Tukey's multiple comparisons test to assess differences between groups at each timepoint. Differences were considered statistically significant if a p-value ≤ 0.05 was observed (95 % confidence level).

Results

Successful GRGDS engraftment in GG

The modification of GG followed a click chemistry approach previously optimized and published by our group [36,37]. Quantification of the total peptide bound to gellan gum using HPLC-based amino acid analysis showed 92.85 nmol of GRGDS per mg of GG (Figure 2.1).

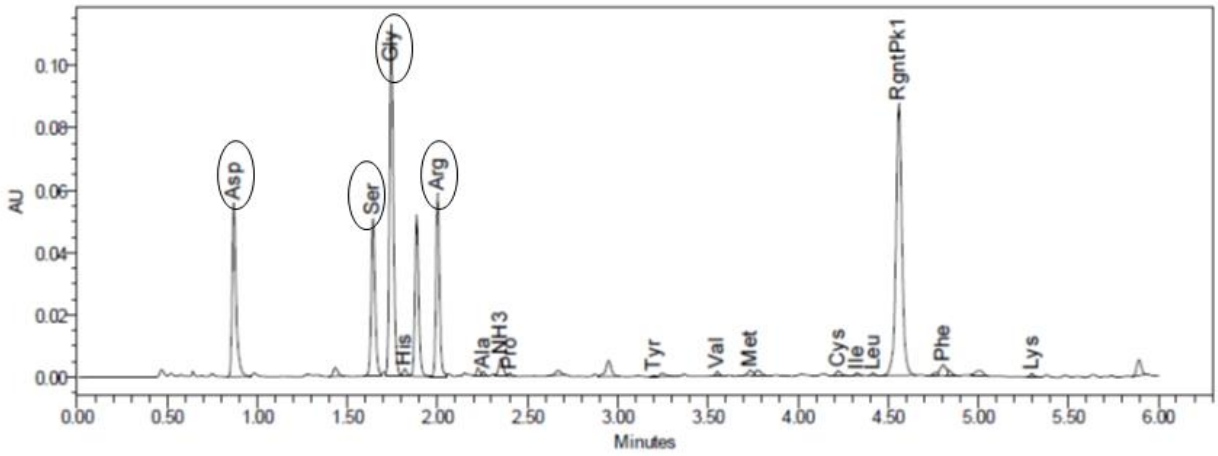

Figure 2.1 – Amino acid analysis allowed to quantify the amount of peptide bound to gellan (92.85 nmol of GRGDS/mg of gellan). Oval forms identify each peptide.

The presence of ASCs is fundamental to increase neurite outgrowth on DRG explants and the vascular assembly of HUVECs

Given the lack of self-regenerative capacity observed in SCI, understanding how this parameter is affected is of pivotal importance during the initial steps of the development of a therapeutic approach to treat the condition (biomaterial-based or not). Thus, modulation of neuritogenesis by co-culturing ASCs and HUVECs in GG-GRGDS was compared to each cell type alone and the hydrogel by itself using a DRG organotypic model for axonal regeneration. Following 7 days of culture it was observed that both ASCs and the co-culture promoted increased neurite outgrowth (Figure 2.2 A). Quantification of the area occupied by neurites provided similar values for GRGDS-GG encapsulating ASCs and the co-culture ($7.83\pm0.75\times10^5$ μm^2 and $8.0\pm1.2\times10^5$ μm^2, respectively), being superior to HUVECs alone ($608757\pm0.86\times10^5$ μm^2) and statistically significantly higher ($p<0.01$) than GG-GRGDS ($2.99\pm0.35\times10^5$ μm^2) (Figure 2.2 B).

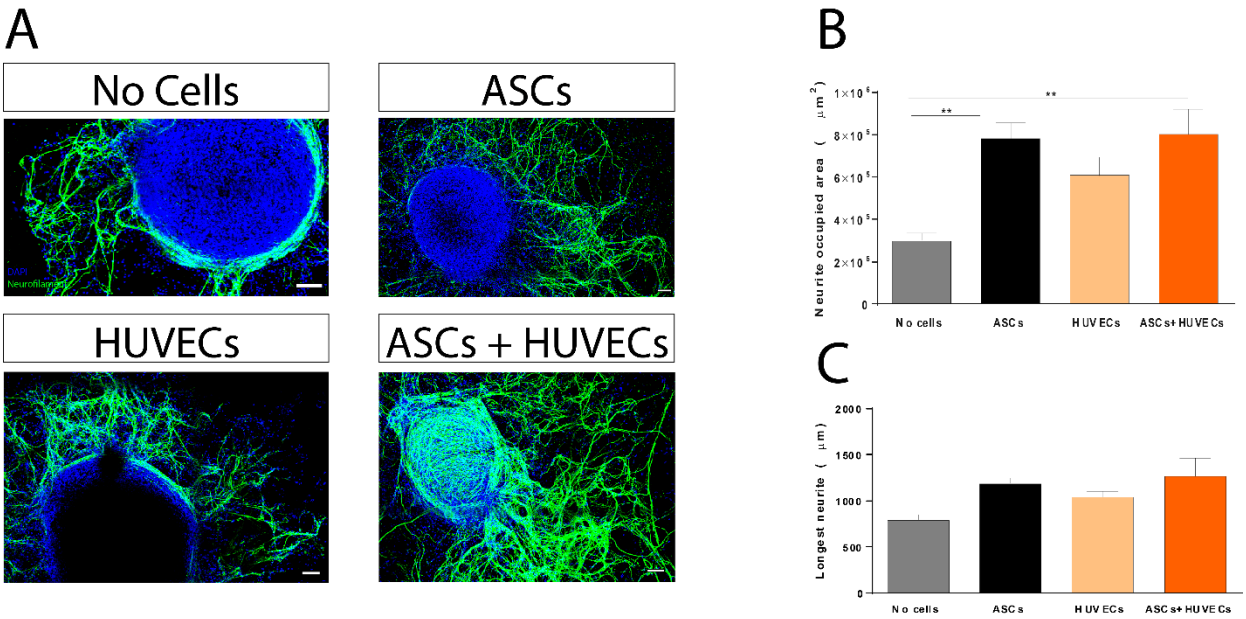

Figure 2.2 – Effect of co-culturing ASCs and HUVECs on GRGDS-modified gellan gum in the neurite outgrowth of DRG explants in comparison to each cell type alone. **A,** Representative images of the conditions. **B,** Co-culture promoted a similar outgrowth to ASCs, being statistically significantly higher than the hydrogel without cells. **C,** The longest neurite followed the same trend but without statistical differences. Scale bar: 100 µm. Values are shown as mean±SEM (n= 8/10); ¨p<0.01.

A biomaterial-based strategy that aims to promote a revascularization therapy for SCI must provide furnish adequate conditions for ECs to assemble into vascular structures. Therefore, this was another parameter analyzed during these experiments. When encapsulated alone in GG-GRGDS hydrogels, HUVECs were found to be interspersed along the hydrogel with no obvious assembly into vascular-like structures. This was in complete contrast to what occurred when co-culturing these ECs with ASCs, where the vascular organization of HUVECs was noticeable (Figure 2.3 A). The presence of ASCs statistically significantly increased several parameters related to vasculature such as vessel area (0.28±0.07 mm vs 1.32 ±0.16 mm; p<0.001), vessel percentage area (6.1±0.90 % vs 14.16±1.78 %; p<0.01), average vessel length (0.12±0.08 mm vs 0.31±0.07 mm; p<0.001),total vessel length (7.79±1.58 mm vs 39.72±5.02 mm; p<0.001), and the number of junctions formed by the vascular bed (19.50±5.39 mm vs 121.30±27.10 mm; p<0.01) (Figure 2.3B, C, D, E, F). These results show that ASCs have the capacity to induce vascular re-organization of biomaterials and how this modulation can be important to create a positive interplay on ECs and finally impact axonal growth.

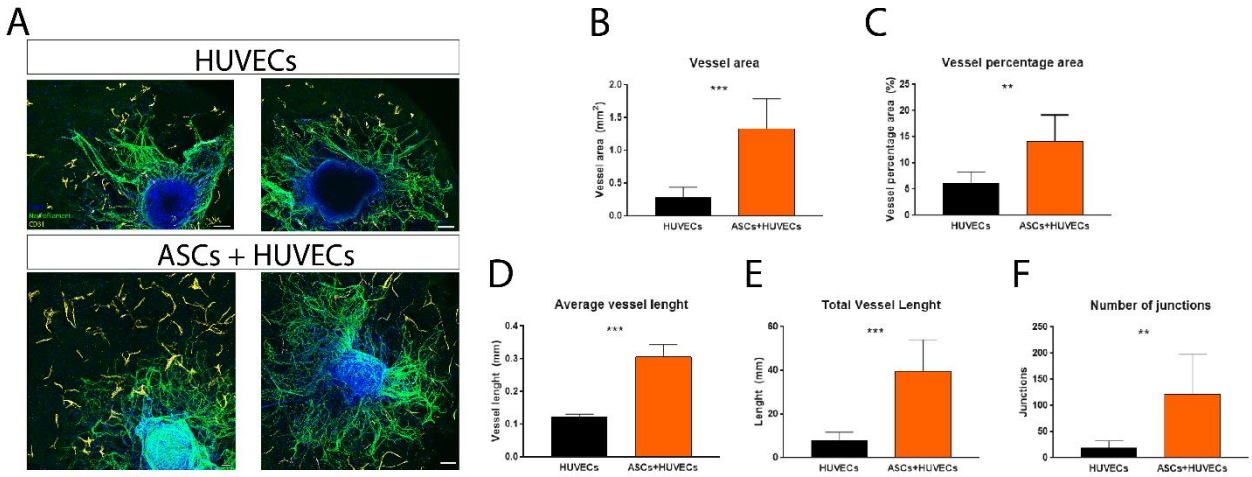

Figure 2.3 – A, Vascular organization of HUVECs inside GG-GRGDS when cultured alone and in co-culture with ASCs. These MSCs promoted the organization of the endothelial cells in vascular-like structures with a statistically significant increase on **B,** vessel area, **C,** vessel percentage area, **D,** average vessel length, **E,** total vessel length and **F,** number of junctions. Scale bar: 100 μm. Data is shown as mean±SEM with n=8/10. ¨p<0.01, ¨¨p<0.001.

GAP-43 expression rapidly increases in DRG from GG-GRGDS encapsulating ASCs and co-culture groups as β-Tubulin III decreases

The temporal dynamics of the genetic expression of GAP-43 (highly expressed in the growth cone of regenerating neurons) and Tubb3 (neuronal cytoskeleton) allowed to understand how the use of ASCs, HUVECs and their co-culture could be modulating neurite extension from DRG in comparison to the hydrogel without cells. Analyzing Figure 2.4 A it is possible to conclude that ASCs and the co-culture upregulated the expression of GAP-43 in DRG neurons as early as 12 h following culture (2.71±0.14 fold for ASCs and 3.47±0.71 fold for ASCs+HUVECs), reaching its maximum at 24 h (ASCs: 5.53±2.8 fold, ASCs+HUVECs: 9.1±4.33 fold) where statistically significant differences were found to HUVECs ($p<0.05$ for ASCs and $p<0.01$ for ASCs+HUVECs) and GG-GRGDS alone ($p<0.01$ for ASCs and $p<0.001$ for ASCs+HUVECs) during the same timepoint. The genetic expression of this axonal growth-related protein markedly decreased at the 4 days timepoint for both conditions where ASCs presented a lesser decrease following 7 days of culture.

GAP-43 expression in DRG cultured together with HUVECs encapsulated in GG-GRGDS was increased at the 12 and 24 h timepoints relative to the hydrogel alone (1.71±0.10 and 1.94±0.46 fold, respectively) but without the dramatic increase detailed for the other two conditions. Interestingly, the expression of Tubb3 followed the opposite path (Figure 2.4 B). Thus, the expression of this neuronal cytoskeleton gene was downregulated for ASCs and ASCs+HUVECs at 12h (ASCs: 0.69±0.23 fold; ASCs+HUVECs: 0.81±0.20 fold) and 24 h of culture (ASCs: 0.42±0.06 fold; ASCs+HUVECs: 0.53±0.31 fold). This gene,

however, was slightly upregulated at 4 days of culture for both conditions (1.39±0.50 fold for ASCs and 2.00±0.92 fold for ASCs+HUVECs) which was followed by its downregulation at 7 days of culture (ASCs: 0.54±0.09 fold; ASCs+HUVECs: 0.62±0.11 fold). The expression of Tubb3 for DRG cultured with HUVECs presented a more homogeneous dynamic (1.046±0.29 fold at 12h; 0.60±0.10 fold at 24h; 1.23±0.25 fold at 4 days; 0.646±0.12 fold at 7 days). These results show that the combination of GG-GRGDS hydrogels with ASCs or ASCS+HUVECs was able to stimulate axonal growth, which was reflected by increased GAP-43 levels at 12 h and 24 h following culture, contrarily to HUVECs where upregulation of this gene was not as markedly as seen for the other two conditions. On the other hand, it seemed that for neurite outgrowth to occur the cytoskeleton of DRG neurons had to be disturbed. These results are in line with what was observed in the neurite outgrowth experiments described in Figure 2.2.

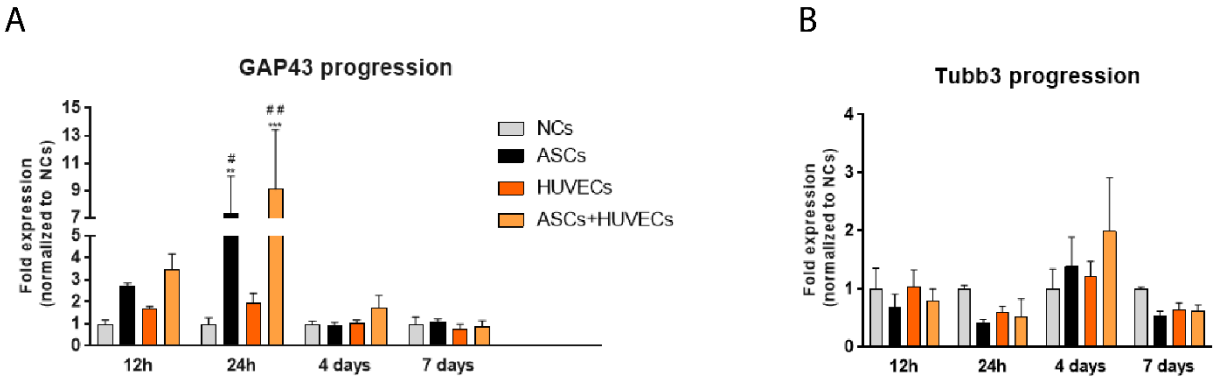

Figure 2.4 – Temporal dynamics of the expression of GAP-43 and βIII-tubulin in DRG cultured on GG-GRGDS encapsulating ASCs, HUVECs, ASCs+HUVECs or no cells. **A,** The co-culture condition increases the expression of GAP43 as early as 12h in comparison to all the other conditions, reaching the maximum at 24h (statistically significant to no cells and HUVECs) and decreasing at latter timepoints (4 and 7 days). **B,** The expression of Tubb3 follows an opposite dynamic and shows that the induction of plasticity is dependent on the downregulation of cytoskeleton genes. Scale bar: 100 μm. Results are shown as mean±SEM (n=4, each represents a pool of 2 DRG). ¨p<0.01 and ¨¨p<0.001 in comparison to no cells; #p<0.05 and ##p<0.01 in comparison to HUVECs.

Neurotrophic and angiogenic signature of the secretome of ASCs+HUVECs is distinct from each cell type alone

The results obtained on DRG experiments showed a clear beneficial effect on HUVECs by the presence of ASCs, with enhancement on their organization into vascular-like structures. This was followed by an increased capacity of the co-culture and ASCs in promoting neurite outgrowth from the explants in relation to HUVECs and prompted the study of the neurotrophic and angiogenic character of their secretomes. The full array of biomolecules detected, and their relative expression can be found in Supplementary

Figure 2.1.

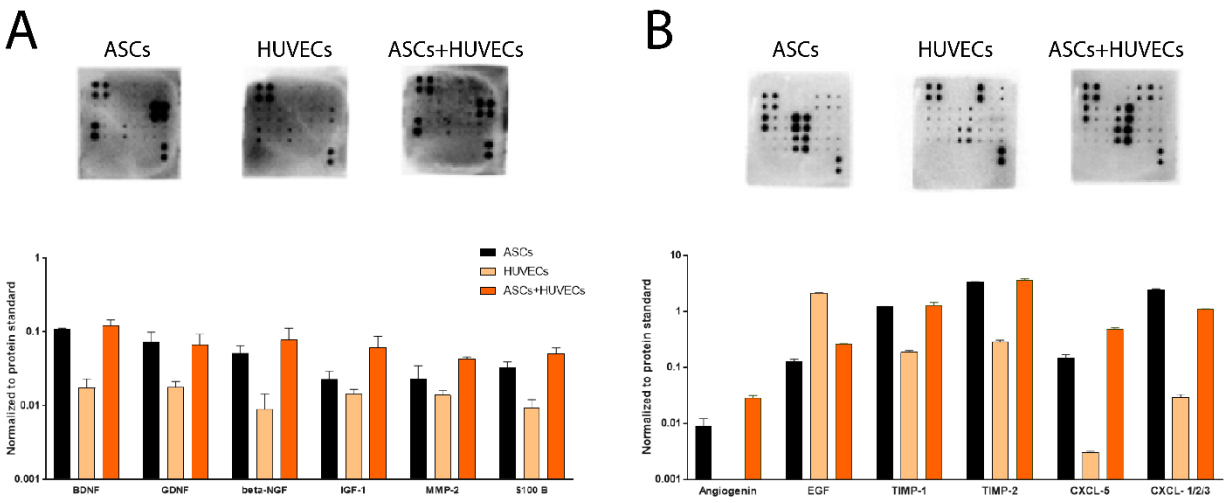

Figure 2.5 – Analysis of the secretomes of ASCs, HUVECs and their co-culture after 7 days of culture in GG-GRGDS allowed to understand the relative expression of a panel of neuroregulatory and angiotrophic molecules. **A,** The secretome of ASCs+HUVECs showed an upregulation on different neurotrophic factors (BDNF, β-NGF, IGF-1 and S-100 B) showing a positive effect of the interaction of both cells on the secretion of these molecules. **B,** The secretome of HUVECs presented decreased amounts of the quantified angiogenic molecules, with exception to EGF, whereas ASCs+HUVECs upregulated Angiogenin and CXCL-5 and ASCs promoted increased expression of CXCL-1/2/3. The relative expression values are shown in a logarithmic scale.

Starting with the neuroregulatory component of the conditioned media, the secretome of HUVECs showed markedly decreased amounts of growth factors associated with neuronal growth and survival, including BDNF, GDNF, β-NGF, IGF-1 or S100-B (Figure 2.5 A). This is the opposite of the other two conditions (ASCs and ASCs+HUVECs) where these neuroregulatory factors were upregulated. In fact, the highest relative expression values for BDNF, GDNF, β-NGF IGF-1 and S100 B were seen in the co-culture (Figure 2.5 A). Additionally, it was also observed high amounts of IL-6 and MCP-1 on the secretome of ASCs and ASCs+HUVECs, two cytokines that have an important role in immune response following neuronal trauma (Supplementary Figure 2.1 A). The analysis of angiogenic components followed the same trend, with the secretome of HUVECs in general presenting decreased expression of the factors, excepting EGF which presented increased relative amounts in the secretome of the ECs. These include TIMP-1 and TIMP-2, being the latter increased in the secretome of the co-culture, and CXCL-1/2/3 which was upregulated in the conditioned media of ASCs. The presence of Angiogenin and CXCL-5 was only observed whenever ASCs were present, showing both relative higher quantities in the secretome of ASCs+HUVECs (Figure 2.5 B). Additionally, we also found similar amounts of bFGF, VEGF-A and VEGF-D in the secretome of

ASCs and ASCs+HUVECs (Supplementary Figure 2.1 B).

Altogether, these results help to shed some insight in the way the secretome dynamics of ASCs might be affected by the presence of other cells on the environment. Thus, we observed a positive impact on the expression of neurotrophic factors when HUVECs were in culture together with ASCs and a very similar angiogenic profile for the secretome of ASCs and ASCs+HUVECs, a fact that may indicate that this modulation might be specific for some components of the secretome.

Vascular recruitment is potentiated by the presence of ASCs

To understand the capacity of GRGDS-modified GG encapsulating ASCs in recruiting blood vessels and induce vascular reorganization these were tested against the biomaterial without cells in an *in vivo* setting: the CAM assay. This model takes advantage of the highly vascularized chorioallantoic membrane (grows by day 7 of chick embryonic development and matures by day 12) to study angiogenesis. It is a cheap and relatively quick way to study angiogenesis, especially for drug screening and implantation of biomaterial-based therapies aiming to transplant cells (due to limited immune responses, which allow the transplant of xenografts) serving as proof-of-concept before evolving to more complex *in vivo* models [43]. Following 3 days of implantation (Figure 2.6A), the combination of hydrogel and ASCs exerted a chemoattractant effect on blood vessels as it significantly increased their convergence (70.17±3.76 blood vessels) when comparing to GRGDS alone (38.71±4.09 blood vessels) (Figure 2.6B). As previously detailed, this recruitment is likely to be mediated by the secretome of ASCs due to its highly rich angiogenic content. Therefore, these results show that ASCs have the potential to redesign the vascular milieu of SCI by promoting vascular attraction and reorganization of spared blood vessels (helping to revascularize the lesion site and prevent damage associated to vascular damage in SCI).

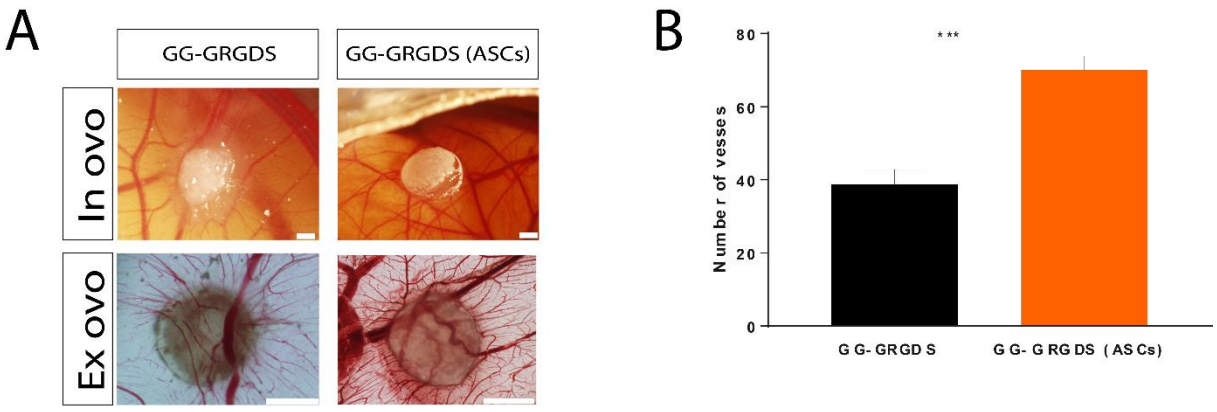

Figure 2.6 – Vessel recruitment capacity of ASCs encapsulated in GG-GRGDS following 3 days of implantation on CAM. **A,** Representative *in ovo* and *ex ovo* images of each condition. **B,** Quantification of the number of vessels

converging to the hydrogels demonstrated that these ASCs significantly impacted this parameter in comparison to the hydrogel without cells, which shows how these cells may affect the SCI vascular milieu following implantation. Scale bar: 1 mm. Results are shown as mean±SEM (n=12/14); ···p<0.001.

Discussion

Vascular damage leading to BSCB disruption occurs in spinal cord trauma or laceration, playing a critical role in defining the severity of SCI. In fact, Noble and Wrathall [44,45] demonstrated that the extension of the cystic cavity was similar to the intraparenchymal hemorrhage originated by vessel destruction and opened up the possibility that controlling this phenomena could lead to attenuate the severity of the condition. Even though the permeability of the BSCB is restored 14 days following injury, it is important to highlight that most vessels are not associated in neurovascular units, which are crucial in regulating appropriate blood flow to the spinal cord [6,46].

Li *et al.*, recently demonstrated that spinal cord tissue caudal to the lesion site is in permanent hypoxia. By artificially elevating O_2 levels, the authors observed a prolonged increased on tissue oxygenation (in opposition to rostral to lesion where the values got back to normal 1 min after the stimulus) probably due to triggering neurovascular coupling, which further dilates vessels and increases oxygen and neuronal activity, originating transient locomotor gains of function [9]. This elegant study clearly underlines the importance of appropriate vascular functional for neuronal homeostasis.

Aiming to reshape the vascular milieu following SCI, in this work we started by understanding the potential of ASCs in modulating this parameter and how it would affect axonal growth. Thus, these MSCs were encapsulated with HUVECs in an in-house biomaterial-based approach (GG-GRGDS hydrogels) and the neurite outgrowth experiments showed that the co-culture provided potential for axonal regeneration similar to ASCs alone and superior to HUVECs or the hydrogel, opening the possibility of positive between both types of cells in the injury environment. In fact, the co-culture (as ASCs alone) proved to impact the internal neuronal growth machinery from early timepoints (12 h at least) as shown by the upregulation of a protein directly connected to axonal growth (GAP-43). This protein is highly expressed in regenerating axons where it acts to potentiate filopodia formation in growth cones (if phosphorylated) or induces microtubule-based outgrowth (if unphosphorylated) [47,48]. One of the molecules that has been shown to upregulate GAP-43 is BDNF [49,50], being essential for the neurotrophic action of the latter. Therefore, this is one of the mechanisms we propose for the neurite outgrowth results here reported.

The beneficial effects of ASCs on the organization of HUVECs were quite visible within the hydrogels, since these ECs were only capable of organizing in vascular-like structures when cultured in the presence

of the MSCs. The characterization of the secretome of ASCs by our [24] and other groups [51–53] has showed an enrichment in angiogenic growth factors which could explain the impact of these MSCs on the vascular organization of HUVECs. Nevertheless, in line with our findings, others reported increased tube-formation capacity and vessel network stability of ECs when co-cultured in the presence of ASCs or other types of MSCs [29,54]. These studies showed that ASCs induced an increased expression of CD31 in ECs and acted on VEGF, hepatocyte growth factor (HGF) and PDGF-BB pathways being their presence imperative for the formation and stabilization of such networks.

The present work also showed that the effect of ASCs on HUVECs probably created a positive synergy that can upregulate a different variety of neurotrophic factors. These molecules belong to the PI3K-Akt pathway, which our group previously identified as one of the effectors of the secretome of ASCs in injured spinal cord [40]. This pathway contributes to cell growth, proliferation and nutrient uptake and its activation has been shown to promote the regeneration of corticospinal tract neurons [55] and optic nerve axons [56], making it a central signaling cascade to drive regeneration.

Moving away from classical neurotrophic factors, we desired to highlight the prevalence of IL-6, and MCP-1 in the secretome of ASCs and ASCs+HUVECs which are classically defined as mediators of the inflammatory response and can also impact neuronal regeneration [57–59]. Willis et al., showed that IL-6 induces neuroprotection in neurons following traumatic brain injury by a *trans*-signaling mechanism [58]. MCP-1 seems to mediate the crosstalk between DRG neurons and macrophages, inducing neurite outgrowth and mobilizing M2 macrophages [59].

The analysis of angiotrophic molecules revealed the presence of several angiotrophic factors such as Angiogenin, EGF, bFGF, PDGF-BB, TPO as well as VEGF-A and VEGF-D in the secretome of ASCs and ASCs+HUVECs. During these experiments it was clear that the secretome of HUVECs showed a clear downregulation, in some cases lack of expression of these factors, a fact that highlights the importance of adding ASCs to provoke their normal homeostasis in GG-GRGDS and might help to explain their incapacity to assembly into vascular-like networks in the absence of the MSCs. Two type of VEGF isoforms (VEGF-A and -D), a key family of angiogenic proteins, were detected on the analyzed secretomes. VEGF-A binds VEGFR1 and VEGFR2 and is crucial for vascular development during embryogenesis, continuing to stimulate angiogenesis postnatally and having also a role in pathological angiogenesis [60]. In addition this isoform is capable exerting neurotrophic and neuroprotective effects (trough flk-1), being a molecule capable of connecting angiogenesis with neuronal development [61].

We also found increased levels of TIMP-1 and TIMP-2 in all the conditioned media collected from ASCs and ASCs+HUVECs collected in GG-GRGDS hydrogels, a possible reflection of the cellular interactions at

the time of recollection. These were collected after 7 days of culture when the cells colonized the entire hydrogel and vascular networks (for the co-culture) were established leading to the inhibition of cellular migration, and the stabilization of the vascular networks formed.

CXCL5 and CXCL1/2/3 also showed increased relative amounts in the secretomes of ASCs+HUVECs and ASCs, respectively. Both chemokines impact angiogenesis after binding to CXCR2 [62,63]. CXCL5 exerts angiogenic effects through the induction of VEGF-A by binding FOXD1 protein to a promoter of the growth factor [62]. CXCL1/2/3 .through CXCR2, leads to the activation and migration of ECs [63]. These results allowed us to understand the relative expression of a myriad of angiogenic and neurotrophic effectors present in the secretome of ASCs and how it can be modulated by the presence of other cells in a 3D environment (in this case HUVECs).

Otherwise a bioinert polymer, previous works have demonstrated that the insertion of RGD motifs into the backbone of gellan gum allows the polymer to activate cellular integrins which in turn induces cellular adhesion, proliferation, survival and regular homeostasis [36,37]. Accordingly, this chemical modification also impacts the quality of the secretome of MSCs since secretome collected from MSCs on GRGDS-modified gellan gum enhanced neuronal survival, their proliferation and metabolism in comparison to native gellan gum [64]. Apart from these chemical cues, the physical properties of the three dimensional environment provided by hydrogels also have a profound impact on cellular behavior [65]. Chaudhuri et al., designed RGD-modified alginate hydrogels with different stress relaxation properties and elegantly showed how the simple modulation of this physical parameter directed MSC differentiation and impacted cellular proliferation independently of RGD density [66]. Taking this example into consideration, the elucidation on how such parameters govern the capacity of GRGDS-GG in promoting for instance the assembling HUVECs into vascular-like structures or the impact the physical properties of the hydrogel have on the secretome of ASCs should be explored in future studies.

Even though our *in vitro* results showed the potential ASCs have to influence angiogenesis and vascular organization of transplanted ECs, these still needed to be validated in an *in vivo-like* setting. The CAM assay enabled to observe that ASCs encapsulated in GG-GRGDS had a significantly higher capacity in recruiting blood vessels towards the hydrogel when compared to GG-GRGDS, a feature that shows the impact of their secretome on reshaping vascular organization and recruitment. This feature is of primordial importance when thinking on the implantation of a vascularization strategy in an animal model of SCI. Therefore, it shows that it might have the capacity to stimulate angiogenesis and with this induce the revascularization of the lesion site and possibly control the infiltration of inflammatory cells from the acute phase of the condition. Finally, this might allow to modulate the severity of the condition.

Conclusions

In this work we started by validating *in vitro* the potential of developing a therapeutic approach aiming to restore normal homeostatic vasculature following SCI and with this to positively modulate inflammation with the final goal of impacting disease severity and motor and autonomic recovery. The co-culture ASCs+HUVECs in GG-GRGDS hydrogels lead to a similar neurite outgrowth and arborization in DRG explants as ASCs alone, impacting genetic expression of proteins involved in regeneration as early as 12 h following culture. Moreover, ASCs were pivotal for the arrangement of HUVECs into vascular-like structures a feature probably due not only to their paracrine action but also to cell-to-cell communication. The neurotrophic part of the secretome of ASCs and HUVECs showed an upregulation in some of these molecules, proving that the interaction between these MSCs and ECs may induce benefits to SCI environment. Regarding the angiotrophic molecules analyzed, the profile of ASCs and co-culture was similar, which helps to prove that the major changes in vascular assembly are majorly mediated by cell-cell contact. Finally, implantation of the hydrogel together with ASCs in the CAM lead to increased recruitment of blood vessels which shows the potential of these cell in reshaping the vascular milieu *in vivo*. Altogether, these results open up a promising possibility of implanting this biomaterial-based cell therapy in a SCI animal to study its impact on revascularization and functional recovery.

Acknowledgments

We want to acknowledge Professor Jeffrey Gimble at the Tulane University Center for Stem Cell Research and Regenerative Medicine and LaCell LLC (New Orleans, Louisiana, USA) for kindly providing the ASCs used in this study. The authors want to acknowledge the financial support from Prémios Santa Casa Neurociências - Prize Melo e Castro for Spinal Cord Injury Research (MC-04/17); from Portuguese Foundation for Science and Technology [Doctoral fellowship (PD/BDE/127835/2016) to L. A. Rocha; Post-doctoral fellowship (SFRH/BPD/117858/2016) to S. Granja and Scientific Employment Stimulus to N. A. Silva (CEECIND/04794/2017)]. This work was funded by FEDER, through the Competitiveness Internationalization Operational Program (POCI), and by National funds, through the Foundation for Science and Technology (FCT), under the scope of the projects POCI-01-0145-FEDER-007038; TUBITAK/0007/2014; PTDC/DTP-FTO/5109/2014; POCI-01-0145-FEDER-029206; POCI-01-0145-FEDER-031392; PTDC/MED-NEU/31417/2017 and NORTE-01-0145-FEDER-029968. This work has also been developed under the scope of the project NORTE-01-0145-FEDER-000013, supported by the Northern Portugal Regional Operational Programme (NORTE 2020), under the Portugal 2020 Partnership Agreement, through the European Regional Development Fund (FEDER).

References

1. James, S. L. *et al.* Global, regional, and national burden of traumatic brain injury and spinal cord injury, 1990–2016: a systematic analysis for the Global Burden of Disease Study 2016. *Lancet Neurol.* **18**, 56–87 (2019).
2. Silva, N. A., Sousa, N., Reis, R. L. & Salgado, A. J. From basics to clinical: A comprehensive review on spinal cord injury. *Prog. Neurobiol.* **114**, 25–57 (2014).
3. Mautes, A. E., Weinzierl, M. R., Donovan, F. & Noble, L. J. Vascular events after spinal cord injury: contribution to secondary pathogenesis. *Phys. Ther.* **80**, 673–87 (2000).
4. Bartanusz, V., Jezova, D., Alajajian, B. & Digicaylioglu, M. The blood-spinal cord barrier: morphology and clinical implications. *Ann. Neurol.* **70**, 194–206 (2011).
5. Tator, C. H. & Koyanagi, I. Vascular mechanisms in the pathophysiology of human spinal cord injury. *J. Neurosurg.* **86**, 483–92 (1997).
6. Casella, G. T. B., Marcillo, A., Bunge, M. B. & Wood, P. M. New vascular tissue rapidly replaces neural parenchyma and vessels destroyed by a contusion injury to the rat spinal cord. *Exp. Neurol.* **173**, 63–76 (2002).
7. Dray, C., Rougon, G. & Debarbieux, F. Quantitative analysis by in vivo imaging of the dynamics of vascular and axonal networks in injured mouse spinal cord. *Proc. Natl. Acad. Sci. U. S. A.* **106**, 9459–64 (2009).
8. Whetstone, W. D., Hsu, J. Y. C., Eisenberg, M., Werb, Z. & Noble-Haeusslein, L. J. Blood-spinal cord barrier after spinal cord injury: Relation to revascularization and wound healing. *J. Neurosci. Res.* **74**, 227–239 (2003).
9. Li, Y. *et al.* Pericytes impair capillary blood flow and motor function after chronic spinal cord injury. *Nat. Med.* **23**, 733–741 (2017).
10. De Laporte, L. *et al.* Vascular endothelial growth factor and fibroblast growth factor 2 delivery from spinal cord bridges to enhance angiogenesis following injury. *J. Biomed. Mater. Res. - Part A* **98 A**, 372–382 (2011).
11. Rauch, M. F. *et al.* Engineering angiogenesis following spinal cord injury: a coculture of neural progenitor and endothelial cells in a degradable polymer implant leads to an increase in vessel density and formation of the blood-spinal cord barrier. *Eur. J. Neurosci.* **29**, 132–45 (2009).
12. Han, S. *et al.* Rescuing vasculature with intravenous angiopoietin-1 and αvβ3 integrin peptide is protective after spinal cord injury. *Brain* **133**, 1026–1042 (2010).
13. Yu, S. *et al.* Angiogenic microspheres promote neural regeneration and motor function recovery

after spinal cord injury in rats. *Sci. Rep.* **6**, 33428 (2016).

14. Duan, H. *et al.* Transcriptome analyses reveal molecular mechanisms underlying functional recovery after spinal cord injury. *Proc. Natl. Acad. Sci.* **112**, 201510176 (2015).
15. Chedly, J. *et al.* Physical chitosan microhydrogels as scaffolds for spinal cord injury restoration and axon regeneration. *Biomaterials* **138**, 91–107 (2017).
16. Ropper, A. E. *et al.* Defining recovery neurobiology of injured spinal cord by synthetic matrix-assisted hMSC implantation. *Proc. Natl. Acad. Sci.* 201616340 (2017) doi:10.1073/pnas.1616340114.
17. Matsushita, T. *et al.* Diffuse and persistent blood–spinal cord barrier disruption after contusive spinal cord injury rapidly recovers following intravenous infusion of bone marrow mesenchymal stem cells. *Exp. Neurol.* **267**, 152–164 (2015).
18. Vawda, R. *et al.* Early Intravenous Infusion of Mesenchymal Stromal Cells Exerts a Tissue Source Age-Dependent Beneficial Effect on Neurovascular Integrity and Neurobehavioral Recovery After Traumatic Cervical Spinal Cord Injury. *Stem Cells Transl. Med.* sctm.18-0192 (2019) doi:10.1002/sctm.18-0192.
19. Morita, T. *et al.* Intravenous infusion of mesenchymal stem cells promotes functional recovery in a model of chronic spinal cord injury. *Neuroscience* **335**, 221–231 (2016).
20. Novikova, L. N., Brohlin, M., Kingham, P. J., Novikov, L. N. & Wiberg, M. Neuroprotective and growth-promoting effects of bone marrow stromal cells after cervical spinal cord injury in adult rats. *Cytotherapy* **13**, 873–887 (2011).
21. Spejo, A. B., Carvalho, J. L., Goes, A. M. & Oliveira, A. L. R. Neuroprotective effects of mesenchymal stem cells on spinal motoneurons following ventral root axotomy: Synapse stability and axonal regeneration. *Neuroscience* **250**, 715–732 (2013).
22. Ribeiro, T. B. *et al.* Neuroprotection and immunomodulation by xenografted human mesenchymal stem cells following spinal cord ventral root avulsion. *Sci. Rep.* **5**, 16167 (2015).
23. Salgado, A. J. *et al.* Mesenchymal stem cells secretome as a modulator of the neurogenic niche: basic insights and therapeutic opportunities. *Front. Cell. Neurosci.* **9**, (2015).
24. Pires, A. O. *et al.* Unveiling the Differences of Secretome of Human Bone Marrow Mesenchymal Stem Cells, Adipose Tissue derived Stem Cells and Human Umbilical Cord Perivascular Cells: A Proteomic Analysis. *Stem Cells Dev.* **25**, 1073–83 (2016).
25. Bunnell, B. A., Flaat, M., Gagliardi, C., Patel, B. & Ripoll, C. Adipose-derived stem cells: isolation, expansion and differentiation. *Methods* **45**, 115–20 (2008).

26. Bronckaers, A. *et al.* Mesenchymal stem/stromal cells as a pharmacological and therapeutic approach to accelerate angiogenesis. *Pharmacol. Ther.* **143**, 181–196 (2014).
27. Verseijden, F. *et al.* Adult human bone marrow- and adipose tissue-derived stromal cells support the formation of prevascular-like structures from endothelial cells in vitro. *Tissue Eng. Part A* **16**, 101–14 (2010).
28. Rohringer, S. *et al.* Mechanisms of vasculogenesis in 3D fibrin matrices mediated by the interaction of adipose-derived stem cells and endothelial cells. *Angiogenesis* (2014) doi:10.1007/s10456-014-9439-0.
29. Merfeld-Clauss, S., Gollahalli, N., March, K. L. & Traktuev, D. O. Adipose tissue progenitor cells directly interact with endothelial cells to induce vascular network formation. *Tissue Eng. - Part A* (2010) doi:10.1089/ten.tea.2009.0635.
30. Li, S., Haigh, K., Haigh, J. J. & Vasudevan, A. Endothelial VEGF Sculpts Cortical Cytoarchitecture. *J. Neurosci.* **33**, 14809–14815 (2013).
31. Lange, C. *et al.* Relief of hypoxia by angiogenesis promotes neural stem cell differentiation by targeting glycolysis. *EMBO J.* **35**, 924–941 (2016).
32. Paredes, I., Himmels, P. & Ruiz de Almodóvar, C. Neurovascular Communication during CNS Development. *Dev. Cell* **45**, 10–32 (2018).
33. Himmels, P. *et al.* Motor neurons control blood vessel patterning in the developing spinal cord. *Nat. Commun.* **8**, (2017).
34. Orive, G., Anitua, E., Pedraz, J. L. & Emerich, D. F. Biomaterials for promoting brain protection, repair and regeneration. *Nat. Rev. Neurosci.* **10**, 682–692 (2009).
35. Khaing, Z. Z., Thomas, R. C., Geissler, S. A. & Schmidt, C. E. Advanced biomaterials for repairing the nervous system: what can hydrogels do for the brain? *Mater. Today* **17**, 332–340 (2014).
36. Silva, N. A. *et al.* The effects of peptide modified gellan gum and olfactory ensheathing glia cells on neural stem/progenitor cell fate. *Biomaterials* **33**, 6345–6354 (2012).
37. Gomes, E. D. *et al.* Combination of a peptide-modified gellan gum hydrogel with cell therapy in a lumbar spinal cord injury animal model. *Biomaterials* **105**, 38–51 (2016).
38. Dubois, S. G. *et al.* Isolation of human adipose-derived stem cells from biopsies and liposuction specimens. in *Methods in molecular biology (Clifton, N.J.)* vol. 449 69–79 (2008).
39. Silva, N. A. *et al.* Modulation of bone marrow mesenchymal stem cell secretome by ECM-like hydrogels. *Biochimie* **95**, 2314–2319 (2013).
40. Gomes, E. D. *et al.* Co-Transplantation of Adipose Tissue-Derived Stromal Cells and Olfactory

Ensheathing Cells for Spinal Cord Injury Repair. *Stem Cells* **36**, 696–708 (2018).

41. Torres-Espín, A., Santos, D., González-Pérez, F., del Valle, J. & Navarro, X. Neurite-J: An Image-J plug-in for axonal growth analysis in organotypic cultures. *J. Neurosci. Methods* **236**, 26–39 (2014).
42. Zudaire, E., Gambardella, L., Kurcz, C. & Vermeren, S. A Computational Tool for Quantitative Analysis of Vascular Networks. *PLoS One* **6**, e27385 (2011).
43. Nowak-Sliwinska, P., Segura, T. & Iruela-Arispe, M. L. The chicken chorioallantoic membrane model in biology, medicine and bioengineering. *Angiogenesis* (2014) doi:10.1007/s10456-014-9440-7.
44. Noble, L. J. & Wrathall, J. R. Correlative analyses of lesion development and functional status after graded spinal cord contusive injuries in the rat. *Exp. Neurol.* **103**, 34–40 (1989).
45. Noble, L. J. & Wrathall, J. R. Distribution and time course of protein extravasation in the rat spinal cord after contusive injury. *Brain Res.* **482**, 57–66 (1989).
46. Goritz, C. *et al.* A Pericyte Origin of Spinal Cord Scar Tissue. *Science (80-.).* **333**, 238–242 (2011).
47. He, Q., Dent, E. W. & Meiri, K. F. Modulation of actin filament behavior by GAP-43 (neuromodulin) is dependent on the phosphorylation status of serine 41, the protein kinase C site. *J. Neurosci.* (1997) doi:10.1523/jneurosci.17-10-03515.1997.
48. Dent, E. W. & Meiri, K. F. Distribution of phosphorylated GAP-43 (neuromodulin) in growth cones directly reflects growth cone behavior. *J. Neurobiol.* (1998) doi:10.1002/(SICI)1097-4695(19980605)35:3<287::AID-NEU6>3.0.CO;2-V.
49. Segal, R. A., Pomeroy, S. L. & Stiles, C. D. Axonal growth and fasciculation linked to differential expression of BDNF and NT3 receptors in developing cerebellar granule cells. *J. Neurosci.* (1995) doi:10.1523/jneurosci.15-07-04970.1995.
50. Gupta, S. K. *et al.* GAP-43 is essential for the neurotrophic effects of BDNF and positive AMPA receptor modulator S18986. *Cell Death Differ.* **16**, 624–637 (2009).
51. Kachgal, S. & Putnam, A. J. Mesenchymal stem cells from adipose and bone marrow promote angiogenesis via distinct cytokine and protease expression mechanisms. *Angiogenesis* (2011) doi:10.1007/s10456-010-9194-9.
52. Nakanishi, C. *et al.* Gene and protein expression analysis of mesenchymal stem cells derived from rat adipose tissue and bone marrow. *Circ. J.* **75**, 2260–8 (2011).
53. Nakagami, H. *et al.* Novel autologous cell therapy in ischemic limb disease through growth factor

secretion by cultured adipose tissue-derived stromal cells. *Arterioscler. Thromb. Vasc. Biol.* (2005) doi:10.1161/01.ATV.0000190701.92007.6d.

54. Holnthoner, W. *et al.* Adipose-derived stem cells induce vascular tube formation of outgrowth endothelial cells in a fibrin matrix. *J. Tissue Eng. Regen. Med.* **9**, 127–136 (2015).
55. Liu, K. *et al.* PTEN deletion enhances the regenerative ability of adult corticospinal neurons. *Nat. Neurosci.* **13**, 1075–81 (2010).
56. Park, K. K. *et al.* Promoting axon regeneration in the adult CNS by modulation of the PTEN/mTOR pathway. *Science* **322**, 963–6 (2008).
57. Leibinger, M. *et al.* Interleukin-6 contributes to CNS axon regeneration upon inflammatory stimulation. *Cell Death Dis.* **4**, e609–e609 (2013).
58. Willis, E. F. *et al.* Repopulating Microglia Promote Brain Repair in an IL-6-Dependent Manner. *Cell* **180**, 833-846.e16 (2020).
59. Kwon, M. J. *et al.* CCL2 Mediates Neuron-Macrophage Interactions to Drive Proregenerative Macrophage Activation Following Preconditioning Injury. *J. Neurosci.* **35**, 15934–15947 (2015).
60. Holmes, D. I. R. & Zachary, I. The vascular endothelial growth factor (VEGF) family: angiogenic factors in health and disease. *Genome Biol.* **6**, 209 (2005).
61. Sondell, M., Sundler, F. & Kanje, M. Vascular endothelial growth factor is a neurotrophic factor which stimulates axonal outgrowth through the flk-1 receptor. *Eur. J. Neurosci.* **12**, 4243–4254 (2000).
62. Chen, C. *et al.* CXCL5 induces tumor angiogenesis via enhancing the expression of FOXD1 mediated by the AKT/NF-κB pathway in colorectal cancer. *Cell Death Dis.* **10**, 178 (2019).
63. Mehrad, B., Keane, M. P. & Strieter, R. M. Chemokines as mediators of angiogenesis. *Thrombosis and Haemostasis* (2007) doi:10.1160/TH07-01-0040.
64. Silva, N. A. *et al.* Modulation of bone marrow mesenchymal stem cell secretome by ECM-like hydrogels. *Biochimie* (2013) doi:10.1016/j.biochi.2013.08.016.
65. Lee, J. H. & Kim, H. W. Emerging properties of hydrogels in tissue engineering. *J. Tissue Eng.* (2018) doi:10.1177/2041731418768285.
66. Chaudhuri, O. *et al.* Hydrogels with tunable stress relaxation regulate stem cell fate and activity. *Nat. Mater.* **15**, 326–334 (2016).

Supplementary material

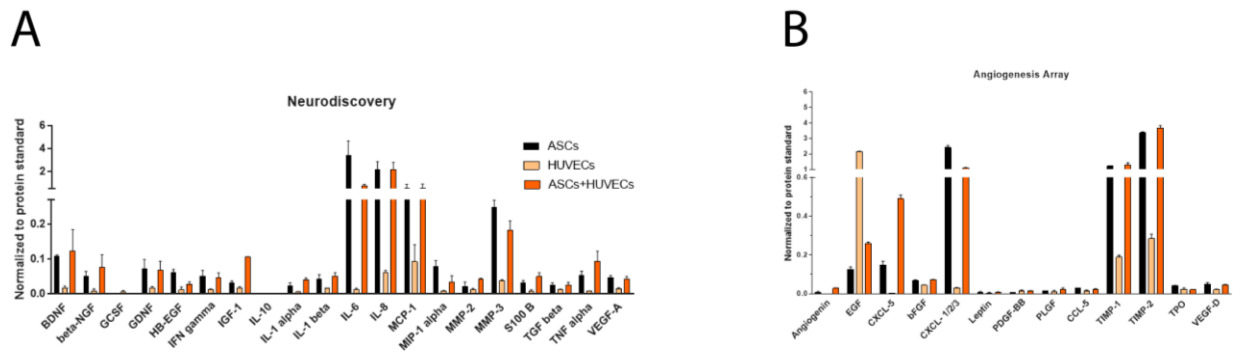

Supplementary Figure 2.1 – Total panel of molecules detected on **A,** Neurodiscovery and **B,** Angiogenesis Array and their relative expression.

CHAPTER 3

L. A. Rocha, C. Mas-Moruno, E. D. Gomes, A. F. B. Räder, H. Kessler, R. A. Sousa, D. A. Learmonth, A. J. Salgado.

Integrin-specific modified gellan gum hydrogels for neuronal and vascular tissue engineering purposes

(Manuscript in preparation)

(2021)

Title

Integrin-specific modified gellan gum hydrogels for neuronal and vascular tissue engineering purposes

Authors

L. A. Rocha[1,2,3], C. Mas-Moruno[4], E. D. Gomes[1,2], A. F. B. Räder[5], H. Kessler[5], R. A. Sousa[3], D. A. Learmonth[3], A. J. Salgado[1,2].

Affiliations

[1]Life and Health Sciences Research Institute (ICVS), School of Medicine, University of Minho, Braga, Portugal.

[2]ICVS/3B's – PT Government Associate Laboratory, Braga, Portugal.

[3]Stemmatters, Biotecnologia e Medicina Regenerativa SA, Barco, Portugal.

[4] Biomaterials, Biomechanics and Tissue Engineering Group (BBT), Department of Materials Science and Engineering, Universitat Politècnica de Catalunya (UPC), Barcelona, Spain.

[5]Technische Universität München, Department Chemie, Institute for Advanced Study, Lichtenbergstrasse, Garching, Germany.

Corresponding author

A. J. Salgado (PhD), Life and Health Sciences Research Institute (ICVS), School of Medicine, University of Minho, Campus Gualtar, 4710-057 Braga, Portugal.

Phone number: +351 253 60 49 47

E-mail: asalgado@med.uminho.pt

Abstract

The biofunctionalization of essentially inert materials is often achieved using linear adhesion peptides that partially lose their conformation upon binding and hence their bioactivity. In this work we studied the use of αvβ3 and α5β1 integrin-selective mimetics to biofunctionalize gellan gum. Both these integrins are highly expressed during angiogenesis, and indeed, faulting vascular repopulation is one of the key hallmarks of SCI and decisively contributes to the poor prognosis associated to the condition. Therefore, the main goals of the work were: to characterize the biological properties of these modifications by studying their capacity to promote the adhesion and spreading of ASCs; understand their impact on neurite outgrowth from DRG (either without encapsulated cells, or encapsulating ASCs, HUVECs and their co-culture); assess their capacity to promote the vascular assembly of human umbilical HUVECs, either with encapsulated ASCs or the hydrogel alone.

Initially, different reaction stoichiometries were tested and characterized by varying the polymer:ligand ratio (10:1, 20:1) and the bioactivity of each condition tested and compared with GG functionalized with RGD employing the same ratios. We observed that the polymer grafted with the αvβ3 mimetic ligand in a 10:1 ratio significantly promoted the extension area of ASCs both at 3 and 7 days of culture in comparison to all the other conditions. Furthermore, the neurite extension from DRG explants was increased when combining the mimetic-functionalized hydrogel with cells (ASCs or ASCs+HUVECs) and ASCs clearly induced the assembly of HUVECs into vascular-like structures. This work shows for the first time the potential of using integrin selective ligands to enhance the biological properties of hydrogels made from bioinert materials in central nervous system applications, and opens the possibility of studying this approach in an in vivo model of SCI.

Keywords: peptidomimetics, integrin-specific ligands, neuronal tissue engineering, vascularization, MSC, neurovascular, secretome.

Introduction

Integrins are fundamental glycoproteic receptors to sense the local cellular environment, where they act essentially to promote the interaction of cells with their ECM. This process is mediated by several proteins that induce integrin activation. Depending on the integrin subtype and ECM protein interacting, distinct cellular phenomena are originated including cytoskeleton reorganization, cell cycle regulation, cell adhesion, cell migration and the trafficking of cell receptors [1]. Integrins encompass two non-covalently attached subunits (α and β) possessing an extracellular domain, a transmembrane region and a noncatalytic cytoplasmic domain [2]. Vertebrates have a total of 24 integrins that result from the combination between 18 α and 8 β subtypes, being this the feature that dictates their affinity towards a given ligand [3].

Their central role on numerous cellular processes has led to extensive structural studies to understand the peptidic sequences that govern such events. A major breakthrough on this field was the discovery that a simple tripeptidic sequence [RGD (Arg-Gly-Asp)] present in a substantial portion of ECM proteins (collagen, fibronectin, vitronectin, laminin and osteopontin), was able to promote extensive cell adhesion [4,5]. Since then, numerous small peptidic sequences that interact with integrins and govern cell adhesion, or other processes like neuronal differentiation or angiogenesis have been discovered. This has given researchers on the field of tissue engineering a vast range of possibilities to functionalize otherwise bioinert materials and provide them with cell instructive cues [6,7]. Previously, we have developed a GRGDS-modified GG hydrogel with enhanced biological properties due to peptidic biofunctionalization to neuronal tissue engineering applications. This hydrogel proved to be suitable for the culture of neuronal cells and ASCs and the transplantation of this biomaterial-cell combination into a severe SCI animal model led to increased motor recovery [8–10]. More recently, envisioning the application of GRGDS-GG to restore local vascularization following SCI we used this peptide modified hydrogel to co-culture ASCs and HUVECs. This co-culture platform induced the formation of vascular-like structures on the hydrogels and originated extensive neurite outgrowth of DRG explants, providing good indications for its use on an animal model of the condition. Nevertheless, simple linear peptides possess low metabolic stability, being prone to enzymatic degradation and partially lose their active conformation upon chemical grafting, and thus integrin affinity [11].

To overcome these drawbacks, the last decades have seen firstly the development of cyclic RGD ligands that restrict the conformational freedom of the molecules and preserve their bioactivity, and eventually the creation of peptidomimetic ligands [12–15]. The latter are non-peptidic molecules that recapitulate the chemical features governing integrin-ECM protein interaction and allow to design synthetic, more stable,

and durable molecules with integrin specificity to instruct particular cellular behaviors [11]. Recently, two distinct peptidomimetics targeting αvβ3 and α5β1 (Figure 3.1 A and B) have shown potential to be used for biomaterial functionalization by clearly proving their capacity to guide cell attachment to metallic surfaces in an integrin-specific manner. Both these peptidomimetic molecules show binding affinity on the nM range to the integrin targets (the α5β1 mimetic has 1.5 nM affinity and the αvβ3 mimetic 1.8 nM), having clearly enhanced affinity relative to linear RGD (Figure 3.1 C) [16–18]. These integrins bind to fibronectin and are present in numerous types cells, playing crucial roles during processes like embryogenesis and angiogenesis [19]. Therefore, both ligands are attractive to be included in biomaterial-based strategies to induce vascularization in alternative to common linear RGD or alternative adhesion motifs by being able to engage important integrins that participate on the angiogenic process in a specific manner. Indeed, faulting vascularization is one of the most common reasons for the failure of biomaterial implantation. Without the presence of specific vascular cues (angiotrophic factors; activation of integrins involved in angiogenesis) or endothelial cells that will mature into stable vascular networks, the process will take days to weeks, eventually leading to cell death by hypoxia and nutrient deprivation [20].

SCI is an extremely debilitating condition that is usually caused by trauma and leads to motor, sensory and autonomic deficiencies. The limited capacity of the CNS to regenerate, combined with the extremely nefarious local environment (hypoxia, uncontrolled inflammation, excitotoxicity, reactive oxygen species) makes SCI extremely complex. One of the major contributors to this complexity lies with the defective vascular repopulation following SCI. The condition is characterized by a dramatic rupture of spinal cord vasculature, which the host fails to replace and leaves the tissue in chronic hypoxia.

To overcome the limitations of the simple linear peptide GG modification, the objective of this work was to characterize and optimize the chemical grafting of the α5β1 and αvβ3 peptidomimetic ligands to GG using different ligand:polymer ratios. We also evaluated the capacity of GG modifications to promote the adhesion and spreading of ASCs and compared it to GG functionalized with linear RGD using similar stoichiometries to understand whether the peptidomimetics promoted increased cellular adhesion. The final aim was to test their use for neural tissue engineering applications using DRG explants and to observe whether the mimetic functionalized GG could promote the formation of vascular-like structures on encapsulated HUVECs as these integrins are pivotal during the process. It was aimed to understand the potential of these biomaterials as cell delivery platforms to induce *in situ* vascularization of SCI sites. To the best of our knowledge this is the first time that such ligands have been utilized to endow bioactivity to three-dimensional hydrogels, which contrasts with their more common application on flat metallic surfaces [16–18].

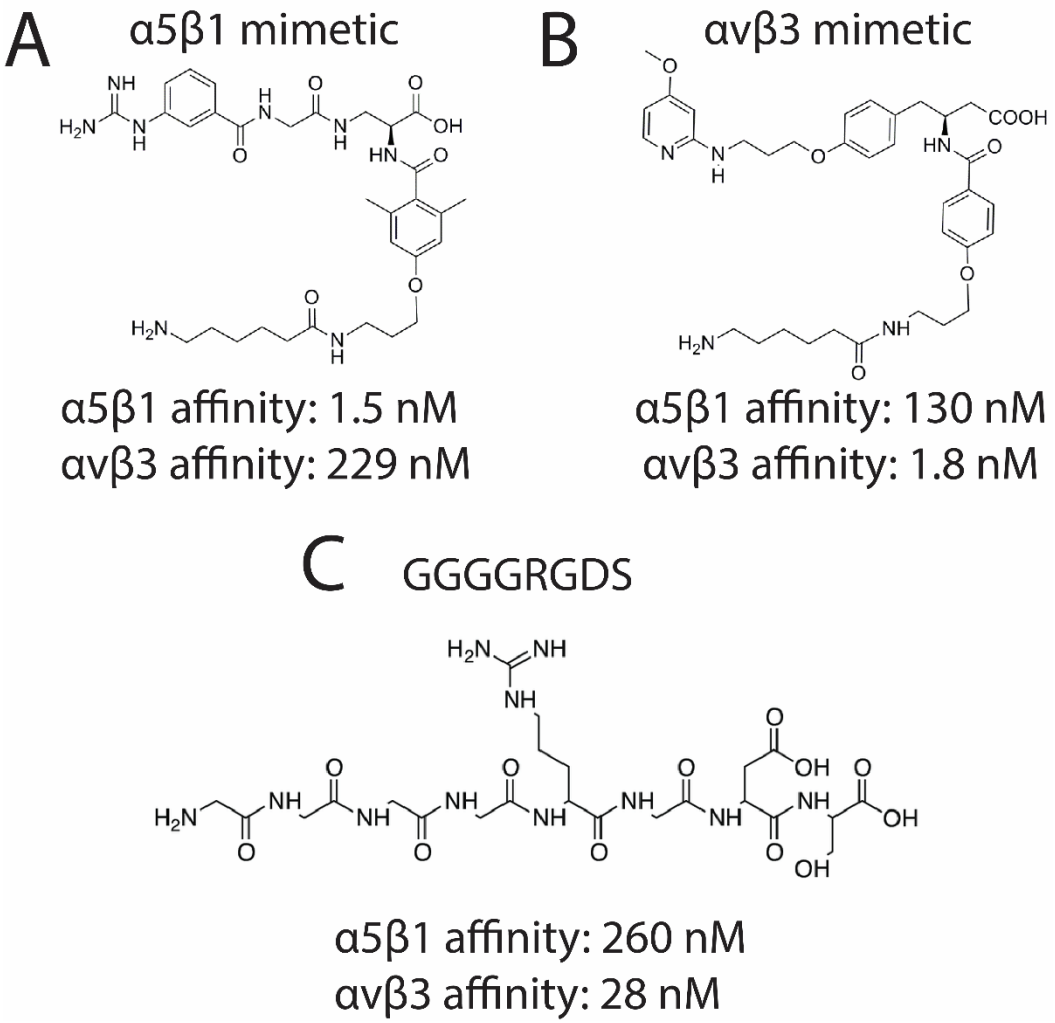

Figure 3.1 – Chemical structure and binding affinities of **A,** the α5β1 mimetic, **B,** the αvβ3 mimetic and **C,** common linear GGGGRGDS. Binding affinities were obtained from 8,20.

Materials and Methods

Gellan gum purification

The purification of GG was done to remove divalent cations and inorganic ash that are present in the commercial product (GelzanTM, Sigma-Aldrich, USA) , following previously published protocols [21,22]. A 1 % (w/V) GG solution was prepared in deionized water (Millipore, Australia) at 65 °C under constant stirring. Once the dissolution of GG was accomplished, a cation exchange resin (Amberlite® IR120, Sigma-Aldrich, USA) was added until the solution reached a pH of 2.5, maintaining the temperature and agitation conditions. After stopping the agitation to allow the resin to settle, the solution was filtered. The recovered GG solution was poured into a pre-heated beaker (95 °C) and the pH of the solution was then adjusted

to 8.7 with a 1 M NaOH (Merck, Germany) and subsequently, allowed to cool to RT. This step was followed by pouring the GGp solution onto ethanol (Carlo Erba, Italy) to allow precipitation of the polymer. Afterwards, the recovery of GGp was accomplished by filtering the mixture using a steel sieve, followed by vacuum filtration. The recovered GGp was then dissolved in water at RT with constant stirring. When the dissolution of GGp was complete, the solution was transferred into a dialysis membrane with a molecular cut-off of 12-14 kDa (Sigma-Aldrich, USA) and dialysed against deionized water during 7 days with daily water exchanges. After completing the dialysis, the content of the membrane was frozen at -20 °C. And finally freeze-dried for 4 days, allowing to recover the polymer as a white, cotton-like, solid.

Chemical grafting of fluorescent analogues of linear RGD, α5β1 and αvβ3 mimetics to GGp

To evaluate the efficiency of the conjugation, as well as the dispersion of each ligand throughout GGp, fluorescent analogues were used. These were modified with carboxyfluorescein (CF) and were a kind donation from the laboratory of Horst Kessler from the Technical University of Munich. The grafting of the molecules was done by firstly activating the -COOH groups of GGp for the formation of an amide bond between the carbohydrate polymer and the ligands. To this end, GGp [0.1 % (w/V)] was dissolved in deionized water at RT and then a 750 mM DMT-MM (Sigma, USA) solution in water was added using a 1:2 polymer:DMT-MM ratio to activate the -COOH groups of the polymer. Subsequently, CF-GGGGRGDS, CF-α5β1 or CF-αvβ3 ligands were added in a water solution at a concentration of 100 μM and reaction proceeded overnight protected from light and under constant magnetic stirring. The reaction mixture was then precipitated using 70 % (V/V) ethanol. After precipitation, the modified polymer was filtered under vacuum to allow the removal of ethanol. Then, the fluorescent ligand conjugate (fGGp) was dissolved in water, frozen in liquid nitrogen and transferred to a freeze dryer, allowing recovery of the polymers as white cotton-like solids. Each fluorescent ligand was conjugated to GGp using a polymer:ligand ratio of 10:1 and 20:1.

Characterization of the coupling efficiency and dispersion of the fluorescent integrin ligands throughout GGp hydrogels

The total amount of fluorescent ligand grafted to GGp under each condition was calculated by measuring the absorption of 0.5 % (w/V) fGGp solutions at 495 nm (the maximum absorption for CF) in a plate reader (Infinite M200 PRO, Tecan Group Ltd., Switzerland) and by interpolating the value in a calibration curve using solutions of 0.5 % (w/V) GGp with defined concentrations of the ligands. The concentrations of the standards were 2 mM, 1.5 mM, 1 mM, 0.5 mM, 0.1 mM, 0.05 mM, and 0.01 mM. Each

modification and standard was prepared in triplicate and the quantity of fluorescent ligand calculated using the average of the absorptions.

To observe the dispersion of the fluorescent ligands throughout fGGp hydrogels using confocal microscopy, 0.8 % (w/V) fGGp solutions from each condition were made, which was followed by the ionic crosslinking of the polymer using 20 % (V/V) of PBS (Gibco, USA), allowing to obtain 0.667 % (w/V) fGGp hydrogels. The volume of the fGGp hydrogels drops was 50 µL and confocal micrographs of each hydrogel were taken using a Zeiss LSM 800 confocal microscope (Carl Zeiss, Jena, Germany).

Chemical grafting of linear RGD, α5β1 and αvβ3 ligands to GGp

The protocol for the biofunctionalization of GGp with the adhesive molecules was performed as described in *Chemical grafting of fluorescent analogues of linear RGD, α5β1 and αvβ3 mimetics to GGp*. GGGGRGDS was kindly provided by Carles Mas-Moruno from the Universitat Politècnica de Catalunya and the α5β1 and αvβ3 peptidomimetics kindly offered by the laboratory of Horst Kessler. Briefly, GGp was dissolved in ultrapure water to obtain a 1 % (w/V) solution. Afterwards, a 750 mM DMT-MM solution in water was added to the dissolved polymer using a polymer:DMT-MM ratio of 1:2 and then a 100 µM water solution encompassing the ligands was poured onto the reaction mixture using the same polymer:ligand ratio in a αvβ3 mimetic water. The reaction continued overnight under magnetic stirring and the modified GGp was precipitated using 70 % (V/V) ethanol. The polymer was recovered by vacuum filtration and then dissolved once again in water to obtain a 1 % (w/V) GGp solution that was quickly frozen on liquid nitrogen and transferred to a freeze dryer to recover the polymer in the solid state. The grafting of RGD to GGp was done using a 10:1 and 20:1 polymer:ligand ratio.

Spectroscopic analysis of the modified GGp

Fourier Transformed Infrared (FTIR) spectra of all GGp modifications and unmodified GGp were obtained using a FTIR Nicolet 6700 in the Attenuate Total Reflectance mode (ATR-FTIR) (256 scans with a data spacing resolution of 2 cm^{-1}). The analysis of the spectra consisted of detecting the presence of the amide bond bands to assess whether the grafting of the ligands was successful.

The chemical composition at the atomic level of each modification was analyzed using X-ray photoelectron spectroscopy (XPS). Spectra were acquired using a non-monochromatic Mg anode X50 source, operating at 150 W, and a Phoibos 150 MCD-9 detector (D8 advance, SPECS Surface Nano Analysis Gmbh, Germany). The detector pass energy was maintained at 25 eV having 0.1 eV steps to record high resolution spectra at a pressure below $7.5x10^{-9}$ mbar. The spectral analysis and peak fittings were made

using Casa XPS software (Version 2.3.16, Casa Software Ltd., UK) and all the binding energies referenced to the C1s signal (284.8 eV). The XPS spectra of three samples of each modification were acquired.

Isolation of ASCs and HUVECs

The isolation of ASCs from the lipoaspirates of consenting donors was done by LaCell LLC, according to a previously reported protocol and with the approval of an institutional review panel at the company [23]. Before each assay, ASCs were cultured at 37 °C and 5 % CO_2 (V/V) in α-MEM (Invitrogen, USA) supplemented with 10 % FBS (Biochrom AG, Germany) and 1 % (V/V) pen/strep (Invitrogen, USA) with medium exchanges every 3 days.

Umbilical cords were obtained from healthy consenting patients of the Gynecology and Obstetrics Service of Braga Hospital under a previously published protocol that was cleared by the review board of the Ethical Commission for Health of Braga Hospital (CESHB) [24]. Briefly, the umbilical cords were rinsed and cleaned with PBS and then a cannula was inserted into the umbilical vein. Blood clots and blood residues were removed by washing the vein with PBS. Afterwards, the other extremity of the umbilical cord was closed with a forceps and the vein filled with α-MEM containing 0.2 % (w/V) (210 U/mL) Type II Collagenase (Gibco, Thermo Fischer Scientific, USA) and 1 % pen/strep. The umbilical cord was then transferred into a cell culture incubator for 15 minutes to allow the digestion of the vein. Before opening the forceps, the cord was massaged to get a homogenous digestion and its content poured into a 50 mL Falcon tube, and subsequently washed with α-MEM containing 10 % FBS (w/V) and 1 % pen/strep, PBS and finally with a syringe filled with air. Subsequently, the suspension was centrifuged for 10 minutes at 1200 rpm which was followed by the removal of the pellet and its resuspension in EGM (R&D Systems, USA) supplemented with 1x EGS (R&D Systems, USA) and 1 % (V/V) pen/strep. This suspension was divided by the wells of a 6-well plate [pre-coated with 1 % (w/V) Type B bovine gelatin (Sigma, USA)] and cultured in EGM supplemented with 1x EGS and 1 % (V/V) pen/strep overnight to allow the attachment of HUVECs. Media was changed the following day to remove unattached cells and debris, and from this point onwards media changes occurred every two days to continue to purify the culture, until cells grew confluent. Then, part of the cells was stored in liquid nitrogen until further used, being the rest transferred to a T75 flask pre-coated with gelatin and cultured as previously described.

Preparation of GGp, RGD, α5β1 and αvβ3-modified GGp hydrogels

The preparation of the RGD-modified GGp (GGp10RGD or GGp20RGD according to 10:1 or 20:1 GGp:RGD ratio, respectively), α5β1 mimetic-modified GGp (GGp10α5 and GGp20α5 applying the same criteria),

αvβ3 mimetic-modified GGp (GGp10αv and GGp20αv according to the initial GGp:αvβ3 ratio) and GGp hydrogels started by exposing the materials to UV light for 15 min to sterilize the sample [9]. These were subsequently dissolved at 0.8 % (w/V) in ultra-pure water and crosslinked using 20 % α-MEM or EGM (when HUVECs alone were encapsulated within the hydrogels) to obtain 0.667 % (w/V) hydrogels. The utilized volume of the hydrogel droplets during the experiments was 50 μL.

3D cell cultures

Adhesion assays

ASCs were cultured as detailed in ***Isolation of ASCs and HUVECs*** and the hydrogels prepared according to ***Preparation of GGp, RGD, α5β1 and αvβ3-modified GGp hydrogels***. The appropriate number of ASCs were resuspended homogenously in the corresponding volume of GGp, GGpRGD, GGpα5 or GGpαv formulation and at a cell density of 30000 ASCs/50 μL of hydrogel. The experiment layout consisted of two timepoints (3 and 7 days) to evaluate the adhesion of ASCs to the hydrogels under the different experimental conditions.

Culture of ASCs, HUVECs and their co-culture for neurite outgrowth experiments

ASCs and HUVECs were cultured as detailed in ***Isolation of ASCs and HUVECs*** and GGp10α5 and GGp10αv hydrogels prepared according to ***Preparation of GGp, RGD, α5β1 and αvβ3-modified GGp hydrogels***. A total of 30000 cells/hydrogel were encapsulated on the three-dimensional matrices. For the co-culture experiments ASCs and HUVECs were encapsulated using a 1:1 ratio, meaning that each hydrogel encompassed 15000 cells of each type, as reported before [24]. The hydrogels were prepared the day before adding DRG explants to their top to allow the cells to adhere to the matrix. These were maintained on α-MEM with 10 % (V/V) FBS and 1 % (V/V) pen/strep (ASCs and co-culture) and on EGM supplemented with 1x EGS and 1 % (V/V) pen/strep for the encapsulated HUVECs.

Isolation and culture dorsal root ganglia explants

The capacity of GGp10α5 and GGp10αv hydrogels to induce axonal growth, either alone or using ASCs, HUVECs and their co-culture, was assessed using DRG explants. The isolation of the explants was done following a previously detailed protocol [8,24,25]. DRG from the thoracic regions of the spine of neonatal pups (P5-7) were removed and placed in cold 1x HBSS without Ca^{2+} and Mg^{2+} (Invitrogen, USA) with 1 % (V/V) pen/strep. Peripheral nerve processes were cleaned from DRG and the explants put on top of the mimetic hydrogels). The culture was maintained under a humidified atmosphere [37 °C and 5 % (V/V) CO_2] and

on Neurobasal medium supplemented with 1x B27 (Invitrogen, USA), 2 mM L-glutamine (Invitrogen, USA), 6 mg/mL D-glucose (Sigma, USA) and 1 % (V/V) pen/strep having medium changes every two days, lasting 7 days. Then, the samples were fixated using PFA to perform ICC to understand neurite outgrowth as well as the morphology of ASCs and HUVECs inside the hydrogels.

Immunocytochemistry and Phalloidin/DAPI staining

The hydrogels from the cell adhesion assays were fixed in 4 % PFA (Panreac, Spain) for 45 minutes at RT following 3 and 7 days of culture. The same protocol was applied to the hydrogels and DRG used during the neurite outgrowth experiments. This step was followed by washing the samples 3 times with PBS and by permeabilizing cell membranes with 0.3 % (V/V) Triton X-100 (Sigma, USA) for 10 minutes. ASCs were stained by incubating them with a PBS solution with 1 µg/mL of DAPI (Invitrogen, USA) and 0.1 µg/mL (Sigma, USA) for 45 minutes at RT.

The ICC protocol to fluorescently label HUVECs and the cytoskeleton of DRG involved to block non-specific binding sites, by incubating samples in PBS with 10 % (V/V) FCS (Biochrom AG, Germany) for 1 h 30 min. Afterwards, the primary antibodies were properly diluted in PBS 10 % FCS and added to the samples for 48 h at 4 °C. Mouse anti-neurofilament 200 kDa antibody (1:200, Millipore, USA) and rabbit anti-CD 31 (1:20, Abcam, United Kingdom) were used to label DRG neurites and to identify HUVECs, respectively. Finally, the samples were washed 3 times using PBS with 0.5 % (V/V) FCS and Alexa Fluor 488 goat anti-rabbit (1:1000, Invitrogen, USA) and Alexa Fluor 647 goat anti-mouse (1:1000, Invitrogen, USA) were diluted in PBS and added to the hydrogels overnight at 4 °C. Imaging was performed on a confocal point-scanning microscope Olympus FV1000.

Calculation of the area/ASC in the cell adhesion studies

The area/ASC was calculated by ImageJ (NIH) to calculate the total area of phalloidin on each micrograph (3 per hydrogel). After defining the scale, the images were converted to 8 bits and then to binary, and finally the area of phalloidin was calculated using the "Analyze Particles" function of the software. Finally, the obtained value is divided by the number of cells present on the corresponding picture to obtain the area/ASC.

Neurite extension and outgrowth analysis

The ImageJ (NIH) plugin Neurite-J [26] was used to calculate the area occupied by the neurites of each DRG explant using a previously developed protocol [8,24]. Firstly the scale was defined, after which the area

referring to the body of the DRG was revealed and the contrast properly corrected to emphasize the neurites. The image is translated to 8 bits and the "Analyze particles" function calculated the area corresponding to the extension the neurites. Neurite-J also enabled to quantify the longest neurite. Following the identification of the DRG body, the plugin automatically creates concentric rings with 25 µm intervals and is defining as the length at which the last ring is capable of intersecting neurites.

Analysis of the vascular organization of HUVECs in GG-GRGDS

The vascular arrangement of HUVECs was evaluated using AngioTool64 Version 0.6a [27] using a previously defined protocol [24]. In brief, the images referring to the fluorescence channel for CD31 were opened and the background and small particles removed by defining the appropriate signal threshold in the software. This correction is followed by the automatic quantification of different parameters related to vascular organization such as total vessel length, vessel area, vessel percentage area and number of junctions.

Statistical analysis

To perform the statistical analysis, GraphPad Prism version 7.04 for Windows (GraphPad Software) was used. The adhesion assays, together with the neurite outgrowth experiments were analyzed by performing one-way ANOVA followed by the Bonferroni post-hoc test. Statistical differences on the vascular arrangement experiments were discriminated using Welch's *t*-test. The observed differences were considered statistically significant whenever a p-value ≤ 0.05 was observed (95 % confidence level).

Results

Gellan gum purification

The purification process makes the polymer easier to handle and dissolve in water at RT and allows better grafting efficiencies when applying protocols that depend on the activation of the carboxyl groups [22]. Of the starting 5.02 g of GG, 4.1 g of GGp were recovered, accounting for a yield of 82 %. This protocol enhances the chemical manipulation of GG for the development of biomaterial-based therapies [28,29].

Grafting efficiency of fluorescent analogues of RGD, α5β1 and αvβ3 mimetics onto GGp.

The first step was to evaluate the efficiency of the coupling reaction for each of the three ligands and the two GGp:ligand ratios utilized (10:1, 20:1), with a recovery yield of 92.4 %. The choice of fluorescent analogs to study these parameters was due to the possibility of conveniently quantifying the amount of ligand bound to GGp (simple spectrophotometry), while observing their dispersion throughout the hydrogels obtained from each condition.

Table 3.1 - Concentration (nM) and mass (mg) of the fluorescent ligands coupled onto the backbone of GGp using the 10:1 and 20:1 GGp:ligand ratios.

	fGGp10	fGGp20
[RGD] (mM)	0.252	0.038
Total mass (mg)	0.627	0.188
[α5β1] (mM)	0.297	0.055
Total mass (mg)	0.739	0.274
[αvβ3] (mM)	0.257	0.043
Total mass (mg)	0.639	0.213

The chemical functionalization involved the activation of the -COOH groups of GGp using DMT-MM, which forms an active GGp ester [30]. This reaction makes the activated carboxylic groups of the polymer extremely susceptible to suffer a nucleophilic attack by the amine groups of the ligands and yields an amide bond between GGp and the adhesion motifs. The use of DMT-MM presents several advantages in comparison to other reagents that activate -COOH groups like carbodiimides. It is more effective and eliminates the need to control the pH of the solution, forming innocuous secondary products that are easily removed through downstream processes such dialysis and polymer precipitation [31].

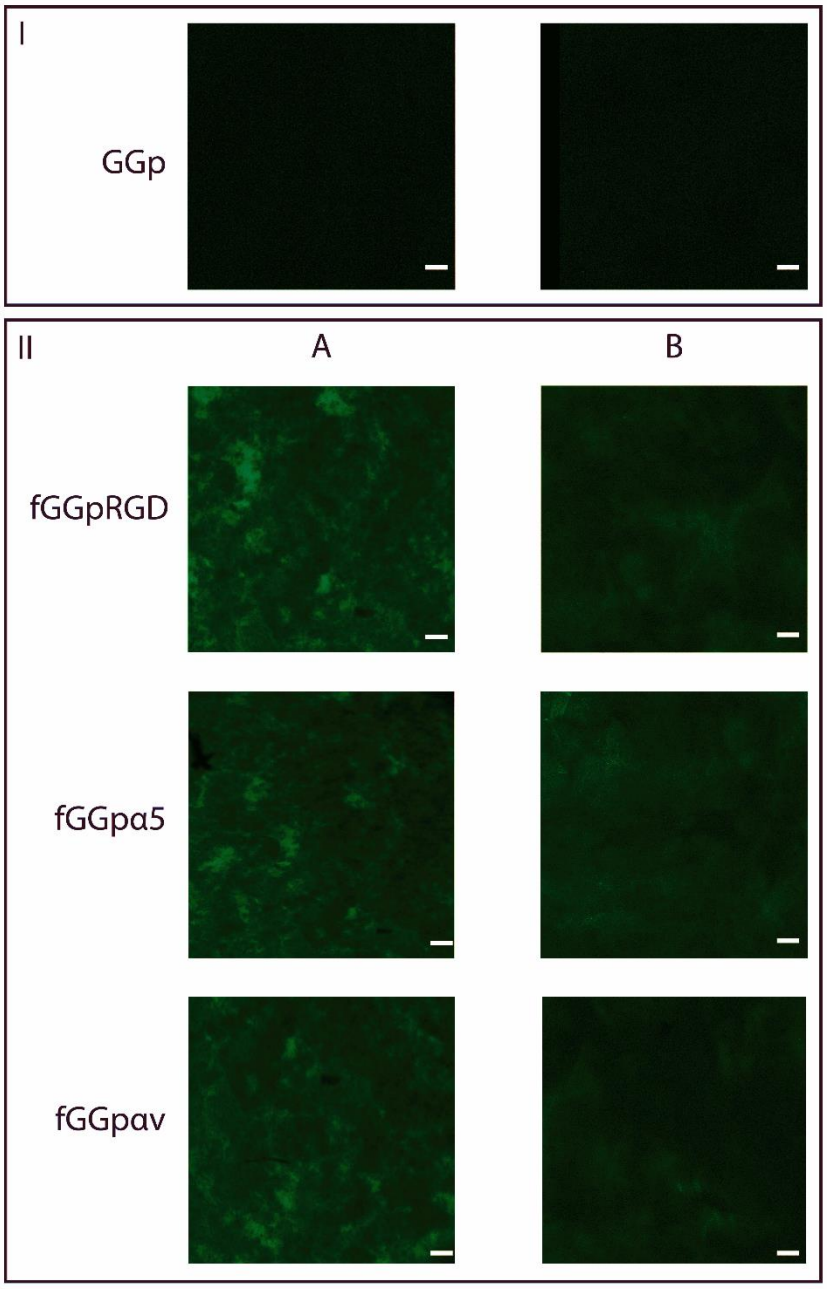

Figure 3.2 – Representative confocal micrographs of GGp hydogels conjugated with fluorescent ligands. **I.** unmodified GGp. **II. A,** 10:1 GGp:ligand ; **B,** fGGp20 . There are no major differences among the same stoichiometry group, however fluorescence clearly decreased on the 20:1 hydrogels, a reflection of the grafting of a lesser quantity of fluorescent molecules.

The analysis of Table 3.1 indicated that the concentration of fluorescent ligand bound to GGp decreases as the GGp:ligand ratio increased from 10:1 to 20:1 for the three molecules, which reflects the decrease of the ligand:GGp stoichiometry. Therefore, the concentration of bound ligands at the 10:1 stoichiometries were 0.252 mM (0.627 mg, 63 % of efficiency) to GGp10RGD, 0.297 mM (0.739 mg and

approximately 74 % of efficiency) to fGGp10α5 and 0.257 mM (0.639 mg, efficiency of 64 %) to fGGp10αv. Regarding the 20:1 ratio, the samples showed bound ligand concentrations of 0.038 mM (0.188 mg, 19 % efficiency) for fGGp20RGD, 0.055 mM (0.274 mg, 27 % efficiency) for fGGp20α5 and 0.043 mM (0.213 mg, 21 % efficiency) for fGGp20αv.

The confocal micrographs obtained (Figure 3.2) enabled to observe that the (spatial) dispersion of fluorescent ligands was relatively homogeneous for all the fGGp10 conditions, whereas the fGGp20 formulations showed clusters of fluorescence along the hydrogels, with significant voids where no ligand was observed (a reflection of the reaction efficiency). Furthermore, fGGp10 hydrogels showed higher intensity of fluorescence in comparison to their fGGp20 counterparts, which correlates with the amount of fluorescent ligands bound to GGp.

Chemical characterization of the grafting of RGD, α5β1 and αvβ3 mimetics onto GGp.

After confirming that the grafting of the fluorescent analogues of each ligand had occurred efficiently, we proceeded to biofunctionalize GGp with the RGD, α5β1 and αvβ3 using the same GGp:ligand ratios (10:1 and 20:1) with a yield of 93,7 %. These two ratios were used to recognize what was the minimal stoichiometric ratio that conferred enhanced bioactivity to the polymer.

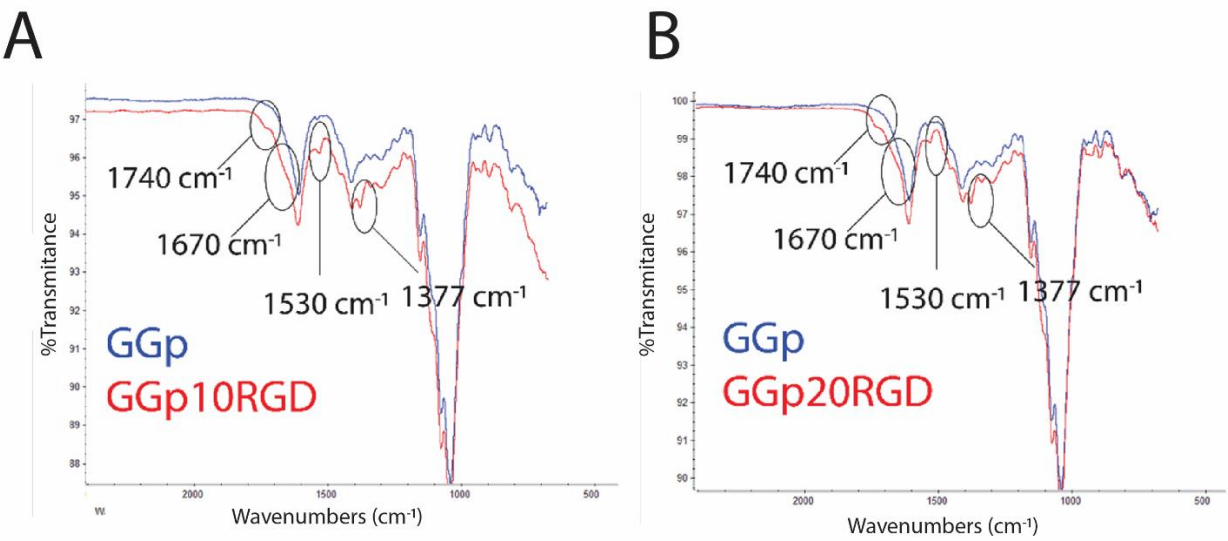

Figure 3.3 – FTIR spectra for modified GGpRGD. **A,** GGp10RGD; **B,** GGp20RGD. The amide bond peaks are highlighted in circles to each modification, accompanied by the corresponding wavelength.

To understand whether the reaction was successful using FTIR and XPS were used (Figure 3.3 for GGpRGD, Figure 3.4 for GGp10α5 and Figure 3.5 GGp10αv). From the FTIR spectra obtained, it is

possible to observe that the modifications (red) show characteristic bands of the amide bond. Indeed, the samples belonging to the biofunctionalized GGp presented peaks for Amide I (1740 and 1670 cm^{-1}) which corresponds to the stretching vibration of the C=O group, Amide II (1530 cm^{-1}) representing the stretching vibrations of the C-N moieties and Amide III (1377 cm^{-1}) reflecting the N-H bending vibrations [4,32]. These bands confirm the insertion of the three ligands onto the backbone of GGp regardless of the stoichiometry.

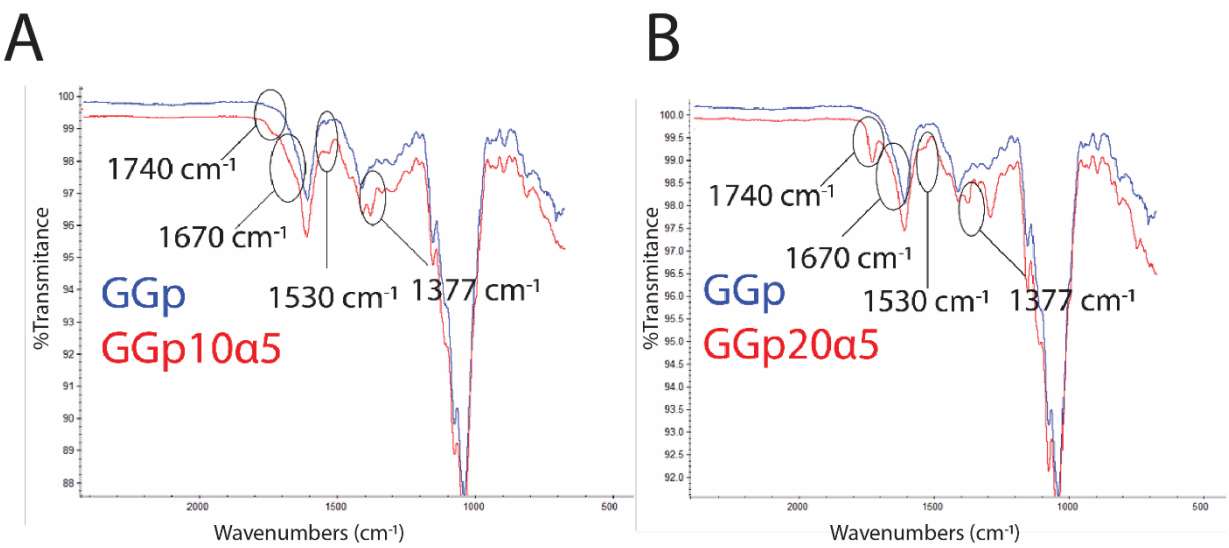

Figure 3.4 – FTIR spectra for modified GGpα5. **A,** GGpα510; **B,** GGpα520. The amide bond peaks are highlighted in circles to each modification, accompanied by the corresponding wavelength.

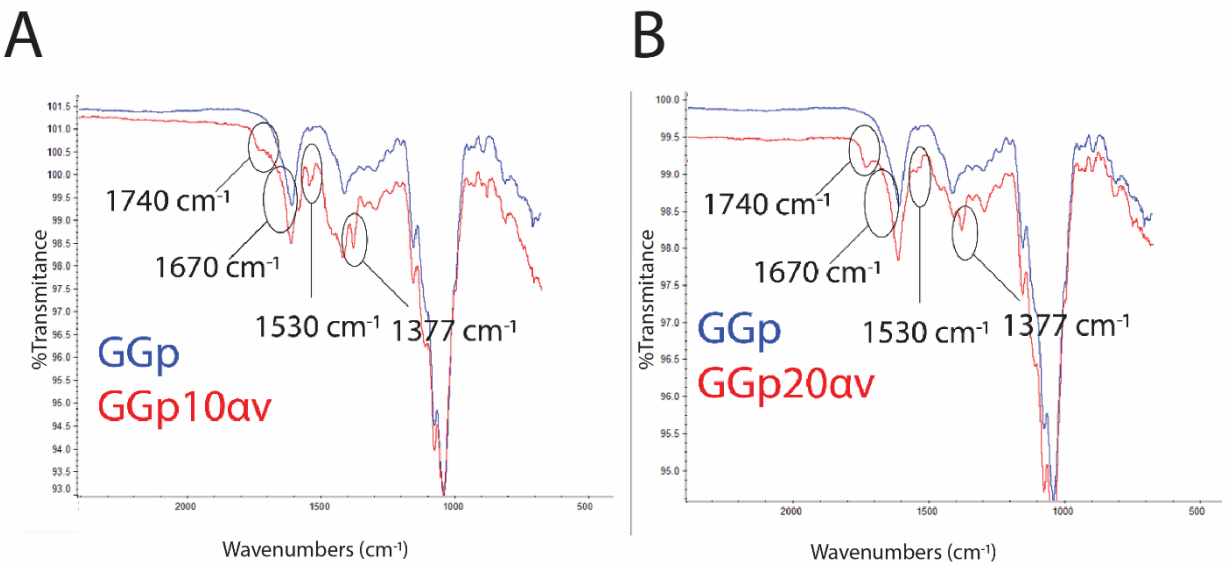

Figure 3.5 – FTIR spectra for modified GGpαv. **A,** GGpαv10; **B,** GGpαv20. The amide bond peaks are highlighted in circles to each modification, accompanied by the corresponding wavelength.

The FTIR analysis was complemented by XPS to assess the elemental composition of the samples. Particularly, we focused on the percentage of nitrogen, since this element is absent on native GGp, is inserted after coupling due to its presence both on the ligands and the amide bond that links polymer and adhesion motif. Table 3.2 details the nitrogen percentage content across modified conditions, with native GGp serving as a negative control. Thus, it was possible to observe that all the modifications clearly possess a higher nitrogen content than GGp (only trace amounts due to contamination from the air exposure since there are no nitrogen atom on its backbone). Additionally, as GGp:ligand ratio increases the N percentage decreases, indicating a decrease in the concentration of grafted adhesion motif from 10:1 to 20:1, something that corroborates what was seen when coupling their fluorescent analogues to the polymer. Maximum incorporation was observed for GGp10α5 (1.625 %), followed by GGp10RGD (1.475 %), GGp10αv (1.44 %), GGp20RGD (1.165 %), GGp20α5 (1.145 %) and finally GGp20αv (0.975 %). As observed by these experimental values there are no significant differences between conditions using the same GGp:ligand ratio, and therefore, it can be assumed that the reaction efficiency is similar between ligands.

Table 3.2 – Amount of nitrogen (N) detected by XPS on native and modified GGp formulations (n=2, two independent batches).

FORMULATION	PERCENTAGE OF N (MEAN±SD)
GGp	0.235±0.133
GGP10RGD	1.475±0.205
GGP20RGD	1.165±0.205
GGP10α5	1.625±0.304
GGP20α5	1.145±0.190
GGP10αV	1.44±0.156
GGP20αV	0.975±0.063

GGp10αv shows the highest biological activity

The characterization of the biofunctionalized gellan gum hydrogels regarding the presence of the adhesion ligands and the efficiency of the chemical reaction was followed by the study of their capacity to promote

the adhesion of ASCs. These experiments aimed to evaluate whether the mimetics were able to enhance the biological properties of GGp in comparison to linear RGD (used in this case as a positive control). Initial experiments included analyzes of cell morphology (to understand whether they were able to adhere to the hydrogels), using the area/cell as a measure of biological output – that is a higher area/cell would mean that cells are more active within the matrix as they increase their cellular processes and direct communication with neighbouring cells. At day 3 of culture it was noticeable that both GGp10αv and GGp20αv promoted increased adhesion (and spreading) of ASCs to the matrix, displaying decreased numbers of round cells (Figure 3.6). More concretely, cells encapsulated in GGp10αv had the highest area/cell (1303.98 μm^2/cell), being statistically significant from all the other conditions (with exception of GGp20αv) (Figure 3.8 A).

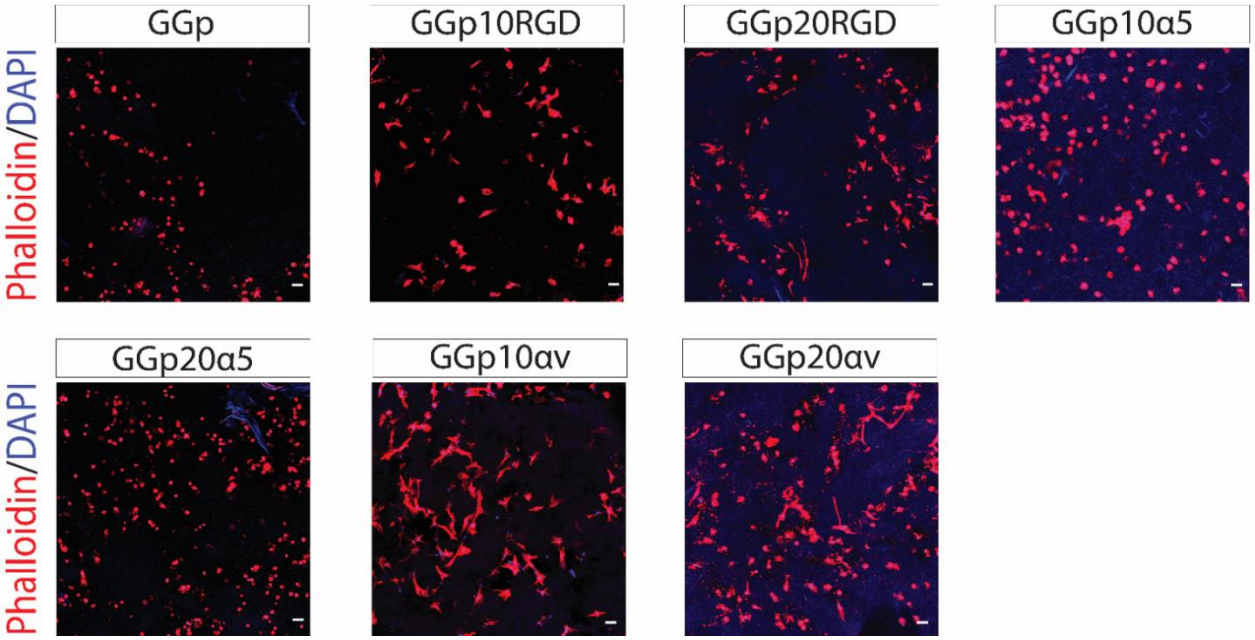

Figure 3.6 – Representative images of the ASCs cultured on native and modified GGp at day 3 of culture. The adhesion of ASCs is clearly enhanced on GGp10αv. Scale bar: 100 μm.

The final timepoint of this experiment (Day 7) underlined this observation, as cells in GGp10αv continued to grow within the hydrogel, the same happening in GGp20αv and GGp10RGD (Figure 3.7). The analysis of area/cell in this timepoint reinforces GGp10αv as the molecule promoting the highest spreading (1721.33 μm^2/cell), being statistically different from the other materials (Figure 3.8 B).

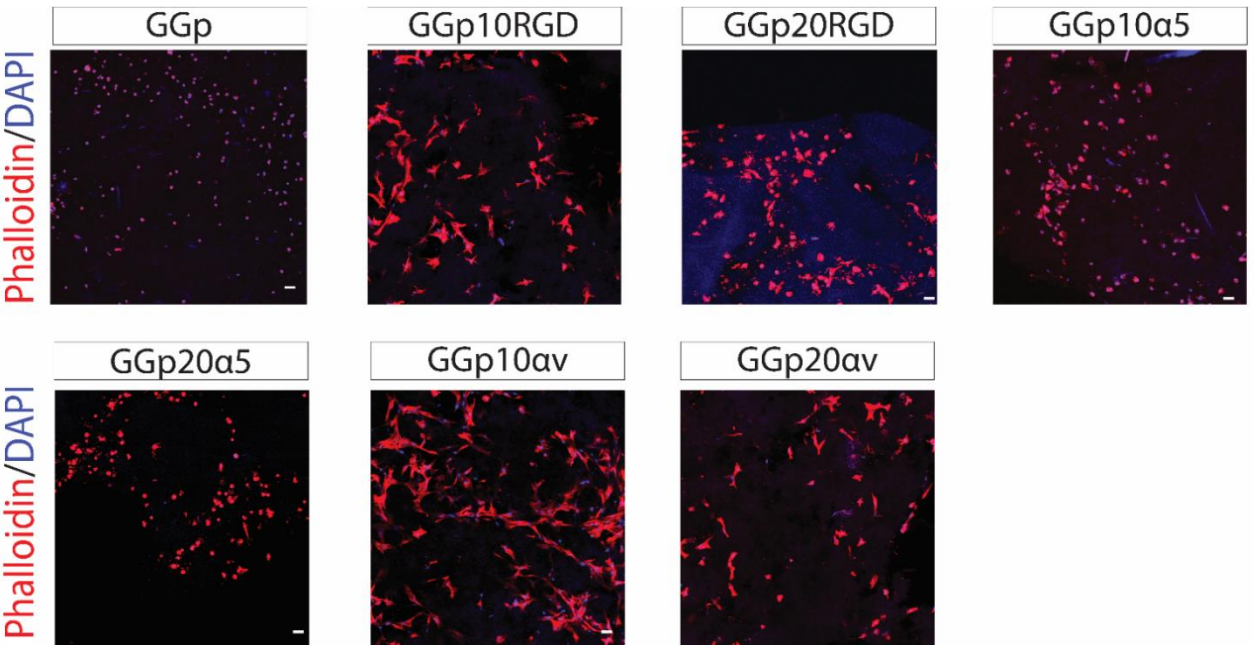

Figure 3.7 – Representative images of each of the studied GGp formulations at day 7 of culture. GGp10αv clearly promoted the adhesion and extensive spreading and interconnection of ASCs to the three-dimensional matrix. Scale bar: 100 μm.

From day 3 to day 7, however, GGp10RGD presented the second highest value concerning this parameter even though very similar to GGp20αv (1097.77 μm^2/cell and 1028.24 μm^2/cell, respectively). This highlights the importance of specific integrin signaling on the normal processes of cells, as the αvβ3 mimetic was able to trigger increased cell adhesion and spreading than RGD even when coupled with higher GGp:ligand ratios. On the other hand, the α5β1 mimetic was unable to induce relevant adhesion and spreading of ASCs to the matrix and had the lowest area/cell of the modified conditions both at day 3 of culture (529.99 μm^2/cell for GGp10α5 and 502.739 μm^2/cell for GGp20α5) and day 7 of culture (850.606 μm^2/cell for GGp10α5 and 514.602 μm^2/cell for GGp20α5). These results are rather surprising since the presence of α5β1 integrin on ASCs, and mesenchymal stem cells in general, is well documented [33–35].

The conjugation of GGp10αv with ASCs promotes significant neurite outgrowth from dorsal root ganglia explants

After understanding the capacity of both mimetics to promote the adhesion and spreading of ASCs within the modified GGp, we evaluated the performance of GGp10αv (the molecule for which the maximum biological activity was observed) and GGp10α5 on the neurite outgrowth of DRG explants. Despite not observing relevant biological activity during the cell adhesion assays, we still evaluated the α5β1 formulation to understand whether the lack of cell adhesion capacity was maintained in the presence of DRG and HUVECs on the culture conditions. We had previously observed the enhancement on ASCs attachment and DRG extension on GG hydrogels modified with laminin-derived peptides, in contrast to their single culture (either ASCs or DRG alone) on the hydrogels (unpublished data). This was probably induced by a positive feedback occurring between DRG and ASCs, originating the increase of the bioactivity of the hydrogels. The culture paradigms involved 4 distinct groups: hydrogel alone, and both GGp10 mimetic formulations encapsulating ASCs, HUVECs and their co-culture.

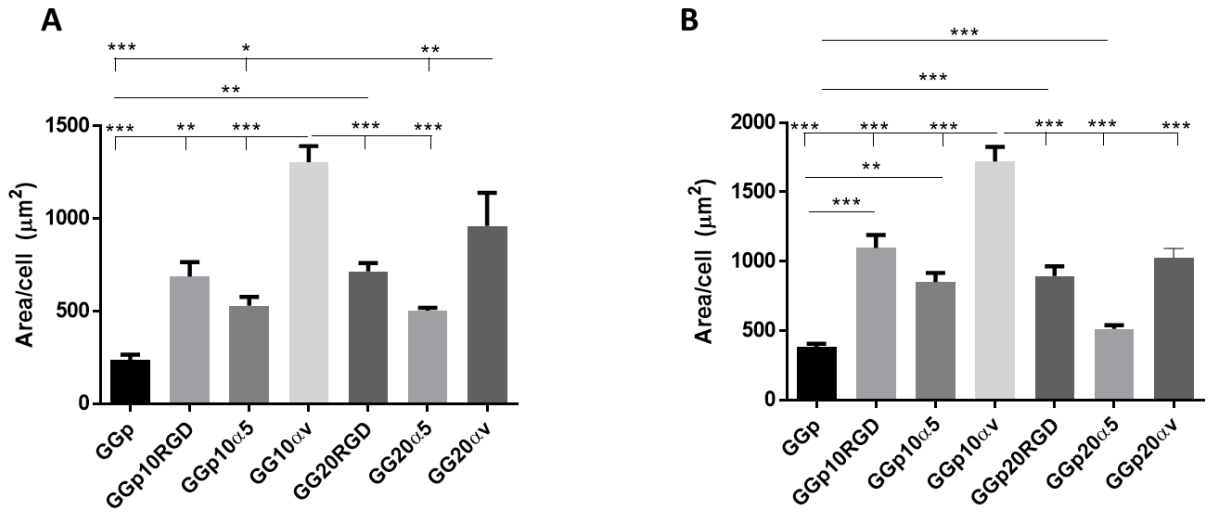

Figure 3.8 – Area/cell (μm²) of ASCs (P6) encapsulated in peptide and peptidomimetic-modified GGp. **A,** at day 3 of culture cells in GGp10αv present the highest value (being statistically different from the other conditions) which reflects their increased adhesion and spreading within these hydrogels. **B,** at day 7, GGp10av continued to induce statistically significant increased spreading in comparison to the other conditions. GGp10RGD and GGp20αv also promoted statistically significant spreading of cells in comparison to GGp10α5 and GGp20α5. Values are shown as mean±SEM (n=3 in 3 independent experiments). *p<0.05; **p<0.01; ***p<0.001.

The observation of Figure 3.9 allows to conclude that GGp10α5 did not induce observable growth of neurites across the different experimental conditions, confirming the lack of capacity of this formulation

to induce the adhesion, spreading and vascular organization of HUVECs. On the other hand, DRG cultured on GGp10αv with encapsulated ASCs (Figure 3.10) had increased neurite outgrowth ($1.057x10^6$ μm^2), with statistical significance from the hydrogels alone ($2.18x10^5$ μm^2, $p<0.01$), GGp10αv encapsulating HUVECs ($2.72x10^5$ μm^2, $p<0.01$) and the co-culture of these cell types ($4.41x10^5$ μm^2, $p<0.05$) (Figure 3.11 A). Regarding the maximum distance of extension of DRG neurites (Figure 3.11 B), both ASCs and ASCs+HUVECs promoted similar values (1084.03 μm and 1003.65 μm, respectively), being statistically different from GGp10αv without cells (214.17 μm, $p<0.001$) and HUVECs (387.52 μm, $p>0.001$).

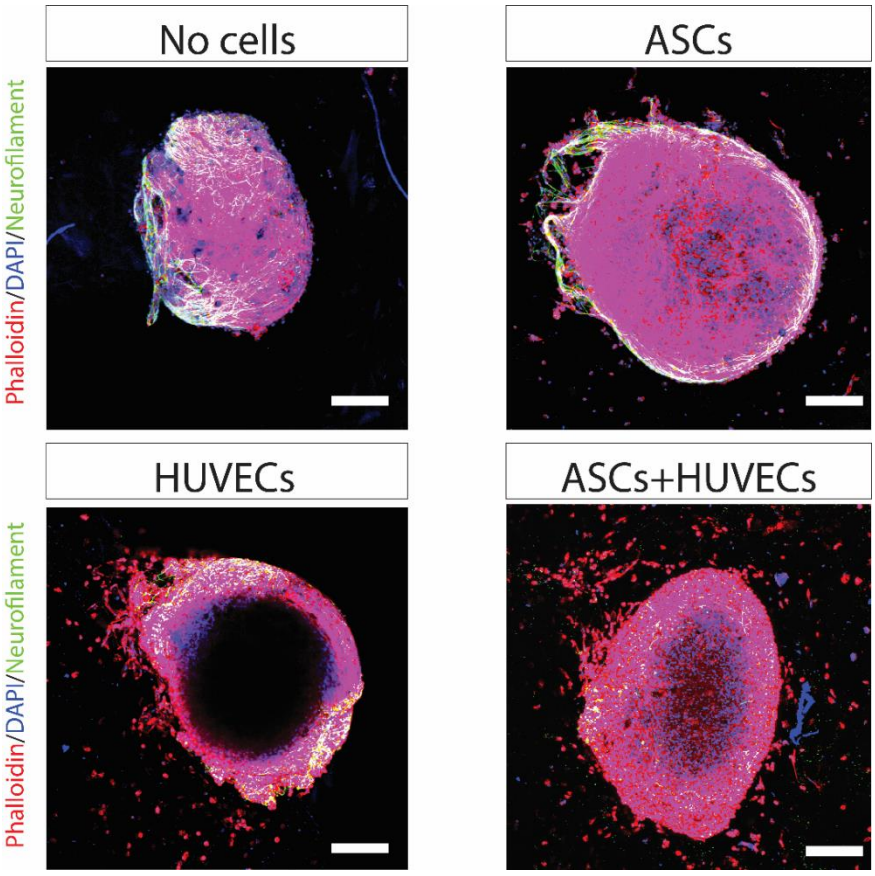

Figure 3.9 – DRG grown on GGp10αv without cells or in the presence of ASCs, HUVECs and ASCs+HUVECs. No biological activity was once again observed within the hydrogels. Scale bar: 100 μm.

As detailed on the introduction, these modifications were made with the final purpose to understand the potential of integrin mimetic ligands to induce the organization of endothelial cells (on this case HUVECs) into vascular-like structures, aiming to deliver them as platforms to induce *in situ* revascularization of SCI epicenter. Similarly to our previously published observations [24], the hydrogel alone (even though possessing enhanced αvβ3 integrin affinity) was not capable to induce the formation of vascular networks (Figure 3.12), which contrasts with the co-culture conditions where HUVECs clearly assembled into such

structures (Figure 3.12). This was noticeable in vascular parameters such as vessel area (0.117 mm^2 for HUVECs and 0.626 mm^2 for ASCs+HUVECs, $p<0.001$), vessel percentage area (5.848 % for HUVECs against 13.995 % for ASCs+HUVECs, $p<0.001$), total vessel length (5.208 mm for HUVECs and 25.158 for ASCs+HUVECs, $p<0.001$), average vessel length (0.083 mm for HUVECs vs 0.219 mm for ASCs+HUVECs, $p<0.001$) and number of junctions (18 for HUVECs vs 112.444 for ASCS+HUVECs, $p<0.001$) (Figure 3.13). These results reinforce the importance of ASCs to stabilize vascular network because even though the hydrogels used during this set of experiences provided an integrin-specific ligand towards $\alpha v\beta 3$, which in turn is extensively involved on the angiogenic process, this signaling cue *per se* was not able to induce the assemble of HUVECs into vascular-like networks.

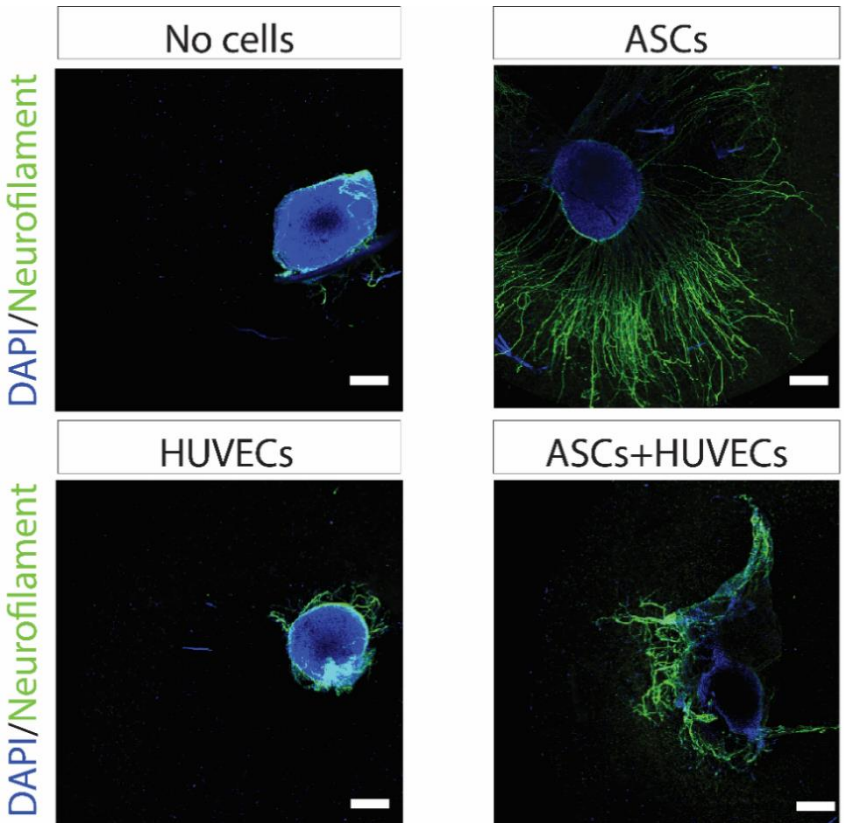

Figure 3.10 – Representative images of DRG neurite outgrowth on GGp10αv without cells, ASCs, HUVECs and ASCs+HUVECs. ASCs and ASCs+HUVECs were the conditions where the growth of neurites was more visible, especially the GGp10αv hydrogels with encapsulated ASCs. Scale bar: 100 μm.

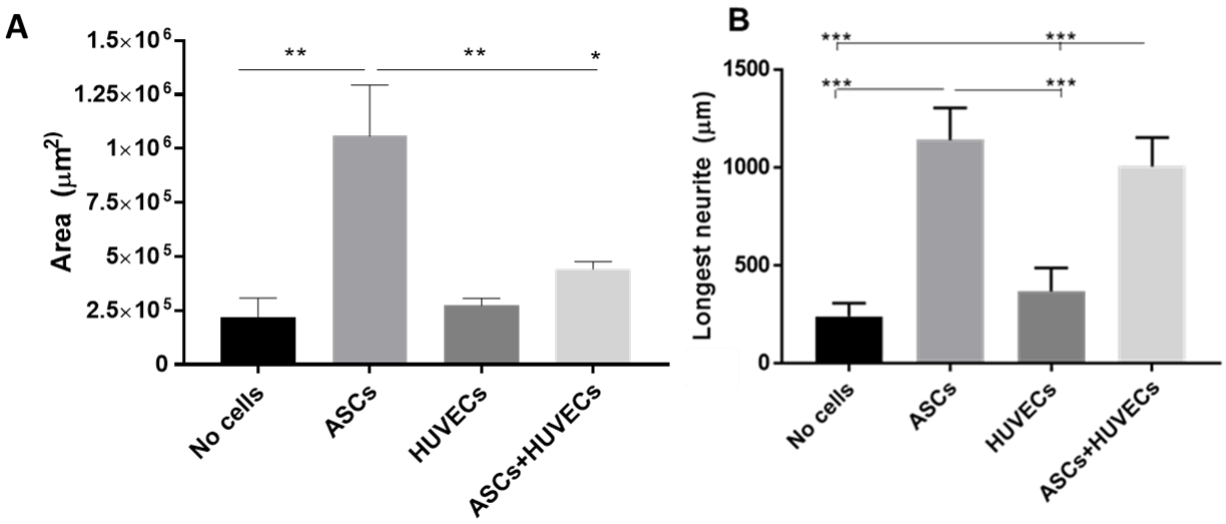

Figure 3.11 – Analysis on the neurite outgrowth area and longest neurite on GGp10av hydrogels. **A,** ASCs promoted significantly greater extension of neurites in comparison to all the other conditions. **B**, regarding the longest neurite (the one which grew furthest from the hydrogel both ASCs and ASCs+HUVECs promoted similar extension, being statistically significant from the hydrogels without cells and encapsulated HUVECs. Values are shown as mean±SEM (n=8/12 and results from 4 independent experiments). *p<0.05; **p<0.01; ***p<0.001.

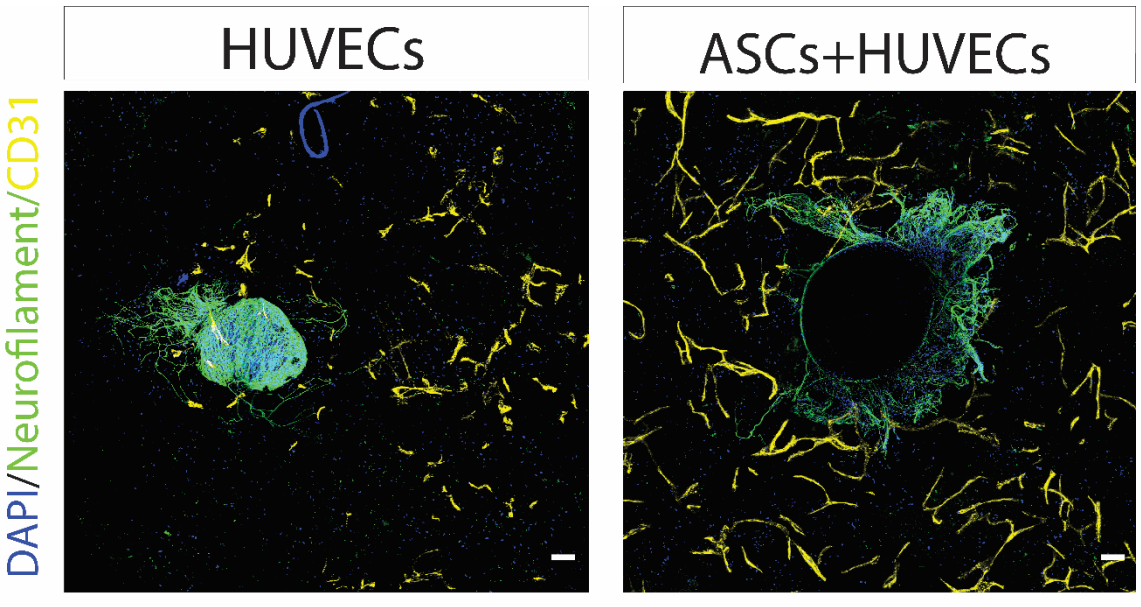

Figure 3.12 – Vascular organization of HUVECs in GGp10αv hydrogels. The presence of ASCs was fundamental for the assembly of these endothelial cells into vascular-like structures. Scale bar: 100 µm.

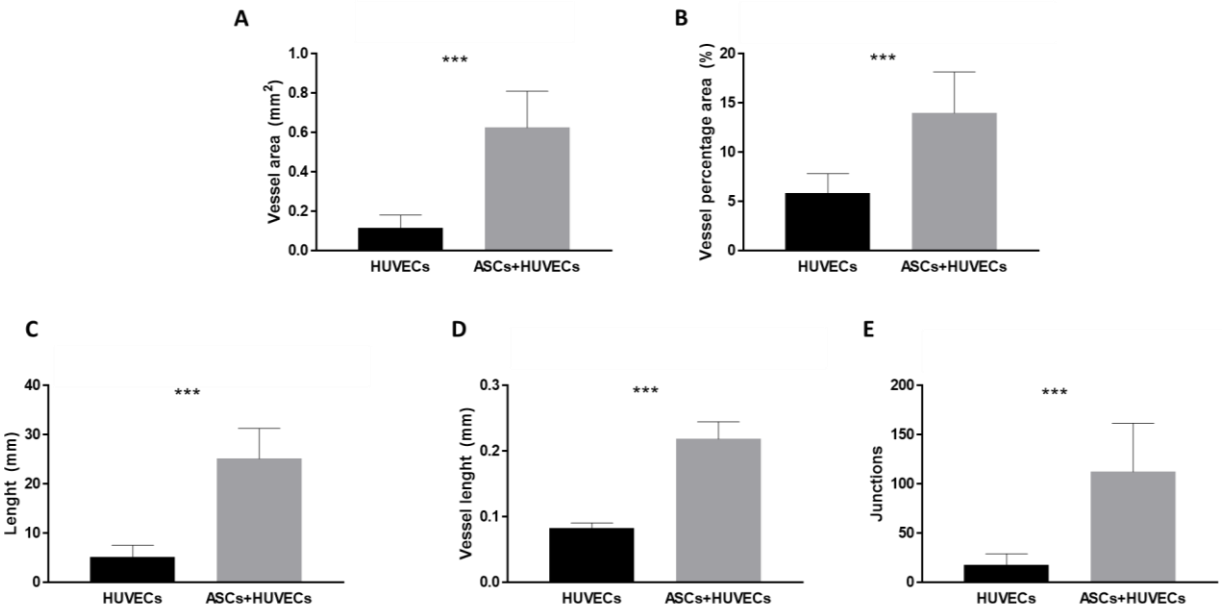

Figure 3.13 – Quantification of diverse parameters associated to vascular organization. The presence of ASCs significantly increased **A,** vessel area, **B,** vessel percentage area, **C,** total vessel length, **D**, average vessel length and **E,** the number of junctions. Data is presented as mean±SEM and is the result of 4 independent experiments (n=8/12). ***p<0.001.

Discussion

The field of Tissue Engineering has long trusted on the use of natural and synthetic polymers to create artificial ECM-like substitutes. These can be created using bioinert materials that are functionalized with cell-instructive chemical cues to induce diverse processes such cell adhesion, proliferation and migration, vascularization, axonal growth or neuronal differentiation [36]. In this regard, the discovery of small peptidic sequences derived from ECM proteins such as RGD, IKVAV (Ile-Lys-Val-Ala-Val), YIGSR (Tyr-Ile-Gly-Ser-Arg) or LDV (Leu-Asp-Val) enabled to recapitulate the interactions between cells and integrins to promote cell adhesion and homeostasis by grafting these sequences onto the backbone of biomaterials lacking such properties. Our research group has previously showed how coupling GRGDS to GG dramatically increased its bioactivity by promoting cell adhesion, proliferation and differentiation of neural progenitors, neurite outgrowth of DRG explants and eventually motor recovery on a severe SCI model [8,9].

However, peptidic sequences are somewhat unstable and prone to degradation by endogenous proteases, do not show a very high integrin affinity and partially lose their bioactive conformation upon grafting [11]. The development of synthetic molecules that perfectly match the binding pocket of integrins, initially

studies which chemical groups are essential for the bioactivity of ECM proteins to a stable ligand with increased integrin affinity that surpass the aforementioned drawbacks of using peptidic adhesion motifs [11]. Peptidomimetics are specifically tailored to activate integrins that drive a biological process of interest, while having the ideal spacer arm length and conformation to allow the sequence maximum bioactivity, representing an important alternative to biofunctionalize inert biomaterials [37]. The peptidomimetic ligands utilized on this work have high affinity towards either α5β1 (1.5 nmol) or αvβ3 (1.8 nmol) integrins [16–18]. Apart from this feature, both are selective for each integrin as αvβ3-expressing and α5β1-expressing fibroblasts only adhered to surfaces functionalized with the corresponding mimetic [18]. These mimetics were chosen as both integrins have been previously described to be present on MSCs and are pivotal during angiogenesis [19,33–35]. Furthermore, the final application of these biomaterials is to induce *in situ* vascularization following SCI and so the activation of αvβ3 and α5β1 might be pivotal. To achieve it, we envision applying them as culture platforms encompassing ASCs+HUVECs that promote the assembly of these endothelial cells into vascular-like structures, as well as and their integration into the spinal cord vasculature of the host.

The previous applications of both ligands were on flat two-dimensional surfaces and since our strategy involves the use of three-dimensional hydrogels the first steps involved the optimization of the chemical grafting of both ligands in comparison to linear RGD, using different stoichiometries. The data gathered did not show relevant differences between the peptide and mimetics regarding coupling efficiency either by quantifying the amount of fluorescent ligand bound, ligand distribution throughout the hydrogels, FTIR and XPS analysis. These techniques confirmed that the grafting strategies were successful and enable to insert the ligands onto GGp, being the formulations where the GGp:ligand stoichiometry was smaller (10:1) the ones with highest amounts of bound adhesive molecules.

The next stage involved understanding whether the modifications promoted the bioactivity of GGp and whether it performed better than linear RGD. The results clearly demonstrated that GGp10αv induced the best results regarding the adhesion and spreading of ASCs to the polymeric matrix both at day 3 and 7 of culture. Thus, it elucidated the enhanced capacity that integrin specific peptidomimetics have in triggering cellular homeostasis and how they can be helpful to develop soft three-dimensional ECM substitutes for regenerative medicine processes. The application of GGp10αv alone, however, was insufficient to induce a significant growth of neurites from DRG explants. This might be explained by the fact that this integrin is not important for neurite outgrowth as demonstrated by Gardiner *et al.* [38], which blocked the β3 subunit and observed no impact on the extension DRG neurites. Therefore, the conditions that promoted increased neurite arborization were the combination between GGp10αv and encapsulated

ASCs or ASCs+HUVECs. The encapsulation of ASCs, in fact, enabled an extensive and significantly higher neurite outgrowth in relation to the other tested conditions. The main driver behind this result is probably the secretome of ASCs, which we previously demonstrated that possesses a cocktail of neurotrophic molecules like BDNF, NGF, GDNF, among other general growth factors including insulin growth factor (IGF) and bFGF [8,24,39]. Most of these molecular effectors activate the PI3k-Akt signaling pathway, which has been shown to enable axonal regeneration on the spinal cord and retina, playing a central role in CNS regeneration [40,41].

Apart from their effect on neurite extension, ASCs also induced the significant assembly of HUVECs into stable vascular-like structures, something that contrasts with the culture of these cells alone on GGp10αv. These results are partially explained by the richness of the secretome of ASCs on angiogenic molecules such as VEGF-A, angiogenin or PDGF [24]. Nevertheless, it was the combination between secretome and direct cell contact that probably led to the establishment of long-lasting vascular-like structures on the co-culture condition. Different studies have showed that the direct contact between ASCs and endothelial cells is fundamental to induce tube-formation and stabilize newly formed vascular networks [42,43]. These MSCs reinforce the expression of common endothelial markers such as CD31 and act on fundamental signaling pathways to vascular assembly like the VEGF, HGF and PDGF-BB pathways. These results help to show that despite the use of integrin-specific ligands provides increased bioactivity to bioinert polymers, complex processes like vascularization might need additional stimuli, such as the presence of other types of cells to occur.

On the other hand, the GGp formulation functionalized with the α5β1 mimetic did not show significant biological activity either during the adhesion studies or the neurite outgrowth studies, despite the presence of this on ASCs and DRG [33–35,38]. Actually, the latter have been previously demonstrated to extend their neurites in a α5β1-dependent manner [38]. These results are rather surprising, especially because the binding of the ligand seemed to be successful and we could not observe any differences between the GGpα5, GGpαv and GGpRGD formulations. The loss of conformation upon grafting cannot be excluded. Although unlikely, since the ligand was designed with the appropriate parameters to present conformational stability and bioactivity, it must be considered because this represents the first time such integrin mimetics were used to functionalize three-dimensional biomaterials. Another possible explanation may reside on the crosslinking of the GGp chains, which might lead to the entanglement of the α5β1 mimetic and consequently to its loss of availability. These considerations need to be further explored to understand the unsatisfactory biological results obtained with this modification.

Despite the less promising results showed by GGpα5 formulations, GGp10αv clearly demonstrated the advantages of using peptidomimetic ligands with integrin specificity to enhance the biological properties of bioinert polymers in comparison to commonly used peptidic adhesion molecules. These encouraging results open excellent perspectives regarding the use of such hydrogels with encapsulated ASCs+HUVECs in a SCI animal model with the purpose to promote the *in-situ* vascular assembly of the transplanted cells and revascularize the lesion site, thus promoting better functional outcomes. The lack of vascular regeneration is pivotal to trigger numerous deleterious events following the lesion and so it might be a pivotal feature to obtain robust motor, sensory and autonomic improvements.

Conclusions

The present work allowed assessment of the potential of using peptidomimetic ligands with integrin specificity to increase the biological properties of otherwise bioinert hydrogels. We clearly demonstrated that the GGp formulations to which the αvβ3 mimetic was grafted enhanced the capacity of the polymer to promote greater adhesion and extension of ASCs in comparison to common RGD motifs. Substantial neurite outgrowth was also achieved using GGp10αv hydrogels with encapsulated ASCs, these being fundamental for the assembly of HUVECs into vascular-like structures within the hydrogels. These results open excellent perspectives regarding the application of this integrin-specific biomaterial in SCI animal models to study its capacity to promote *in-situ* organization of transplanted HUVECs into vascular networks and consequently functional recovery following lesion. This was, to our knowledge, the first time that peptidomimetic ligands bearing integrin specificity were used to enhance the bioactivity of inert hydrogels.

Acknowledgements

The authors acknowledge Professor Jeffrey Gimble at the Tulane University Center for Stem Cell Research and Regenerative Medicine and LaCell LLC (New Orleans, Louisiana, USA) for kindly providing the ASCs used in this study. The authors want to acknowledge the financial support from Prémios Santa Casa Neurociências - Prize Melo e Castro for Spinal Cord Injury Research (MC-04/17); from Portuguese Foundation for Science and Technology (PD/BDE/127835/2016) to L. A. Rocha and (SFH/BD/103075/2014) to E.D. Gomes. This work was funded by FEDER, through the Competitiveness Internationalization Operational Program (POCI), and by National funds, through the Foundation for

Science and Technology (FCT), under the scope of the projects POCI-01-0145-FEDER-007038; TUBITAK/0007/2014; PTDC/DTP-FTO/5109/2014; POCI-01-0145-FEDER-029206; POCI-01-0145-FEDER-031392; PTDC/MED-NEU/31417/2017 and NORTE-01-0145-FEDER-029968. This work has also been developed under the scope of the project NORTE-01-0145-FEDER-000013, supported by the Northern Portugal Regional Operational Programme (NORTE 2020), under the Portugal 2020 Partnership Agreement, through the European Regional Development Fund (FEDER).

References

1. Shattil, S. J., Kim, C. & Ginsberg, M. H. The final steps of integrin activation: the end game. *Nat. Rev. Mol. Cell Biol.* **11**, 288–300 (2010).
2. Rocha, L. A., Learmonth, D. A., Sousa, R. A. & Salgado, A. J. αvβ3 and α5β1 integrin-specific ligands: From tumor angiogenesis inhibitors to vascularization promoters in regenerative medicine? *Biotechnol. Adv.* **36**, 208–227 (2018).
3. Hynes, R. O. Integrins: bidirectional, allosteric signaling machines. *Cell* **110**, 673–87 (2002).
4. Hersel, U., Dahmen, C. & Kessler, H. RGD modified polymers: biomaterials for stimulated cell adhesion and beyond. *Biomaterials* **24**, 4385–415 (2003).
5. Pierschbacher, M. D. & Ruoslahti, E. Variants of the cell recognition site of fibronectin that retain attachment-promoting activity. *Proc. Natl. Acad. Sci. U. S. A.* **81**, 5985–5988 (1984).
6. Bicho, D., Ajami, S., Liu, C., Reis, R. L. & Oliveira, J. M. Peptide-biofunctionalization of biomaterials for osteochondral tissue regeneration in early stage osteoarthritis: Challenges and opportunities. *Journal of Materials Chemistry B* (2019) doi:10.1039/c8tb03173h.
7. Karimi, F., O'Connor, A. J., Qiao, G. G. & Heath, D. E. Integrin Clustering Matters: A Review of Biomaterials Functionalized with Multivalent Integrin-Binding Ligands to Improve Cell Adhesion, Migration, Differentiation, Angiogenesis, and Biomedical Device Integration. *Advanced Healthcare Materials* (2018) doi:10.1002/adhm.201701324.
8. Gomes, E. D. *et al.* Co-Transplantation of Adipose Tissue-Derived Stromal Cells and Olfactory Ensheathing Cells for Spinal Cord Injury Repair. *Stem Cells* **36**, 696–708 (2018).
9. Silva, N. A. *et al.* The effects of peptide modified gellan gum and olfactory ensheathing glia cells on neural stem/progenitor cell fate. *Biomaterials* **33**, 6345–6354 (2012).
10. Assunção-Silva, R. C. *et al.* Induction of neurite outgrowth in 3D hydrogel-based environments. *Biomed. Mater.* **10**, 051001 (2015).
11. Mas-Moruno, C. *et al.* αvβ3- or α5β1-Integrin-Selective Peptidomimetics for Surface Coating. *Angew. Chemie - Int. Ed.* **55**, 7048–7067 (2016).
12. Ku, T. W. *et al.* Direct design of a potent non-peptide fibrinogen receptor antagonist based on the structure and conformation of a highly constrained cyclic RGD peptide. *J. Am. Chem. Soc.* **115**, 8861–8862 (1993).
13. Reardon, D. A., Nabors, L. B., Stupp, R. & Mikkelsen, T. Cilengitide: An integrin-targeting arginine-glycine-aspartic acid peptide with promising activity for glioblastoma multiforme. *Expert Opinion on Investigational Drugs* (2008) doi:10.1517/13543784.17.8.1225.

14. Rerat, V. *et al.* αvβ3 Integrin-Targeting Arg-Gly-Asp (RGD) Peptidomimetics Containing Oligoethylene Glycol (OEG) Spacers. *J. Med. Chem.* **52**, 7029–7043 (2009).
15. Marchini, M. *et al.* Cyclic RGD peptidomimetics containing bifunctional diketopiperazine scaffolds as new potent integrin ligands. *Chem. - A Eur. J.* **18**, 6195–6207 (2012).
16. Fraioli, R. *et al.* Mimicking bone extracellular matrix: Integrin-binding peptidomimetics enhance osteoblast-like cells adhesion, proliferation, and differentiation on titanium. *Colloids Surfaces B Biointerfaces* **128**, 191–200 (2015).
17. Rechenmacher, F. *et al.* A molecular toolkit for the functionalization of titanium-based biomaterials that selectively control integrin-mediated cell adhesion. *Chem. - A Eur. J.* **19**, 9218–9223 (2013).
18. Rechenmacher, F. *et al.* Functionalizing αvβ3- or α5β1-selective integrin antagonists for surface coating: A method to discriminate integrin subtypes in vitro. *Angew. Chemie - Int. Ed.* **52**, 1572–1575 (2013).
19. Avraamides, C. J., Garmy-Susini, B. & Varner, J. A. Integrins in angiogenesis and lymphangiogenesis. *Nat. Rev. Cancer* **8**, 604–617 (2008).
20. Rouwkema, J. & Khademhosseini, A. Vascularization and Angiogenesis in Tissue Engineering: Beyond Creating Static Networks. *Trends Biotechnol.* **34**, 733–745 (2016).
21. Kirchmajer, D. M., Steinhoff, B., Warren, H., Clark, R. & In Het Panhuis, M. Enhanced gelation properties of purified gellan gum. *Carbohydr. Res.* **388**, 125–129 (2014).
22. Doner, L. W. Rapid purification of commercial gellan gum to highly soluble and gellable monovalent cation salts. *Carbohydr. Polym.* **32**, 245–247 (1997).
23. Dubois, S. G. *et al.* Isolation of human adipose-derived stem cells from biopsies and liposuction specimens. in *Methods in molecular biology (Clifton, N.J.)* vol. 449 69–79 (2008).
24. Rocha, L. A. *et al.* In vitro Evaluation of ASCs and HUVECs Co-cultures in 3D Biodegradable Hydrogels on Neurite Outgrowth and Vascular Organization. *Front. Cell Dev. Biol.* **8**, (2020).
25. Gomes, E. D. *et al.* Combination of a peptide-modified gellan gum hydrogel with cell therapy in a lumbar spinal cord injury animal model. *Biomaterials* **105**, 38–51 (2016).
26. Torres-Espín, A., Santos, D., González-Pérez, F., del Valle, J. & Navarro, X. Neurite-J: An Image-J plug-in for axonal growth analysis in organotypic cultures. *J. Neurosci. Methods* **236**, 26–39 (2014).
27. Zudaire, E., Gambardella, L., Kurcz, C. & Vermeren, S. A Computational Tool for Quantitative Analysis of Vascular Networks. *PLoS One* **6**, e27385 (2011).
28. Ferris, C. J., Gilmore, K. J., Wallace, G. G. & Panhuis, M. In Het. Modified gellan gum hydrogels

for tissue engineering applications. *Soft Matter* **9**, 3705 (2013).

29. Lozano, R. *et al.* 3D printing of layered brain-like structures using peptide modified gellan gum substrates. *Biomaterials* **67**, 264–273 (2015).
30. D'Este, M., Eglin, D. & Alini, M. A systematic analysis of DMTMM vs EDC/NHS for ligation of amines to hyaluronan in water. *Carbohydr. Polym.* **108**, 239–46 (2014).
31. Farkaš, P. & Bystrický, S. Efficient activation of carboxyl polysaccharides for the preparation of conjugates. *Carbohydr. Polym.* (2007) doi:10.1016/j.carbpol.2006.07.013.
32. Stodolak-Zych, E. *et al.* Modification of chitosan fibers with short peptides as a model of synthetic extracellular matrix. *J. Mol. Struct.* (2020) doi:10.1016/j.molstruc.2020.128061.
33. Gronthos, S., Simmons, P. J., Graves, S. E. & G. Robey, P. Integrin-mediated interactions between human bone marrow stromal precursor cells and the extracellular matrix. *Bone* (2001) doi:10.1016/S8756-3282(00)00424-5.
34. Frith, J. E., Mills, R. J., Hudson, J. E. & Cooper-White, J. J. Tailored Integrin–Extracellular Matrix Interactions to Direct Human Mesenchymal Stem Cell Differentiation. *Stem Cells Dev.* **21**, 2442–2456 (2012).
35. Goessler, U. R. *et al.* Integrin expression in stem cells from bone marrow and adipose tissue during chondrogenic differentiation. *Int. J. Mol. Med.* (2008) doi:10.3892/ijmm.21.3.271.
36. Rocha, L. A. *et al.* Cell and Tissue Instructive Materials for Central Nervous System Repair. *Adv. Funct. Mater.* 1909083 (2020) doi:10.1002/adfm.201909083.
37. Kapp, T. G. *et al.* A Comprehensive Evaluation of the Activity and Selectivity Profile of Ligands for RGD-binding Integrins. *Sci. Rep.* **7**, 39805 (2017).
38. Gardiner, N. J. *et al.* Preconditioning injury-induced neurite outgrowth of adult rat sensory neurons on fibronectin is mediated by mobilisation of axonal α5 integrin. *Mol. Cell. Neurosci.* **35**, 249–260 (2007).
39. Pires, A. O. *et al.* Unveiling the Differences of Secretome of Human Bone Marrow Mesenchymal Stem Cells, Adipose Tissue derived Stem Cells and Human Umbilical Cord Perivascular Cells: A Proteomic Analysis. *Stem Cells Dev.* **25**, 1073–83 (2016).
40. Liu, K. *et al.* PTEN deletion enhances the regenerative ability of adult corticospinal neurons. *Nat. Neurosci.* **13**, 1075–81 (2010).
41. Park, K. K. *et al.* Promoting axon regeneration in the adult CNS by modulation of the PTEN/mTOR pathway. *Science* **322**, 963–6 (2008).
42. Merfeld-Clauss, S., Gollahalli, N., March, K. L. & Traktuev, D. O. Adipose tissue progenitor cells

directly interact with endothelial cells to induce vascular network formation. *Tissue Eng. - Part A* (2010) doi:10.1089/ten.tea.2009.0635.

43. Holnthoner, W. *et al.* Adipose-derived stem cells induce vascular tube formation of outgrowth endothelial cells in a fibrin matrix. *J. Tissue Eng. Regen. Med.* **9**, 127–136 (2015).

CHAPTER 4

L.A. Rocha, C.M. Moruno, E.D. Gomes, R. Lima, J. Campos, J. Cibrão, D. Silva, A. F. B. Räder, H. Kessler, N.A. Silva, R.A. Sousa, D.A. Learmonth, A.J. Salgado

Evaluation of peptidomimetic-modified and GRGDS-modified gellan gum hydrogels encompassing ASCs and HUVECs in the recovery and systemic inflammation following spinal cord injury

(In preparation)

(2021)

Title

Evaluation of peptidomimetic-modified and GRGDS-modified gellan gum hydrogels encompassing ASCs and HUVECs in the recovery and systemic inflammation following spinal cord injury

Authors

L.A. Rocha[1,2,3], C.M. Moruno[4], E.D. Gomes[1,2], R. Lima[1,2], J. Campos[1,2], J. Cibrão[1,2], D. Silva[1,2], A. F. B. Räder[5], H. Kessler[5], N.A. Silva[1,2] R.A. Sousa[3], D.A. Learmonth[3], A.J. Salgado[1,2]

Affiliations

[1]Life and Health Sciences Research Institute (ICVS), School of Medicine, University of Minho, Braga, Portugal.

[2]ICVS/3B's – PT Government Associate Laboratory, Braga, Portugal.

[3]Stemmatters, Biotecnologia e Medicina Regenerativa SA, Barco, Portugal.

[4] Biomaterials, Biomechanics and Tissue Engineering Group (BBT), Department of Materials Science and Metallurgical Engineering, Universitat Politècnica de Catalunya (UPC), 08019 Barcelona, Spain

[5]Technische Universität München, Department Chemie, Institute for Advanced Study, Lichtenbergstrasse, Garching, Germany.

Corresponding author

A. J. Salgado (PhD), Life and Health Sciences Research Institute (ICVS), School of Medicine, University of Minho, Campus Gualtar, 4710-057 Braga, Portugal.

Phone number: +351 253 60 49 47

E-mail: asalgado@med.uminho.pt

Abstract

Spinal cord injury (SCI) is an extremely debilitating condition for which its care remains mostly palliative. Part of this limited prognosis is due to the vascular disruption occurring immediately after SCI and its faulting endogenous response. Therefore, the present work envisioned to implant two distinct biomaterial-based approaches encapsulating ASCs and HUVECs into a transection rat model of SCI. With it, we intended to understand the impact of a GRGDS-modified gellan gum (GG-GRGDS) hydrogel and of a αvβ3-modified gellan gum (GGp10αv) on the motor and sensory recovery following SCI, as well as the systemic inflammatory profile in different stages of the condition. Even though the final BBB scores of the two cell transplantation groups were similar, the results demonstrated that GGp10αv+cells was the only treatment that promoted an overall statistically significant increase on BBB scores in comparison to injured animals. Moreover, both hydrogel-based therapies enhanced the sensory perception of treated animals. Even though on the acute phase of SCI both cell therapies induced an upregulation on anti-inflammatory cytokines, on animals transplanted GGp10αv+cells this was accompanied by a reduction on pro-inflammatory cytokines possibly indicating a stronger immunomodulatory action of the therapy. This effect was lost on the latter timepoints (3 and 8 weeks post-SCI) narrowing it to the acute phase of SCI. Despite the promising data, these results need to be further explored by histological analysis of the injured tissue. This analysis will allow to understand the impact of the therapeutic approaches on different neuronal populations, local inflammation, regeneration and on the vascular response (vascular phenotype and integration of transplanted HUVECs) to further elucidate the mechanisms that led to the behavioral improvements.

Keywords: peptidomimetics, integrin-specific ligands, spinal cord injury, vascularization, MSC, neurovascular.

Introduction

SCI represents an extremely disabling medical problem for which there is no current effective treatment. Recent estimations indicate that a total of 27 million people worldwide live with comorbidities, or permanent impairments, that are consequence of SCI [1]. The vast majority of lesions occur by contusions originated by traumatic events such as falls or traffic accidents, being the cervical region of the spinal cord the most commonly affected [2]. Although the knowledge acquired in the last decades on the pathophysiology of the disease, as well as on the management of patients, have improved, their treatment remains mostly palliative. The reason behind this lies on the complexity of events triggered following SCI. Thus, following mechanical trauma the BSCB is disrupted originating tissue edema and swelling, the uncontrolled infiltration of inflammatory cells, excitotoxicity, ionic imbalance, mitochondrial dysfunction, ROS [3]. The natural resolution of SCI involves the formation of a glial scar, that even though contains the damage and the spreading of neurotoxic agents, at the same time creates a physical barrier for axons to grow and regenerate [4]. To aggravate the problem, either due to their epigenetic nature that naturally represses neuronal regenerative programs or the inhibitory environment found on SCI lesion tissue (myelin debris and other repulsive molecules, deposition of CSPGs) the perspectives of some degree of recovery are scarce [3]. Therefore, SCI leads to extensive neuronal damage, accompanied by motor, autonomic and sensory impairments.

Vascular disruption following SCI plays a central role on the pathophysiology of the condition where it contributes to initiate the already mentioned cascade of deleterious events and to the chronic hypoxic state of injured tissue [5,6]. Although a strong angiogenic response is observed during the first days after SCI, most of the newly formed vessels do not subsist and the ones that survive do not associate with neurons and astrocytes to form neurovascular units [7–9]. Therefore, apart from the insufficient oxygen influx to SCI tissue, the local environment remains exposed to systemic neurotoxic agents due to inefficient BSCB reestablishment. This opened the possibility of promoting the revascularization of the SCI milieu as a way of modulating the progression of the disease and achieve better functional outcomes [10–14].

A possible approach to do so is through the transplantation of cells to either replace the lost vasculature or to stimulate the proliferation of endogenous ECs and the formation of new vessels [13,15–17]. Mesenchymal stem cells (MSCs) have shown to promote the latter due to their strong paracrine angiogenic signaling and impact on the stabilization of vascular networks by direct MSC-EC contact [18]. Firstly reported by Friedenstein and coworkers [19], the initial rationale to apply MSCs for regenerative medicine applications involved their multipotency, allowing to replace damage cells and promote tissue regeneration [20]. However, numerous studies demonstrated that the positive results obtained from their use expanded beyond their

capacity to differentiate into distinct cell types, and included the trophic support provided by the panel of soluble molecules and vesicles that MSCs secrete to the extracellular milieu (their secretome) [21,22]. Apart from angiotrophic factors, these include neuroregulatory and neurotrophic molecules, immunomodulatory cytokines and chemokines and distinct growth factors and microRNAs (miRNAs) that promote cell survival and proliferation [23]. ASCs are a subpopulation of MSCs that are easily isolated from lipoaspirates (otherwise a medical waste product) with a marked presence of molecules that target excitotoxicity, which makes this type of MSCs attractive to apply in SCI [24]. Their potential has been demonstrated in different preclinical models of SCI [25,26] and prompted their study in human patients, where the cell infusion did not elicit signs of adverse effects, whilst having some indications of impacting the neurological status of the patients [27,28].

The major drawback associated to cell transplantation lies on their low survival rate due to their low integration into the host tissue, forcing the use of enormous amounts of cells to obtain a clinical effect [29]. A possible way to address this issue is to use biomaterial platforms that act as substitutes of the native ECM providing trophic support and the adequate signaling cues for cell homeostasis [30]. These can be designed to possess similar mechanical properties to native tissue, thus facilitating the integration of biomaterial/cell constructs [31]. A trend on the field is to incorporate peptidic motifs into the backbone of bioinert materials that confer them biological activity by simple chemical reactions. Probably the most used of these sequences is GRGDS, a ubiquitous motif amongst ECM proteins, with strong cell adhesion properties [32]. Previously, our research group has applied this rationale and modified GG with the GRGDS motif and proved that the incorporation of the adhesion sequence enhanced the adhesion and proliferation of cells to the matrix, whilst promoting the neurite extension from dorsal root ganglia explants [33–35]. Moreover, its implantation as an artificial ECM substitute encapsulating ASCs and olfactory ensheathing cells (OECs) into an animal model of SCI promoted a significant recovery on motor function [35]. However, linear peptides are extremely prone to enzymatic degradation and can easily partially lose their bioactive conformation, hence their efficiency to promoted cellular processes [36]. Recent years have seen the development of synthetic ligands (peptidomimetics) that are specifically tailored to maximize the interaction with the binding pockets of cell receptors to engage the activation of specific cellular processes and have a more stable conformation, whilst being less susceptible to degradation [37].

We have demonstrated on Chapter 2 and 3 of this thesis that ASCs are instrumental for the organization of HUVECs on stable vascular-like structures when cultured on GG-GRGDS and GGp10αv, a mandatory prerequisite for the development of successful vascular constructs. Taken this together, the objective of the present work was to evaluate the capacity of GRGDS-modified GG and αvβ3 integrin-specific modified

GG, encapsulating ASCs and HUVECs, to promote the motor and sensory recovery of a T8 transection rat model of SCI. Moreover, the impact of our treatment on the systemic expression of a defined array of serum cytokines in distinct phases of the conditions (acute, intermediate and chronic) was also evaluated to understand its impact on the systemic response to the injury.

Material and Methods

Cell isolation and culture

Human ASCs were obtained by LaCell LLC (New Orleans, USA) from the lipoaspirates obtained from consenting donors according to Dubois *et al.*[38], under a protocol previously approved by an institutional review panel at LaCell LLC. Following their isolation, ASCs were cultured in α-MEM (Invitrogen, USA) supplemented with 10 % FBS (Biochrom AG, Germany), and 1 % (V/V) penicillin-streptomycin (Invitrogen, USA). The cells were kept at 37 ◦C and 5 % CO2 (V/V) and medium exchanged every 3 days until further use.

The isolation of HUVECs followed a previously published protocol [39] that was approved by the review board of the Ethical Commission for Health of Braga Hospital (CESHB). The cells were obtained from the umbilical cord of healthy consenting patients from the Gynecology and Obstetrics Service of Hospital de Braga. Briefly, the umbilical cord was rinsed and cleaned with PBS and then a cannula was inserted in the umbilical vein. This was followed by the washing of the vein with PBS to remove excesses of blood and clots. Then, the opposed extremity of the cord was closed with forceps and the vein filled with α-MEM containing 0.2 % (w/V) (210 U/mL) Type I Collagenase (Gibco, Thermo Fischer Scientific, USA) and 1 % pen/strep. The cord was transferred to a cell culture incubator for 15 minutes to allow the proper digestion of the endothelium of the umbilical vein. Following this period, the cord was massaged and its content transferred to a 50 mL Falcon tube being then washed with α-MEM, PBS and a syringe filled with air. The suspension was then centrifuged at 1200 rpm for 10 minutes to obtain the cellular pellet. After resuspending the pellet in EGM (R&D Systems, USA) supplemented with 1x EGS (R&D Systems, USA) and 1 % (V/V) pen/strep the suspension was divided into a 6-well plate [pre-coated with 1 % (w/V) Type B bovine gelatin (Sigma, USA)] and cultured overnight in the same media to allow the attachment of HUVECs. The media was exchanged to remove debris and unattached cells, being up from this moment changed every two days to keep purifying the culture. After reaching confluence, part of the cells were transferred to a T75 flask pre-coated with gelatin and cultured using the already described conditions, while the rest were stored in liquid nitrogen until further use.

Chemical modification of GG with GRGDS

The biofunctionalization of GG with GRGDS was performed in accordance to previously described protocols [34,35,39]. Succinctly, a GG (Sigma, USA) 1 % (w/V) solution was prepared in 100 mM MES (Sigma, USA) buffer at pH 5.5 and 37 °C. Then, a 750 mM DMT-MM (Sigma, USA) water solution was prepared and added using a 1:4 molar ratio (GG:DMT-MM). This step was followed by the addition of furfurylamine

(Acros Organics, Belgium) to the solution at the same molar ratio and the reaction allowed to proceed for 24 h. The obtained product was dialyzed in a membrane with a molecular cutoff of 12-14 kDa (Spectrum Labs, USA) for 5 days alternatively against distilled water or PBS (0.1 M, pH 7.2) to allow the purification of the modified polymer. The recovery of GG-furan as a white powder was achieved by lyophilization. The immobilization of maleimide-modified GRGDS (GRGDS-maleimide) proceeded by first dissolving 1.2 mg/mL GG-furan in 100 mM MES buffer at pH 5.5 and 37 °C. Afterwards, mal-GRGDS (Anaspec, USA) was added using a 1:5 molar ratio (furan:maleimide), for 48 h and under vigorous agitation. To purify GG-GRGDS the solution was dialyzed (molecular cutoff of 12-14 kDa) against distilled water and PBS (0.1 M, pH 7.2) alternatively during 5 days. Finally, the lyophilization of the product allowed to obtain GRGDS-modified GG (GG-GRGDS) as a white powder.

Gellan gum purification

The purification of GG was performed following published protocols [40,41]. Thus, a 1 % (w/V) GG solution was dissolved in deionized water at 65 °C and under constant stirring. This was followed by the addition of a cation exchange resin (Amberlite® IR120, Sigma-Aldrich, USA) until the solution reached a pH of 2.5. Then, the agitation was stopped to allow the resin to settle and the solution filtered. Afterwards, the solution was poured into a pre-heated beaker (95 °C) and the pH adjusted to 8.7 using 1 M NaOH (Merck, Germany). The dispersion was allowed to cool to RT and then poured onto 70 % (V/V) ethanol (Carlo Erba, Italy) to precipitate GG. GGp was recovered by filtering the mixture using a steel sieve, being this followed by vacuum filtration. Subsequently, GGp was dissolved in water at RT with constant stirring and the solution transferred into a dialysis membrane with a molecular cutoff of 12-14 kDa (Sigma-Aldrich, USA). Dialysis continued for a period of 7 days with daily water exchanges. Afterwards, the content of the membrane was frozen at a -20 °C and freeze-dried for 4 days. The procedure allowed to obtain the polymer as a white, cotton-like, solid (yield of 81.67 %).

Chemical grafting of αvβ3 mimetic to GGp

The modification of GGp with the αvβ3 mimetic started by preparing a 1 % (w/V) GGp water solution, to which a 750 mM DMT-MM water solution was added following the complete dissolution of the polymer using a polymer:DMT-MM ratio of 1:2. Subsequently, a solution of 100 μM αvβ3 mimetic in water was added to the reaction mixture using a 10:1 polymer:αvβ3 mimetic ratio. The reaction proceeded overnight under magnetic stirring. Then, GGp10αv was precipitated using 70 % (V/V) ethanol, being the modified polymer recovered by vacuum filtration. Recovered GGp10αv was then dissolved in water to obtain a 1 %

(w/V) GGp solution, which upon dissolution was rapidly frozen on liquid nitrogen and transferred to a freeze dryer to recover the polymer in the solid, cotton-like, state (recovery yield of 93.7 %).

Synthesis of GG-GRGDS and GGp10αv hydrogels

GG-GRGDS and unmodified GG were weighed and then sterilized by exposure to UV lights for 15 min, a method previously used by Silva *et al*[34]. Following this step, a 1 % (w/V) solution containing equal amounts of GG-GRGDS and GG was prepared by dissolving the mixture in water at 40 °C overnight. Before cell encapsulation, the GG-GRGDS solution was ionically crosslinked using 10 % (V/V) of a 0.3 % (w/V) $CaCl_2$ water solution [to a final $CaCl_2$ concentration of 0.03 % (w/V) and 0.91 % of GG-GRGDS].

The preparation of the GGp10αv started by exposing the materials to UV lights for 15 min to allow their sterilization [34]. Then, GGp10αv was dissolved in water at a 0.8 % (w/V) concentration and crosslinked using 20 % α-MEM. The hydrogel volume utilized in the *in vivo* experiments was 5 µL.

Encapsulation of ASCs and HUVECs on GG-GRGDS and GGp10αv

ASCs and HUVECs were cultured as previously detailed (section 4.2.1) and the corresponding hydrogels prepared according to section 4.2.5. The encapsulation of ASCs and HUVECs was done using a 1:1 ratio of each cell type. Briefly, after trypsinization the cellular suspensions corresponding to ASCs and HUVECs were mixed and then centrifuged at 1200 rpm for 5 minutes to obtain the cell pellet. Then, the corresponding volume of GG-GRGDS or GGp10αv was added to obtain a cell density of 2 million cells (1 million ASCs and 1 million HUVECs)/50 µL of hydrogel.

In Vivo experiments

Animals and groups

The animal care committee of ICVS approved all the animal protocols, and these were performed in accordance with standardized animal care guidelines [42].

The *in vivo* experiments were performed using Eight-weeks-old female Wistar rats (Charles River, France) which were accommodated in light and temperature-controlled rooms and fed with standard diet. These experiments were divided in two independent sets and consisted of six distinct: (I) Animals subjected to SCI (Inj, n=9); (II) SCI animals treated with GG-GRGDS alone (RGD, n=7), (III) SCI animals treated with a transplantation of ASCs and HUVECs (RGD + Cells, n=5); (IV) SCI animals treated with GGp10αv (n=4); (V) SCI animals treated with GGp10αv encapsulating ASCs and HUVECs (GGp10αv+Cells, n=8); (VI) Animals to which only a laminectomy was performed (Sham, n=5). Animals on the groups that received

the combination of hydrogel and cells received a total of 200,000 cells (100,000 ASCs and 100,000 HUVECs), encapsulated in 5 µL of hydrogel. The hydrogel was pipetted into the void that appeared as consequence of the spinal cord transection using a positive displacement pipette.

Spinal Cord Injury Surgery

The animals were anesthetized using a ketamine (100 mg/ml, Imalgene/Merial, France) and medetomidine hydrochloride (1 mg/ml, Domitor/Pfizer, USA) mixture (1.5:1) that was injected intraperitoneally. Subsequently, the fur from the surgical site was shaved and the skin disinfected with ethanol 70% and chlorohexidine. This was followed by a dorsal midline incision from T7-T13 was done and the retraction of the paravertebral muscles. Then, after performing a laminectomy at T8, the spinous processes were removed to expose the spinal cord. The spinal cord was transected at T8 level by cutting it using a pair of straight micro scissors, being the area cleaned until a void of approximately 5 mm was visible. Then, the animals received the corresponding treatment and both the paravertebral muscles and skin were closed with Vicryl sutures (Johnson and Johnson, USA). Animals in the injured group were closed immediately after injury. Sham animals were only subjected to the laminectomy procedure, after which they were closed using the previously referred procedure. Post-operative care was given to all SCI rats.

Post-operative care

Immediately after the SCI surgeries, rats were put under heat lamps and received a subcutaneous injection containing vitamins (Duphalyte/Pfizer, USA), 0.9 % NaCl, carprofen (5 mg/ml, Rimadyl/Pfizer, USA) (anti-inflammatory), butorphanol (10 mg/ml, Butomidor/Richter Pharma AG, Austria) (analgesic) and enrofloxacin (5 mg/ml, Baytril/Bayer, Germany) (antibiotic), besides atipamezole (5 mg/ml, Antisedan/Pfizer, USA) a drug used in order to revert anesthesia. Bladder evacuation was done manually twice a day or until the animals were capable of regain its control. The rats continued to receive daily subcutaneous injections having all the described components with exception to atipamezole. The administration of Carprofen was stopped three days post-injury. During the treatment and recovery period the animals were examined to assess whether they presented symptoms of illness or potential adverse reactions to the treatment. Finally, the diet was changed, and animals started receiving a diet with a high caloric-content (Mucedola 4RF25, Italy) and the food was presented to the rats in the cage.

Behavioral Analysis

Basso, Beattie, Bresnahan (BBB) Test

The motor behavior was evaluated using the BBB Locomotor Rating Scale [43]. The test started 3 days post-injury, proceeding then once a week (starting exactly one week following injury) up to a total of 8 weeks. During the BBB test rats were placed in an open arena with no obstacles, being allowed to move freely, and locomotion of the affected hindlimbs was rated by two blinded observers for 4 minutes. The animal locomotion profile was evaluated and a score attributed to its performance.

Von Frey

The mechanical sensitivity was assessed every 2 weeks during the *in vivo* experiments (a total of 4 evaluations during the 8 week period) using the Von Frey test [44,45]. The test started by placing the rats on an elevated grid, which was covered with a transparent box, and the animals left acclimatizing to the experimental conditions for 5 minutes. Then, a series of calibrated Von Frey filaments (15.0 g, 8.0 g, 6.0 g, 4.0 g, 2.0 g, 1.0 g, 0.6 g, 0.4 g) (North Coast Medical Inc., USA) were used to determine the 50 % likelihood of obtaining a paw withdrawal response (50 % threshold) using the up-down method [46]. Testing paradigm consisted in probing the hind paws of each animal in the sural dermatome using the already referred filaments. The test started with the 2.0 g and continued until obtaining 6 measurements around the threshold point. In case the animal responded to the filament (X) (observed as a brisk withdraw of the limb or licking of the limb) the next filament to be tested would be the immediately bellow one. In opposition, a negative (O) would mean that the following probe would occur using the immediately upward filament. Paw movements associated to locomotion or weight shifting were not considered as a response to the filaments. The 50 % response threshold was calculated using the following formula:

$$50\%g\ threshold = \frac{10^{Xf+K.\delta}}{10000}$$

where: X_f= logarithmic value of the last Von Frey filament; k= tabular value corresponding to the pattern of positive and negative responses (X and 0 sequence; δ= logarithm of the mean difference between stimuli (0.224).

If no responses to the filaments was observed, including to the maximal force filament (15.0 g), or in alternative, in cases where all the tested filaments (from 2.0 to 0.4 g) generated a reaction, the values of 15 and 0.25 were assumed as the 50 % withdrawal threshold, respectively.

Swimming Test

The swimming test allowed to observe spontaneous motility and was performed 8 weeks post-injury. Briefly, each rat was placed at the border of a pool with 170 cm of diameter, and a central platform with 12 cm of diameter. Three trials were given to each animal find the platform, having each a maximum of 2 minutes. Then, the average velocity of each animal was determined through an infra-red camera, associated to the VideoTrack software (Viewpoint, France).

Serum cytokine profile

Blood was collected from the tail vein of the animals 48h and 3 weeks following injury. During the sacrifice of the animals (8 weeks post-SCI), the blood was directly gathered from the heart of the animals using a syringe with a 19 G needle. The blood could coagulate for 30 minutes and was then subjected to centrifugation (15,000 rpm for 15 minutes) to separate the serum. To evaluate the cytokine profile of the previously obtained serums it was used the Rat Cytokine Array C2 (RayBiotech, United States) following the guidelines provided by the manufacturers. The Sapphire Biomolecular Imager (Azure Biosystems, United States) allowed to obtain the chemiluminescence image of each membrane. The intensity of each dot was quantified using the AzureSpot software (Azure Biosystems, United States) by designing a 12×8 dot grid which was adjusted to include each individual point. Absolute values were normalized for the mean of the positive control of each membrane and the background subtracted to allow the comparison between membranes and sera

Animal sacrifice

Animals were sacrificed 8 weeks after post-SCI after being deeply anesthetized by an intraperitoneal injection of 200 mg/mL sodium pentobarbital (Eutasil, Ceva Saúde Animal, Portugal) and perfused through the ascending aorta with 0.9 % (V/V) NaCl, being followed by 4 % (V/V) PFA. After performing a rough dissection of the spine and spinal cord centered on the injury site, the tissue were fixated in 4 % (V/V) PFA overnight. Then, a more cautious dissection of the spinal cord was done and the tissues carefully placed on a solution of sucrose of sucrose [30 % (w/V)]. After 24 h, about 2.5 to 3 cms of spinal cord tissues around the lesion site were involved in frozen section medium (Neg-50, Thermo Scientific, USA) for further histological analysis. Spinal cords collected for proteomic studies were only perfused with 0.9 % (V/V) as already described and then rostral (0.5 cms above the lesion), caudal (0.5 cms bellow the injury) and lesion epicenter were frozen in liquid nitrogen before being stored at -80 ◦C.

Statistical Analysis

The statistical analyses were performed using GraphPad Prism version 7.04 for Windows (GraphPad Software, USA). The statistical comparisons among groups were assessed by two-way ANOVA followed by the Tukey's post-hoc test. Differences were considered statistically significant if a p-value ≤ 0.05 was observed (95 % confidence level).

Results

Combination of hydrogels and cells promotes motor recovery

Our *in vitro* results (Chapter 2 and Chapter 3) have demonstrated that ASCs play a vital role in the vascular assembly of HUVECs, when these ECs were encapsulated both in GG-GRGDS and GGp10αv. Accordingly, we decided to implant both GG-GRGDS and GGp10αv encapsulating both ASCs and HUVECs to enhance the capacity of both types of hydrogels to develop vascularized constructs (Figure 4.1 A).

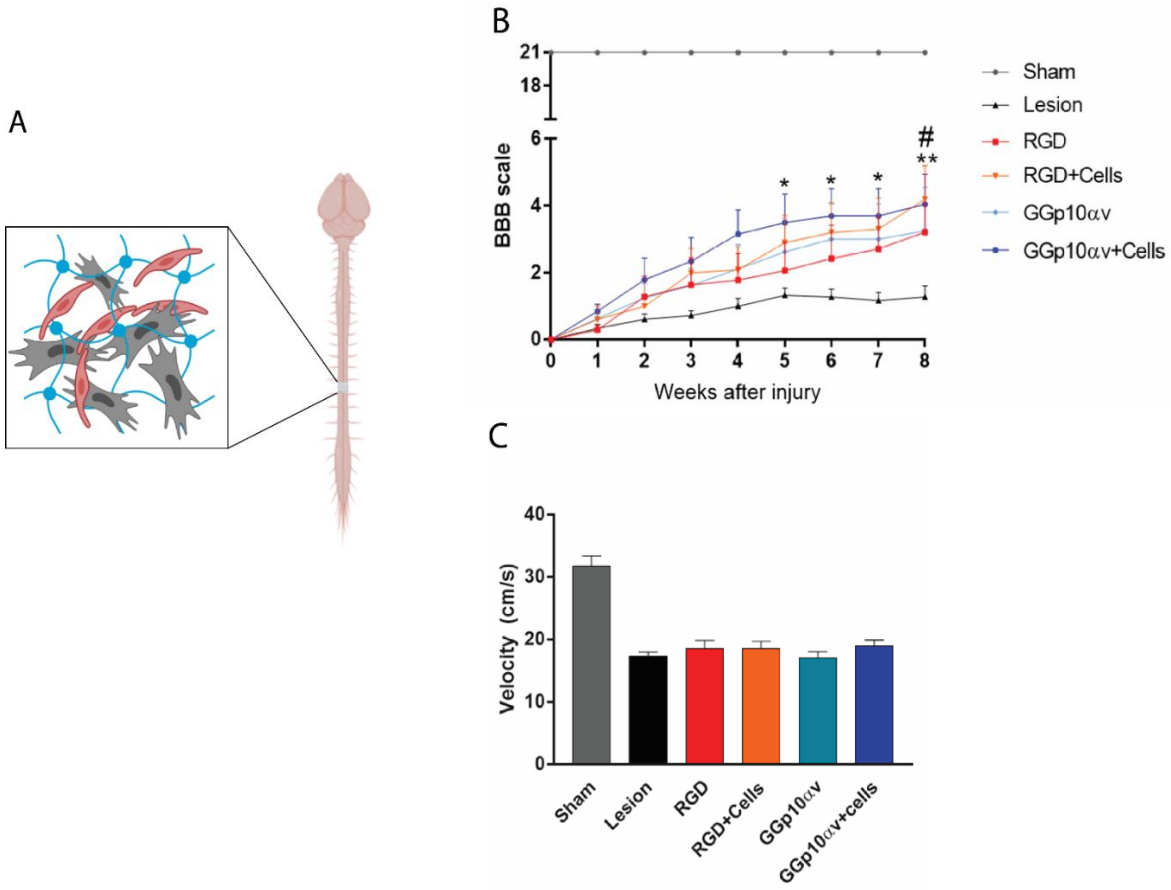

Figure 4.1 – A, Schematic representation of the proposed hydrogel-based therapy, showing ASCs (grey cells) and HUVECs (red cells) encapsulated within GRGDS-modified GG and αvβ3-modified GGp following implantation on the transected cord. **B,** BBB locomotor scale assessment of the different experimental groups. GGp10αv promoted a significant motor recovery in comparison to injured animals from week 4 of the in vivo ($p<0.05$ from week 4-7, $p<0.01$ on week 8), whereas GG-GRGDS only had a significantly higher BBB score when compared to the same group on week 8 ($p<0.05$). **C,** Mean velocity of the animals of each experimental paradigm on the swimming test did not show differences among injured animals and treated animals. Data is shown as mean±SEM (n=4/10). *$p<0.05$; **$p<0.01$ between GGp10αv and injured animals; #$p<0.05$ between GG-GRGDS and injured animals.

Regarding the locomotor behavior, animals in the treated groups presented increased BBB scores in comparison to injured animals. However, only rats receiving the combination between both hydrogels and

cells had statistically significantly higher BBB scores from lesioned animals. In fact, GGp10αv+cells promoted significantly higher BBB scores from week 4 up until the end of the *in vivo* (4.05±0.902 vs 1.28±0.334 at week 8), being the overall performance of animals in the test statistically higher than SCI animals (p=0.0455). Regarding GG-GRGDS+cells, the only timepoint where it a statistically higher BBB score was on week 8 (4.20±1.204 vs 1.28 ± 0.334). The final BBB scores of the *in vivo* meant that animals in both groups that received the combination of hydrogels and cells were able on average to slightly move the three joints of the hindlimbs, whereas the mean BBB score of lesioned animals traduced in the slight movement of one joint (usually the knee) (Figure 4.1 B).

Contrastingly, the swimming test did not reveal differences between injured and treated animals concerning their mean velocity on water (Figure 4.1 C).

Sensory recovery following injury

Transection spinal cord injuries cause the total loss of sensation bellow the injury level, and so this is one of the most important parameters to evaluate functional recovery. The Von Frey test allowed to observe that animals on the treated groups showed increased sensitivity in comparison to injured animals throughout the test (Figure 4.2). For instance, animals on the RGD group were the most responsive to the Von Frey filaments in the 4 timepoints, being statistically significant from the injured group, and showing higher sensitivity than sham animals. GG-GRGDS treated rats were next on the hierarchy and showed significantly lower 50 % Threshold values when comparing to transected animals on week 2, week 6 and week 8 of the *in vivo*, remaining below sham animals across the 4 timepoints. Regarding the αvβ3-modified GGp group, its average 50 % Threshold value was significantly lower than injured animals from the second timepoint of the test (week 4) and, with exception to this measurement, higher than both RGD groups. Finally, the implantation of GGp10αv encapsulating ASCs and HUVECs steadily promoted the regain of sensitivity to these rats, being their 50 % Threshold statistically lower than the one presented by transected animals on week 8 of the *in vivo*. Contrastingly to the other treated groups, these animals remain less reactive to Von Frey filaments than Sham animals. Finally, injured animals remain almost unresponsive to the filaments in a clear indication of permanent sensory loss following SCI.

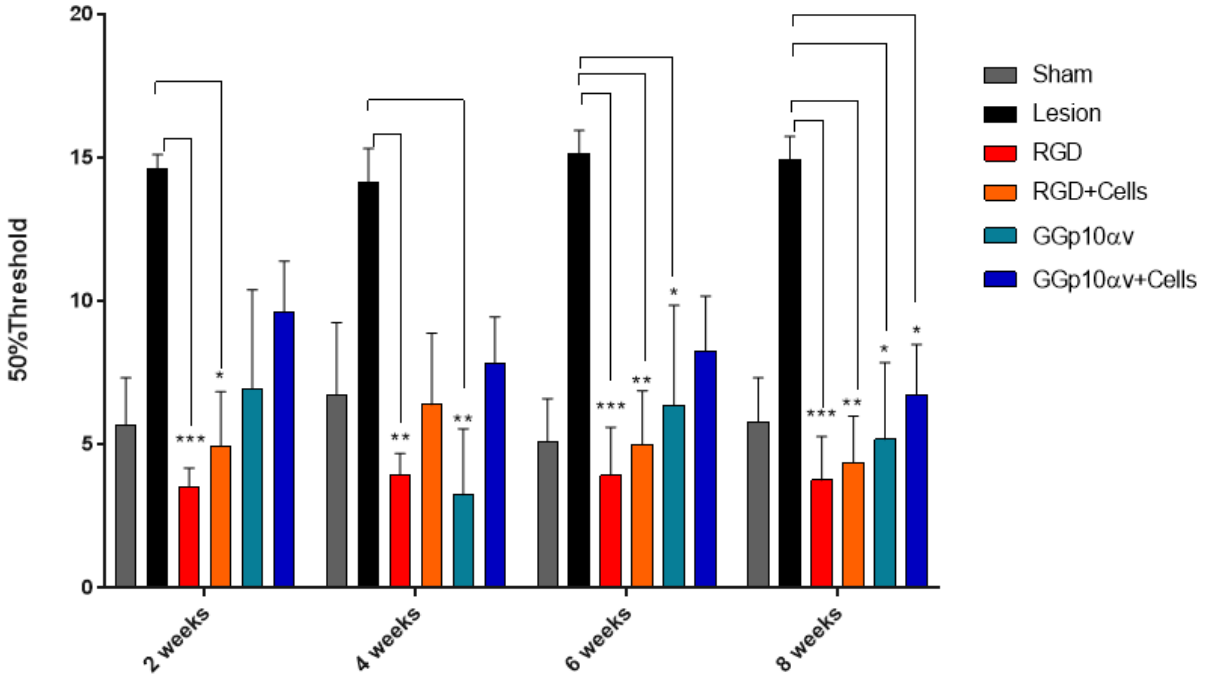

Figure 4.2 – Sensory evaluation of the studied animals using the Von Frey filament test. Animals on the treated groups increased sensory recovery when comparing to SCI animals. With exception to rats that received GGp10αv+cells, the other experimental groups showed signs of hypersensitivity as their 50 % threshold was consistently lower than the value obtained for the Sham animals. Data is presented as mean±SEM (n=4/10). *p<0.05; **p<0.01; p<0.001.

Modulation of systemic inflammation on different stages of SCI

The strong and uncontrolled systemic inflammatory response that follows SCI is one of the most fundamental features for the exacerbation and expansion of damage to the injured spinal cord. Therefore, successful therapies should positively impact this phenomenon and drive it towards a regenerative phenotype. Thus, we assessed a defined panel of cytokines (Rat Cytokine Array C2 from Raybiotech) on different stages of the condition (48 h, 3 and 8 weeks post-SCI) to understand whether our hydrogel-based response could modulate the systemic inflammation associated to SCI (Figure 4.3, 4.4 and 4.5). 48 h after SCI the GGp10αv+cells group showed a marked decrease on several inflammatory cytokines (IL-1 α, IL-1 β, TNF-α and MCP-1) in comparison to all the other groups and simultaneously demonstrating an increase in different anti-inflammatory cytokines (IL-4, IL-10 and IL-13) in comparison to injured animals. On the same timepoint, rats with GGp10αv+cells also had higher serum levels of IL-6. Regarding the modulation of pro-inflammatory cytokines by GG-GRGDS 48 h post-SCI, it was found an increased

expression of the aforementioned pro-inflammatory cytokines in comparison to injured animals. However, animals within this group present the highest serum quantities of IL-4, IL-13, and IL-10 (Fig 4.3 B).

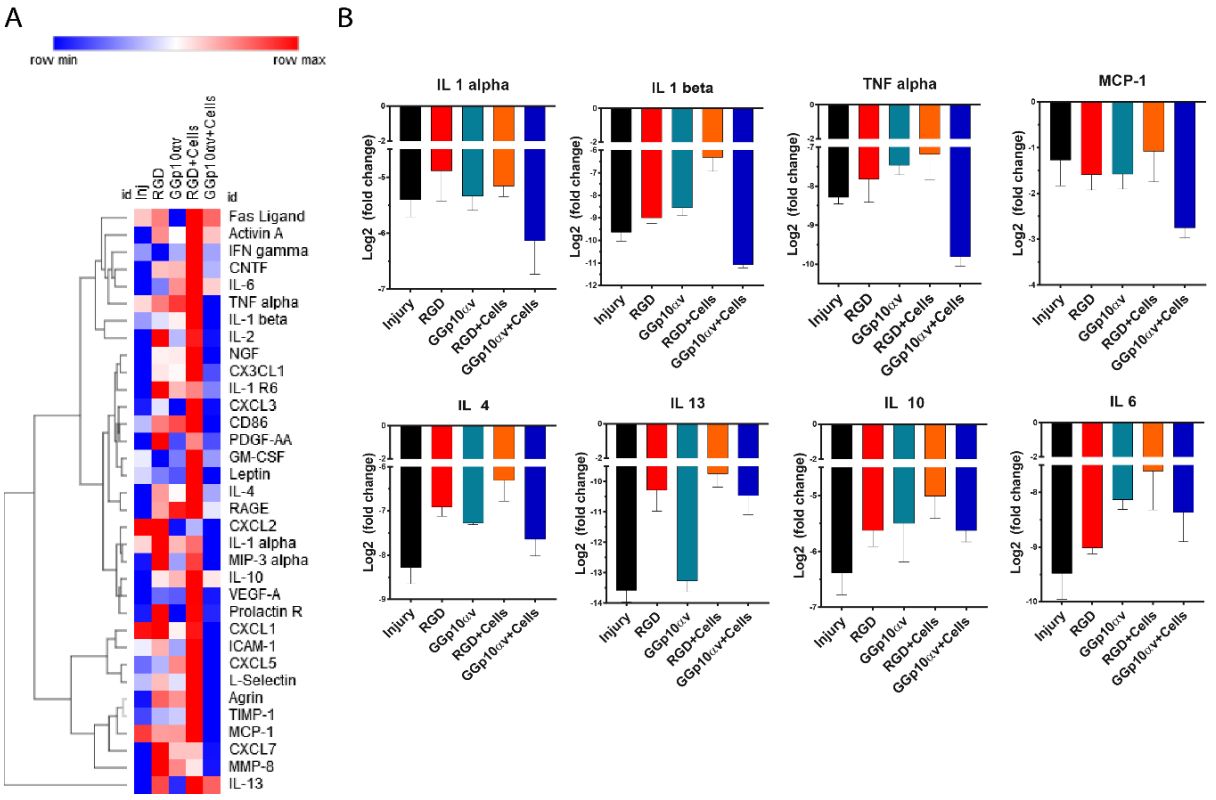

Figure 4.3 – Molecular analysis of the recollected sera 48 h following SCI using Rat Cytokine Array C2 from Raybiotech. **A,** Representative heat map of the panel for the different groups was generated using the BROAD Institute's R implementation of Morpheus with Euclidean distance hierarchical clustering. **B,** Relative expression of selected anti-inflammatory and pro-inflammatory cytokines with a known role on SCI. Data are shown as mean Log2 (fold change) relative to the normalization of each cytokine to the internal controls of each membrane.

After 3 weeks, the SCI animals on the GGp10αv+cells continued to have a lower expression of IL – 1 β and TNF-α than SCI animals, a similar expression of IL-1 α and a slight increase on MCP-1. The same tendency was observed on GG-GRGDS+cells animals. Interestingly, rats in the GGp10αv group presented the lowest amounts of IL-1 α, IL- β and TNF-α during this timepoint. At the same timepoint rats that received GGp10αv+cells had the highest serum amounts of both IL-4 and IL-10 and lower quantities of IL-13 than lesioned animals. Concerning GG-GRGDS+cells, these animals only had an upregulation on IL-4 in comparison to injured animals 3 weeks after SCI (Fig 4.4 B). It is also worth noting that during the

first two timepoints, the M1 macrophage marker CD86 was downregulated in GGp10αv+cells relative to injured animals.

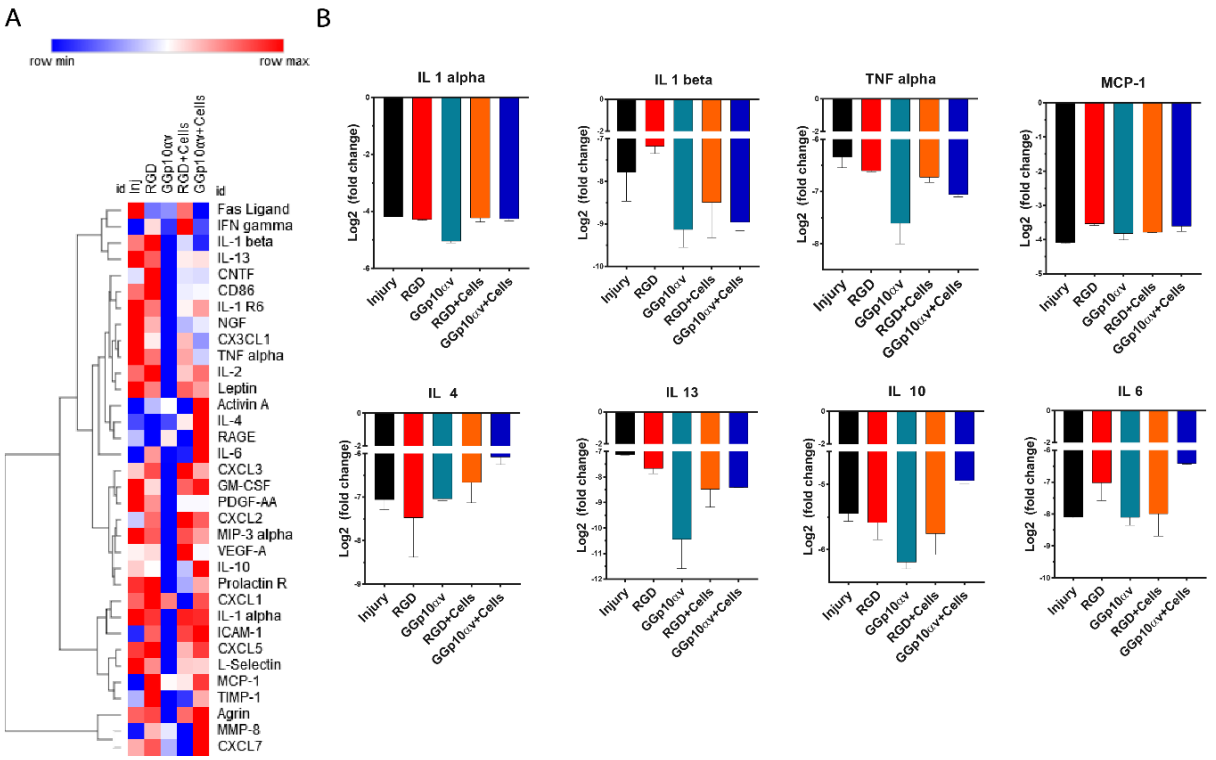

Figure 4.4 – Analysis of the recollected sera 3 weeks following SCI. **A,** Representative heat map of the panel for the different groups was generated using the BROAD Institute's R implementation of Morpheus with Euclidean distance hierarchical clustering. **B,** Relative expression of selected anti-inflammatory and pro-inflammatory cytokines with a known role on SCI. Data are shown as mean Log2 (fold change) relative to the normalization of each cytokine to the internal controls of each membrane.

The final timepoint analyzed (8 weeks post-SCI) continued to show a strong decrease on IL-1 β on GGp10αv+cells when comparing to the other groups, and a downregulation of TNF-α relative to injured animals. On the other hand, rats that received this treatment had a small downregulation on IL-1 α and MCP-1 in comparison to injured animals. The lowest amounts of TNF-α were seen on both GG-GRGDS groups, with rats transplanted with GG-GRGDS+cells also showing a downregulation on IL-1 β in comparison to injured animals. The levels of IL-10 remained the highest for GGp10αv+cells and these animals experienced a decrease on IL-4 from 3 to 8 weeks after SCI, having similar quantities to SCI rats.

The latter showed the highest amounts of both IL-13 and IL-6 and a comparable expression of IL-4 relative to GG-GRGDS (Fig 4.5 B).

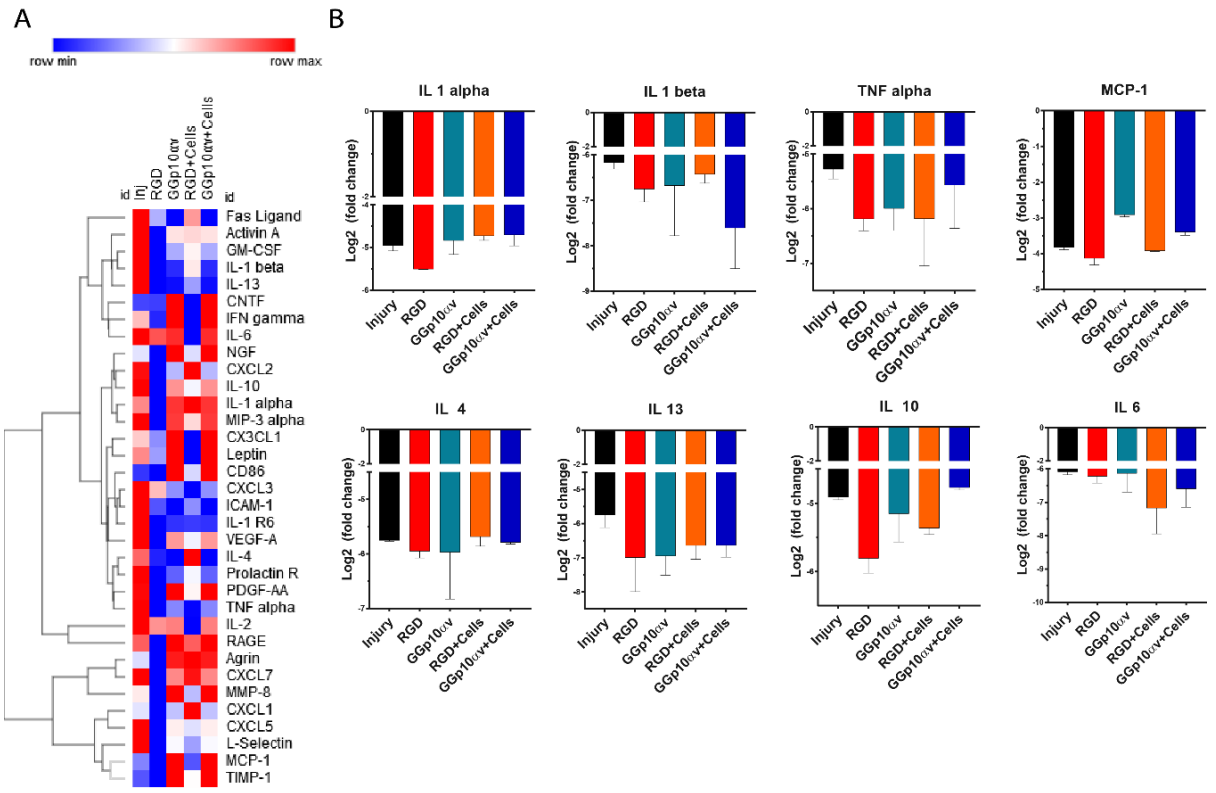

Figure 4.5 - Analysis of the recollected sera from the animals studied during the in vivo 8 weeks after SCI. The molecular analysis was performed using the Rat Cytokine Array C2 from Raybiotech. **A,** Representative heat map of the panel for the different groups was generated using the BROAD Institute's R implementation of Morpheus with Euclidean distance hierarchical clustering. **B,** Relative expression of selected anti-inflammatory and pro-inflammatory cytokines with a known role on SCI. Data are shown as mean Log2 (fold change) relative to the normalization of each cytokine to the internal controls of each membrane.

Discussion

The development of biomaterial-based strategies to enhance the motor, sensory and autonomic recovery after SCI has witnessed an increment during the last few years. This is mainly a reflex on the acknowledgment that these therapies are a privileged way of efficiently delivering cells to the injured spinal cord, protecting them from the nefarious local environment, and providing physical and chemical cues to instruct the behavior of the transplanted cells [47,48]. Moreover, these cues can be extended to include immunomodulatory or axonal growth molecules to ensure a more holistic approach to an extremely complex biological problem [49–51].

On this work we have utilized GG hydrogels encompassing distinct types of cell adhesive motives. One of such hydrogels was based on a previously developed GRGDS-modified GG that had already proved to be capable of enhance cell behavior in comparison to native GG, support neurite outgrowth and the vascular arrangement of HUVECs when co-cultured with ASCs [34,35]. Additionally, this GRGDS-based hydrogel had previously enhanced the locomotor behavior of rats in a severe SCI animal model [35]. The other approach consisted on the first application of an αvβ3 integrin-specific peptidomimetic modified GG hydrogel, that previously demonstrated to grant further biological properties to the polymer relative to linear RGD (when comparing 1:10 and 1:20 ligand:polymer modification ratios). Even though integrin αvβ3 is highly expressed during the angiogenic process in ECs, it was observed that HUVECs would only assemble into vascular-like structures in the presence of ASCs.

As the final aim of the work was to develop a hydrogel-based therapy to promote the revascularization of the SCI injury site, we utilized both modified hydrogels encapsulating the co-culture of ASCs and HUVECs. Despite transection injury models are not the most clinically relevant (the majority of lesions occurs by spinal cord contusion), it grants a reproducible model to study the regenerative and integration capacity of biomaterials (either encapsulating cells or not) by creating a gap that can be easily filled by the proposed therapy [52]. The motor recovery assessment using the BBB scale demonstrated that animals that received GGp10αv+cells presented the most robust recovery (despite the final BBB score of these and the GG-GRGDS+cells animals being similar), with statistical significance relative to injured animals from week 4 up until the end of the *in vivo*. Furthermore, GGp10αv+cells was the only group that promoted a significant overall improvement on the BBB score in comparison to injured animals.

Despite these motor improvements, there were no differences on the swimming velocity among groups, as excluding sham animals, no rats could produce movement using the hindlimbs (videos not shown). These differences could be explained by discrepancies regarding the sensory input that rats experience in water against what they experience in direct contact with the table used for the BBB test. It is fairly

understood that sensory input can be fundamental to engage the activation of propriospinal motor networks and central pattern generators (CPGs) following SCI [53,54]. Additionally, there are different reports in the literature where recovery following SCI was enhanced by sensory stimulation [55,56]. Indeed, all the therapeutic approaches provided the recovery of sensation along the *in vivo*, contrasting to SCI animals which remained mostly unresponsive to the Von Frey filaments. Therefore, a probable mechanism involved on the motor recovery observed on both GGp10αv+cells and GG-GRGDS+cells groups would involve the induction of plasticity and reorganization of propriospinal motor and sensory networks rather than the regeneration of supraspinal fibers. Moreover, we have previously identified on the secretome of ASCs a variety of molecules belonging to the Akt pathway, which represents an important signaling cascade to drive neuronal growth and plasticity [39,57–59]. Nevertheless, this plasticity hypothesis can be only validated after a thorough histological characterization of serotonergic and other excitatory fibers that engage the activation of CPGs caudally to the injury site.

A major feature of ASCs lies on their capacity to immunomodulate injured environments towards regenerative phenotypes [60]. The analysis of the sera of the animals revealed a strong shift towards a more anti-inflammatory profile in animals treated with GGp10αv+cells during the most critical stage of SCI (the acute phase, 48 h post-SCI). These animals had decreased levels of the pro-inflammatory mediators IL-1 α, IL-1 β, TNF-α and MCP-1. Regarding IL-1, Sato and coworkers [61] elegantly demonstrated that both isoforms contribute to exacerbate the inflammatory damage following SCI. The authors demonstrated that both isoforms act by activating macrophages and microglia, contributing to increased lesion area and poorer motor outcomes than IL-1 knockout mice. A different work has also showed that the sole deletion of IL-1 α protects oligodendrocytes for degeneration during the acute phase of SCI [62]. Numerous studies have pointed out to a deleterious effect of TNF-α on the pathophysiology of SCI, with cytokine contributing to initiate the Wallerian Degeneration process, to exacerbate the activity of IL-1 β, for the activation process of macrophages or neuronal apoptosis [63–65]. The expression of MCP-1 (CCL2) has been shown to be upregulated in the acute phase of SCI and has been additionally associated to the development of pain and also as a promoter of immune cell infiltration and microglia activation in different CNS and peripheral nervous system conditions [66–68].

The opposite pattern concerning anti-inflammatory molecules was observed on the 48 h post-SCI timepoint. Thus, it was found an increased expression of IL-4, IL-10 and IL-13 in animals treated with GGp10αv+cells. Recently, it has been demonstrated that the systemic administration of IL-4 decreases the expression of myeloid markers and iNOS, whilst driving microglia and macrophages towards a more regenerative phenotype, thus acting as a neuroprotective therapy [69,70]. IL-10 possesses a similar effect on

inflammation, and its administration promoted a reduction on TNF- α, leading to axonal preservation and neuronal survival following SCI, and enhancing motor recovery [71–73]. The anti-inflammatory cytokine IL-13 has been demonstrated to possess a role in directing microglia and macrophages into phenotypes more prone to regeneration in traumatic brain injury and multiple sclerosis animal models [74,75]. The delivery of IL-13 expressing MSCs into an animal model of SCI lead to a decrease in lesion size, less axonal demyelination, while modulating the inflammatory environment and contributing to better motor outcomes [76].

The expression of these anti-inflammatory cytokines was further enhanced on GG-GRGDS treated animals 48 h after SCI, which may have acted to counteract the increased expression of the highlighted pro-inflammatory cytokines. Nevertheless, GGp10αv+cells seemed to have a stronger effect on the immunomodulation of the systemic inflammation during this period. Interestingly, the 48 h post-SCI was the timepoint where this shift was more evident, suggesting that our therapeutic approach acts preferably during the acute phase concerning systemic immunomodulation. Nevertheless, the inflammatory response *in situ* should be characterized to understand whether this systemic shift traduced into a more anti-inflammatory profile on the lesioned spinal cord.

The expression of IL-6 was also elevated in both conditions where the combination of hydrogel and cells was applied. Although the role of this particular cytokine remains to be fully elucidated with some studies pointing out to a deleterious effect on the pathophysiology of SCI [77,78], it was recently found that IL-6 can also have a beneficial role on CNS trauma through neuroprotection [79].

Another mechanism of action that could also explain the motor and sensory behavioral outcomes could be related with a decrease on the inflammatory cell infiltration on SCI lesion site. This could be due to the formation and integration into the host vasculature of HUVEC-derived vascular assemblies and to the action of MSCs on vascular permeability following SCI. Accordingly, several studies have shown that the modulation of SCI vascularization, namely the reduction of vascular permeability, decreases the infiltration of inflammatory cells [80]. On this regard, the Fehlings Lab has published a series of works where it shows that the infusion of different types of MSCs decreased vascular permeability after SCI and contributed to less prominent intraparenchymal hemorrhage [13,16]. Moreover, we have also demonstrated that the administration of GG-GRGDS together with ASCs and OECs decreased inflammatory cell infiltration after SCI [35]. Despite these indications provided by the literature and former studies, the histological characterization is needed to validate this hypothesis and to assess whether transplanted HUVECs anastomosed into the host vasculature.

Conclusions

Integrin-specific peptidomimetics might represent the next iteration concerning the biofunctionalization of hydrogels for CNS applications, as these are more stable (both in conformation and bioavailability) and enable to specifically engage integrins of interest to guide intended biological phenomena. In this work we compared the potential of two GG-based hydrogels (one functionalized with a αvβ3 mimetic and another coupled with linear GRGDS) encapsulating ASCs and HUVECs in promoting the recovery in a transection model of SCI. Although leading to the same motor final BBB score, the peptidomimetic modified GG has led to a more robust BBB profile. On the other hand, both approaches could promote the sensory recovery on SCI animals. Serum analysis has also demonstrated that GGp10αv induced a stronger shift towards a systemic anti-inflammatory profile during the acute phase of SCI. Despite these indications, future work should elucidate the main mechanisms of action that mediated these effects, including the impact of this therapeutic on the vascular response following SCI.

Acknowledgements

The authors acknowledge Professor Jeffrey Gimble at the Tulane University Center for Stem Cell Research and Regenerative Medicine and LaCell LLC (New Orleans, Louisiana, USA) for kindly providing the ASCs used in this study. The authors want to additionally acknowledge the financial support from Prémios Santa Casa Neurociências - Prize Melo e Castro for Spinal Cord Injury Research (MC-04/17); from Portuguese Foundation for Science and Technology [Doctoral fellowship (PD/BDE/127835/2016) to L. A. Rocha, R.A. Lima (PD/BDE/127836/2016) and D. Silva (PD/BDE/127835), E.D. Gomes (SFH/BD/103075/2014) Scientific Employment Stimulus to N. A. Silva (CEECIND/04794/2017)]. This work was funded by FEDER, through the Competitiveness Internationalization Operational Program (POCI), and by National funds, through the Foundation for Science and Technology (FCT), under the scope of the projects POCI-01-0145-FEDER-007038; TUBITAK/0007/2014; PTDC/DTP-FTO/5109/2014; POCI-01-0145-FEDER-029206; POCI-01-0145-FEDER-031392; PTDC/MED-NEU/31417/2017 and NORTE-01-0145-FEDER-029968. This work has also been developed under the scope of the project NORTE-01-0145-FEDER-000013, supported by the Northern Portugal Regional Operational Programme (NORTE 2020), under the Portugal 2020 Partnership Agreement, through the European Regional Development Fund (FEDER).

References

1. James, S. L. *et al.* Global, regional, and national burden of traumatic brain injury and spinal cord injury, 1990–2016: a systematic analysis for the Global Burden of Disease Study 2016. *Lancet Neurol.* **18**, 56–87 (2019).
2. Ahuja, C. S. *et al.* Traumatic spinal cord injury. *Nat. Rev. Dis. Prim.* **3**, 17018 (2017).
3. Tran, A. P., Warren, P. M. & Silver, J. The biology of regeneration failure and success after spinal cord injury. *Physiol. Rev.* **98**, 881–917 (2018).
4. Silva, N. A., Sousa, N., Reis, R. L. & Salgado, A. J. From basics to clinical: A comprehensive review on spinal cord injury. *Prog. Neurobiol.* **114**, 25–57 (2014).
5. Sinescu, C. *et al.* Molecular basis of vascular events following spinal cord injury. *J. Med. Life* **3**, 254–261 (2010).
6. Li, Y. *et al.* Pericytes impair capillary blood flow and motor function after chronic spinal cord injury. *Nat. Med.* **23**, 733–741 (2017).
7. Ng, M. T. L., Stammers, A. T. & Kwon, B. K. Vascular Disruption and the Role of Angiogenic Proteins After Spinal Cord Injury. *Transl. Stroke Res.* **2**, 474–491 (2011).
8. Casella, G. T. B., Marcillo, A., Bunge, M. B. & Wood, P. M. New vascular tissue rapidly replaces neural parenchyma and vessels destroyed by a contusion injury to the rat spinal cord. *Exp. Neurol.* **173**, 63–76 (2002).
9. Dray, C., Rougon, G. & Debarbieux, F. Quantitative analysis by in vivo imaging of the dynamics of vascular and axonal networks in injured mouse spinal cord. *Proc. Natl. Acad. Sci. U. S. A.* **106**, 9459–64 (2009).
10. Han, S. *et al.* Rescuing vasculature with intravenous angiopoietin-1 and αvβ3 integrin peptide is protective after spinal cord injury. *Brain* **133**, 1026–1042 (2010).
11. Ni, S. *et al.* UTX/KDM6A Deletion Promotes Recovery of Spinal Cord Injury by Epigenetically Regulating Vascular Regeneration. *Mol. Ther.* **27**, 2134–2146 (2019).
12. Chio, J. C. T. *et al.* The effects of human immunoglobulin G on enhancing tissue protection and neurobehavioral recovery after traumatic cervical spinal cord injury are mediated through the neurovascular unit. *J. Neuroinflammation* **16**, 1–18 (2019).
13. Badner, A. *et al.* Early Intravenous Delivery of Human Brain Stromal Cells Modulates Systemic Inflammation and Leads to Vasoprotection in Traumatic Spinal Cord Injury. *Stem Cells Transl. Med.* **5**, 991–1003 (2016).

14. Tran, K. A. *et al.* Vascularization of self-assembled peptide scaffolds for spinal cord injury repair. *Acta Biomater.* **104**, 76–84 (2020).
15. Kamei, N. *et al.* Contribution of bone marrow-derived endothelial progenitor cells to neovascularization and astrogliosis following spinal cord injury. *J. Neurosci. Res.* **90**, 2281–2292 (2012).
16. Vawda, R. *et al.* Early Intravenous Infusion of Mesenchymal Stromal Cells Exerts a Tissue Source Age-Dependent Beneficial Effect on Neurovascular Integrity and Neurobehavioral Recovery After Traumatic Cervical Spinal Cord Injury. *Stem Cells Transl. Med.* **8**, 639–649 (2019).
17. Rauch, M. F. *et al.* Engineering angiogenesis following spinal cord injury: a coculture of neural progenitor and endothelial cells in a degradable polymer implant leads to an increase in vessel density and formation of the blood-spinal cord barrier. *Eur. J. Neurosci.* **29**, 132–45 (2009).
18. Bronckaers, A. *et al.* Mesenchymal stem/stromal cells as a pharmacological and therapeutic approach to accelerate angiogenesis. *Pharmacol. Ther.* **143**, 181–196 (2014).
19. Friedenstein, A. J., Piatetzky-Shapiro, I. & Petrakova, & K. V. *Osteogenesis in transplants of bone marrow cells*. *Embryol. exp. Morph* vol. 16 (1966).
20. Han, Y. *et al.* Mesenchymal Stem Cells for Regenerative Medicine. *Cells* **8**, (2019).
21. Uccelli, A., Moretta, L. & Pistoia, V. Mesenchymal stem cells in health and disease. *Nature Reviews Immunology* vol. 8 726–736 (2008).
22. Andrzejewska, A., Lukomska, B. & Janowski, M. Concise Review: Mesenchymal Stem Cells: From Roots to Boost. *Stem Cells* **37**, 855–864 (2019).
23. Eleuteri, S. & Fierabracci, A. Insights into the secretome of mesenchymal stem cells and its potential applications. *International Journal of Molecular Sciences* vol. 20 (2019).
24. Pires, A. O. *et al.* Unveiling the Differences of Secretome of Human Bone Marrow Mesenchymal Stem Cells, Adipose Tissue-Derived Stem Cells, and Human Umbilical Cord Perivascular Cells: A Proteomic Analysis. *Stem Cells Dev.* **25**, 1073–1083 (2016).
25. Kolar, M. K., Kingham, P. J., Novikova, L. N., Wiberg, M. & Novikov, L. N. The Therapeutic Effects of Human Adipose-Derived Stem Cells in a Rat Cervical Spinal Cord Injury Model. *Stem Cells Dev.* **23**, 1659–1674 (2014).
26. Menezes, K. *et al.* Human mesenchymal cells from adipose tissue deposit laminin and promote regeneration of injured spinal cord in rats. *PLoS One* **9**, (2014).
27. Hur, J. W. *et al.* Intrathecal transplantation of autologous adipose-derived mesenchymal stem cells for treating spinal cord injury: A human trial. *J. Spinal Cord Med.* (2016)

doi:10.1179/2045772315Y.0000000048.

28. Bydon, M. *et al.* CELLTOP Clinical Trial: First Report From a Phase 1 Trial of Autologous Adipose Tissue-Derived Mesenchymal Stem Cells in the Treatment of Paralysis Due to Traumatic Spinal Cord Injury. *Mayo Clin. Proc.* **95**, 406–414 (2020).
29. Anderson, A. J. *et al.* Achieving stable human stem cell engraftment and survival in the CNS: is the future of regenerative medicine immunodeficient? *Regen. Med.* **6**, 367–406 (2011).
30. Führmann, T., Anandakumaran, P. N. & Shoichet, M. S. Combinatorial Therapies After Spinal Cord Injury: How Can Biomaterials Help? *Adv. Healthc. Mater.* **6**, 1–21 (2017).
31. Marcus, M. *et al.* Interactions of Neurons with Physical Environments. *Adv. Healthc. Mater.* **6**, (2017).
32. Holzapfel, B. M. *et al.* How smart do biomaterials need to be? A translational science and clinical point of view. *Adv. Drug Deliv. Rev.* **65**, 581–603 (2013).
33. Assunção-Silva, R. C. *et al.* Induction of neurite outgrowth in 3D hydrogel-based environments. *Biomed. Mater.* **10**, 051001 (2015).
34. Silva, N. A. *et al.* The effects of peptide modified gellan gum and olfactory ensheathing glia cells on neural stem/progenitor cell fate. *Biomaterials* **33**, 6345–6354 (2012).
35. Gomes, E. D. *et al.* Combination of a peptide-modified gellan gum hydrogel with cell therapy in a lumbar spinal cord injury animal model. *Biomaterials* **105**, 38–51 (2016).
36. Mas-Moruno, C. *et al.* αvβ3- or α5β1-Integrin-Selective Peptidomimetics for Surface Coating. *Angew. Chemie - Int. Ed.* **55**, 7048–7067 (2016).
37. Kapp, T. G. *et al.* A Comprehensive Evaluation of the Activity and Selectivity Profile of Ligands for RGD-binding Integrins. *Sci. Rep.* **7**, 39805 (2017).
38. Dubois, S. G. *et al.* Isolation of human adipose-derived stem cells from biopsies and liposuction specimens. in *Methods in molecular biology (Clifton, N.J.)* vol. 449 69–79 (2008).
39. Rocha, L. A. *et al.* In vitro Evaluation of ASCs and HUVECs Co-cultures in 3D Biodegradable Hydrogels on Neurite Outgrowth and Vascular Organization. *Front. Cell Dev. Biol.* **8**, (2020).
40. Kirchmajer, D. M., Steinhoff, B., Warren, H., Clark, R. & In Het Panhuis, M. Enhanced gelation properties of purified gellan gum. *Carbohydr. Res.* **388**, 125–129 (2014).
41. Doner, L. W. Rapid purification of commercial gellan gum to highly soluble and gellable monovalent cation salts. *Carbohydr. Polym.* **32**, 245–247 (1997).
42. Zutphen, L. F. van, Baumans, V. & Beynen, A. C. *Principles of Laboratory Animal Science*. *Laboratory Animals* (2001).

43. Bass, D. M., Beattie, M. S. & Bresnahan, J. C. A Sensitive and Reliable Locomotor Rating Scale for Open Field Testing in Rats. *J. Neurotrauma* **12**, 1–21 (1995).

44. Guimarães, M. R. *et al.* Evidence for lack of direct causality between pain and affective disturbances in a rat peripheral neuropathy model. *Genes. Brain. Behav.* **18**, e12542 (2019).

45. Gomes, E. D. *et al.* Combination of a Gellan Gum-Based Hydrogel With Cell Therapy for the Treatment of Cervical Spinal Cord Injury. *Front. Bioeng. Biotechnol.* (2020) doi:10.3389/fbioe.2020.00984.

46. Chaplan, S. R., Bach, F. W., Pogrel, J. W., Chung, J. M. & Yaksh, T. L. Quantitative assessment of tactile allodynia in the rat paw. *J. Neurosci. Methods* (1994) doi:10.1016/0165-0270(94)90144-9.

47. Khaing, Z. Z., Thomas, R. C., Geissler, S. A. & Schmidt, C. E. Advanced biomaterials for repairing the nervous system: what can hydrogels do for the brain? *Mater. Today* **17**, 332–340 (2014).

48. Maclean, F. L., Rodriguez, A. L., Parish, C. L., Williams, R. J. & Nisbet, D. R. Integrating Biomaterials and Stem Cells for Neural Regeneration. *Stem Cells Dev.* **25**, 214–226 (2016).

49. Papa, S. *et al.* Mesenchymal stem cells encapsulated into biomimetic hydrogel scaffold gradually release CCL2 chemokine in situ preserving cytoarchitecture and promoting functional recovery in spinal cord injury. *J. Control. Release* (2018) doi:10.1016/j.jconrel.2018.03.034.

50. Liu, S. *et al.* Regulated viral BDNF delivery in combination with Schwann cells promotes axonal regeneration through capillary alginate hydrogels after spinal cord injury. *Acta Biomater.* **60**, 167–180 (2017).

51. Nguyen, L. H. *et al.* Three-dimensional aligned nanofibers-hydrogel scaffold for controlled non-viral drug/gene delivery to direct axon regeneration in spinal cord injury treatment. *Sci. Rep.* (2017) doi:10.1038/srep42212.

52. Lukovic, D. *et al.* Complete rat spinal cord transection as a faithful model of spinal cord injury for translational cell transplantation. *Sci. Rep.* **5**, 9640 (2015).

53. Rossignol, S., Dubuc, R. & Gossard, J. P. Dynamic sensorimotor interactions in locomotion. *Physiological Reviews* (2006) doi:10.1152/physrev.00028.2005.

54. Rossignol, S. & Frigon, A. Recovery of locomotion after spinal cord injury: Some facts and mechanisms. *Annu. Rev. Neurosci.* (2011) doi:10.1146/annurev-neuro-061010-113746.

55. Gad, P. *et al.* Neuromodulation of motor-evoked potentials during stepping in spinal rats. *J. Neurophysiol.* (2013) doi:10.1152/jn.00169.2013.

56. Shah, P. K. *et al.* Variability in step training enhances locomotor recovery after a spinal cord injury.

Eur. J. Neurosci. (2012) doi:10.1111/j.1460-9568.2012.08106.x.

57. Gomes, E. D. *et al.* Co-Transplantation of Adipose Tissue-Derived Stromal Cells and Olfactory Ensheathing Cells for Spinal Cord Injury Repair. *Stem Cells* **36**, 696–708 (2018).
58. Liu, K. *et al.* PTEN deletion enhances the regenerative ability of adult corticospinal neurons. *Nat. Neurosci.* **13**, 1075–81 (2010).
59. Sánchez-Alegría, K., Flores-León, M., Avila-Muñoz, E., Rodríguez-Corona, N. & Arias, C. PI3K signaling in neurons: A central node for the control of multiple functions. *International Journal of Molecular Sciences* (2018) doi:10.3390/ijms19123725.
60. Kokai, L. E., Marra, K. & Rubin, J. P. Adipose stem cells: biology and clinical applications for tissue repair and regeneration. *Transl. Res.* **163**, 399–408 (2014).
61. Sato, A. *et al.* Interleukin-1 participates in the classical and alternative activation of microglia/macrophages after spinal cord injury. *J. Neuroinflammation* (2012) doi:10.1186/1742-2094-9-65.
62. Bastien, D. *et al.* IL-1α gene deletion protects oligodendrocytes after spinal cord injury through upregulation of the survival factor Tox3. *J. Neurosci.* (2015) doi:10.1523/JNEUROSCI.0498-15.2015.
63. Guido, S., Sebastian, J. & Schroeter, M. Detrimental and Beneficial Effects of Injury-Induced Inflammation and Cytokine Expression in the Nervous System. in *Advances in experimental medicine and biology* vol. 513 87–113 (2003).
64. Fong, Y. *et al.* Cachectin/TNF or IL-1α induced cachexia with redistribution of body proteins. *Am. J. Physiol. - Regul. Integr. Comp. Physiol.* (1989) doi:10.1152/ajpregu.1989.256.3.r659.
65. Yune, T. Y. *et al.* Increased production of tumor necrosis factor-α induces apoptosis after traumatic spinal cord injury in rats. *J. Neurotrauma* (2003) doi:10.1089/08977150360547116.
66. Van Steenwinckel, J. *et al.* CCL2 Released from Neuronal Synaptic Vesicles in the Spinal Cord Is a Major Mediator of Local Inflammation and Pain after Peripheral Nerve Injury. *J. Neurosci.* **31**, 5865–5875 (2011).
67. Kim, R. Y. *et al.* Astrocyte CCL2 sustains immune cell infiltration in chronic experimental autoimmune encephalomyelitis. *J. Neuroimmunol.* (2014) doi:10.1016/j.jneuroim.2014.06.009.
68. Kwon, B. K. *et al.* Cerebrospinal fluid inflammatory cytokines and biomarkers of injury severity in acute human spinal cord injury. *J. Neurotrauma* (2010) doi:10.1089/neu.2009.1080.
69. Francos-Quijorna, I., Amo-Aparicio, J., Martinez-Muriana, A. & López-Vales, R. IL-4 drives microglia and macrophages toward a phenotype conducive for tissue repair and functional recovery after

spinal cord injury. *Glia* **64**, 2079–2092 (2016).

70. Lima, R. *et al.* Systemic interleukin-4 administration after spinal cord injury modulates inflammation and promotes neuroprotection. *Pharmaceuticals* (2017) doi:10.3390/ph10040083.
71. Bethea, J. R. *et al.* Systemically administered interleukin-10 reduces tumor necrosis factor- alpha production and significantly improves functional recovery following traumatic spinal cord injury in rats. *J. Neurotrauma* (1999) doi:10.1089/neu.1999.16.851.
72. Zhou, Z., Peng, X., Insolera, R., Fink, D. J. & Mata, M. IL-10 promotes neuronal survival following spinal cord injury. *Exp. Neurol.* (2009) doi:10.1016/j.expneurol.2009.08.018.
73. Hellenbrand, D. J. *et al.* Sustained interleukin-10 delivery reduces inflammation and improves motor function after spinal cord injury. *J. Neuroinflammation* **16**, 93 (2019).
74. Guglielmetti, C. *et al.* Interleukin-13 immune gene therapy prevents CNS inflammation and demyelination via alternative activation of microglia and macrophages. *Glia* **64**, 2181–2200 (2016).
75. Miao, W. *et al.* IL-13 Ameliorates Neuroinflammation and Promotes Functional Recovery after Traumatic Brain Injury. *J. Immunol.* **204**, 1486–1498 (2020).
76. Dooley, D. *et al.* Cell-Based Delivery of Interleukin-13 Directs Alternative Activation of Macrophages Resulting in Improved Functional Outcome after Spinal Cord Injury. *Stem Cell Reports* (2016) doi:10.1016/j.stemcr.2016.11.005.
77. Okada, S. *et al.* Blockade of interleukin-6 receptor suppresses reactive astrogliosis and ameliorates functional recovery in experimental spinal cord injury. *J. Neurosci. Res.* **76**, 265–76 (2004).
78. Guerrero, A. R. *et al.* Blockade of interleukin-6 signaling inhibits the classic pathway and promotes an alternative pathway of macrophage activation after spinal cord injury in mice. *J. Neuroinflammation* (2012) doi:10.1186/1742-2094-9-40.
79. Willis, E. F. *et al.* Repopulating Microglia Promote Brain Repair in an IL-6-Dependent Manner. *Cell* **180**, 833-846.e16 (2020).
80. Rocha, L. A., Sousa, R. A., Learmonth, D. A. & Salgado, A. J. The role of biomaterials as angiogenic modulators of spinal cord injury: Mimetics of the spinal cord, cell and angiogenic factor delivery agents. *Front. Pharmacol.* **9**, (2018).

CHAPTER 5

General discussion and future perspectives

Discussion

SCI remains as one the most fascinating biological problems that remain to be solved. The extremely complex interplays between neuronal and non-neuronal cells, the sequence of secondary events acting in a positive feedback mechanism that exponentiate damage and the lack of epigenetic predisposition of adult CNS to regenerate, make the development of an effective SCI treatment extremely difficult [1,2]. Simultaneously to the spinal cord insult, the BSCB is disrupted and this phenomena is responsible for the initiation of a myriad of secondary events, including: (I) intraparenchymal hemorrhage; (II) uncontrolled infiltration of systemic inflammatory cells and neurotoxic molecules; (III) tissue hypoxia; (IV) deficiencies on nutrient and waste product exchanges; (V) mitochondrial dysfunctions; (VI) cell apoptosis [3,4].

This vascular damage is irreversible, leaving the spinal cord (especially the injury site and caudal areas) in a chronic state of hypoxia that contribute for cellular imbalances and a deleterious local environment [5,6]. Therefore, we envisioned the development of a biomaterial-based therapy to promote the revascularization following SCI, and eventually functional recovery. Given the fact that the angiogenic response after SCI fails to provide efficient vascular perfusion, we chose to guide our approach towards EC transplantation. This was coupled with the presence of ASCs, a type of MSC that has been shown to enhance the vascular organization of ECs [7,8]. Furthermore, these cells have an extremely enriched secretome on angiotrophic, neurotrophic and immunomodulatory factors, present low immunogenicity and are easily isolated from hospital waste products, being an ideal candidate for SCI cell therapies [9].

The final element of our therapeutic proposition included a biofunctionalized GG-based hydrogel that was intended to provide the appropriate cues for cells to grow and proliferate, whilst protecting them from the harsh conditions of the SCI lesion site. We started by using a previously developed GG hydrogel modified with the linear adhesive motif GRGDS and finally optimized the ideal grafting conditions of two integrin-specific ($\alpha v\beta 3$ and $\alpha 5\beta 1$) peptidomimetics to GGp. These ligands were chosen as both integrins are highly expressed on ECs during the angiogenic process and are also present on ASCs [10]. The chemical modifications intended to engage specific integrin activity, something that the GRGDS sequence does not address, and with it provide enhanced biological activity to GGp formulations.

The initial axonal growth experiments using GG-GRGDS and the DRG model demonstrated that the co-culture of ASCs and HUVECs had a comparable neurite elongation as ASCs alone with statistical significance relative to the hydrogel alone (Chapter 2). These results were connected to an induction on the overexpression of the axonal growth protein GAP-43 during early timepoints, and simultaneously to the decreased expression of Tubb3 allowing probably to induce plasticity by cytoskeleton disassembly.

This might be partially explained by the enhanced presence of several neurotrophic factors on the secretome of the co-culture, in which BDNF (a key upregulator of GAP-43) is included [11,12]. A very important result that highlighted the importance of ASCs on our therapeutic paradigm was the observation that within GG-GRGDS, HUVECs were only capable to form long lasting, stable, vascular-like structures when ASCs were present. This happened despite the co-culture conditions encompassing half the amount of HUVECs to when these ECs were cultured alone (15000 vs 30000, respectively) and the competition of both ASCs and HUVECs for GRGDS binding sites. Whether when cultured alone the ECs transiently organized in vascular-like structures and the lack of ASCs to stabilize these networks led to their disassembly remains to be shown and would be an interesting experiment to do. This would allow to understand whether GG-GRGDS by itself has the appropriate cues to promote the initial vascular organization regardless the vascular stabilizing properties conferred by ASCs, or not. The capacity of ASCs in reshaping the vascular milieu was additionally proved by the CAM assay, a technique that is usually utilized to test vascular therapies. Thus, we demonstrated that ASCs could significantly chemoattract blood vessels towards GG-GRGDS, demonstrating the importance of the angiotrophic portion of their secretome. Nevertheless, the histological analysis of the membranes was not executed, and this would be something useful to complement our analysis, allowing to assess the permeation of GG-GRGDS to invading vasculature. Other techniques such as the plug assay could also be considered to evaluate this parameter [13].

The following research questions involved comprehending whether the biofunctionalization of GGp with two integrin-specific mimetics (against $\alpha5\beta1$ and $\alpha v\beta3$ integrins) would enhance the biological properties of the polymer in comparison to linear RGD analogues using the same reaction stoichiometries (1:10 and 1:20 ligand:polymer ratio) (Chapter 3). Following the necessary chemical characterization, which proved that the all the ligands were successfully engrafted into the backbone of GGp, the cell adhesion studies revealed that the hydrogels that were modified with the $\alpha v\beta3$ mimetic showed enhanced biological activity in comparison to both the $\alpha5\beta1$ and RGD modified GGp. This was more evident for GGp10αv, being this the condition the one that presented the best outcomes for this parameter. Subsequently, DRG experiments demonstrated that the conditions where ASCs were cultured alone on GGp10αv promoted enhanced neurite outgrowth in comparison to the hydrogel and HUVECs alone, as well as the co-culture of both cell types. This result does not corroborate the DRG experiments of Chapter 2, where the co-culture lead to similar neurite outgrowth as ASCs alone. Hypothesis that can be raised to explain this include the modulation of the secretome produced by the co-culture towards a less neurotrophic phenotype or to a decrease on the bioactivity of both ASCs and HUVECs within GGp10αv. The latter was

not observed since ASCs had their normal, fibroblast-like morphology, when co-cultured with HUVECs, and the ECs clearly assembled into vascular-like structures in the presence of MSCs. However, the characterization of the secretome of the co-culture in αvβ3 mimetic modified GGp was not performed and remains to be addressed. Only after this thorough analysis one could confirm, or not, the aforementioned hypothesis. Even though presented with an integrin-specific ligand that is highly involved in angiogenesis, HUVECs could not assemble into stable vascular-like networks. This confirms the complexity of the vascularization process and demonstrates that integrin specific signalling by itself may not be enough to promote the process. Angiogenesis results from the coordinated expression of different growth factors, in specific gradients, and from the interaction between ECs, smooth muscle cells, pericytes, among other types of cells where MSCs are included. Despite this, it was once again demonstrated that the presence of ASCs provides the adequate guidance to drive ECs towards a vascular arrangement, being fundamental to include on the proposed therapy.

Contrasting with the potential demonstrated by GGpαv, there was no noticeable biological activity on GGpα5 formulations, either on cell adhesion and DRG assays, despite the presence of α5β1 integrin being documented both on ASCs and DRG. The characterization techniques applied to assess the success of the chemical coupling to GGp showed no difference regarding GGpαv and GGpRGD and so one can assume that the ligand was coupled into the backbone of GGp with success. Additional reasons for this could lie on the loss of conformation of the ligand following its engraftment or its entanglement following the crosslinking of the polymeric chains of GGp. These hypotheses could be addressed, at least partially, by performing simple cell adhesion assays with a specific line of highly expressing α5β1 fibroblasts, that were previously utilized to validate the selectivity of this ligand to the integrin [14].

The last part of the work (Chapter 4) consisted in evaluating both GG-GRGDS and GGp10αv encapsulating ASCs and HUVECs on the motor and sensory recovery of a T8 transection rat model. Given the immunomodulatory capacity of ASCs the systemic characterization of a panel of cytokines was also performed during three distinct phases of the condition (acute, intermediate, and chronic). The transection model is not the most clinically relevant as most injuries occur by spinal cord contusion but nevertheless recapitulates all the hallmarks of SCI and represents a reliable way of evaluating biomaterial implantation by providing a gap that can be filled by the therapy [15]. The motor recovery results demonstrated that although the final BBB scores of both GG-GRGDS+cells and GGp10αv+cells groups were similar the mimetic modified GGp lead to a more robust recovery, traducing on an overall statistically significant increase in comparison to non-treated SCI animals. The sensory gains were also evident for both biomaterial-based therapies, possibly indicating that these were able to promote local excitatory fiber

plasticity, enhancing recovery. In fact, the motor gains cannot be dissociated from the sensory improvements as the activation of CPGs to generate propriospinal-dependent movement has been shown to be modulated by sensory enhancements [16,17]. Indeed, this is the most probable cellular mechanism that led to the observed recovery since hindlimb motor function is highly dependent on these circuitries [18,19]. Nevertheless, the elucidation of this question will only be answered after the histological analysis of these spinal cords to serotonergic and other excitatory fibers caudally to the lesion site on the CPG area. The recollected sera of these animals has demonstrated that GGp10αv+cells strongly reduced the expression of pro-inflammatory cytokines like IL-1 α and β or TNF-α, upregulating anti-inflammatory molecules such as IL-4, IL-10 and IL-13 in comparison to SCI animals during the acute phase of SCI (48 h post-SCI). This phenotype was not as strong on the other analyzed timepoints suggesting a crucial impact of the therapy on inflammation during the first stages of SCI. Although GG-GRGDS+cells was not capable to produce the same pro-inflammatory cytokine depression, the therapeutic paradigm showed the highest values for the referred anti-inflammatory cytokines 48 h after SCI, confirming the immunomodulatory nature of ASC-based therapies. It is extremely interesting that even though the treatment was applied locally it still had the capacity to modulate the systemic inflammatory response, as some studies indicate that this characteristic of MSCs is achieved if delivered via intravenous infusion [20–24]. Additionally, the local action of HUVECs cannot be also excluded as their successful integration into the host vasculature would lead to a decrease of vascular permeability and possibly act to contain the inflammatory cells and mediators from freely infiltrating the lesioned spinal cord. However, this can only be validated after assessing the dissected spinal cords and search for EC, BSCB and human cell markers. The same is valid for local inflammatory cell modulation, something observed in previous studies from our lab. Furthermore, the exact molecular mechanisms where MSCs exert their effects are still poorly understood. To elucidate it a subset of spinal cords were sent for proteomic analysis and will shed light on the local modulation of these therapies.

Future perspectives

Independently of the interesting results obtained during this thesis, some important parameters were not addressed and should be considered to further improve our hydrogel-based vascular cell therapy. First, it is widely understood that the physical properties of biomaterials are capable *per se* to induce specific cell behavior, influencing stem cell differentiation, integrin-mediated mechanotransduction or even neuronal migration [25–27]. The proposed hydrogels were not optimized to match the mechanical properties of native CNS and so rheological and dynamic mechanical analysis should be performed to fully characterize this feature and refine it. Another important limitation lies on the utilized transection model due to the lack of relevance from a clinical standpoint. Therefore, further work should be performed on contusive SCI models, and if possible, on the cervical region as these represent the most frequent types of lesions. This would lead to the establishment of novel routes of administration, as there would not be e visible cavity to be filled. However, it should be emphasized that injectable hydrogels are perhaps the most probable candidates to succeed on SCI clinical translation.

The EC source used should also be different since HUVECs fail to display CNS phenotypes, where specialized transporters and barrier markers are included, and are not a type of microvascular EC. Although the isolation of microvascular cells from rat spinal cord is possible, its yield is probably not satisfactory to correspond to the demand of these studies [28]. On this regard, the derivation of spinal cord microvascular ECs from iPSCs should be considered, as such approaches are already available for their brain counterpart a translatable source of specific CNS ECs [29,30].

The ever-evolving SCI field has witness major breakthroughs during the last decade, but the clinical gains to this day remain extremely limited. The complexity of the condition has always pushed researchers to theorize and test combinatorial approaches modulating different SCI events [31,32]. However, their design should take into consideration whether the events to be modulated are overlapped, or even have a common origin. It is now well established that perhaps the most important reason for the lack of neuronal regeneration following SCI does not lie on extrinsic factors such as CSPG deposition or the glial scar, but on the epigenetic drifts experienced by neurons throughout their maturation that suppress this ability [33]. Once these are unblocked, neurons can regenerate independently of the SCI environment [34,35]. Indeed, to achieve it neurons need to revert to embryonic transcription programs [36]. These exciting findings are now being applied to develop *in situ* reprogramming cycles that can transiently relapse neuronal cells to embryonic development with interesting results in different CNS disease models [37,38]. Other game changing field lies on the application of techniques such as epidural stimulation, brain machine interfaces and artificial intelligence (AI) to either bypass the spinal cord lesion site and momentarily activate neuronal

circuits to produce movement, or to establish new approaches in rehabilitative care [39]. Particularly the use of AI for SCI research holds great promise as it may provide a way to deeply understand the complex activation patterns of neuronal circuits that produce movement. This will increase our understanding on these groups of neurons on unimagined ways, offering the possibility to be then coupled with brain computer interface technologies that allow SCI patients to relearn how to perform motor tasks.

As we wait for this future, the contribution of vascular damage for the poor prognosis faced by SCI patients should not be undermined. On this regard, the development of biomaterial-based therapies aiming to serve as cell transplantation vehicles to replace the lost vasculature remains an interesting alternative. To our knowledge this work represents the first time synthetic peptidomimetic ligands were covalently coupled to hydrogels, demonstrating their potential in providing enhanced biological outcomes in comparison to linear RGD peptides. It is worth noting that the GRGDS coupling procedures developed in our lab use a stoichiometric excess of peptide, whereas the functionalization protocols for the peptidomimetics applied an inverse logic, being the polymer in excess and not the ligand. Moreover, whenever the stoichiometries were the same, GGp10αv always showed to provide better biological outcomes. Therefore, this work may represent the first step towards biomaterial-based vascularization therapies providing specific integrin activation for CNS applications.

Concluding remarks

The work developed during this thesis allowed to develop vascularizable hydrogels to tackle SCI or other CNS vascular diseases. We started by understanding the behavior of HUVECs on a previously developed GG-GRGDS hydrogel to attest that the assembly of these ECs into vascular-like networks only occurred in the presence of ASCs. To assess whether the modification of GGp with integrin specific peptidomimetic ligands for αvβ3 and α5β1 lead to enhanced bioactivity, we used two different polymer:ligand stoichiometries (10:1 and 20:1) and compared it with GGpRGD using the same ratios. It was clear that αvb3 formulations had enhanced bioactivity, specially GGp10αv, as it promoted significantly increased adhesion of ASCs to the matrix. Nevertheless, we only observed the formation of vascular assemblies when HUVECs were co-cultured with ASCs, reinforcing the importance of these MSCs in the maturation and stabilization of vascular networks. Finally, we studied the effects of both GG-GRGDS and GGp10αv encapsulating ASCs and HUVECs on the motor and sensory recovery of a T8 transection model of SCI. We demonstrated that GGp10αv+cells lead to an overall statistically significant motor recovery. Regarding the sensory recovery, all the treated groups has significant gains in comparison to injured animals at the final timepoint of the in vivo (8 weeks). The analysis of the serum of the of the animals using a defined panel of cytokines showed that GGp10αv+cells decreased the expression of pro-inflammatory mediators IL-1 α, IL-1 β, TNF-α and MCP-1 and by the upregulation of the anti-inflammatory cytokines IL-4 and IL-10 during the acute phase of SCI (48 h after injury). These in vivo results, although absent of proteomic and histological data, point out to a neuroprotective role of GGp10αv+cells following SCI.

References

1. Tran, A. P., Warren, P. M. & Silver, J. The biology of regeneration failure and success after spinal cord injury. *Physiol. Rev.* **98**, 881–917 (2018).
2. Silva, N. A., Sousa, N., Reis, R. L. & Salgado, A. J. From basics to clinical: A comprehensive review on spinal cord injury. *Prog. Neurobiol.* **114**, 25–57 (2014).
3. Popa, C. *et al.* Vascular dysfunctions following spinal cord injury. *J. Med. Life* **3**, 275–85 (2010).
4. Ng, M. T. L., Stammers, A. T. & Kwon, B. K. Vascular Disruption and the Role of Angiogenic Proteins After Spinal Cord Injury. *Transl. Stroke Res.* **2**, 474–491 (2011).
5. Li, Y. *et al.* Pericytes impair capillary blood flow and motor function after chronic spinal cord injury. *Nat. Med.* **23**, 733–741 (2017).
6. Rocha, L. A., Sousa, R. A., Learmonth, D. A. & Salgado, A. J. The role of biomaterials as angiogenic modulators of spinal cord injury: Mimetics of the spinal cord, cell and angiogenic factor delivery agents. *Front. Pharmacol.* **9**, (2018).
7. Holnthoner, W. *et al.* Adipose-derived stem cells induce vascular tube formation of outgrowth endothelial cells in a fibrin matrix. *J. Tissue Eng. Regen. Med.* **9**, 127–136 (2015).
8. Merfeld-Clauss, S., Gollahalli, N., March, K. L. & Traktuev, D. O. Adipose tissue progenitor cells directly interact with endothelial cells to induce vascular network formation. *Tissue Eng. - Part A* (2010) doi:10.1089/ten.tea.2009.0635.
9. Pires, A. O. *et al.* Unveiling the Differences of Secretome of Human Bone Marrow Mesenchymal Stem Cells, Adipose Tissue-Derived Stem Cells, and Human Umbilical Cord Perivascular Cells: A Proteomic Analysis. *Stem Cells Dev.* **25**, 1073–1083 (2016).
10. Rocha, L. A., Learmonth, D. A., Sousa, R. A. & Salgado, A. J. αvβ3 and α5β1 integrin-specific ligands: From tumor angiogenesis inhibitors to vascularization promoters in regenerative medicine? *Biotechnol. Adv.* **36**, 208–227 (2018).
11. Segal, R. A., Pomeroy, S. L. & Stiles, C. D. Axonal growth and fasciculation linked to differential expression of BDNF and NT3 receptors in developing cerebellar granule cells. *J. Neurosci.* (1995) doi:10.1523/jneurosci.15-07-04970.1995.
12. Gupta, S. K. *et al.* GAP-43 is essential for the neurotrophic effects of BDNF and positive AMPA receptor modulator S18986. *Cell Death Differ.* **16**, 624–637 (2009).
13. Coltrini, D. *et al.* Matrigel plug assay: evaluation of the angiogenic response by reverse transcription-quantitative PCR. *Angiogenesis* **16**, 469–477 (2013).
14. Rechenmacher, F. *et al.* A molecular toolkit for the functionalization of titanium-based biomaterials that selectively control integrin-mediated cell adhesion. *Chem. - A Eur. J.* **19**, 9218–9223 (2013).
15. Lukovic, D. *et al.* Complete rat spinal cord transection as a faithful model of spinal cord injury for

translational cell transplantation. *Sci. Rep.* **5**, 9640 (2015).

16. Gad, P. *et al.* Neuromodulation of motor-evoked potentials during stepping in spinal rats. *J. Neurophysiol.* (2013) doi:10.1152/jn.00169.2013.
17. Shah, P. K. *et al.* Variability in step training enhances locomotor recovery after a spinal cord injury. *Eur. J. Neurosci.* (2012) doi:10.1111/j.1460-9568.2012.08106.x.
18. Rossignol, S., Dubuc, R. & Gossard, J. P. Dynamic sensorimotor interactions in locomotion. *Physiological Reviews* (2006) doi:10.1152/physrev.00028.2005.
19. Rossignol, S. & Frigon, A. Recovery of locomotion after spinal cord injury: Some facts and mechanisms. *Annu. Rev. Neurosci.* (2011) doi:10.1146/annurev-neuro-061010-113746.
20. Matsushita, T. *et al.* Diffuse and persistent blood–spinal cord barrier disruption after contusive spinal cord injury rapidly recovers following intravenous infusion of bone marrow mesenchymal stem cells. *Exp. Neurol.* **267**, 152–164 (2015).
21. Osaka, M. *et al.* Intravenous administration of mesenchymal stem cells derived from bone marrow after contusive spinal cord injury improves functional outcome. *Brain Res.* **1343**, 226–235 (2010).
22. Morita, T. *et al.* Intravenous infusion of mesenchymal stem cells promotes functional recovery in a model of chronic spinal cord injury. *Neuroscience* **335**, 221–231 (2016).
23. Vawda, R. *et al.* Early Intravenous Infusion of Mesenchymal Stromal Cells Exerts a Tissue Source Age-Dependent Beneficial Effect on Neurovascular Integrity and Neurobehavioral Recovery After Traumatic Cervical Spinal Cord Injury. *Stem Cells Transl. Med.* sctm.18-0192 (2019) doi:10.1002/sctm.18-0192.
24. Badner, A. *et al.* Early Intravenous Delivery of Human Brain Stromal Cells Modulates Systemic Inflammation and Leads to Vasoprotection in Traumatic Spinal Cord Injury. *Stem Cells Transl. Med.* **5**, 991–1003 (2016).
25. Marcus, M. *et al.* Interactions of Neurons with Physical Environments. *Adv. Healthc. Mater.* **6**, (2017).
26. Engler, A. J., Sen, S., Sweeney, H. L. & Discher, D. E. Matrix Elasticity Directs Stem Cell Lineage Specification. *Cell* **126**, 677–689 (2006).
27. Leipzig, N. D. & Shoichet, M. S. The effect of substrate stiffness on adult neural stem cell behavior. *Biomaterials* **30**, 6867–6878 (2009).
28. Ge, S. & Pachter, J. S. Isolation and culture of microvascular endothelial cells from murine spinal cord. *J. Neuroimmunol.* **177**, 209–214 (2006).
29. Vatine, G. D. *et al.* Human iPSC-Derived Blood-Brain Barrier Chips Enable Disease Modeling and Personalized Medicine Applications. *Cell Stem Cell* **24**, 995-1005.e6 (2019).
30. Minami, H. *et al.* Generation of Brain Microvascular Endothelial-Like Cells from Human Induced Pluripotent Stem Cells by Co-Culture with C6 Glioma Cells. *PLoS One* **10**, e0128890 (2015).

31. Führmann, T., Anandakumaran, P. N. & Shoichet, M. S. Combinatorial Therapies After Spinal Cord Injury: How Can Biomaterials Help? *Adv. Healthc. Mater.* **6**, 1–21 (2017).
32. Griffin, J. M. & Bradke, F. Therapeutic repair for spinal cord injury: combinatory approaches to address a multifaceted problem. *EMBO Mol. Med.* (2020) doi:10.15252/emmm.201911505.
33. Hutson, T. H. *et al.* Cbp-dependent histone acetylation mediates axon regeneration induced by environmental enrichment in rodent spinal cord injury models. *Sci. Transl. Med.* (2019) doi:10.1126/scitranslmed.aaw2064.
34. Anderson, M. A. *et al.* Required growth facilitators propel axon regeneration across complete spinal cord injury. *Nature* **561**, 396–400 (2018).
35. Anderson, M. A. *et al.* Astrocyte scar formation aids central nervous system axon regeneration. *Nature* **532**, 195–200 (2016).
36. Poplawski, G. H. D. *et al.* Injured adult neurons regress to an embryonic transcriptional growth state. *Nature* **581**, 77–82 (2020).
37. Su, Z., Niu, W., Liu, M. L., Zou, Y. & Zhang, C. L. In vivo conversion of astrocytes to neurons in the injured adult spinal cord. *Nat. Commun.* (2014) doi:10.1038/ncomms4338.
38. Jorstad, N. L. *et al.* Stimulation of functional neuronal regeneration from Müller glia in adult mice. *Nature* **548**, 103–107 (2017).
39. James, N. D., McMahon, S. B., Field-Fote, E. C. & Bradbury, E. J. Neuromodulation in the restoration of function after spinal cord injury. *Lancet Neurol.* **17**, 905–917 (2018).